Stimulus-Responsive Block Copolymer Nano-Objects *via* Polymerisation-Induced Self-Assembly

Joseph Roy Lovett

Department of Chemistry

The University of Sheffield

Submitted to the University of Sheffield in fulfilment of the requirements for the award of Doctor of Philosophy

March 2016

Declaration

The work described in this thesis was carried out at the University of Sheffield under the supervision of Professor Steven P. Armes between October 2012 and March 2016 and has not been submitted, either wholly or in part, for this or any other degree. All the work is the original work of the author, except where acknowledged.

Signature: _____

Joseph Roy Lovett March 2016

Acknowledgements

Joseph Lovett and the Never Ending Student Life. 8 years, 8 long years ago I remember settling into my new student halls thinking “What am I doing here?”. I never would have thought chemistry would have taken me this far. Perhaps the most saddening thing, as I exit studenthood, is that my free burgers from Maccy Ds are ending. Anyway, I have countless people to thank that have helped me on my merry way during my time in Sheffield.

Firstly, to Steve FRS. Prof. PISA. Sir RAFTalot. How can one man have so many ideas!? (Not a bad strike rate either). As I’m writing this now I can hear him come up with another. Thank you for all your help and guidance these last 4 years, you’ve really had a positive *affect* on my terrible English. Your door was always open when I had any problems, I really appreciate that. Thanks for the opportunity to work in such a fantastic group.

I would like to thank the University of Sheffield and GEO Specialty Chemicals for funding the research. In particular to my contacts, Mark Smallridge and Rob Cracknell, at GEO.

Big thanks to the girls in accounts, Denise, Louise, Rachel and Brit, without you the department couldn’t run how it does. Pete (sexy tiger), Nick, Dan the glass blowing man and Simon cheers for all the banter. Pauline and Sharon, thanks for supplying cracking cuppa of teas throughout my PhD. To Chris and Svet thanks for dealing with all my TEM issues. Thanks to our collaborators Chris Clarkson and Mark Geoghegan.

To my lab dads (it’s a modern world) Nick and Lee. Thanks for answering all my countless queries. I have so many people to thank that have been through the Armes revolving door. Liam: explorer, PadDerry, Rymurk, Penners, Dean ‘the mincer’ Cocker, Babs, Vicki, Lizzy, Marksy, Dave, Morsey and Morsey (Mable), Grand Master Jeppe, Kate, Simon, Andreas, Carlo Yin, Amy, Beulah, Canning, Kay, Greg, Irene, Sasha, Craig, Byard, Erik, Herr, Marzena and so many others. Thanks for making this a really enjoyable time.

To Sam, Ross, Matt and Greg for making me feel like nothing changes when I go home. Nick, Rich, Oli, Sam, Rob, Jack and Walton, I hope the good times keep rolling. J’adore Hardcore. Cheers to man mountain Jarmani, Rutland, Excell, Hiwa and to all the footballers.

Big thanks to my big sisters ‘weak ankles’ Vicki (shame we never got that Lovett and Lovett or Lovett^2 paper) and Fran ‘the crazy horse lady’ for you continued love and support all these years. To their respective partners Methers and Ian, Christmas 2015 will never be forgotten. Come on Eileen. Huge thanks to Grandma for the past 25+ years. Without you I never would have got here. Big thanks to the entirety of my extended family, especially to a certain uncle: that party popper up the bottom 18 years ago probably got me on the right track.

To Zoë (I hope you appreciate the umlaut) thanks for all your patience, meal cooking and support during these last few months. We shall celebrate in style with a fillet en croute mmmmmmmmm. I am now your equal. Not forgetting the fur balls, Alfie and Toby, who’s stupidity never fails to make me smile.

Finally to mum and dad. How you dealt with me as I was growing up I’ll never know, but thanks for sticking with me. Your constant support and unconditional love to me means more to me than you will ever know. I hope I’ve made you proud. This is for you.

Publications

Primary Publications

(1) Lovett, J. R.; Warren, N. J.; Ratcliffe, L. P.; Kocik, M. K.; Armes, S. P. 'pH-Responsive Non-ionic Diblock Copolymers: Ionization of Carboxylic Acid End-Groups Induces an Order-Order Morphological Transition' *Angew. Chem., Int. Ed.* **2015**, *54*, 1279

(2) Clarkson, C. G.; Lovett, J. R.; Madsen, J.; Armes, S. P.; Geoghegan, M. 'Characterization of Diblock Copolymer Order-Order Transitions in Semidilute Aqueous Solution Using Fluorescence Correlation Spectroscopy' *Macrmol. Rapid Commun.* **2015**, *36*, 1572

(3) Lovett, J. R.; Warren, N. J.; Smallridge M. J.; Cracknell R. B.; Armes, S. P. 'Order−Order Morphological Transitions for Dual Stimulus Responsive Diblock Copolymer Vesicles' *Macromolecules.* **2016**, 49, 1016

(4) Lovett, J. R.; Ratcliffe, L. P.; Warren, N. J.; Smallridge M. J.; Cracknell R. B.; Saunders B. R.; Armes, S. P. 'A Robust Cross-Linking Stratrgy for Block Copolymer Worms Prepared *via* Polymerization-Induced Self-Assembly' *Macromolecules.* **2016**, 49, 2928

(5) Lovett, J. R.; Mable, C. J.; Warren, N. J.; Ratcliffe, L. P.;Armes, S. P. 'Acid-responsive diblock copolymer nano-objects *via* Polymeriation-Induced Self-Assembly' *manuscript in preperation*

Secondary Publications

(1) Penfold, N. J .W.; Lovett, J. R.; Warren, N. J.; Verstraete, P.; Smets, J.; Armes, S. P. 'pH-Responsive Non-Ionic Diblock Copolymers: Protonation of a Morpholine End-Group Induces an Order-Order Transition' *Polym. Chem.* **2016**, *7*, 79

(2) Mitchell, D. E.; Lovett, J. R.; Armes, S. P.; Gibson, M. I. 'Combining Biomietic Block Copolymer Worms with an Ice-Inhibiting Polymer for the Solvent-free Cryopreservation of Red Blood Cells' *Angew. Chem., Int. Ed.* **2016**, *55*, 2801

(3) Williams, N.; Penfold, N. J .W.; Lovett, J. R.; Warren, N. J.; Douglas, C. W. I.; Doroshenko, N.; Verstraete, P.; Smets, J.; Armes, S. P. 'Bespoke Cationic Nano-objects *via* RAFT Aqueous Dispersion Polymerisation' *Polym. Chem.* **2016**, DOI: 10.1039/C6PY00696E

(4) Jesson, C.; Pearce, C.; Simon, H.; Werner, A.; Lovett, J. R.; Warren, N. J.; Armes, S. P. 'Convenient Removal of RAFT End-groups for The Preparation of Colourless Block Copolymer Worm Gels' *manuscript in preparation*

Other Publications

(1) Lovett, J. R.; Fielding, L. A.; Buxton, R.; Armes, S. P. 'One-Pot Preparation of Conducting Polymer-Coated Silica Particles: Model Highly Absorbing Aerosols' *Adv. Funct. Mater.* **2014**, *24*, 1290

(2) Wozniakiewicz, P. J.; Price, M. C.; Armes, S. P.; Burchell, M. J.; Cole, M. J.; Fielding, L. A.; Hillier, J. K.; Lovett, J. R. 'Micron-scale hypervelocity impact craters: Dependence of crater ellipticity and rim morphology on impact trajectory, projectile size, velocity, and shape' *Meteorit. Planet. Sci.* **2014**, *49*, 1929

Conferences

July 2012 *Poster Presentation* at 'The Polymer Conference', Warwick, UK.

August 2013 *Poster Presentation* at 10th IUPAC International Conference on Advanced Polymers via Macromolecular Engineering, Durham, UK.

July 2014 *Poster Presentation* at Macro Group UK Young Researchers Meeting, Durham, UK.

August 2014 *Poster and Oral Presentations* at ACS Fall meeting, San Francisco, USA.

June 2015 *Oral Presentation* at European Polymer Congress 2015 (EPF 2015), Dresden, Germany

August 2015 *Oral Presentations* at ACS Fall meeting, Boston, USA.

Abstract

The work in this thesis focuses on stimulus-responsive poly(glycerol monomethacrylate)-poly(2-hydroxypropyl methacrylate) (PGMA-PHPMA) diblock copolymer nano-objects prepared by polymerisation-induced self-assembly (PISA) using reversible addition-fragmentation chain transfer (RAFT) aqueous dispersion polymerisation.

PGMA-PHPMA worms form soft free-standing gels at room temperature due to multiple inter-worm contacts. Cooling this gel induces a worm-to-sphere transition due to surface plasticisation of the core-forming PHPMA block, which leads to degelation. In this thesis it is demonstrated that these worms are also pH-responsive when prepared with a carboxylic acid-functionalised RAFT agent. Ionisation of the terminal carboxylic acid on the PGMA stabiliser block increases the hydrophilic character of this block and hence drives the worm-to-sphere transition. A control experiment using an analogous non-ionic ester RAFT agent only led to pH-insensitive worms. The pH-responsive behaviour of a series of analogous HOOC-PGMA-PHPMA vesicles prepared with a fixed PGMA degree of polymerisation (DP) and a variable PHPMA DP is explored. For relatively short PHPMA DPs, order-order transitions are observed on ionising the carboxylic acid end-group. However, longer PHPMA DPs yield pH-insensitive vesicles as the greater hydrophilicity from the ionised end-groups is insufficient to induce a morphological transition. Furthermore, the dual responsive nature of these vesicles to both pH and temperature triggers is investigated.

The effect of statistically copolymerising various amounts of pH-responsive 2-(diisopropylamino)ethyl methacrylate (DPA) residues in the core of PGMA-P(HPMA-DPA) spheres, worms or vesicles is explored. Kinetic studies of the chain extension revealed that DPA monomer is initially consumed faster than HPMA. This yields a DPA-rich sequence next to the block junction point, which allows order-order transitions to lower order morphologies to take place.

Finally, core cross-linked worms are prepared by chain-extending PGMA with HPMA and glycidyl methacrylate (GlyMA), followed by post-polymerisation reaction with 3-aminopropyl triethoxysilane (APTES). The primary amine in APTES ring opens the epoxy group in GlyMA and undergoes a concomitant hydrolysis-condensation reaction to covalently cross-link the worm cores. Oscillatory rheology studies indicate that core cross-linking affords stiffer worm gels that are no longer thermo-responsive. Furthermore, utilising similar epoxy-based chemistry enabled the preparation of fluorescently-labelled worms.

Contents

Common Abbreviations

AA	acrylic acid
ACVA	4,4'-azobis(4-cyanopentanoic acid)
APTES	3-aminopropyl triethoxysilane
ATRP	atom transfer radical polymerisation
BzMA	benzyl methacrylate
CGT	critical gelation temperature
CMC	critical micelle concentration
CPADB	4-cyano-4-(phenylcarbonothioylthio) pentanoic acid
CPDB	2-cyano-2-propyl dithiobenzoate
CRP	controlled radical polymerisation
CTA	chain transfer agent
DAAM	diacetone acrylamide
DLS	dynamic light scattering
DMAAM	*N*,*N*-dimethylacrylamide
DMF	dimethylformamide
DMSO	dimethyl sulfoxide
DP	degree of polymerisation
DPA	2-diisopropylaminoethyl methacrylate
FCS	fluorescence correlation spectroscopy
FRP	free radical polymerisation
G'	storage modulus
G"	loss modulus
GlyMA	glycidyl methacrylate
GMA	glycerol monomethacrylate
GPC	gel permeation chromatography
HEMA	2-hydroxyethyl methacrylate
HPLC	high-performance liquid chromatography
HPMA	2-hydroxypropyl methacrylate
LAM	less activated monomer
LAP	living anionic polymerisation
LCST	lower critical solution temperature
Macro-CTA	macromolecular chain transfer agent

MAM	more activated monomer
Me-PETTC	4-cyano-4-(2-phenylethanesulfanylthiocarbonyl)-sulfanylmethyl pentanoate
M_n	number-average molecular weight
MPC	2-(methacryloyloxy)ethyl phosphorylcholine
M_w	weight-average molecular weight
NIPAM	*N*-isopropylacrylamide
NMP	nitroxide mediated polymerisation
NMR	nuclear magnetic resonance
PDI	polydispersity index
PEO	poly(ethylene oxide)
PEOMA	poly(ethylene oxide) methyl ether methacrylate
PETTC	4-cyano-4-(2-phenylethanesulfanylthiocarbonyl)-sulfanylpentanoic acid
PISA	polymerisation-induced self-assembly
PMMA	poly(methyl methacrylate)
PS	polystyrene
RAFT	reversible addition fragmentation transfer
SDS	sodium dodecyl sulfate
TEM	transmission electron microscopy
THF	tetrahydrofuran
TMSP	sodium trimethylsilyl propanoate
UV-vis	ultraviolet-visible
VA-044	2,2'-azobis[2-(2-imidazolin-2-yl)propane]dihydrochloride

Chapter 1:

Introduction

1.1 Polymer Science

Over the past century or so, the use of polymers in everyday life has increased significantly. With an ever-increasing polymer design complexity, advances in polymer techniques have had to match this development. The first example of modern polymer science was reported by Braconnot in the 1830s, who developed derivatives from the naturally occurring polymer cellulose.[1] However, the true long-chained nature of polymers was not properly recognised for another century. Prior to polymers, the highest known molecular weight of a chemical structure was of the order of 500 Daltons. Moreover, it was long thought that polymers merely consisted of aggregates of smaller molecules. It was not until the 1920s that Staudinger proposed the long-chain nature of polymers.[2] In 1929, this hypothesis was proved correct by a series of reactions performed by Carothers, who categorised polymers as either condensation or addition depending on structural differences between the polymer and its monomer(s).[3] Condensation polymers are synthesised by a reaction that involves elimination of a small molecules. In contrast, addition polymers are formed without loss of small molecules and possess precisely the same chemical composition as the corresponding monomer(s). However, this classification leads to inconsistencies. For example, polyurethanes have the same elemental composition as their monomer, but are structurally much more similar to a condensation polymer. Therefore, in 1953 Flory classified polymerisations as chain or step depending on their formation reaction mechanism.[4] Chain polymerisations proceed by the sequential addition of monomers at a reactive centre. Conversely, step-growth polymerisations form dimers and oligomers before the generation of long-chain polymers.

Unlike small molecules, polymers do not possess a unique molecular weight. Each polymer consists of a variable number of monomer repeat units, resulting in a molecular weight distribution.[5] The two most common moments of the molecular weight distribution are the number-average molecular weight (M_n) and the weight-average molecular weight (M_w), which are defined as follows:

$$\langle M_n \rangle = \frac{\sum n_i M_i}{\sum n_i} \quad (1.1)$$

$$\langle M_w \rangle = \frac{\sum w_i M_i}{\sum w_i} = \frac{\sum n_i M_i^2}{\sum n_i M_i} \quad (1.2)$$

Where M is the molecular weight of the repeat unit (or monomer) and n is the number of chains. M_w is biased towards higher molecular weight chains. Thus, its molecular distribution is skewed in favour of the higher molecular weight species. Combined, M_w and M_n give useful information on the molecular weight distributions of polymers. The M_w/M_n is known as the polydispersity index of the polymer and is always greater than unity since $M_w > M_n$.

1.2 Free Radical Polymerisation (FRP)

Free radical polymerisation (FRP) is the most popular commercial technique as a wide range of vinyl monomers can be conveniently polymerised in various solvents without the requirement for protection group chemistry.[6] Moreover, as radical polymerisations are unaffected by protic impurities, they can be carried out in bulk, solution, dispersion and emulsion conditions.[7] However, FRP reactions must be conducted in an inert atmosphere as oxygen acts as a retarder. FRP is an example of a chain polymerisation with a radical-based reactive centre. These radicals are generated by an external source, typically by thermal or irradiate degradation of an initiator molecule. There are four essential stages in FRP; initiation, propagation, termination and transfer; a full detailed mechanism is shown in **Figure 1.1**.[4-8]

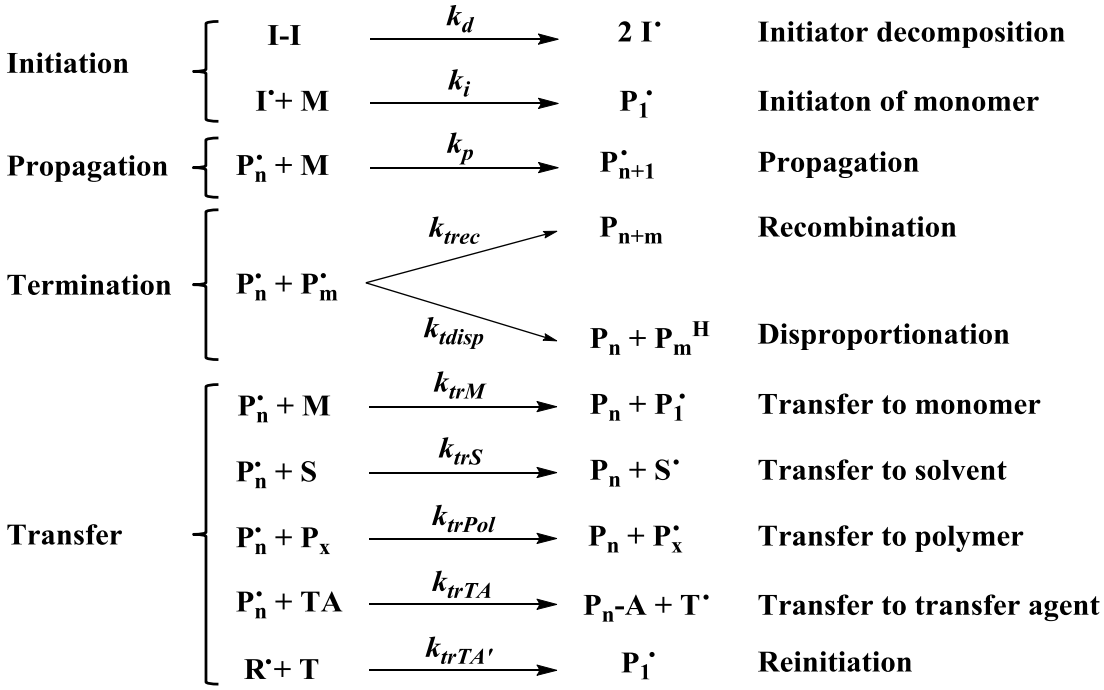

Figure 1.1 Elementary steps for free radical polymerisation.[7]

Initiation consists of two steps; generation of free radicals *via* thermal decomposition and their subsequent initiation of monomer. The first step typically proceeds by homolytic cleavage of an initiator molecule I to give two primary radicals $I^{\bullet}$. These radicals then react with a monomer unit M to generate a new active centre $P_1^{\bullet}$. Since the rate of initiator decomposition is relatively slow compared to the rate of reaction of the primary radicals with monomer, the overall rate of initiation R_i is given by:

$$R_i = \frac{d[P_I^{\cdot}]}{dt} = 2k_d f[I] \qquad (1.3)$$

Here, k_d is the rate constant for decomposition, f is the initiator efficiency and the numerical factor of two signifies that two radicals are generated per initiator molecule. The initiator efficiency indicates the ability of the primary radical to initiate a monomer. Equation **1.3** is only valid for thermal initiation, which is applicable to this thesis. Following initiation, monomer units sequentially add to

produce polymer radicals $P_n^{\bullet}$ during propagation. It is assumed that the rate constant for propagation (k_p) and termination (k_t) are both independent of the size of the radical species. Therefore, the rate of propagation (R_p) is assumed to be equal for each monomer addition, as indicated by equation **1.4**.

$$\boldsymbol{R_p = -\frac{d[M]}{dt} = k_p[P_n^{\bullet}][M]} \quad (\mathbf{1.4})$$

Here, k_p is typically ~ 10^2 to 10^4 M^{-1} s^{-1}.[7,9] Propagation continues until two polymer radicals $P_n^{\bullet}$ and $P_m^{\bullet}$ react with one each other, resulting in the annihilation of both radicals. The two most common termination mechanisms are combination and disproportionation. The former occurs when two polymer radicals react together to form one dormant chain with a mean degree of polymerisation (DP) equal to the sum of the DPs of the two original polymer radicals. Alternatively, disproportionation can occur when one polymer radical abstracts hydrogen from another, resulting in the formation of saturated and unsaturated polymer chains. The respective rates of these reactions are shown in equations **1.5** and **1.6**.

$$\boldsymbol{R_{trec} = k_{trec}[P_n^{\bullet}][P_m^{\bullet}]} \quad (\mathbf{1.5})$$

$$\boldsymbol{R_{tdisp} = k_{tdisp}[P_n^{\bullet}][P_m^{\bullet}]} \quad (\mathbf{1.6})$$

Depending on the monomer type, the extent to which of these termination mechanisms occur can differ. For example, styrene normally terminates by combination, whereas methacrylates tend to terminate mainly by disproportionation. Furthermore, the relative degrees of each mechanism can have a large effect on the polydispersity and the molecular weight of the polymers. The overall rate of termination (R_t) is expressed as:

$$R_t = 2k_t[P^{\cdot}]^2 \qquad (1.7)$$

Here, the rate constant for termination (k_t), is equal to the sum of the rate constant for termination by combination (k_{trec}) and the rate constant for termination by disproportionation (k_{tdisp}). Termination is extremely fast ($k_t > 10^8$ M^{-1} s^{-1}) compared to propagation.[9] Therefore, to grow long polymer chains by FRP it is essential that R_t is relatively slow compared to R_p. This is achieved by using low radical concentrations since R_t is second-order with respect to the radical concentrations (see equation **1.7)**, whereas R_p is first-order (see equation **1.4**).

In FRP the polymer radicals also tend to undergo chain transfer reactions with monomer, solvent, dormant polymer chains or transfer agents (see **Figure 1.1**). These side reactions should have little or no effect on the overall kinetics since the reactions are fast and no radicals are destroyed. However, these side reactions can result in cross-linking or branching. Hence they can have a considerable effect on the polydispersity and molecular weight of the resulting polymer. The overall rate of polymerisation (R_{polym}) is only affected by the initiation, propagation and termination steps. More simply, the overall rate of polymerisation is approximately equal to the rate of propagation. However, quantifying the polymer radical concentration is difficult. This problem can be overcome by assuming steady-state kinetics, or $R_i \approx R_t$. Combining and rearranging equations **1.3** and **1.7** gives an expression for the concentration of polymer radicals [$\mathbf{P}^{\bullet}$]:

$$[P^{\cdot}] = \sqrt{\frac{fk_d[I]}{k_t}} \qquad (1.8)$$

This expression can be substituted into equation **1.4** to give the overall rate of polymerisation (R_{polym}):

$$R_{polym} = k_P[M]\sqrt{\frac{fk_d[I]}{k_t}} \quad (1.9)$$

Equation **1.9** indicates that R_{polym} is proportional to both [M] and [I]$^{1/2}$ provided that the initiator efficiency (f) is high. In cases where efficiency is low, the R_{polym} is only a function of [M]. Somewhat counterintuitively, many free radical polymerisations exhibit a significant increase in rate towards the end of the reaction.[5] This is known as auto-acceleration and is most prevalent in the bulk or at high concentrations. Because of the high solution viscosity, polymer radicals diffuse more slowly, resulting in a reduction in the rate of termination (k_t), and thus an increase in the overall kinetics. In contrast, the smaller monomer units are able to diffuse freely, allowing for propagation to be maintained. Although widely used on an industrial scale, FRP offers limited control on the polymer molecular weight, polydispersity and essentially no control over the polymer architecture.

1.3 Living Anionic Polymerisation (LAP)

Living anionic polymerisation (LAP) is another example of chain polymerisation. Unlike FRP, which involves radical-based active centres, LAP propagates through anionic species. The first truly living polymerisation was reported in 1956 by Szwarc and co-workers, who conducted the anionic polymerisation of styrene in tetrahydrofuran.[10] The remarkable feature of such living polymerisations is that there is no termination (or transfer) step in the polymerisation mechanism, provided all protic impurities are absent.[6] Termination is prevented because carbanions are unable to react with one another. An intrinsic feature of LAP is that the rate of initiation is far greater than that of propagation ($R_i >> R_p$). This means that initiation is complete prior to any propagation and results in the uniform growth of polymer chains. Furthermore, as the concentration of propagating species remains constant throughout the polymerisation (even at 100 % conversion), polymers with narrow molecular weight distributions are obtained ($M_w/M_n < 1.20$). Hence, a characteristic linear evolution of polymer molecular weight with conversion

is observed. In stark contrast, FRP produces high molecular weights even at low conversions (see **Figure 1.2**).

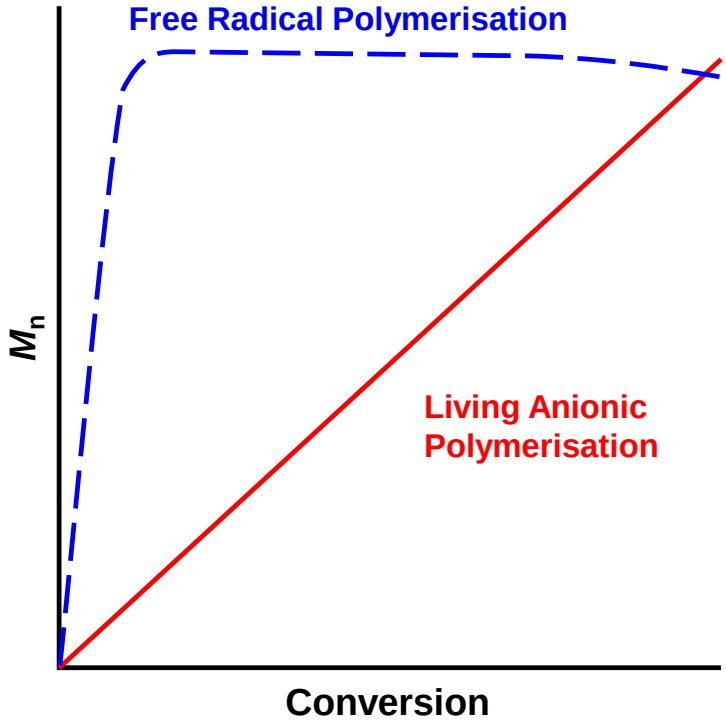

Figure 1.2 Variation of number-average molecular weight (M_n) with monomer conversion for non-living free radical polymerisation (dashed line) and living anionic polymerisation (solid line).

Another advantage of the living character of anionic polymerisation is that well-defined block copolymers can be prepared with good control over composition by sequential monomer addition. Furthermore, if no transfer or branching side-reactions occur during the polymerisation, the mean DP can be calculated according to equation **1.10**.

$$DP = \frac{[M]_0}{[I]_0} \qquad (1.10)$$

Here $[M]_0$ and $[I]_0$ are the respective initial concentrations of the monomer and initiator prior to polymerisation. Additionally, the M_n of the polymer can be

calculated by multiplying the DP of the polymer by the molecular weight of the monomer repeat unit.

Although living anionic polymerisation is a well-established technique, it has some drawbacks: protic solvents (such as water or alcohols) and electrophiles react with and terminate the active centre. Therefore, reactions must be conducted under rigorously anhydrous conditions using extremely pure reagents and aprotic solvents. Unlike FRP, LAP is more selective and is limited to monomers that possess electron-withdrawing groups. It is noteworthy that living cationic polymerisation is also possible.[11] However, termination reactions and β-proton transfer reactions to either monomer or the counterion are more prevalent than in LAP.[7] Despite these restrictions, cationic living polymerisation has been shown to be successful as long as the initiator, monomer and solvent are judiciously selected.[12-15] Other examples of living polymerisation include ring-opening[16] and group transfer polymerisation,[17] but these are beyond the scope of this thesis.

1.4 Controlled Radical Polymerisation (CRP)

Over the last two decades or so, there have been many advances in the development of living radical polymerisations. Such reactions are highly desirable as almost all vinyl monomers can be polymerised by radical polymerisation. A living or controlled radical polymerisation (CRP) is often termed 'pseudo-living' as termination is only suppressed relative to propagation, rather than eliminated. If the rates of propagation and termination in FRP are considered; the rate of propagation is directly proportional to the polymer radical concentration ($k_p \propto [P^\bullet]$), whereas the rate of termination is proportional to the square of the polymer radical concentration ($k_t \propto [P^\bullet]^2$). Hence by reducing $[P^\bullet]$, the rate of termination is reduced relative to the rate of propagation. This can be achieved by deactivating or reducing the reactivity of polymer radicals, thus preventing radical coupling and producing a more controlled polymerisation. A key aspect of CRP is the dynamic equilibrium between dormant and active states. There are two types of such equilibria, which are known as reversible termination (**Scheme 1.1a**) and reversible transfer (**Scheme 1.1b**).[6,7,18] The former equilibrium is more common and includes both nitroxide-mediated

polymerisation (NMP) and atom transfer radical polymerisation (ATRP), where X is a nitroxide species or a halogen atom respectively. Both topics will be covered briefly in **sections 1.4.1 and 1.4.2** respectively.

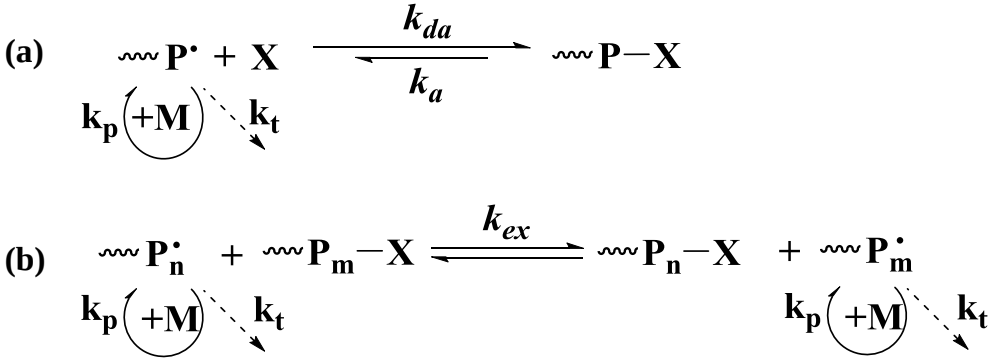

Scheme 1.1 Dynamic equilibria formed in (a) reversible termination and (b) reversible transfer, which enables controlled radical polymerisation.[6,7]

Reversible termination utilises the persistent radical effect.[19-21] This proceeds by homolytic cleavage of an initiator, which yields one reactive radical and one stable (or persistent radical, X). The reactive radical initiates polymerisation, allowing for polymers to grow over an equal time scale. These propagating chains ($P^{\bullet}$) are rapidly capped and deactivated by the persistent radical, where k_{da} is the rate of deactivation. This dormant species can be reactivated and propagation can continue, where k_a is the rate of activation. These two rate constants determine the living character of the polymerisation. It is essential that the equilibrium lies in favour of the dormant species (i.e., $k_{da} > k_a$) in order to reduce the propagating radical concentration, and therefore suppress termination. However, the concentration of the propagating radical must be high enough for propagation to occur. When the propagating species is in its active state ($P^{\bullet}$) both propagation (k_p) and termination (k_t) can take place. In contrast, the persistent radical is incapable of termination with itself, and only reversibly couples with a propagating chain. Hence, when termination occurs there is gradual accumulation of X. This shifts the equilibrium in favour of the dormant propagating species and further reduces the concentration of the propagating radical species. In contrast, reversible transfer does not involve the persistent radical effect (see **Scheme 1.1b**). Instead, it proceeds by a

mechanism more similar to FRP, where the steady-state kinetics are established by relatively slow initiation and fast termination. Control over the polymerisation is facilitated by using a transfer agent, which moves from one propagating chain to another. When the polymer radicals are capped by the transfer agent they are in a dormant unreactive state. However, when they are (briefly) in their radical form they are able to propagate (and terminate). It is essential that transfer is fast relative to propagation ($k_{ex} >> k_p$) and the concentration of the transfer agent is significantly higher than the primary radical flux to achieve good control. This is the basis for reversible addition-fragmentation chain transfer (RAFT) polymerisation, which will be discussed in more detail in **section 1.4.3**.

In both mechanisms it is critical that the rate of exchange from an active to a dormant species is faster than the rate of propagation. This allows for control over the target molecular weight and affords narrow polydispersities (M_w/M_n < 1.30, rather than M_w/M_n > 1.50 for FRP) as the growing chains spend the majority of their time in a dormant state.[18] Like LAP, the polymer M_n evolves linearly with conversion (see **Figure 1.2**). Furthermore, well-defined block (or star or graft) copolymers (see **Figure 1.3**) can be prepared by sequential monomer.

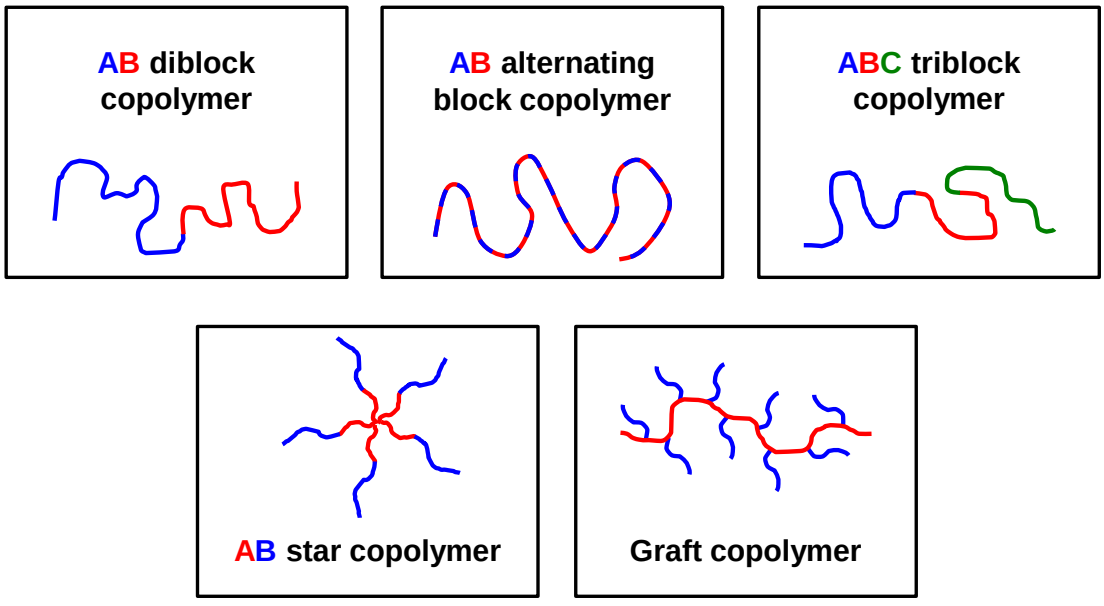

Figure 1.3 Graphical illustration of the most common block copolymer architectures.[8,22]

1.4.1 Nitroxide Mediated Polymerisation (NMP)

NMP follows the reversible termination mechanism and relies on the persistent radical effect.[23-25] Key to this mechanism is the reversible homolytic cleavage of a relatively weak C-O bond to produce an active propagating radical species and a stable/persistent radical (see **Scheme 1.2**). As previously discussed, the persistent radical (nitroxide species) is unable to terminate with itself and can only react with a propagating radical. In this case, self-termination of the nitroxide species is prevented primarily by steric hindrance. Reactions can be initiated by either an alkoxyamine or by using a conventional initiator with a nitroxide species, which forms an alkoxyamine *in situ*. NMP is arguably the simplest CRP technique, particularly since the development of so-called universal alkoxyamines which allow the controlled polymerisation of several monomer classes.[23,25,26]

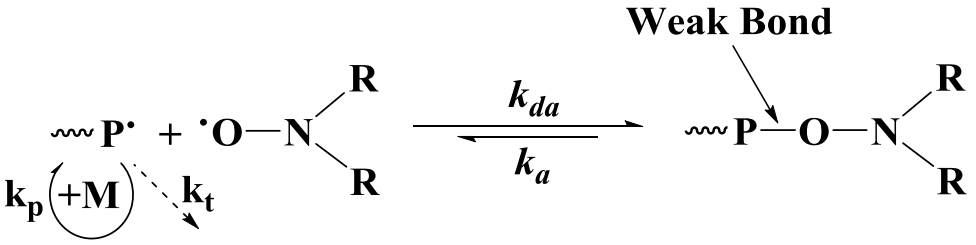

Scheme 1.2 Reversible termination equilibrium for NMP-based reactions.[24]

Originally, nitroxide species were utilised as irreversible radical traps to investigate reactions between initiators and radicals.[24,27] However, it was only in 1993 when Georges *et al*. reported the synthesis of polystyrene using 2,2,6,6-tetramethylpiperidinyloxy (TEMPO) which possessed a narrow molecular weight distribution that NMP became of widespread interest.[28] Here the nitroxide species reversibly capped a propagating chain enabling a controlled polymerisation. Since then, the temperature required to reactivate the dormant chains have been reduced by optimisation of the nitroxide specie for specific monomer classes.[23] This is achieved by adjusting the steric and electronic properties of the nitroxide, which govern the rate of homolysis of the alkoxyamine C-O bond.[29] Nowadays, there is quite an extensive library of nitroxide and alkoxyamine species available. Despite these advances, controlled polymerisation of methacrylates by NMP have had limited

success due a hydrogen abstraction side reaction. Nevertheless, some recent progress has been made to address this problem.[30,31]

1.4.2 Atom Transfer Radical Polymerisation (ATRP)

ATRP was independently developed by Wang and Matyjaszewski[32] and Sawamoto and co-workers[33] in 1995. Since then, there have been many examples of well-defined polymers with varying functionalities that have been prepared using ATRP.[34-36] Like NMP, ATRP relies on the persistent radical effect. The main dynamic equilibrium is shown in **Scheme 1.3** where X is a halide (usually Br or Cl) and Mt^m/L is a metal catalyst (with oxidation state m and ligand(s) L). Typically, the metal catalyst is Cu-based but many other transition metals have also been reported, such as Fe, Ru, Ni.[37]

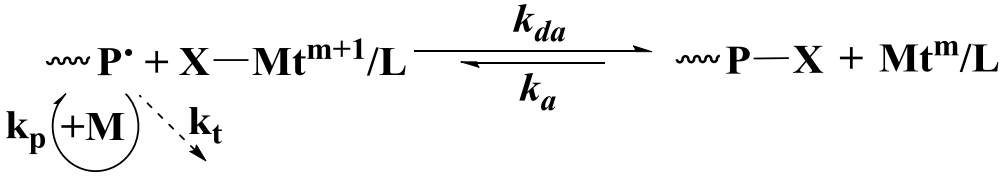

Scheme 1.3 Reversible termination equilibrium for ATRP based reactions.[34]

The basic principle of ATRP involves homolytic cleavage of an initiator comprising a labile halide bond (usually an alkyl halide) by a transitional metal catalyst. This results in the oxidation of the catalyst and formation of a reactive alkyl radical, which can propagate, terminate to form dead polymer chains or undergo reversible reactions with the metal catalyst to form halogen-capped dormant chains. Thus conventional ATRP must be conducted in the absence of oxygen or oxidants to prevent irreversible oxidation of the catalyst. Reversible capping is mediated by the metal catalyst, which undergoes redox reactions. This equilibrium strongly favours the dormant species ($k_{da} >> k_a$), which enables the controlled simultaneous growth of propagating chains. The mean DP of the resulting polymer chains prepared by ATRP is equal to the monomer concentration divided by the initiator concentration (see equation **1.10**), and is not affected by the concentration of the metal catalyst. The rate of ATRP is governed by the following expression:

$$R_{polym} = k_p[M][P^{\cdot}] = k_p K_{ATRP}\left(\frac{[PX][Mt^m/L][M]}{[X-Mt^{m+1}/L]}\right) \quad (1.11)$$

Here K_{ATRP} is the atom transfer equilibrium constant and is equal to k_a/k_{da}.[18,38] The equilibrium constants in ATRP, and therefore rate, are strongly dependent on the structure of the metal catalyst and its ligands, the initiator and the monomer type. It is noteworthy that the equilibrium constants also increase strongly with temperature. To obtain well-controlled polymerisations with efficient rates of polymerisation, each of these parameters must be judiciously chosen. In general, the initiator reactivity is inversely proportional to the R-X bond dissociation energy.[39] Therefore the rate of initiation increases with higher degrees of substitution around the halogen, more activating substituents around the halogen (e.g., α-carbonyls) and by the leaving group ability of the halogen (i.e., I > Br > Cl).[40,41] Furthermore, this makes up the basis of the principle of 'halogen exchange', whereby a polymer made of a less active monomer can be chain-extended with a more active monomer (e.g., chain extension of poly(n-butyl acrylate) with poly(methyl methacrylate)).[42,43]

A prerequisite for ATRP is that the transition metal catalyst must be able to expand its coordination sphere and have two readily accessible oxidation states one apart from one another (e.g., Cu(I)/Cu(II)). Moreover, the metal catalyst ideally must be soluble in the reaction solvent. Solubility can be facilitated by the choice of ligand(s), which also has an effect on K_{ATRP}. Nitrogen-containing ligands are commonly used because they do not bind strongly to polar solvents.[7] The activity of metal catalysts is governed by the structure of the ligands (cyclic-bridged > branched > cyclic > linear), the nature of the N atom (imine > aliphatic amine), the number of linking units between each N (2 > 3) and steric effects.[41,44]

A significant drawback of ATRP is the requirement to remove the metal catalyst after the polymerisation. Such impurities are well known to be harmful to living organisms. Various methods for removal of metal catalysts have been developed (e.g., silica chromatography, use of supported catalysts etc.), but the cost and time of its removal are usually uneconomic.[36] Furthermore, termination in

conventional ATRP results in the build-up of the deactivator species X-Mt^{m+1}/L and reduced polymerisation rates, see equation **1.11**. In cases where the degree of radical termination is greater than that of the initial metal catalyst the polymerisation will completely halt. However, significant progress has been made to combat these two major issues.[35,45] For example, activators generated by electron transfer (AGET) was developed in 2005, whereby the metal catalyst is added in its deactivated form and a (sub)stoichiometric amount of reducing agent (such as tin(II) 2-ethylhexanoate, ascorbic acid or triethylamine) is used to activate the metal complex and initiate polymerisations *in situ*.[46-49] Subsequently, this led to recognition that using excess reducing agent enables the regeneration of Mt^{m}/L from Mt^{m+1}/L by a technique called 'activators regenerated by electron transfer' (ARGET).[50,51] Therefore, reduced concentrations of the metal catalyst (sometimes less than 10 ppm) can be used without diminishing the rate of polymerisation, which depends on the ratio of concentrations of the activator (Mt^{m}/L) and deactivator (X-Mt^{m+1}/L) metal catalyst, see equation **1.11**.[45] Initiators for continuous activator regeneration (ICAR) proceeds by the same principle. However, in this case the metal catalyst is regenerated by free radical initiators which slowly decompose throughout the reaction.[52] More recently, Matyjaszewski and co-workers have reported electrochemically-mediated ATRP (eATRP), where the relative concentrations of oxidised and reduced metal catalyst can be controlled *via* an applied electrochemical potential.[53]

1.4.3 Reversible Addition Fragmentation Transfer (RAFT) Polymerisation

RAFT was first developed in 1998 by Rizzardo and co-workers at CSIRO.[54] Unlike NMP and ATRP, RAFT controls chain growth through reversible (chain) transfer and does not rely on the persistent radical effect. RAFT polymerisation follows the same mechanism as FRP but is mediated by a RAFT chain transfer agent (CTA), which transfers from one propagating chain to another to control the polymerisation. The main steps in the RAFT mechanism are shown in **Figure 1.4**.[54-59]

1. Initiation

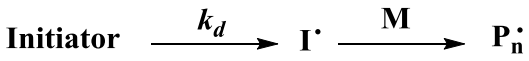

2. Reversible chain transfer

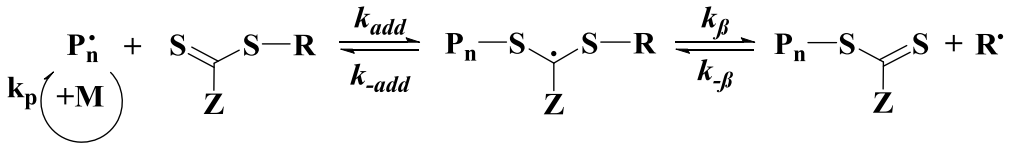

3. Reinitiation

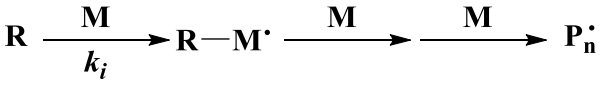

4. Chain equilibration

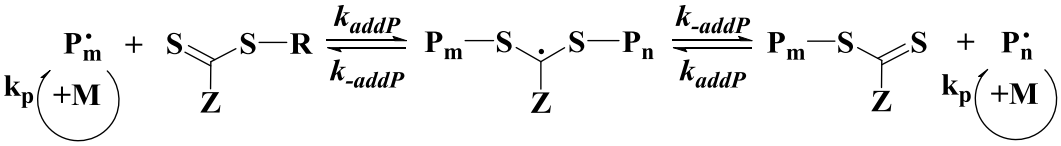

5. Termination

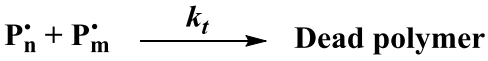

Figure 1.4 The RAFT mechanism illustrating the initiation, reversible chain transfer, re-initiation, chain equilibration and termination steps.[56-59]

Generation of free radicals (step 1 in **Figure 1.4**) occurs as in FRP and typically proceeds by the homolytic cleavage of initiator molecules by either heat or UV radiation. These radicals can then react with monomer and a propagating chain is formed ($P_n^{\bullet}$). This species quickly reacts with the CTA (step 2) and undergoes fragmentation to afford either the original CTA or a polymeric CTA and a new radical source ($R^{\bullet}$). The latter is able to re-initiate more monomer (step 3) and produce another propagating chain ($P_m^{\bullet}$). These polymer chains continue to propagate in the chain equilibrium step (step 4), whereby they undergo a rapid reversible equilibrium between active and dormant states. As with FRP, radical-radical reactions result in termination and the production of dead chains (step 5). For

an efficient RAFT polymerisation, the initial CTA (or macro-CTA) should possess a reactive C=S bond (high k_{add}). The intermediate species should fragment quickly with no side reactions in favour of release of the R$^{\bullet}$ group (i.e., $k_{\beta} > k_{-add}$), which is capable of monomer re-initiation ($k_i > k_p$). In the main chain equilibrium it is essential that the rate of transfer is faster than the rate of propagation to obtain a well-controlled polymerisation. It is this rapid equilibrium which allows the polymer chains to propagate equally and therefore possess uniform chain lengths and low polydispersities. It is essential that the polymer chains retain the CTA end-group to preserve their 'living' character, especially for the synthesis of well-defined block copolymers. The generalised chemical structure of a CTA and its characteristic features are depicted below in **Figure 1.5**.

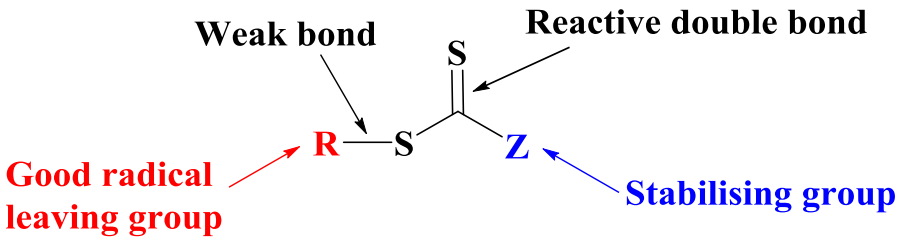

Figure 1.5 Generic depiction of the chemical structure of a RAFT CTA highlighting it's the key components.

Common examples of effective RAFT CTAs include dithioesters,[54] trithiocarbonates,[60] dithiocarbamates[61,62] and xanthates.[63] Ultimately, the choice of the CTA and its Z and R groups are governed by the monomer, although solubility must also be taken into consideration.[57-59,64-66] The rate of addition of a propagating radical to the CTA is determined by the stabilising Z group. In general, strong stabilising groups favour the formation of the intermediate radical and increase the reactivity of the C=S bond. Furthermore, electron-withdrawing groups enhance the C=S bond activity, whereas interacting adjacent heteroatoms reduce its activity (i.e., dithiocarbamates and xanthates).[65] Fragmentation of the R group is mainly controlled by its electronic and steric properties. Typically, more electrophilic and/or bulkier radicals are better leaving groups, but the ability of the radical to re-initiate must also be considered. For efficient polymerisation, it is important that R is a better leaving group than the propagating species.[66] To obtain well-controlled polymerisations and

narrow molecular weight distributions, it is critical to match the reactivity of the CTA with that of the monomer. A set of guidelines for selection of the correct CTA for a given monomer class have been reported by Moad and co-workers, see **Figure 1.6**.[58] There are two types of monomer; more-activated monomers (MAMs) and less-activated monomers (LAMs). MAMs are those where the double bond is conjugated to a carbonyl group (such as methyl methacrylate (MMA), 2-hydroxypropyl methacrylamide (HPMAM), methyl acrylate (MA), acrylamide (AM)), a nitrile (such as acrylonitrile (AN)) or an aromatic (for example styrene (St)). LAMs are those where the double bond is adjacent an unsaturated carbon or a heteroatom lone pair (such as vinyl acetate (VAc), N-vinylpyrrolidone (NVP) or N-vinylcarbazole (NVC)).

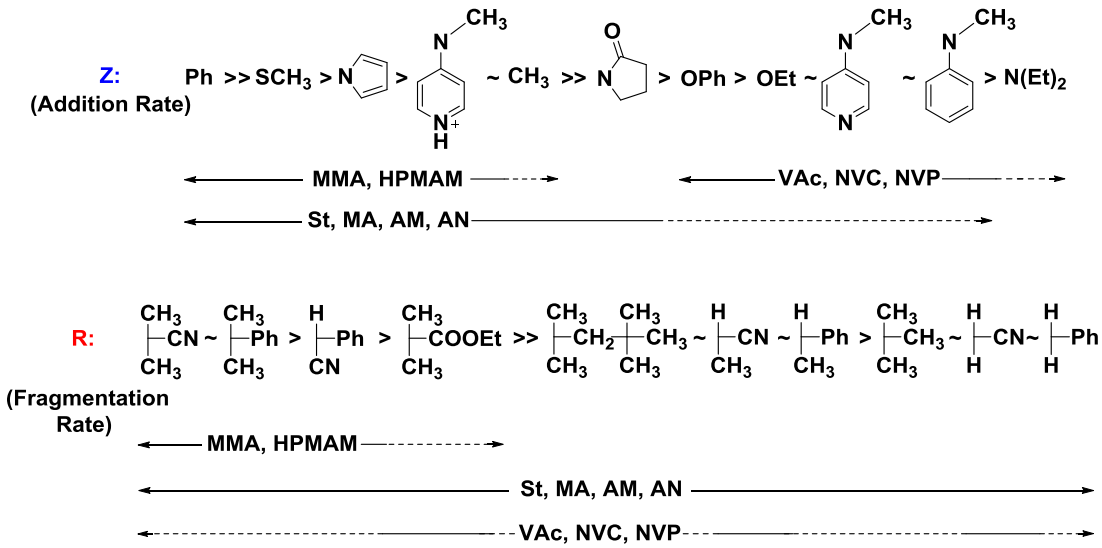

Figure 1.6 Guidelines for selection of RAFT agents for polymerisation of various monomers as reported by Moad and co-workers.[58] Solid lines represent good control, whereas dashed lines indicate partial control.

In general, well-controlled polymerisation of MAMs can be achieved using dithioesters or trithiocarbonates, whereas poorly-controlled polymerisations are usually observed when dithiocarbamates or xanthates are employed. For LAMs, the opposite behaviour is observed. In principle, the rate of a RAFT polymerisation should follow the kinetics of the corresponding FRP as the chain transfer side-reactions have no effect on the overall rate. However, inhibition at the beginning of

the reaction and retardation during the reaction are regularly observed.[58,59] In some cases, this can be attributed to inappropriate selection of the CTA and the Z and R groups. For example, the polymerisation of LAMs with dithioesters or trithiocarbonates is usually accompanied by both inhibition and retardation, because of the relatively high stability of the intermediate relative to the leaving ability of the propagating radical. Polymerisations of MAMs by dithiocarbamates or xanthates are ineffective, due to the relatively poor reactivity of the CTAs to the monomer. However, they can be effective when the heteroatom is part of an aromatic ring or if electron-withdrawing groups are present.[58,59,64] Retardation becomes more pronounced with increasing CTA concentration, particularly when dithiobenzoates are employed.[18,58,64] Two main mechanisms for the phenomena have been proposed; side reactions with intermediates[67] and slow fragmentation of the intermediate.[68] There is still some controversy on this subject.[69] Despite this, low polydispersity polymers can be prepared. Inhibition has been attributed to slow fragmentation of the initial intermediate to afford $R^{\bullet}$ followed slow re-initiation of new polymer chains.[70,71]

In theory, only two different CTAs are required to achieve reasonably controlled polymerisation for the majority of the monomers (see **Figure 1.6**):[24,58,59] one CTA designed for the synthesis of the MAMs (such as a tertiary cyanoalkyl trithiocarbonate) and the other for the polymerisation of LAMs (for example, a cyanoalkyl dithiocarbamate or xanthate). However, different CTAs may be required for certain solvents or if specific end-group functionality is required. More recently, so-called switchable or universal CTAs have been designed that enable the controlled polymerisation of both LAMs and MAMs.[72,73] Thang and co-workers demonstrated that the deprotonated form of N-(4-pyridinyl)-N-methyldithiocarbamates could mediate the polymerisations of LAMs, but when protonated these CTAs could be used to prepare MAMs (see **Figure 1.7**). Moreover, such CTAs provide a facile route for the synthesis of polyMAM-polyLAM block copolymers, which cannot be prepared by conventional RAFT methods. It is essential that the two blocks are prepared in the correct order due to the poor leaving group ability of the polyLAMs relative to the polyMAMs.

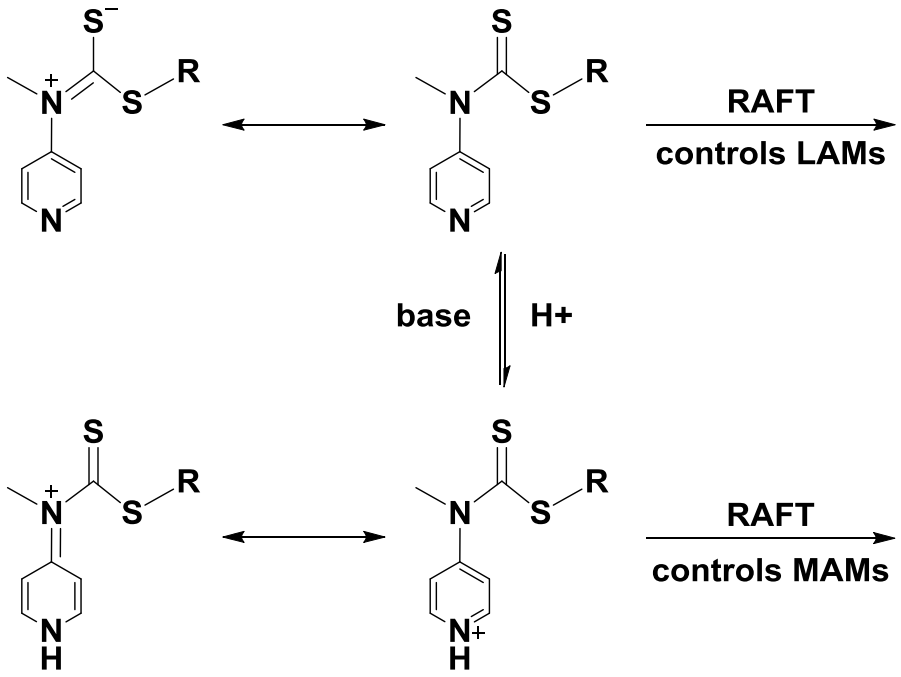

Figure 1.7 Chemical structures of a switchable N-(4-pyridinyl)-N-methyldithiocarbamate CTA in its deprotonated and protonated form and their resonance forms.[72,73]

Unlike other examples of CRP, the concentration of the mediator (i.e., CTA) affects the number of polymer chains formed and hence the target DP. The overall number of growing chains is determined by the sum of the CTA concentration and the concentration of radicals that are capable of initiation.[6] Assuming that the monomer reaches 100% conversion, the target DP is given by the following expression:

$$\boldsymbol{DP = \frac{[M]_0}{([CTA]_0 + 2f[I]_0)}} \qquad \textbf{(1.12)}$$

However, high concentrations of CTA with large chain-transfer constants are typically used, whereas the initiator is used in relatively low concentrations and only slowly decomposes. Therefore, the number of polymer chains formed due to the initiator is normally negligible compared to those capped by the CTA (i.e., $[CTA]_0 >> 2f[I]_0$). Under such conditions, the DP can be simplified to give:

$$DP = \frac{[M]_0}{[CTA]_0} \quad (1.13)$$

RAFT is arguably the most versatile 'living' technique as well-controlled polymerisations of a wide range of monomers are possible when a suitable RAFT agent is selected.[7] Unlike NMP and ATRP, RAFT can be used to efficiently polymerise LAMs.[58] Furthermore, acidic monomers can be polymerised in their unprotected forms, whereas ATRP normally requires protecting group chemistry.[74,75] However, the sulphur-based CTA (and resulting polymer) are malodorous and also possess intrinsic colour and must be removed for many potential applications. Several methods have been developed to remove the CTA end-group or to exploit its chemistry for functionalisation.[76,77] Some common examples include: (i) reactions with nucleophiles or reducing agents to yield thiol groups, which can be functionalised further; (ii) thermolysis to afford an alkene end-group; (iii) radical-induced reactions with initiators to remove sulfur end-groups. Furthermore, RAFT has proved an elegant method for the preparation of block copolymers by sequential monomer addition.[58] This thesis focuses on the preparation of methacrylate-based diblock copolymers using RAFT polymerisation. Thus diothioester and trithiocarbonate RAFT agents can be employed to obtain well-controlled polymerisations.

1.5 Conventional Heterogeneous Polymerisation in Water

Over the past few decades, considerable effort has been made in the preparation of monodisperse latex particles by various different polymerisation methods.[78] These include emulsion, suspension, precipitation or dispersion polymerisations. However, this section will focus on conventional aqueous emulsion polymerisation and aqueous dispersion polymerisation formulations. The basis of both these methods is the formation of a water-insoluble polymer in the presence of a stabiliser to form colloidally stable latexes. A typical emulsion formulation consists of water, a water-soluble initiator, surfactant and a vinyl monomer of limited water-solubility (although often additives may also be present).[79] On application of shear,

surfactant micelles and large polydisperse surfactant-stabilised monomer droplets are formed (see **Figure 1.8a**). Initiation of monomer takes place in the aqueous phase, whereas particle nucleation can occur through two routes: (i) homogenous nucleation or (ii) heterogeneous-nucleation which occurs within surfactant micelles.[78] The former produces oligomeric radicals that remain relatively water-soluble. On reaching a critical length, these growing chains become surface-active and either enter a pre-existing micelle or aggregate with surfactant to form a micelle (see **Figure 1.8b**).[80,81] The polymer chain propagates rapidly as the local monomer concentration in these micelles is relatively high. Monomer now migrates from the reservoir droplets to the polymerising particles. At any given time during the emulsion polymerisation, the particles contain either one or zero radical species due to rapid radical annihilation. Eventually, the monomer reservoirs become completely consumed and only monomer within the growing particles reacts (**Figure 1.8c**). Typically, emulsion polymerisation produces particles of the order of 100-500 nm.[79] One example of an emulsion polymerisation is the preparation of polystyrene latexes using potassium persulfate initiator and cetyltrimethylammonium bromide as a cationic surfactant.[82]

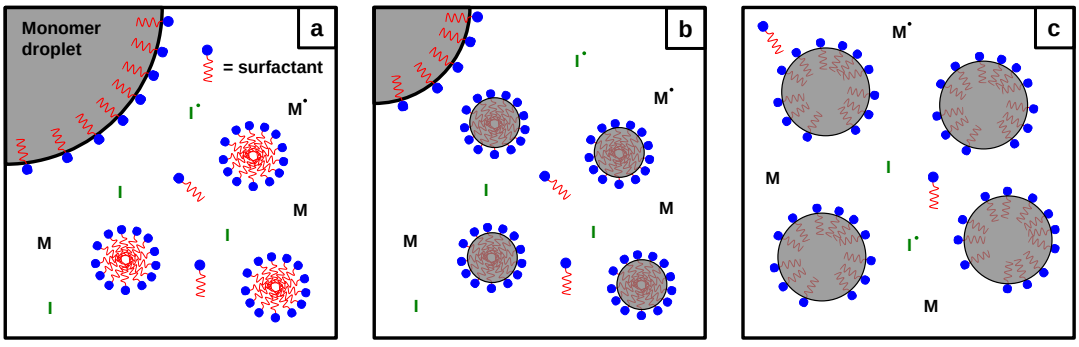

Figure 1.8 Schematic illustration of the main components and three stages of aqueous emulsion polymerisation: I is the initiator molecule, I$^{\bullet}$ is the radical initiator, M is the monomer and M$^{\bullet}$ represents the propagating radicals.[78]

In contrast, an aqueous dispersion polymerisation formulation consists of water, a water-soluble monomer, a water-soluble initiator and a polymeric stabiliser. Importantly, the water-soluble monomer polymerises to afford a water-insoluble polymer. There are very few monomers that fulfil this criterion in water, whereas

there are many examples of dispersion polymerisation formulations in polar or non-polar media.[83,84] The generally accepted mechanism for formation of particles by dispersion polymerisation is as follows.[78,84] Initially all the components in the reaction solution are fully soluble. Monomer reacts with initiator radicals and forms a soluble propagating oligomer. However, at a critical DP this chain becomes insoluble and aggregates with other chains to form nascent particles and the stabiliser starts to adsorb on their surface. These particles then coalesce with other unstable particles until sufficient amounts of stabiliser are adsorbed on the surface to form colloidally stable particles. In the absence of a suitable stabiliser, a precipitation polymerisation is obtained.

As mentioned above, there are currently very few literature reports of particles prepared by aqueous dispersion polymerisation. For example, Armes *et al*. prepared polypyrrole latexes in the presence of various stabilisers.[85-87] These included poly(*N*-vinylpyrrolidone) (PNVP), poly(vinyl alcohol), poly(ethylene oxide) (PEO), sodium dodecylbenzenesulfonate. More recently, Ali and co-workers prepared 100 – 1000 nm diameter poly(2-hydroxypropyl methacrylate) (PHPMA) latexes, by free radical aqueous dispersion polymerisation of HPMA in the presence of a PNVP or sodium dodecyl sulfate (SDS) steric stabiliser (**Figure 1.9**).[88] Incorporating a dimethacrylate cross-linker, produced latexes that exhibited microgel character in good solvents for the PHPMA chains (e.g., methanol).

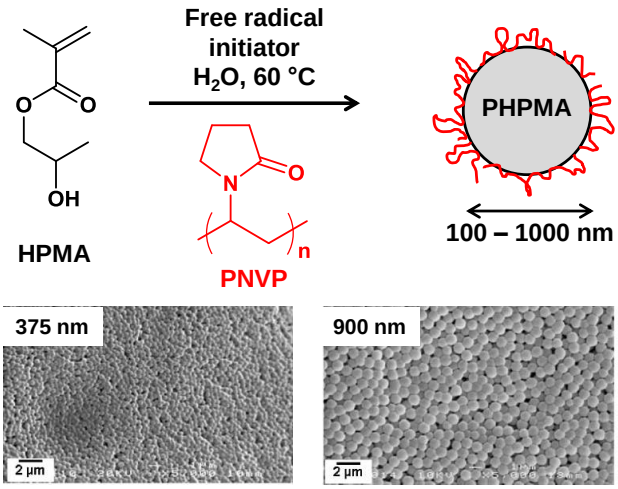

Figure 1.9 Preparation of PHPMA latexes by aqueous dispersion polymerisation of HPMA in the presence of a PNVP polymeric stabiliser.[88]

1.6 Self-Assembly of Amphiphiles

1.6.1 Water and the hydrophobic effect

Water is one of the most abundant molecules on Earth and is essential for life. Considering its relatively low molecular weight alone (18 g mol^{-1}), water should be a gas at room temperature and atmospheric pressure. However, water actually melts at 0 °C and boils at 100 °C. This is because of extensive intermolecular forces known as hydrogen bonds. Such bonds are predominately electrostatic attractions which form between an electronegative atom (such as oxygen) and a hydrogen atom bound to an electronegative atom. Typically, the strength of a hydrogen bond for neutral molecules lies between 10 and 65 kJ mol^{-1} and are significantly stronger than that of van der Waal forces (1 kJ mol^{-1}).[89] Furthermore, unlike van der Waals, hydrogen bonds express some directionality. Therefore, water adopts a tetrahedral coordination as the two lone electron pairs on the oxygen atom and the two bound hydrogen atoms in a water molecule are each able to form hydrogen bonds with other water molecules.

Water is often called a 'universal solvent' as it is capable of dissolving many different ionic or polar solids, which is usually due to the formation of hydrogen bonds between the substrate and water molecules. In contrast, hydrophobic molecules (e.g., a hydrocarbon chain) are unable to form hydrogen bonds. Therefore, water molecules surrounding a hydrophobic molecule must lose at least one hydrogen bond, although this is thermodynamically unfavourable. Thus water molecules rearrange themselves to form a cage (or clathrate) around hydrophobic molecules in order to maximise the number of hydrogen bonds. This reordering of water molecules is known as the hydrophobic effect.[90-92] Although thermodynamically favourable, the increased order in the system is entropically highly unfavourable. The entropic penalty increases with the surface area of the hydrophobic substrate. Thus mixing water with hydrophobic molecules normally results in phase separation.

1.6.2 Thermodynamics for self-assembly of surfactants

The hydrophobic effect accounts for some interesting phenomenon in water, including the spontaneous self-assembly of amphiphiles in aqueous solution. An amphiphilic surfactant consists of a hydrophilic head group and a hydrophobic tail. The head group is solvated in aqueous solution, whereas the hydrophobic tail drives aggregation. The self-assembly of such amphiphiles is governed by weaker interactions such as hydrogen bonding, van der Waal and electrostatic interactions. **Figure 1.10** illustrates the equilibrium of single amphiphilic molecules (unimers or monomers) and their aggregates.

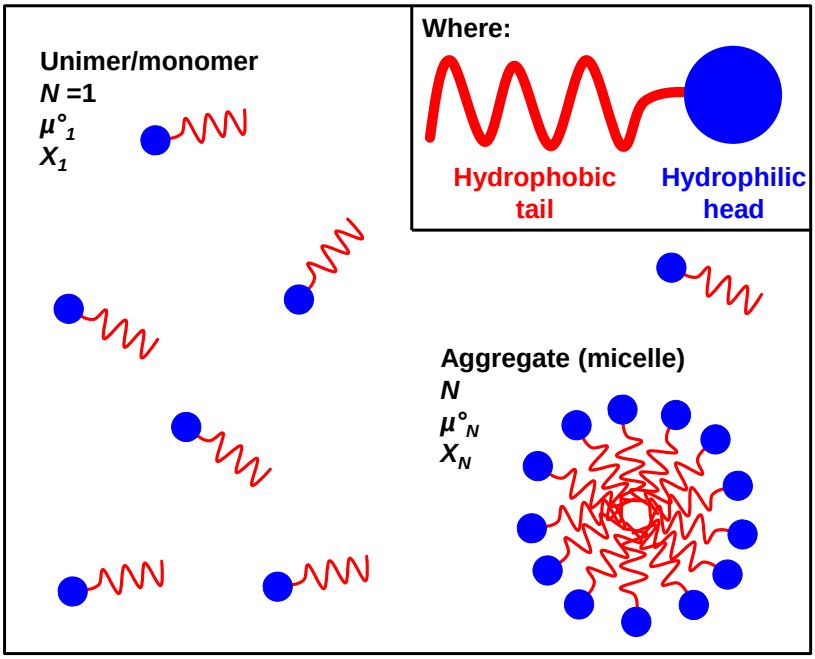

Figure 1.10 Schematic representation of the self-assembly of amphiphilic unimers (or monomers) to form an aggregate (e.g., micelles) in aqueous solution and their corresponding parameters used in thermodynamic equations.[92]

The equilibrium constant, K, for this exchange between unimers and aggregates can be written as:[92]

$$K = \frac{k_1}{k_N} = exp\left[-N\frac{(\mu_N^o - \mu_1^o)}{k_B T}\right] \quad (1.14)$$

Here k_1 and k_N are the rates of association (aggregation) and dissociation respectively, N is the aggregation number, k_B is the Botlzmann constant and T represents the absolute temperature. If we consider equation **1.14**, it is apparent that for aggregation to take place K must be positive (as $k_1 > k_N$). Therefore, the chemical potential of a unimer, $\mu°_1$, must be larger than the chemical potential of an aggregate, $\mu°_N$, with an aggregation number N. Equation **1.14** can also be written in terms of X_N (concentration/activity fraction of molecules existing as part of an aggregate N unimers):

$$\boldsymbol{X_N = N\left\{X_1\, exp\left[\frac{(\mu_1^o - \mu_N^o)}{k_B \mathrm{T}}\right]\right\}^N} \qquad (\mathbf{1.15})$$

Here X_1 is the concentration/activity of an isolated unimer and the total solute concentration, C, is equal to:

$$\boldsymbol{C = X_1 + X_2 + X_3 + \cdots = \sum_{N=1}^{\infty} X_N} \qquad (\mathbf{1.16})$$

C (and X_N) cannot exceed unity. It is also important to note that the above equations assume ideal mixing in dilute solutions so that inter-aggregate interactions can be ignored. Formation of aggregates from unimers requires the chemical potentials of the aggregated molecules to be lower than that of isolated unimers (i.e., $\mu°_1 > \mu°_N$) and that $\mu°_N$ decreases with increasing N. However, the dependence of $\mu°_N$ on N is related to the geometry and shape of the aggregate. If it is assumed that $-\alpha k_B\mathrm{T}$ is equal to the 'bond' energy between molecules in an aggregate relative to isolated unimers (where α is a constant related to monomer-monomer and monomer-solvent interactions) then, for a one-dimensional aggregate (i.e., a chain), the total interaction free energy $N\mu°_N$ for an aggregate made up of N molecules can be described as:[92]

$$N\mu_N^o = -(N-1)\alpha k_B T \quad (1.17)$$

where (N – 1) represents terminal unbound monomers at each end of the chain. Equation **1.17** can be rearranged to be expressed in terms of $\mu°_N$:

$$\mu_N^o = \mu_\infty^o + \frac{\alpha k_B T}{N} \quad (1.18)$$

Here $\mu°_\infty$ defines the bulk energy of a molecule in an infinite aggregate. Similar calculations can be conducted for two-dimensional structures (e.g., disc) and three-dimensional structures (e.g., micelles or spheres). In the case of the former, N is proportional to the area of a disc (πr^2) and the number of unbound molecules is proportional to the circumference of the disc ($2\pi r$). For three-dimensional structures, the number of bound molecules is proportional to the volume of a sphere ($4/3\ \pi r^3$) and the number of unbound molecules is proportional to the area of a sphere ($4\pi r^2$).Therefore, equation **1.18** can be generalised to give:

$$\mu_N^o = \mu_\infty^o + \frac{\alpha k_B T}{N^P} \quad (1.19)$$

where P is dependent on the geometry of the aggregate. For example, in a three-dimensional structure P = 1/3. From equation **1.19** it is clear that $\mu°_N$ decreases with increasing N, regardless of geometry. However, other parameters have to be considered for self-assembly, such as concentration. The concentration at which aggregation first occurs is known as the critical aggregation concentration, which is more commonly known as the critical micelle concentration (CMC). Typically, micellisation occurs at low concentrations, as the entropic cost of forming an ordered system is more favourable than unimer dissolution due to the hydrophobic effect. Inspecting equation **1.15**, we can see that this occurs as X_1 approaches $\exp[-(\mu°_1 - \mu°_N) / k_B T]$, as X_N cannot exceed unity. Increasing the concentration of amphiphilic

molecules in solution beyond this point, results in an increased concentration of molecules within an aggregate, whereas the concentration of molecules in their unimeric state remains relatively constant (see **Figure 1.11** below).

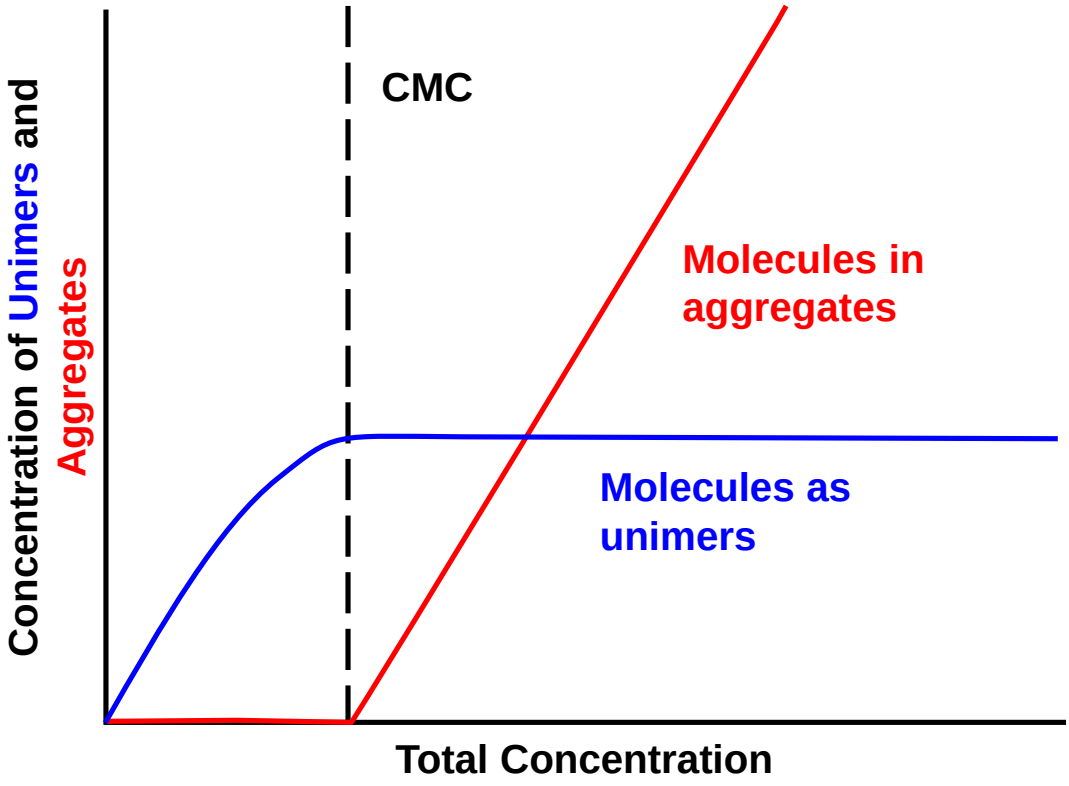

Figure 1.11 Graphical representation of the concentration of unimers and aggregates against total concentration. The point at which unimers start to aggregate is known as the critical micelle concentration (CMC).[92]

1.6.3 The packing parameter

As discussed above, amphiphilic molecules are capable of spontaneous self-assembly in aqueous solution (assuming the concentration of the amphiphilic molecule is greater than its CMC). Up to this point, only spherical micelles have been considered, but three-dimensional assemblies are not limited to this single geometry (others include worms, vesicles, lamellae, etc.). The final morphology of self-assemblies is related to the packing of the amphiphilic molecules. The two major forces that govern self-assembly of surfactants in aqueous solution are the repulsion between neighbouring hydrophilic head-groups (caused by steric hindrance and

preference for interaction with water), and the attraction of the hydrophobic chains at the hydrocarbon-water interface (i.e., opposing forces).[92] Both of these interactions have an effect on the surface area occupied per head-group (*a*). Typically, the positive interfacial energy per unit area, γ, for a hydrocarbon-water interface is approximately 50 mJ m^{-2} (this value is sensitive to the length of the hydrocarbon chain). However, γ is likely to be lower for aggregated amphiphilic molecules because of head-group repulsion. Therefore the interfacial free energy of a molecule in an aggregate can be written as:

$$\mu_N^o = \gamma a + \frac{K}{a} \qquad (1.20)$$

where K is a constant. If it is assumed that the repulsive and attractive forces are operating in the same plane, then the point minimum energy is given by $d\mu°_N / da = 0$. This expression gives the optimal head-group area, a_0. However, this is a rather crude approximation, as specific head-group interactions and the effect of interfacial curvature on $\mu°_N$ are neglected. Nevertheless, this a_0 value still provides useful insights for the self-assembly of amphiphilic molecules. The geometry also depends on the volume of the hydrocarbon chain, *v*, and the maximum effective chain length or critical chain length, l_c, which gives the dimensionless packing parameter, *p*:[92]

$$p = \frac{v}{a_0 l_c} \qquad (1.21)$$

Figure 1.12 indicates how the packing parameter affects the morphology of the aggregates formed by an amphiphilic surfactant molecule. Some of the more common geometries/morphologies are illustrated with their respective packing parameters, including spheres ($p < 1/3$), cylindrical micelles or worms (where $1/3 < p < 1/2$) and vesicles ($p > 1/2$).[92,93]

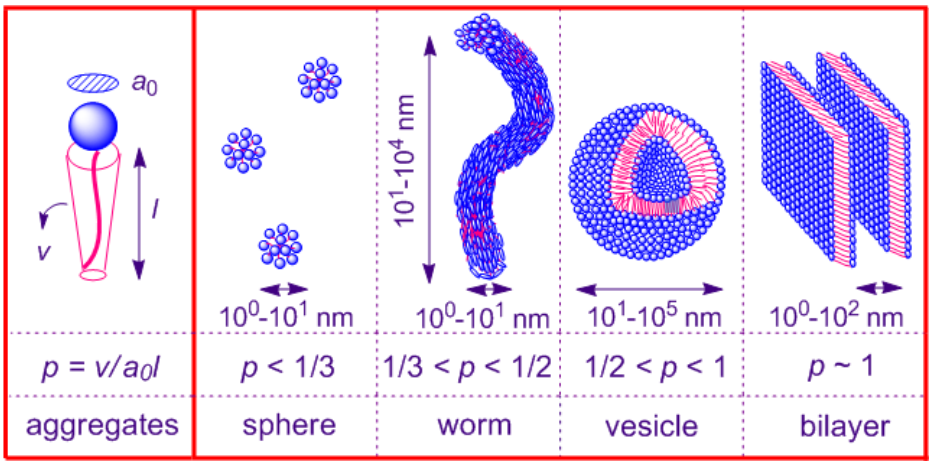

Figure 1.12 Graphical illustration of the relationship between the packing parameter, *p*, and the morphology adopted by surfactant aggregates.[93]

1.6.4 Self-assembly of diblock copolymers

The spontaneous self-assembly of molecules is not limited to surfactants. Since the advent of controlled/living polymerisation, a large variety of well-defined AB diblock copolymers have been prepared. Such diblock copolymers can self-assemble in the bulk (i.e., no solvent) or in a solvent that is selective for one block. First we shall consider the self-assembly diblock copolymers in bulk. An AB diblock copolymer comprising two distinctively different blocks can undergo microphase separation below a specific temperature (known as the order-disorder temperature) into various morphologies.[94-97] It is essential that the A and B blocks are covalently bound together; otherwise macrophase separation would be observed rather than microphase separation. For spontaneous self-assembly to take place the Gibbs energy of mixing (ΔG_{mix}) must be positive, see equation **1.22**. Diblock copolymer self-assembly in the bulk is driven by an unfavourable mixing enthalpy (ΔH_{mix}) with a small mixing entropy (ΔS_{mix}).

$$\Delta \mathbf{G_{mix}} = \Delta \mathbf{H_{mix}} - \mathbf{T}\Delta \mathbf{S_{mix}} \qquad (\mathbf{1.22})$$

The extent of microphase separation for diblock copolymers in the solid state depends on three factors:[94] (i) the volume fraction of the A and B blocks (denoted as

f_A and f_B respectively, (ii) the total degree polymerisation of the diblock copolymer (N) and (iii) the temperature dependent Flory-Huggins parameter (χ_{AB}), which describes the incompatibility of components A and B and is given by:

$$\boldsymbol{\chi_{AB} = \left(\frac{z}{k_B T}\right)\left[\varepsilon_{AB} - \frac{1}{2}(\varepsilon_{AA} + \varepsilon_{BB})\right]} \qquad \textbf{(1.23)}$$

Here z is the number of nearest neighbours per molecule, k_BT is the thermal energy and ε_{AB}, ε_{AA} and ε_{BB} are the respective interaction energies between repeat units. From equation **1.23** it is observed that if the A-B interaction energy is greater than the A-A and B-B interactions [i.e., $\varepsilon_{AB} > 1/2\ (\varepsilon_{AA} + \varepsilon_{BB})$], then χ_{AB} will be negative and mixing is preferred. Therefore the A-B interaction energy must be lower than that of A-A and B-B (i.e., $\chi_{AB} > 0$) to drive microphase separation. The degree of microphase separation of diblock copolymers is determined by the segregation product (χN). For lower χN (often from increasing temperature), the compatibility between the two blocks increases and mixing is preferred to microphase separation.

Several theories (e.g., self-consistent mean-field) have been used to predict the phase separation behaviour of block copolymers in the bulk.[98-101] These are now in good agreement with experimental findings (see **Figure 1.13**).[94,96,102] At high χN ($\chi N > 100$), segregation between blocks is sufficiently strong that the domains are nearly pure. This is known as the strong segregation limit. In contrast, if $\chi N < 10$, segregation is incomplete and is close to the order-disorder transition. This is known as the weak segregation limit. At χN values above this critical value, order-order transitions from body-centred cubic spheres to hexagonally-packed cylinders to bicontinuous gyroid to lamellae are observed on increasing the volume fraction of one block up to 0.5 (see **Figure 1.13**).[96]

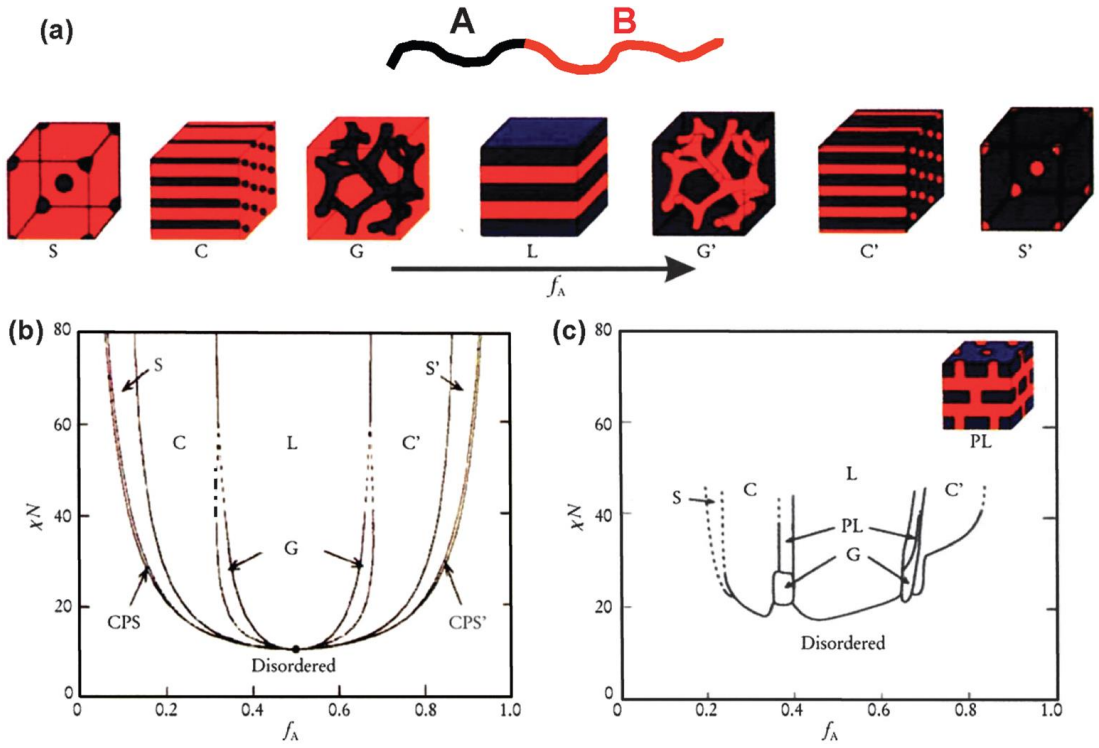

Figure 1.13 (a) Graphical illustrations of various morphologies of AB diblock copolymer melts with an increasing volume fraction of component A (f_A). Where S and S' are body-centred-cubic spheres, C and C' are hexagonally-packed cyclinders, G and G' are gyroid and L is lamellae. (b) Theoretical phase diagram of AB diblock copolymer melts depending on f_A and the segregation product (χN) predicted by self-consistent mean-field theory. (c) Experimental phase diagram constructed for polyisopropene-polystyrene diblock copolymers where polysiopropene is the A block and PL represents a perforated lamella phase.[96,102]

The addition of a solvent to a diblock copolymer increases the complexity of its self-assembly behaviour, as interactions between polymer and solvent must now be taken into account.[95,103,104] Nevertheless, amphiphilic diblock copolymers (i.e., where one block is hydrophilic and the other is hydrophobic) undergo spontaneous self-assembly in aqueous solution to form various morphologies.[105-109] Such systems can be viewed as being analogous to the small molecule surfactants discussed earlier. Similarly, the packing parameter still holds for diblock copolymers in a selective solvent (see **Figure 1.14**).[110] However, block copolymers typically exhibit much lower CMCs compared to surfactants. For example, CMCs determined for polystyrene-poly(acrylic acid) (PS-PAA) diblock copolymers are approximately 5-6 orders of magnitude lower than that of SDS.[111,112] Furthermore, block copolymer

aggregates are significantly more stable as the exchange between unimers and aggregates is much slower than for surfactant aggregates.[95]

Traditionally, diblock copolymer self-assembly is achieved by post-polymerisation techniques such as direct dissolution,[113] solvent switching,[106,114,115] pH switching[116] or thin film rehydration.[117,118] Such processes are usually conducted in dilute solutions (e.g., < 1 % w/w copolymer). However, the recent development of polymerisation-induced self-assembly (PISA) allows the direct preparation of many complex copolymer morphologies in concentrated solution (> 10 % w/w copolymer). This approach is discussed in detail in **section 1.7** below.

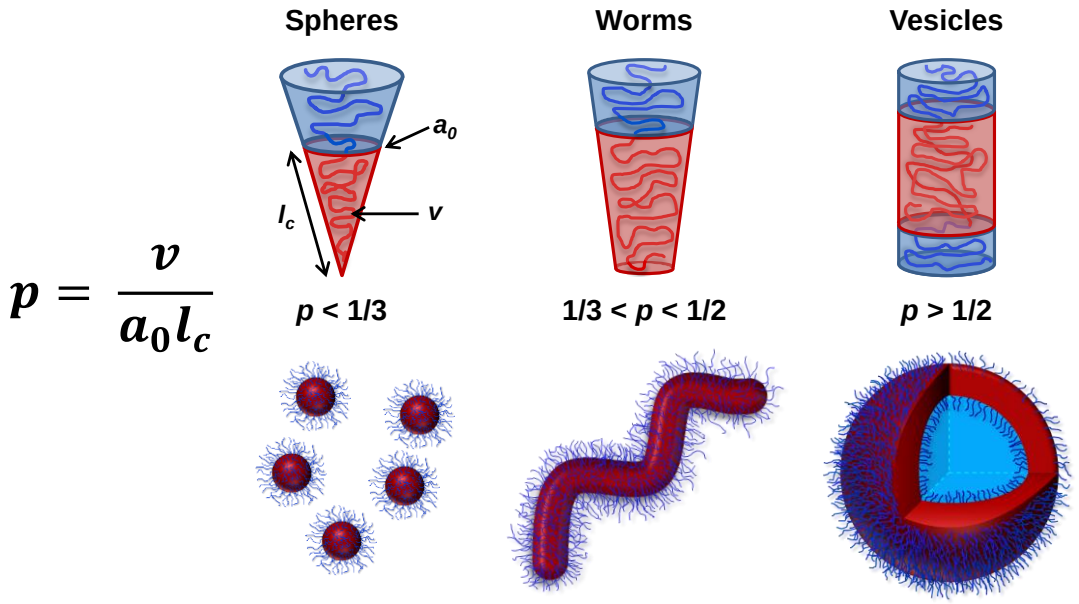

Figure 1.14 Graphical illustration of how the dimensionless packing parameter, *p*, is related to the morphology of a diblock copolymer in selective solvent.

1.7 Polymerisation-Induced Self-Assembly (PISA)

Over the past 10 years, there has been increasing interest in preparing self-assembled diblock copolymer nano-objects *in situ* by utilising heterogeneous polymerisation using PISA.[119] Typically, a soluble homopolymer is chain-extended with a second monomer that, when polymerised, forms an insoluble core-forming

block, hence driving *in situ* self-assembly to form sterically-stabilised nanoparticles (see **Figure 1.15**). PISA enables the direct 'one-pot' preparation of nanoparticles rather than the multiple steps normally required using post-polymerisation processing. Furthermore, PISA has been successfully conducted at high copolymer concentrations (> 30 % w/w).[120-122] In principle, PISA can be conducted using any living radical polymerisation technique.[119,123-129] However, the majority of PISA papers utilise RAFT polymerisation. Most relevant to the work described in this thesis is PISA *via* RAFT aqueous emulsion polymerisation (where the second monomer is *water-immiscible*) and PISA by RAFT aqueous dispersion polymerisation (where the second monomer is *water-miscible*). These formulations will be discussed in more detail in **sections 1.7.1** and **1.7.2**, respectively. It is noteworthy that PISA is not limited to water; it has been reported for other polar solvents[130-134] (such as methanol and ethanol), non-polar solvents,[134-136] and more recently ionic liquids[137]. However, such PISA formulations are beyond the scope of this thesis and will not be discussed further.

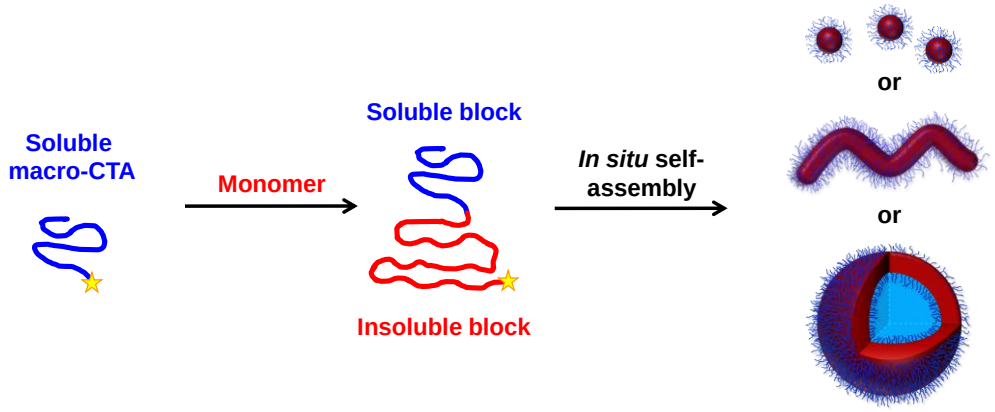

Figure 1.15 Graphical representation of the *in situ* formation of nanoparticles by polymerisation-induced self-assembly (PISA). A soluble macro-CTA is chain-extended in a suitable solvent with a monomer that when polymerised, becomes insoluble. This drives *in situ* self-assembly to form a wide range of sterically-stabilised nano-objects (spheres, worms or vesicles).

1.7.1 PISA by RAFT aqueous emulsion polymerisation

Initial attempts to utilise RAFT chemistry in *conventional* aqueous emulsion polymerisation suffered from several problems, such as colloidal instability and poor

molecular weight control.[138,139] One possible explanation was suggested to be poor transfer of the RAFT agent across the aqueous phase.[140] Hawkett and co-workers addressed these problems by chain-extending a short PAA macromolecular chain transfer agent (macro-CTA) by RAFT aqueous emulsion polymerisation (in the absence of a surfactant) using a slow feed of *n*-butyl acrylate (BA).[141] The diblock copolymer self-assembled *in situ* to form nano-objects of 60 nm diameter, in a surfactant-free technique now known as PISA. THF gel permeation chromatography (GPC) studies of this polymerisation indicated a linear evolution of molecular weight with conversion (see diamond data set in **Figure 1.16**). However, as the reaction proceeded some loss of control over the polymerisation was observed (M_w/M_n > 1.40), with the appearance of a high molecular weight shoulder (see **Figure 1.16**). The same group further developed this formulation by preparing ABC triblock copolymer nanoparticles where the B and C blocks were either PS or PBA.[142,143]

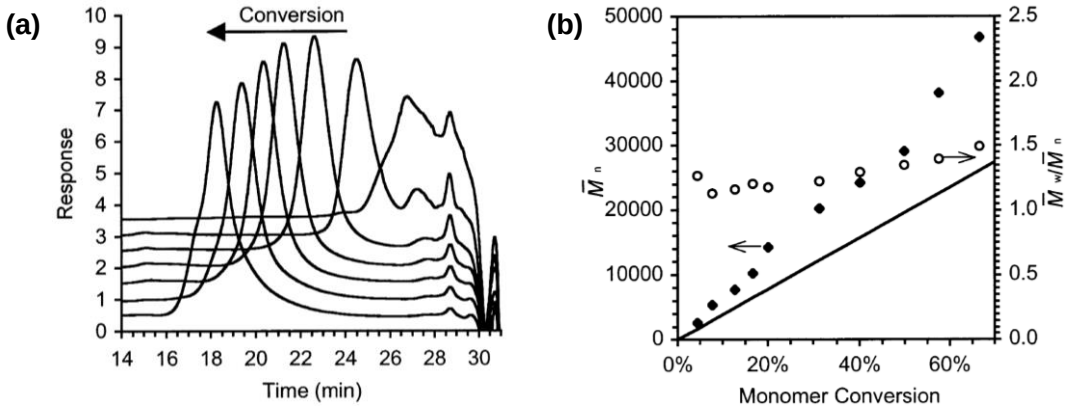

Figure 1.16 (a) THF GPC traces obtained during chain extension of a PAA macro-CTA with BA and (b) molecular weight (diamonds) and polydispersity (circles) data versus polystyrene standards for the same RAFT polymerisation. Note that the solid black line indicates theoretical molecular weight.[141]

Since these initial reports, several other research groups have explored the preparation of diblock copolymer nano-objects using PISA by RAFT aqueous emulsion polymerisation.[121,144-157] In particular, Charleux and co-workers have worked extensively in this area.[144-154] Their first report in this field was the chain-extension of a protonated poly(2-(diethylamino)ethyl methacrylate) (PDEA) macro-CTA (synthesised by RAFT solution polymerisation in ethanol) with styrene to

prepare diblock copolymer spheres.[144] However, it was initially thought that the amphiphilic block copolymers would stabilise conventional latex particles. Hence no attention was paid to the polydispersity of the resulting copolymer. Following this initial report, Charleux *et al*. prepared a PEO macro-CTA by esterification of a monohydroxyl PEO with a carboxylic acid-functionalised RAFT agent.[151] This was subsequently chain-extended with either styrene or BA by RAFT aqueous emulsion polymerisation to yield well-defined block copolymers ($M_w/M_n \approx 1.20$), which self-assembled to form nanoparticles of up to 500 nm in diameter. Since then, the same research team has have utilised several types of stabiliser blocks (e.g., methacrylates,[144-149] PEO,[150,151] acrylates[152,153] and acrylamides[154]) and core-forming blocks (e.g., styrene,[146-149,151-153] acrylates[146,150,151,154] and methacrylates[145,146,150]) to prepare diblock copolymer nano-objects by RAFT aqueous emulsion polymerisation. By optimising reaction conditions, it was demonstrated that diblock copolymers possessing narrow molecular weight distributions ($M_w/M_n < 1.30$) can be obtained with high monomer conversions (> 95 %). Moreover, sequential monomer addition enables the one-pot synthesis of diblock copolymer nano-objects in water.[146-148]

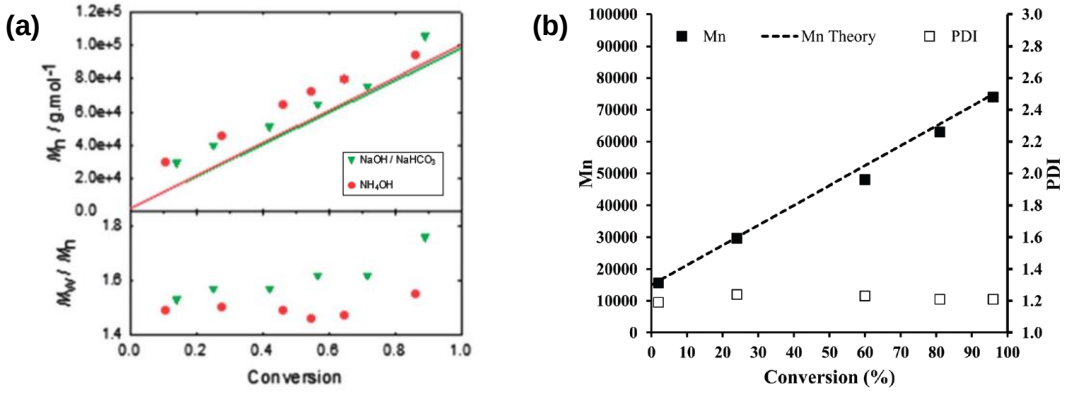

Figure 1.17 Evolution of M_n and polydispersity (M_w/M_n or PDI) during the synthesis of: (a) PAA-PBA[155] and (b) P(PEOA-*stat*-HEAA)-PS[156] diblock copolymer spheres prepared by PISA *via* RAFT aqueous emulsion polymerisation.

In closely related research, Rieger *et al.* chain-extended a PAA macro-CTA using BA by RAFT aqueous emulsion polymerisation to prepare high molecular weight PAA-PBA spheres using PISA ($M_n \approx 100$ kg mol^{-1} by THF GPC).[155] However, these reactions were poorly controlled with M_w/M_n values typically greater

than 1.50 (see **Figure 1.17a**). Similarly, Davis and co-workers prepared high molecular diblock copolymer spheres ($M_n \approx 70$ kg mol^{-1} by dimethyl acetamide GPC) by PISA.[156] More specifically, a poly(*N*-hydroxyethyl acrylamide)-*stat*-poly((ethylene oxide) methyl ether acrylate) or P(PEOA-*stat*-HEAA) macro-CTA was chain-extended with styrene using RAFT aqueous emulsion polymerisation. In contrast to the previous example, these diblock copolymer chains possessed narrow molecular weight distributions ($M_w/M_n \approx 1.20$), see **Figure 1.17b**. Moreover, by increasing the styrene concentration in the formulation, diblock copolymers with molecular weights upto 1,000 kg mol^{-1} were prepared possessing a relatively low polydispersity of 1.39.

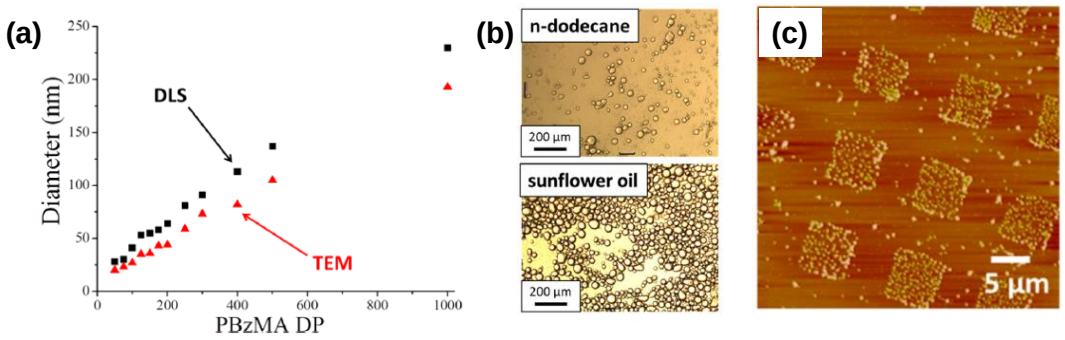

Figure 1.18 (a) Linear relationship between mean particle diameter and PBzMA DP for a series of $PGMA_{51}$-$PBzMA_x$ spheres, as measured by TEM and DLS. (b) Optical microscopy images obtained for oil-in-water emulsions formed using $PGMA_{51}$-$PBzMA_{100}$ spheres as Pickering emulsifiers. (c) AFM images of $PGMA_{51}$-$PBzMA_{100}$ nanoparticles adsorbed onto the surface of a micropatterened phenylboronic acid-functionalised silicon wafer.[121]

In related work, Cunningham and co-workers prepared a series of poly(gylcerol monomethacrylate)-poly(benzyl methacrylate) (PGMA-PBzMA) spheres by PISA *via* RAFT aqueous emulsion polymerisation.[121] The mean sphere diameter increased monotonically from 20 to 200 nm when targeting higher PBzMA DPs, as judged by dynamic light scattering (DLS) and transmission electron microscopy (TEM) (see **Figure 1.18a**). Such nanoparticles were also shown to act as efficient oil-in-water Pickering emulsifiers for several oils (see **Figure 1.18b**). Furthermore, the cis-diol moiety on the PGMA stabiliser enabled pH-modulated nanoparticle adsorption to be demonstrated on a selectively patterned planar surface

using boronic acid chemistry. This could be imaged using atomic force microscopy (AFM) (see **Figure 1.18c**). More recently, D'Agosto utilised an alkoxyamine-functionalised trithiocarbonate CTA to prepare a PAA macro-CTA by RAFT solution polymerisation in dioxane.[157] This was then chain-extended with styrene by RAFT aqueous emulsion polymerisation to form alkoxyamine-decorated spherical latexes.

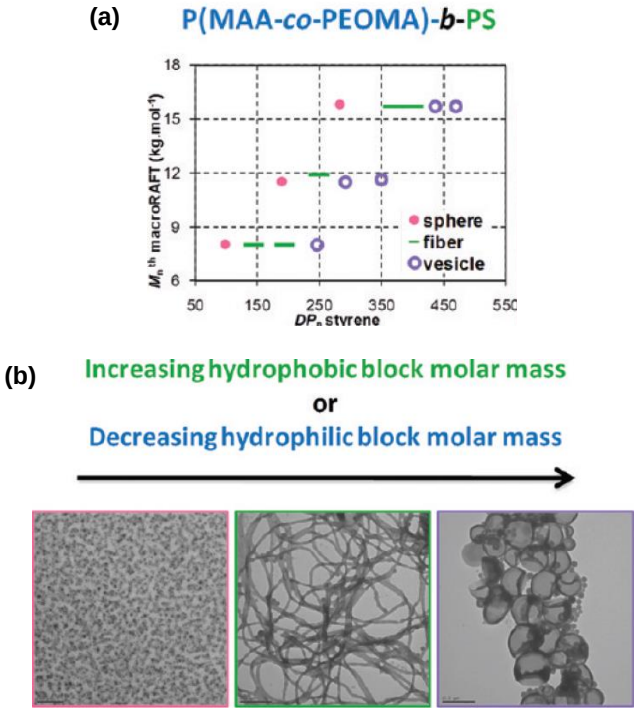

Figure 1.19 (a) Predictive phase diagram for the PISA synthesis of P(MAA-co-PEOMA)-PS diblock copolymer nano-objects *via* RAFT aqueous emulsion polymerisation, where the molar mass of the stabiliser and core-forming blocks are systematically varied. (b) TEM images of P(MAA-co-PEOMA)-PS diblock copolymer spheres, worms and vesicles.[147]

Unlike conventional emulsion polymerisation, RAFT aqueous emulsion polymerisation enables the preparation of so-called higher order copolymer morphologies such as worms (or fibers) and vesicles.[147,152,153,158] For example, Charleux and co-workers reported that spheres, worms or vesicles could be prepared when styrene was polymerised in the presence of a hydrophilic poly(methacrylic acid-*co*-poly(ethylene oxide) methyl ether methacrylate) or P(MAA-*co*-PEOMA) macro-CTA.[147] By increasing the molar mass/DP of the hydrophobic block (PS) or

reducing the molar mass/DP of the hydrophilic block resulted in the formation of higher order morphologies (see **Figure 1.19**). However, most RAFT aqueous emulsion polymerisation formulations yield only kinetically trapped spheres.[121,146,148,150,154-157] This problem is still not fully understood. Conversely, PISA by RAFT *aqueous dispersion* polymerisation is a much more reliable method for the synthesis of higher order morphologies, which is discussed in **section 1.7.2**.

1.7.2 PISA by RAFT aqueous dispersion polymerisation

As previously discussed above, RAFT aqueous dispersion polymerisations comprise initially homogeneous solutions, since the macro-CTA, monomer (and initiator) are all water-soluble. However, the monomer polymerises to form a water-insoluble polymer and, at a critical point during the reaction, the diblock copolymer undergoes self-assembly. The soluble block acts as a steric stabiliser and prevents macroscopic precipitation. In practise, only a very few monomers fulfil the criterion for aqueous dispersion polymerisation, some of which will discussed below. Recently, there have been two excellent review articles in this area.[128,159]

The first example of RAFT aqueous dispersion polymerisation was conducted in 2007 by Hawker and co-workers.[160] A poly(*N*,*N*′-dimethylacrylamide) (PDMAAM) macro-CTA was chain-extended with *N*-isopropylacrylamide (NIPAM) to prepare spherical nanoparticles at 70 °C (see **Figure 1.20**). However, when these particles were cooled to room temperature dissolution took place. This is because the PNPAM core possesses a lower critical solution temperature (LCST) of 32 °C. Therefore these particles were cross-linked using bisacrylamide to prepare nanogels, which are colloidally stable at room temperature. Furthermore, zeta potential measurements indicated that the nano-objects exhibited anionic charge due to the carboxylic acid functional CTA employed for the RAFT synthesis. Similarly, Charleux *et al.* prepared thermo-responsive micelles by polymerising *N*,*N*-diethylacrylamide (DEAAM) in the presence of a PEO macro-CTA.[161,162] Again, addition of a bisacrylamide cross-linker was required to produce colloidally stable particles at room temperature, as the PDEAAM core-forming block exhibited an LCST of approximately 32 °C.

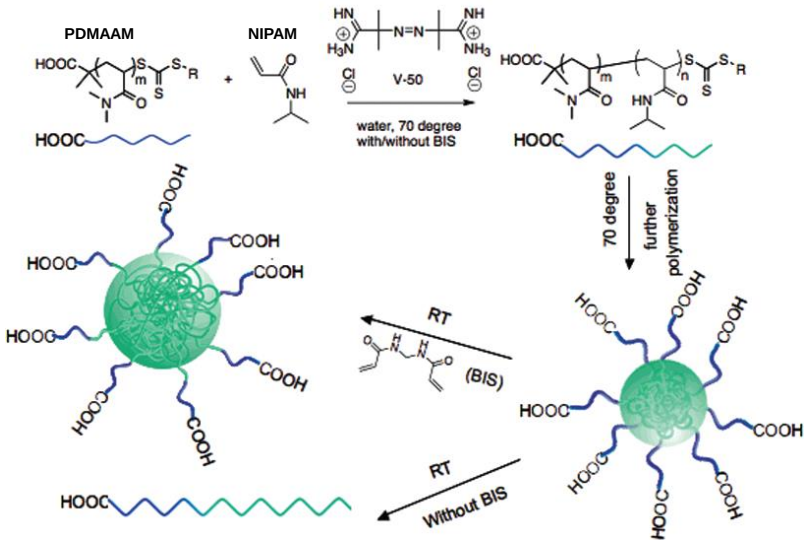

Figure 1.20 Schematic representation of the chain-extension of a PDMAAM macro-CTA with NIPAM by RAFT aqueous dispersion polymerisation, and the subsequent cross-linking to obtain spherical nano-objects.[160]

An *et al.* have published several PISA studies using RAFT aqueous dispersion polymerisation.[122,163-165] For example, a PEO-based macro-CTA was chain-extended with a mixture of di(ethylene glycol) methyl ether methacrylate (MEO_2MA), PEOMA and poly(ethylene glycol) dimethacrylate (PEGDMA) cross-linker to produce nanogels in water (**Figure 1.21**).[163] It was also demonstrated that the nanogel dimensions could be reduced by either increasing stabiliser block DP, lowering the core-forming block DP or reducing the solids concentration. Furthermore, such nanoparticles demonstrated excellent biocompatibility owing to their high ethylene glycol content.

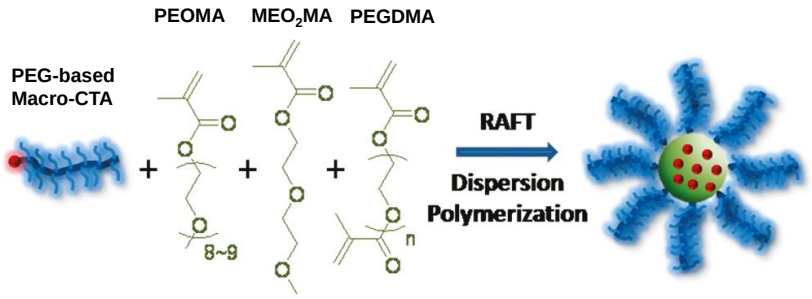

Figure 1.21 Schematic illustration of the statistical copolymerisation of a PEG-based macro-CTA with PEOMA, MEO_2MA and PEGDMA using a RAFT aqueous dispersion polymerisation formulation.[163]

An and co-workers also synthesised diblock copolymer spheres by copolymerising a PPEOMA macro-CTA with 2-methoxyethyl acrylate (MEA) by RAFT aqueous dispersion polymerisation.[122] Such nanoparticles could be prepared at high solid concentrations (up to 32 % w/v) and possessed relatively narrow size distributions, as judged by DLS. Very recently, the team prepared poly(*N*,*N*-dimethylacrylamide)-poly(diacetone acrylamide) (PDMAAM-PDAAM) diblock copolymers using RAFT aqueous dispersion polymerisation at 10-20 % solids.[165] Such copolymers possessed narrow molecular weight distributions (M_w/M_n typically lower than 1.20) and self-assembled to form either spheres or vesicles depending on the DP of the core-forming block DP (**Figure 1.22**). Moreover, the ketone group on the PDAAM block enabled the particle cores to be functionalised.

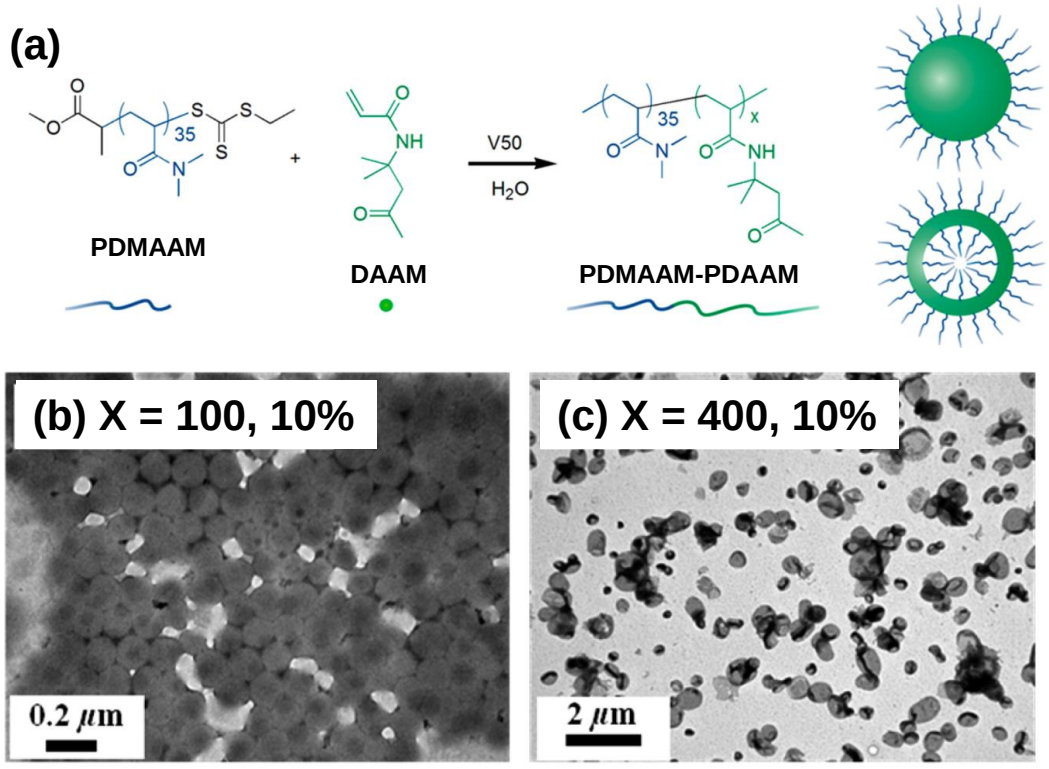

Figure 1.22 (a) Schematic illustration of the chain extension of a PDMAAM macro-CTA with DAAM by PISA *via* RAFT aqueous dispersion polymerisation. TEM images obtained for (b) $PDMAAM_{35}$-$PDAAM_{100}$ spheres and (c) $PDMAAM_{35}$-$PDAAM_{100}$ vesicles.[165]

Armes and co-workers have worked extensively on PISA syntheses over the past 6 years or so.[166-177] Their first example was the chain extension of a $PGMA_{65}$

macro-CTA with varying amounts of HPMA by PISA *via* RAFT aqueous dispersion polymerisation at 70 °C and 10 % w/w solids (**Figure 1.23**).[166] According to DLS studies, the particle diameter increased when targeting longer PHPMA core-forming block DPs. Furthermore, synthesis of a $PGMA_{65}$-$PHPMA_{300}$ diblock copolymer at 20 % w/w solids led to the formation of polydisperse vesicles, rather than spheres. However, relatively large amounts of unreacted macro-CTA were observed by DMF GPC, and high polydispersities were obtained (M_w/M_n > 1.50) due to high dimethacrylate impurities in the HPMA monomer.

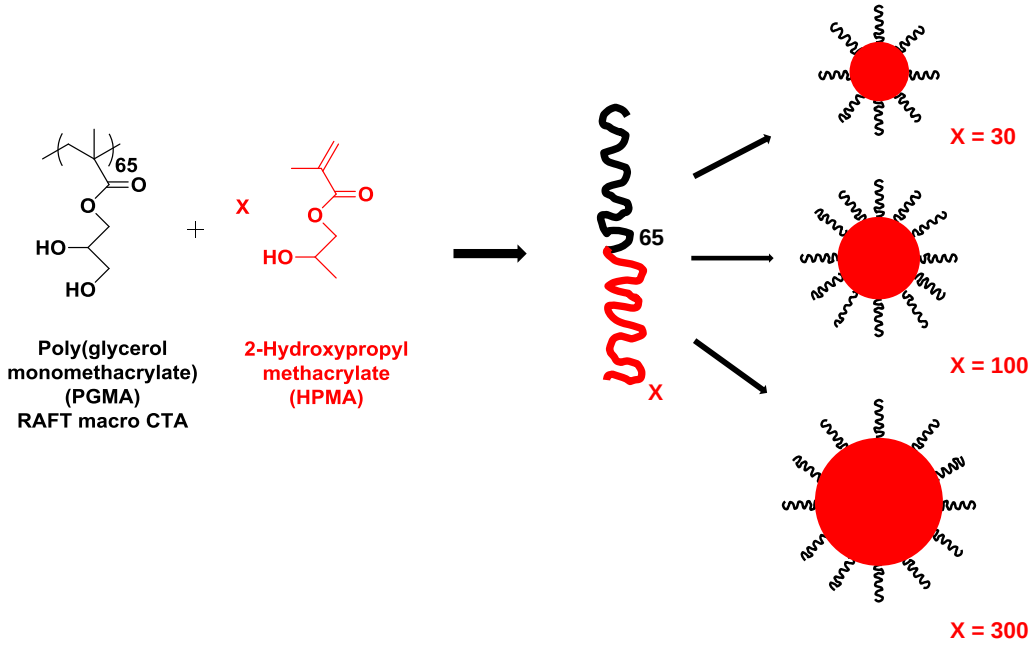

Figure 1.23 Schematic representation of the chain extension of a PGMA macro-CTA *via* RAFT aqueous dispersion polymerisation of HPMA to form spheres.[166]

Monitoring the formation of $PGMA_{47}$-$PHPMA_{200}$ diblock copolymer vesicles by ^{1}H NMR and TEM led to some rather fascinating insights regarding the PISA mechanism.[167] Firstly, a significant increase in the rate of polymerisation was observed by ^{1}H NMR at the same time point corresponding to micellar nucleation, as judged by TEM (**Figure 1.24a**). It was suggested that unreacted HPMA monomer migrates into the core of the nascent growing particles, increasing the local concentration and thus the rate of polymerisation. As the PHPMA block continued to grow, the copolymer morphology changed from spheres to worms to branched

worms to 'jellyfish' and finally to vesicles (**Figure 1.24b**). This morphology evolution can be rationalised in terms of the packing parameter, because the PHPMA block DP increases during the polymerisation while the PGMA DP remains constant. Therefore the packing parameter gradually increases as the polymerisation proceeds.

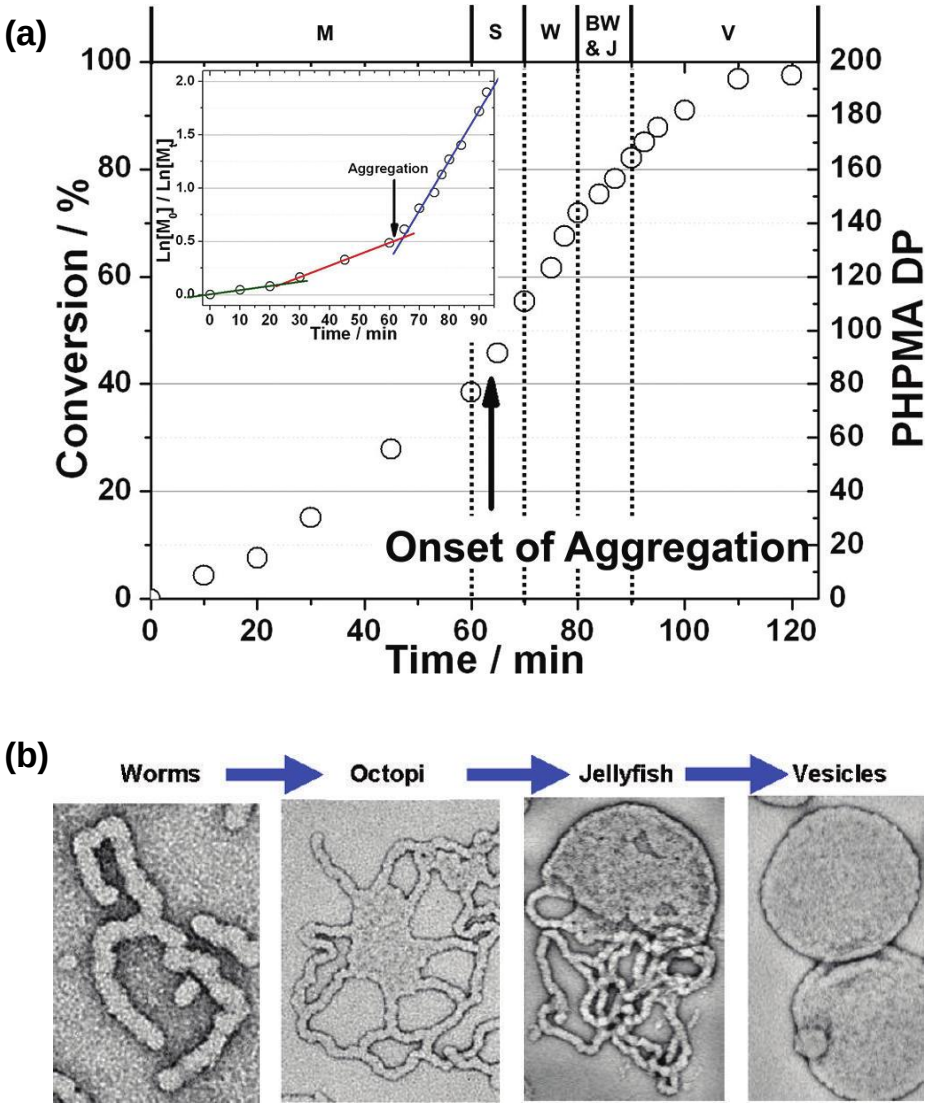

Figure 1.24 (a) ^{1}H NMR kinetics of the chain extension of a $PGMA_{47}$ macro-CTA with 200 units of HPMA by RAFT aqueous dispersion polymerisation. The kinetic data comprise five distinct regimes where M represents molecularly dissolved chains, S represents spheres, W represents worms, BW represents branches worms, J represents jellyfish and V represents vesicles. The inset semi-logarithmic plot indicates the change in rate during the reaction. (b) TEM images obtained during the synthesis of $PGMA_{47}$-$PHPMA_{200}$ diblock copolymers illustrating the morphology transition from worms to vesicles.[167]

Detailed phase diagrams have been constructed by chain-extending three different PGMA macro-CTA DPs, with differing target PHPMA DPs and variable copolymer concentrations.[168] Post mortem TEM analysis was used to assign the final morphology for each formulation (see **Figure 1.25a-c**). The final morphology depended on three factors: (i) the DP of the PGMA stabiliser block, (ii) the DP of the PHPMA core-forming block and (iii) the overall concentration. By fixing the overall copolymer concentration at 20 % w/w solids, a master phase diagram has been constructed that allows for the reproducible synthesis of a desired morphology (**Figure 1.25d**).[178] It is noteworthy that when the PGMA block DP is approximately 40-60, there is essentially no concentration dependence for the copolymer morphology.

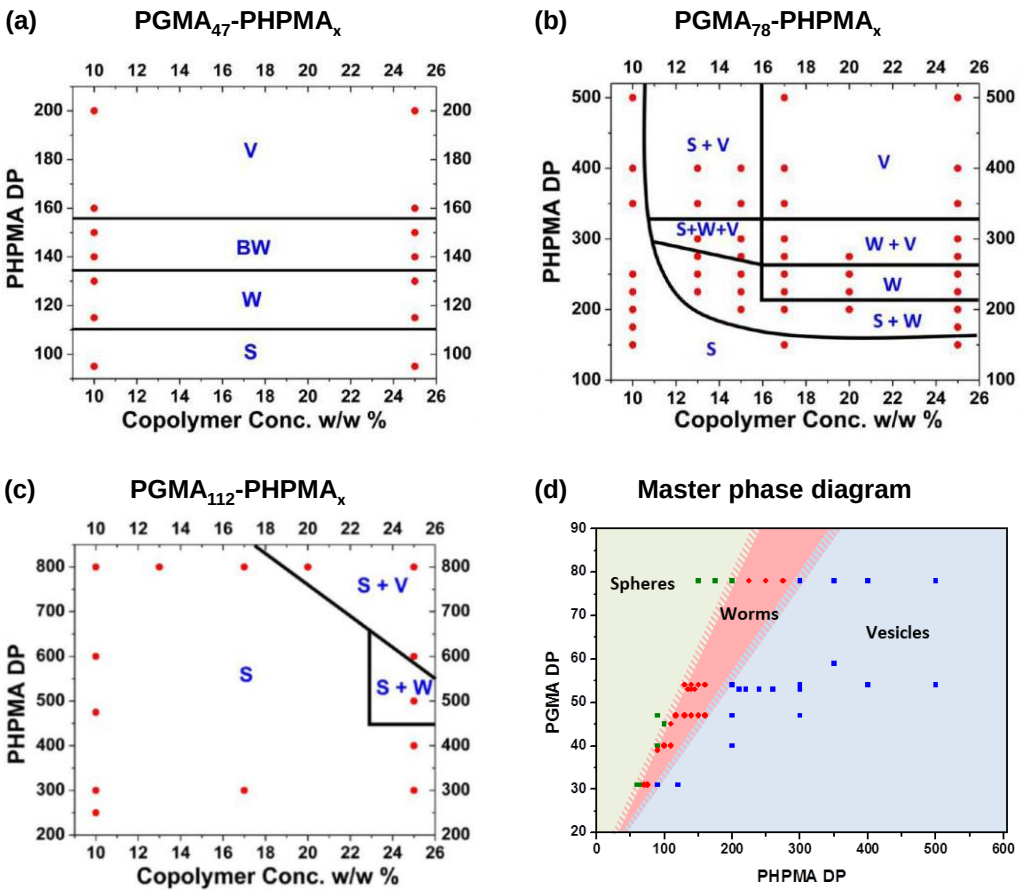

Figure 1.25 Phase diagrams constructed for PGMA-PHPMA diblock copolymers at various copolymer concentrations and PHPMA DPs when the PGMA macro-CTA DP is (a) 47, (b) 78 and (c) 112. (d) A master phase diagram of PGMA DP versus PHPMA DP at a fixed copolymer concentration of 20 % w/w solids.[168,178]

Since the first report by Li and Armes, the PGMA-PHPMA formulation has been optimised, leading to relatively narrow molecular-weight distributions (M_w/M_n < 1.20) and high blocking efficiencies.[168] This was developed further by Ratcliffe *et al.* to produce a convenient one-pot formulation.[169] More specifically, glycidyl methacrylate (GlyMA), a cheap water-immiscible monomer, was converted to the expensive speciality monomer GMA by an epoxide ring-opening reaction conducted in water.[169] This GMA was subsequently polymerised in the presence of a RAFT agent to prepare a PGMA macro-CTA, which was then chain-extended with HPMA to form either spheres, worms or vesicles, depending on the targeted PHPMA DP.

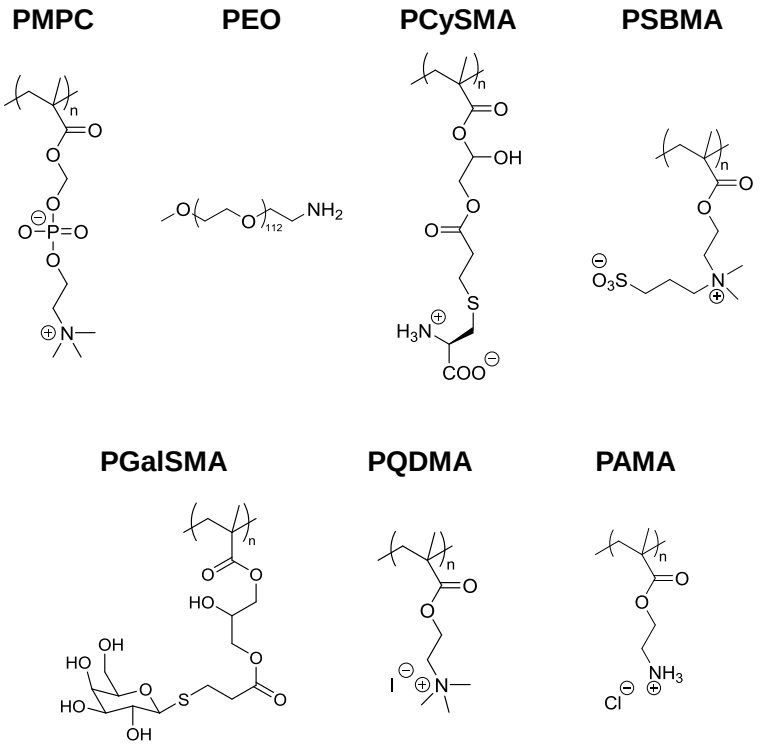

Figure 1.26 Chemical structures for various steric stabiliser blocks used by Armes and co-workers in the chain extension of HPMA by RAFT aqueous dispersion polymerisation.[170-176]

More recently, Armes and co-workers have reported the chain extension of several other water-soluble macro-CTAs (see **Figure 1.26**) with HPMA to prepare various copolymer morphologies. These include poly(2-(methacryloyloxy) ethylphosphorylcholine) (PMPC),[170] PEO,[171] poly(L-cysteine-based methacrylate) (PCysMA),[172] poly(2-(methacryloyloxy)ethyl dimethyl-(3-sulfopropyl) ammonium

hydroxide) (PSBMA)[173]. Furthermore, the same team has also investigated block copolymerising HPMA with binary mixtures of PGMA and other macro-CTAs (such as poly(galactose methacrylate) (PGalSMA),[174] poly(quaternized 2-(dimethylamino) ethyl methacrylate) (PQDMA)[175] or poly(2-aminoethyl methacrylate) (PAMA)[176]) to prepare spheres, worms or vesicles. In the case of polyelectrolyte stabilisers, it is usually necessary to add a non-ionic macro-CTA to the formulation in order to obtain higher order morphologies. Otherwise, the morphology is limited to spherical nanoparticles due to strong lateral electrostatic repulsion between the adjacent stabiliser blocks in the coronal layer.[177]

More recently, Sumerlin *et al*. were also able to prepare spheres, worms or vesicles by chain-extending a PDMAAM-PAA-based macro-CTA with NIPAM.[179] However, like early research in this field, these nano-objects had to be cross-linked to obtain colloidally stable nanoparticles at room temperature. In this case a diamine is reacted with the carboxylic acid from the AA residues in the presence of a carbodiimide. Sugihara and co-workers were able to prepare various PEO-MEA diblock copolymer nano-objects by PISA *via* RAFT aqueous dispersion polymerisation.[180] Cai and co-workers reported the chain extension of a water-soluble poly(2-hydroxypropyl methacrylamide) (PHPMAM) macro-CTA with DAAM and a small amount of AMA comonomer to form spheres.[181] The NH_3^+ groups on the AMA units in the core-forming block were reacted with pyridine-2,6-dicarboxaldehyde, which enabled coordination to zinc(II).

1.8 Thesis Outline

This thesis focuses on the preparation of well-defined stimuli-responsive PGMA-PHPMA based diblock copolymer nano-objects by PISA *via* RAFT aqueous dispersion polymerisation. Chapter 2 describes the synthesis of pH-responsive PGMA-PHPMA worm gels by utilising an acid-functionalised RAFT agent. Ionisation of the terminal carboxylic acid end-group, derived from the CTA, induces a worm-to-sphere order-order transition and hence degelation. In Chapter 3, this approach is extended to prepare a series of PGMA-PHPMA vesicles possessing a terminal carboxylic acid on each PGMA stabiliser block. The effect of the PHPMA

core-forming block DP on the pH-responsive nature of these vesicular particles is explored. Furthermore, their thermo-responsive and hence dual stimuli-responsive (i.e., pH and temperature) behaviour is also investigated. In Chapter 4 varying amounts of 2-diisopropylaminoethyl methacrylate (DPA) are statistically copolymerised with HPMA to yield three series of PGMA-P(HPMA-DPA) diblock copolymer worms, vesicles and spheres. Unlike in Chapters 2 and 3, the pH-responsive moiety is now located within the core, rather than at the periphery of the nano-objects. Similarly, the pH-responsive nature of these nanoparticles is explored. Finally, in Chapter 5 anisotropic worms prepared by PISA are covalently cross-linked *via* post-polymerisation reaction with 3-aminopropyl triethoxysilane (APTES). Here, a PGMA macro-CTA is chain-extended with varying amounts of HPMA and GlyMA to prepare a series of worms. The epoxide groups on the GlyMA react with ATPES, which cross-links the worm cores by hydrolysis-condensation reactions. Their rheological properties and resistance to ionic surfactant or methanol are investigated before and after worm cross-linking.

1.9 References

(1) Braconnot, H.; Braconnot *Ann. Chim., Phys.* **1833**, *52*, 290.

(2) Staudinger, H. *Berichte der deutschen chemischen Gesellschaft (A and B Series)* **1920**, *53*, 1073.

(3) Carothers, W. H. *J. Am. Chem. Soc.* **1929**, *51*, 2548.

(4) Flory, P. J. *Principles of Polymer Chemistry*; Cornell University Press: New York, **1953**.

(5) Cowie, J. M. G. *Polymers: Chemistry and Physics of Modern Materials*; Nelson Thornes: Cheltenham, **2002**.

(6) Odian, G. *Principles of Polymerization*; Fourth ed.; Wiley: Hoboken, **2004**.

(7) Matyjaszewski, K.; Gnanou, Y.; Leibler, L. *Macromolecular Engineering: Precise Synthesis, Materials Properties, Applications*; Wiley: Weinheim, **2007**; Vol. 1.

(8) Hiemenz, P. C.; Lodge, T. P. *Polymer Chemistry*; 2nd ed.; CRC Press: New York, **2007**.

(9) Braunecker, W. A.; Matyjaszewski, K. *Prog. Polym. Sci.* **2007**, *32*, 93.

(10) Szwarc, M.; Levy, M.; Milkovich, R. *J. Am. Chem. Soc.* **1956**, *78*, 2656.

(11) Webster, O. W. *Science* **1991**, *251*, 887.

(12) Miyamoto, M.; Sawamoto, M.; Higashimura, T. *Macromolecules* **1984**, *17*, 265.

(13) Dreyfuss, M. P.; Dreyfuss, P. *Polymer* **1965**, *6*, 93.

(14) Sawamoto, M. *Prog. Polym. Sci.* **1991**, *16*, 111.

(15) Faust, R.; Kennedy, J. P. *Polym. Bull.* **1986**, *15*, 317.

(16) Schrock, R. R. *Accounts Chem. Res.* **1990**, *23*, 158.

(17) Webster, O. W.; Hertler, W. R.; Sogah, D. Y.; Farnham, W. B.; Rajanbabu, T. V. *J. Am. Chem. Soc.* **1983**, *105*, 5706.

(18) Goto, A.; Fukuda, T. *Prog. Polym. Sci.* **2004**, *29*, 329.

(19) Otsu, T.; Yoshida, M. *Makromol. Chem., Rapid Commun.* **1982**, *3*, 127.

(20) Otsu, T.; Yoshida, M.; Tazaki, T. *Makromol. Chem., Rapid Commun.* **1982**, *3*, 133.

(21) Fischer, H. *Chem. Rev.* **2001**, *101*, 3581.

(22) Matyjaszewski, K. *Science* **2011**, *333*, 1104.

(23) Hawker, C. J.; Bosman, A. W.; Harth, E. *Chem. Rev.* **2001**, *101*, 3661.

(24) Moad, G.; Rizzardo, E.; Thang, S. H. *Accounts Chem. Res.* **2008**, *41*, 1133.

(25) Nicolas, J.; Guillaneuf, Y.; Lefay, C.; Bertin, D.; Gigmes, D.; Charleux, B. *Prog. Polym. Sci.* **2013**, *38*, 63.

(26) Benoit, D.; Chaplinski, V.; Braslau, R.; Hawker, C. J. *J. Am. Chem. Soc.* **1999**, *121*, 3904.

(27) Rizzardo, E.; Solomon, D. H. *Polym. Bull.* **1979**, *1*, 529.

(28) Georges, M. K.; Veregin, R. P. N.; Kazmaier, P. M.; Hamer, G. K. *Macromolecules* **1993**, *26*, 2987.

(29) Moad, G.; Rizzardo, E. *Macromolecules* **1995**, *28*, 8722.

(30) Guillaneuf, Y.; Gigmes, D.; Marque, S. R. A.; Astolfi, P.; Greci, L.; Tordo, P.; Bertin, D. *Macromolecules* **2007**, *40*, 3108.

(31) Detrembleur, C.; Jerome, C.; De Winter, J.; Gerbaux, P.; Clement, J. L.; Guillaneuf, Y.; Gigmes, D. *Polym. Chem.* **2014**, *5*, 335.

(32) Wang, J.-S.; Matyjaszewski, K. *J. Am. Chem. Soc.* **1995**, *117*, 5614.

(33) Kato, M.; Kamigaito, M.; Sawamoto, M.; Higashimura, T. *Macromolecules* **1995**, *28*, 1721.

(34) Coessens, V.; Pintauer, T.; Matyjaszewski, K. *Prog. Polym. Sci.* **2001**, *26*, 337.

(35) Matyjaszewski, K. *Macromolecules* **2012**, *45*, 4015.

(36) Tsarevsky, N. V.; Matyjaszewski, K. *Chem. Rev.* **2007**, *107*, 2270.

(37) di Lena, F.; Matyjaszewski, K. *Prog. Polym. Sci.* **2010**, *35*, 959.

(38) Matyjaszewski, K.; Patten, T. E.; Xia, J. *J. Am. Chem. Soc.* **1997**, *119*, 674.

(39) Gillies, M. B.; Matyjaszewski, K.; Norrby, P.-O.; Pintauer, T.; Poli, R.; Richard, P. *Macromolecules* **2003**, *36*, 8551.

(40) Tang, W.; Matyjaszewski, K. *Macromolecules* **2007**, *40*, 1858.

(41) Tang, W.; Kwak, Y.; Braunecker, W.; Tsarevsky, N. V.; Coote, M. L.; Matyjaszewski, K. *J. Am. Chem. Soc.* **2008**, *130*, 10702.

(42) Shipp, D. A.; Wang, J.-L.; Matyjaszewski, K. *Macromolecules* **1998**, *31*, 8005.

(43) Peng, C.-H.; Kong, J.; Seeliger, F.; Matyjaszewski, K. *Macromolecules* **2011**, *44*, 7546.

(44) Tang, W.; Matyjaszewski, K. *Macromolecules* **2006**, *39*, 4953.

(45) Pintauer, T.; Matyjaszewski, K. *Chem. Soc. Rev.* **2008**, *37*, 1087.

(46) Jakubowski, W.; Matyjaszewski, K. *Macromolecules* **2005**, *38*, 4139.

(47) Min, K.; Gao, H. F.; Matyjaszewski, K. *J. Am. Chem. Soc.* **2005**, *127*, 3825.

(48) Min, K.; Jakubowski, W.; Matyjaszewski, K. *Macromol. Rapid Commun.* **2006**, *27*, 594.

(49) Tang, H.; Radosz, M.; Shen, Y. *Macromol. Rapid Commun.* **2006**, *27*, 1127.

(50) Jakubowski, W.; Min, K.; Matyjaszewski, K. *Macromolecules* **2006**, *39*, 39.

(51) Jakubowski, W.; Matyjaszewski, K. *Angew. Chem., Int. Ed.* **2006**, *45*, 4482.

(52) Matyjaszewski, K.; Jakubowski, W.; Min, K.; Tang, W.; Huang, J.; Braunecker, W. A.; Tsarevsky, N. V. *Proc. Natl. Acad. Sci. U. S. A.* **2006**, *103*, 15309.

(53) Magenau, A. J. D.; Strandwitz, N. C.; Gennaro, A.; Matyjaszewski, K. *Science* **2011**, *332*, 81.

(54) Chiefari, J.; Chong, Y. K.; Ercole, F.; Krstina, J.; Jeffery, J.; Le, T. P. T.; Mayadunne, R. T. A.; Meijs, G. F.; Moad, C. L.; Moad, G.; Rizzardo, E.; Thang, S. H. *Macromolecules* **1998**, *31*, 5559.

(55) Hawthorne, D. G.; Moad, G.; Rizzardo, E.; Thang, S. H. *Macromolecules* **1999**, *32*, 5457.

(56) Moad, G.; Rizzardo, E.; Thang, S. H. *Aust. J. Chem.* **2005**, *58*, 379.

(57) Moad, G.; Rizzardo, E.; Thang, S. H. *Aust. J. Chem.* **2009**, *62*, 1402.

(58) Moad, G.; Rizzardo, E.; Thang, S. H. *Aust. J. Chem.* **2012**, *65*, 985.

(59) Barner-Kowolik, C. *Handbook of RAFT Polymerization*; Wiley WCH: Weinheim, **2008**.

(60) Mayadunne, R. T. A.; Rizzardo, E.; Chiefari, J.; Krstina, J.; Moad, G.; Postma, A.; Thang, S. H. *Macromolecules* **2000**, *33*, 243.

(61) Mayadunne, R. T. A.; Rizzardo, E.; Chiefari, J.; Chong, Y. K.; Moad, G.; Thang, S. H. *Macromolecules* **1999**, *32*, 6977.

(62) Destarac, M.; Charmot, D.; Franck, X.; Zard, S. Z. *Macromol. Rapid Commun.* **2000**, *21*, 1035.

(63) Charmot, D.; Corpart, P.; Adam, H.; Zard, S. Z.; Biadatti, T.; Bouhadir, G. *Macromolecular Symposia* **2000**, *150*, 23.

(64) Perrier, S.; Takolpuckdee, P. *J. Polym. Sci. A Polym. Chem.* **2005**, *43*, 5347.

(65) Chiefari, J.; Mayadunne, R. T. A.; Moad, C. L.; Moad, G.; Rizzardo, E.; Postma, A.; Skidmore, M. A.; Thang, S. H. *Macromolecules* **2003**, *36*, 2273.

(66) Chong, Y. K.; Krstina, J.; Le, T. P. T.; Moad, G.; Postma, A.; Rizzardo, E.; Thang, S. H. *Macromolecules* **2003**, *36*, 2256.

(67) Monteiro, M. J.; de Brouwer, H. *Macromolecules* **2001**, *34*, 349.

(68) Barner-Kowollik, C.; Quinn, J. F.; Morsley, D. R.; Davis, T. P. *J. Polym. Sci., Part A: Polym. Chem.* **2001**, *39*, 1353.

(69) Barner-Kowollik, C.; Buback, M.; Charleux, B.; Coote, M. L.; Drache, M.; Fukuda, T.; Goto, A.; Klumperman, B.; Lowe, A. B.; McLeary, J. B.; Moad, G.; Monteiro, M. J.; Sanderson, R. D.; Tonge, M. P.; Vana, P. *J. Polym. Sci., Part A: Polym. Chem.* **2006**, *44*, 5809.

(70) Perrier, S.; Barner-Kowollik, C.; Quinn, J. F.; Vana, P.; Davis, T. P. *Macromolecules* **2002**, *35*, 8300.

(71) Donovan, M. S.; Lowe, A. B.; Sumerlin, B. S.; McCormick, C. L. *Macromolecules* **2002**, *35*, 4123.

(72) Benaglia, M.; Chiefari, J.; Chong, Y. K.; Moad, G.; Rizzardo, E.; Thang, S. H. *J. Am. Chem. Soc.* **2009**, *131*, 6914.

(73) Keddie, D. J.; Guerrero-Sanchez, C.; Moad, G.; Rizzardo, E.; Thang, S. H. *Macromolecules* **2011**, *44*, 6738.

(74) Patten, T. E.; Matyjaszewski, K. *Adv. Mater.* **1998**, *10*, 901.

(75) Ashford, E. J.; Naldi, V.; O'Dell, R.; Billingham, N. C.; Armes, S. P. *Chem. Commun.* **1999**, 1285.

(76) Willcock, H.; O'Reilly, R. K. *Polym. Chem.* **2010**, *1*, 149.

(77) Moad, G.; Rizzardo, E.; Thang, S. H. *Polym. Int.* **2011**, *60*, 9.

(78) Gilbert, R. G. *Emulsion Polymerisation*; Academic Press: London, **1990**.

(79) Qun, W.; Shoukuan, F.; Tongyin, Y. *Prog. Polym. Sci.* **1994**, *19*, 703.

(80) Smith, W. V.; Ewart, R. H. *J. Chem. Phys.* **1948**, *16*, 592.

(81) Harkins, W. D. *J. Am. Chem. Soc.* **1947**, *69*, 1428.

(82) Gu, S.; Mogi, T.; Konno, M. *J. Colloid Interface Sci.* **1998**, *207*, 113.

(83) Richez, A. P.; Yow, H. N.; Biggs, S.; Cayre, O. J. *Prog. Polym. Sci.* **2013**, *38*, 897.

(84) Kawaguchi, S.; Ito, K. In *Polymer Particles*:; Springer: Berlin, 2005.

(85) Armes, S. P.; Vincent, B. *Journal of the Chemical Society, Chemical Communications* **1987**, 288.

(86) DeArmitt, C.; Armes, S. P. *Langmuir* **1993**, *9*, 652.

(87) Armes, S. P.; Aldissi, M.; Idzorek, G. C.; Keaton, P. W.; Rowton, L. J.; Stradling, G. L.; Collopy, M. T.; McColl, D. B. *J. Colloid Interface Sci.* **1991**, *141*, 119.

(88) Ali, A. M. I.; Pareek, P.; Sewell, L.; Schmid, A.; Fujii, S.; Armes, S. P.; Shirley, I. M. *Soft Matter* **2007**, *3*, 1003.

(89) Aakeroy, C. B.; Seddon, K. R. *Chem. Soc. Rev.* **1993**, *22*, 397.

(90) Tanford, C. *Science* **1978**, *200*, 1012.

(91) Chandler, D. *Nature* **2005**, *437*, 640.

(92) Israelachvili, J. N. *Intermolecular and Surface Forces*; Third Edition ed.; Academic Press: London, **2011**.

(93) Chu, Z.; Dreiss, C. A.; Feng, Y. *Chem. Soc. Rev.* **2013**, *42*, 7174.

(94) Bates, F. S.; Fredrickson, G. H. *Phys. Today* **1999**, *52*, 32.

(95) Krikorian, V.; Kang, Y.; Thomas, E. L. In *Macromolecular Engineering*; Wiley-VCH: Weinheim, Germany, 2007; Vol. 3.

(96) Mai, Y.; Eisenberg, A. *Chem. Soc. Rev.* **2012**, *41*, 5969.

(97) Orilall, M. C.; Wiesner, U. *Chem. Soc. Rev.* **2011**, *40*, 520.

(98) Leibler, L. *Macromolecules* **1980**, *13*, 1602.

(99) Bates, F. S.; Fredrickson, G. H. *Annu. Rev. Phys. Chem.* **1990**, *41*, 525.

(100) Matsen, M. W.; Schick, M. *Macromolecules* **1994**, *27*, 6761.

(101) Matsen, M. W.; Bates, F. S. *Macromolecules* **1996**, *29*, 1091.

(102) Khandpur, A. K.; Foerster, S.; Bates, F. S.; Hamley, I. W.; Ryan, A. J.; Bras, W.; Almdal, K.; Mortensen, K. *Macromolecules* **1995**, *28*, 8796.

(103) Huang, C.-I.; Lodge, T. P. *Macromolecules* **1998**, *31*, 3556.

(104) Alexandridis, P.; Spontak, R. J. *Curr. Opin. Colloid Interface Sci*, **1999**, *4*, 130.

(105) Zhang, L.; Eisenberg, A. *Science* **1995**, *268*, 1728.

(106) Zhang, L.; Eisenberg, A. *Polym. Adv. Tech.* **1998**, *9*, 677.

(107) Jain, S.; Bates, F. S. *Science* **2003**, *300*, 460.

(108) Rodríguez-Hernández, J.; Chécot, F.; Gnanou, Y.; Lecommandoux, S. *Prog. Polym. Sci.* **2005**, *30*, 691.

(109) Letchford, K.; Burt, H. *Eur. J. Pharm. Biopharm.* **2007**, *65*, 259.

(110) Blanazs, A.; Armes, S. P.; Ryan, A. J. *Macromol. Rapid Commun.* **2009**, *30*, 267.

(111) Moroi, Y.; Motomura, K.; Matuura, R. *J. Colloid Interface Sci.* **1974**, *46*, 111.

(112) Khougaz, K.; Zhong, X. F.; Eisenberg, A. *Macromolecules* **1996**, *29*, 3937.

(113) Won, Y.-Y.; Davis, H. T.; Bates, F. S. *Science* **1999**, *283*, 960.

(114) Bellomo, E. G.; Wyrsta, M. D.; Pakstis, L.; Pochan, D. J.; Deming, T. J. *Nat. Mater.* **2004**, *3*, 244.

(115) Cui, H.; Chen, Z.; Zhong, S.; Wooley, K. L.; Pochan, D. J. *Science* **2007**, *317*, 647.

(116) Du, J.; Tang, Y.; Lewis, A. L.; Armes, S. P. *J. Am. Chem. Soc.* **2005**, *127*, 17982.

(117) Arifin, D. R.; Palmer, A. F. *Biomacromolecules* **2005**, *6*, 2172.

(118) Ghoroghchian, P. P.; Frail, P. R.; Susumu, K.; Blessington, D.; Brannan, A. K.; Bates, F. S.; Chance, B.; Hammer, D. A.; Therien, M. J. *Proc. Natl. Acad. Sci. U. S. A.* **2005**, *102*, 2922.

(119) Charleux, B.; Delaittre, G.; Rieger, J.; D'Agosto, F. *Macromolecules* **2012**, *45*, 6753.

(120) Derry, M. J.; Fielding, L. A.; Armes, S. P. *Polym. Chem.* **2015**, *6*, 3054.

(121) Cunningham, V. J.; Alswieleh, A. M.; Thompson, K. L.; Williams, M.; Leggett, G. J.; Armes, S. P.; Musa, O. M. *Macromolecules* **2014**, *47*, 5613.

(122) Liu, G. Y.; Qiu, Q.; Shen, W. Q.; An, Z. S. *Macromolecules* **2011**, *44*, 5237.

(123) Delaittre, G.; Nicolas, J.; Lefay, C.; Save, M.; Charleux, B. *Chem. Commun.* **2005**, 614.

(124) Delaittre, G.; Save, M.; Gaborieau, M.; Castignolles, P.; Rieger, J.; Charleux, B. *Polym. Chem.* **2012**, *3*, 1526.

(125) Kim, K. H.; Kim, J.; Jo, W. H. *Polymer* **2005**, *46*, 2836.

(126) Sugihara, S.; Sugihara, K.; Armes, S. P.; Ahmad, H.; Lewis, A. L. *Macromolecules* **2010**, *43*, 6321.

(127) Rieger, J. *Macromol. Rapid Commun.* **2015**, *36*, 1458.

(128) Warren, N. J.; Armes, S. P. *J. Am. Chem. Soc.* **2014**, *136*, 10174.

(129) Delaittre, G.; Save, M.; Charleux, B. *Macromol. Rapid Commun.* **2007**, *28*, 1528.

(130) He, W.-D.; Sun, X.-L.; Wan, W.-M.; Pan, C.-Y. *Macromolecules* **2011**, *44*, 3358.

(131) Wan, W.-M.; Pan, C.-Y. *Polym. Chem.* **2010**, *1*, 1475.

(132) Jones, E. R.; Semsarilar, M.; Blanazs, A.; Armes, S. P. *Macromolecules* **2012**, *45*, 5091.

(133) Semsarilar, M.; Jones, E. R.; Blanazs, A.; Armes, S. P. *Adv. Mater.* **2012**, *24*, 3378.

(134) Derry, M. J.; Fielding, L. A.; Armes, S. P. *Prog. Polym. Sci.* **2016**, *52*, 1.

(135) Fielding, L. A.; Derry, M. J.; Ladmiral, V.; Rosselgong, J.; Rodrigues, A. M.; Ratcliffe, L. P. D.; Sugihara, S.; Armes, S. P. *Chem. Sci.* **2013**, *4*, 2081.

(136) Pei, Y.; Thurairajah, L.; Sugita, O. R.; Lowe, A. B. *Macromolecules* **2014**, *48*, 236.

(137) Zhang, Q.; Zhu, S. *ACS Macro Lett.* **2015**, *4*, 755.

(138) Monteiro, M. J.; Hodgson, M.; De Brouwer, H. *J. Polym. Sci., Part A: Polym. Chem.* **2000**, *38*, 3864.

(139) Monteiro, M. J.; de Barbeyrac, J. *Macromolecules* **2001**, *34*, 4416.

(140) Butté, A.; Storti, G.; Morbidelli, M. *Macromolecules* **2001**, *34*, 5885.

(141) Ferguson, C. J.; Hughes, R. J.; Pham, B. T. T.; Hawkett, B. S.; Gilbert, R. G.; Serelis, A. K.; Such, C. H. *Macromolecules* **2002**, *35*, 9243.

(142) Ganeva, D. E.; Sprong, E.; de Bruyn, H.; Warr, G. G.; Such, C. H.; Hawkett, B. S. *Macromolecules* **2007**, *40*, 6181.

(143) Ferguson, C. J.; Hughes, R. J.; Nguyen, D.; Pham, B. T. T.; Gilbert, R. G.; Serelis, A. K.; Such, C. H.; Hawkett, B. S. *Macromolecules* **2005**, *38*, 2191.

(144) Manguian, M.; Save, M.; Charleux, B. *Macromol. Rapid Commun.* **2006**, *27*, 399.

(145) Zhang, X.; Rieger, J.; Charleux, B. *Polym. Chem.* **2012**, *3*, 1502.

(146) Chaduc, I.; Girod, M.; Antoine, R.; Charleux, B.; D'Agosto, F.; Lansalot, M. *Macromolecules* **2012**, *45*, 5881.

(147) Zhang, W.; D'Agosto, F.; Boyron, O.; Rieger, J.; Charleux, B. *Macromolecules* **2012**, *45*, 4075.

(148) Zhang, W.; D'Agosto, F.; Boyron, O.; Rieger, J.; Charleux, B. *Macromolecules* **2011**, *44*, 7584.

(149) Zhang, X.; Boissé, S.; Zhang, W.; Beaunier, P.; D'Agosto, F.; Rieger, J.; Charleux, B. *Macromolecules* **2011**, *44*, 4149.

(150) Rieger, J.; Osterwinter, G.; Bui, C.; Stoffelbach, F.; Charleux, B. *Macromolecules* **2009**, *42*, 5518.

(151) Rieger, J.; Stoffelbach, F.; Bui, C.; Alaimo, D.; Jerome, C.; Charleux, B. *Macromolecules* **2008**, *41*, 4065.

(152) Boisse, S.; Rieger, J.; Belal, K.; Di-Cicco, A.; Beaunier, P.; Li, M.-H.; Charleux, B. *Chem. Commun.* **2010**, *46*, 1950.

(153) Boissé, S.; Rieger, J.; Pembouong, G.; Beaunier, P.; Charleux, B. *J. Polym. Sci. A Polym. Chem.* **2011**, *49*, 3346.

(154) Rieger, J.; Zhang, W.; Stoffelbach, F.; Charleux, B. *Macromolecules* **2010**, *43*, 6302.

(155) Chenal, M.; Bouteiller, L.; Rieger, J. *Polym. Chem.* **2013**, *4*, 752.

(156) Truong, N. P.; Dussert, M. V.; Whittaker, M. R.; Quinn, J. F.; Davis, T. P. *Polym. Chem.* **2015**, *6*, 3865.

(157) St Thomas, C.; Guerrero-Santos, R.; D'Agosto, F. *Polym. Chem.* **2015**, *6*, 5405.

(158) Zhang, B.; Yan, X.; Alcouffe, P.; Charlot, A.; Fleury, E.; Bernard, J. *ACS Macro Lett.* **2015**, *4*, 1008.

(159) Rieger, J. *Macromol. Rapid Commun.* **2015**, *36*, 1458.

(160) An, Z.; Shi, Q.; Tang, W.; Tsung, C.-K.; Hawker, C. J.; Stucky, G. D. *J. Am. Chem. Soc.* **2007**, *129*, 14493.

(161) Rieger, J.; Grazon, C.; Charleux, B.; Alaimo, D.; Jerome, C. *J. Polym. Sci., Part A: Polym. Chem.* **2009**, *47*, 2373.

(162) Grazon, C.; Rieger, J.; Sanson, N.; Charleux, B. *Soft Matter* **2011**, *7*, 3482.

(163) Shen, W. Q.; Chang, Y. L.; Liu, G. Y.; Wang, H. F.; Cao, A. N.; An, Z. S. *Macromolecules* **2011**, *44*, 2524.

(164) Liu, G.; Qiu, Q.; An, Z. *Polym. Chem.* **2012**, *3*, 504.

(165) Zhou, W.; Qu, Q.; Xu, Y.; An, Z. *ACS Macro Lett.* **2015**, *4*, 495.

(166) Li, Y.; Armes, S. P. *Angew. Chem., Int. Ed.* **2010**, *49*, 4042.

(167) Blanazs, A.; Madsen, J.; Battaglia, G.; Ryan, A. J.; Armes, S. P. *J. Am. Chem. Soc.* **2011**, *133*, 16581.

(168) Blanazs, A.; Ryan, A. J.; Armes, S. P. *Macromolecules* **2012**, *45*, 5099.

(169) Ratcliffe, L. P. D.; Ryan, A. J.; Armes, S. P. *Macromolecules* **2013**, *46*, 769.

(170) Sugihara, S.; Blanazs, A.; Armes, S. P.; Ryan, A. J.; Lewis, A. L. *J. Am. Chem. Soc.* **2011**, *133*, 15707.

(171) Warren, N. J.; Mykhaylyk, O. O.; Mahmood, D.; Ryan, A. J.; Armes, S. P. *J. Am. Chem. Soc.* **2014**, *136*, 1023.

(172) Ladmiral, V.; Charlot, A.; Semsarilar, M.; Armes, S. P. *Polym. Chem.* **2015**, *6*, 1805.

(173) Doncom, K. E. B.; Warren, N. J.; Armes, S. P. *Polym. Chem.* **2015**, *6*, 7264.

(174) Ladmiral, V.; Semsarilar, M.; Canton, I.; Armes, S. P. *J. Am. Chem. Soc.* **2013**, *135*, 13574.

(175) Semsarilar, M.; Ladmiral, V.; Blanazs, A.; Armes, S. P. *Langmuir* **2013**, *29*, 7416.

(176) Williams, M.; Penfold, N. J. W.; Armes, S. P. *Polym. Chem.* **2016**, *7*, 384.

(177) Semsarilar, M.; Ladmiral, V.; Blanazs, A.; Armes, S. P. *Langmuir* **2011**, *28*, 914.

(178) Warren, N. J.; Ladmiral, V.; Derry, M. J.; Lovett, J. R.; Mykhaylyk, O. O.; Armes, S. P. *Manuscript in preparation*.

(179) Figg, C. A.; Simula, A.; Gebre, K. A.; Tucker, B. S.; Haddleton, D. M.; Sumerlin, B. S. *Chem. Sci.* **2015**, *6*, 1230.

(180) Sugihara, S.; Ma'Radzi, A. H.; Ida, S.; Irie, S.; Kikukawa, T.; Maeda, Y. *Polymer* **2015**, *76*, 17.

(181) Jiang, Y.; Xu, N.; Han, J.; Yu, Q.; Guo, L.; Gao, P.; Lu, X.; Cai, Y. *Polym. Chem.* **2015**, *6*, 4955.

Chapter 2:

Worm-to-Sphere Transition of Poly(glycerol monomethacrylate)-Poly(2-hydroxypropyl methacrylate) Diblock Copolymer Nano-Objects Driven By Ionisation of End-Groups

2.1 Introduction

There has been substantial and sustained interest in the field of stimulus-responsive or so-called smart polymers over the last two decades.[1-7] Thermal[2,3] and pH[4,5] stimuli have been particularly well studied for water-soluble polymers, which can be exploited for various biological applications.[7-14] For example, pH-responsive polymers have been extensively studied in the context of cancer treatment since the extracellular pH within the local environment of tumours is well known to be acidic.[15,16] Thus in principle the delivery and release of an active ingredient can be achieved by encapsulation within a suitable polymeric nano-object.[17,18]

Perhaps one of the most widely studied thermo-responsive polymers is poly(*N*-isopropylacrylamide) (PNIPAM). PNIPAM undergoes a coil-to-globule transition in aqueous solution, with phase separation occurring above 32 °C, which is known as the lower critical solution temperature (LCST).[19] Such thermal transitions are typically driven by entropy, which makes mixing unfavourable above certain temperatures. The LCST of PNIPAM is potentially useful for various biological applications, such as controlled release[20], biomolecule purification[21] and tissue engineering.[22] Other examples of water-soluble polymers that exhibit LCST behaviour include poly(*N*,*N*-diethylacrylamide),[23] poly(ethylene oxide),[24] poly(vinyl methyl ether),[25] poly(*N*-ethylacrylamide),[26] poly(2-hydroxypropyl acrylate) (PHPA),[26] poly(*N*-vinylcaprolactam),[27] and poly(2-hydroxyethyl methacrylate) (PHEMA).[28] The LCST behaviour of such polymers can be tuned by incorporating suitable comonomer(s).[26,29] However, addition of hydrophilic or hydrophobic end-groups can also cause significant variations in the LCST.[30-32] For example, Stöver's group reported that the LCST of PNIPAM homopolymers, prepared by atom transfer radical polymerisation (ATRP), can be tuned from 45 to 34 °C depending on the nature of the end-group of the initiator chosen (such as $–NH_2$ or –NHPh).[31] However, there have been relatively few literature examples of end-group chemistry that are able to induce or facilitate an order-order or order-disorder transition. Gibson *et al.* utilised pyridyl disulfide linkages so as to introduce hydrophilic end-groups in order to raise the LCST of PNIPAM. This strategy enabled a coil-to-globule transition to be achieved at constant temperature *via* selective cleavage of the hydrophilic end-

group using glutathione.[33] O'Reilly and co-workers used a quaternary amine-functionalised reversible addition-fragmentation transfer (RAFT) chain transfer agent (CTA) to prepare a PNIPAM-based diblock copolymer, which self-assembled to form spheres at room temperature.[34] However, heating above the LCST of the PNIPAM stabiliser altered the packing parameter of the copolymer (see **Figure 2.1**). This induced a morphological sphere-to-vesicle transition (rather than macroscopic precipitation) because the cationic charge conferred by the CTA-derived end-group located on the PNIPAM chains ensured colloidal stability.[34]

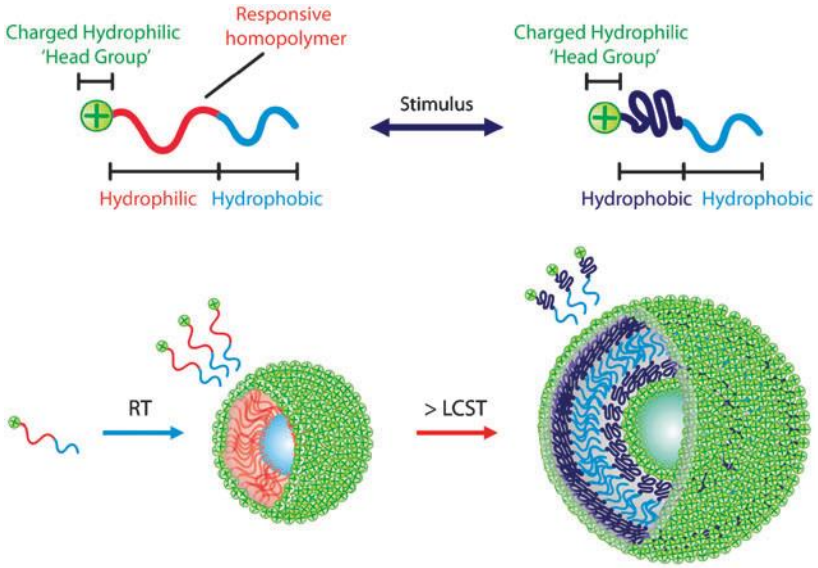

Figure 2.1 Schematic illustration of the change in water solubility of a PNIPAM-based block copolymer induced on heating. This leads to a vesicle-to-sphere transformation.[34]

Recently, Du and co-workers reported that a terminal alkynyl end-group was capable of driving the self-assembly of hydrophilic PNIPAM and poly[oligo(ethylene glycol) methacrylate] homopolymers to form various morphologies in aqueous solution.[35] Warr *et al*. used a carboxylic acid-functionalised CTA with a hydrophobic dodecyl chain to prepare a series of PNIPAM oligomers, which self-assembled in water to form micelles.[32] The LCST of such oligomers varied from 7 °C to 33 °C on increasing the chain length of PNIPAM. However, ionising the carboxylic acid end-group completely suppressed the LCST behaviour in all cases. Similarly, Weaver and co-workers prepared a series of near-monodisperse

PHEMA homopolymers by ATRP, and demonstrated LCST behaviour in aqueous solutions at pH 6.5 within a narrow mean degree of polymerisation (DP) range of 30 to 45.[28] In contrast, PHEMA homopolymers with chain lengths larger than 45 units were water insoluble. However, lowering the pH of the solution to 2.2 dramatically increased their water solubility. This was attributed to the morpholine end-group derived from the ATRP initiator used in their synthesis, which becomes protonated at low pH and so enhances water solubility. In related work, Vo *et al*. reported that the water solubility of PHPA homopolymers prepared by RAFT polymerisation depend on the solution pH when using a carboxylic acid-functionalised CTA.[36] Biocompatible nanoparticles that undergo either order-order or order-disorder morphology transitions upon exposure to a physiologically-relevant or applied stimulus are of particular interest for potential drug delivery applications.[7,37-39]

In 2010 Armes and co-workers prepared a series of sterically stabilised nanoparticles by polymerisation-induced self-assembly (PISA).[40] More specifically, a water-soluble poly(glycerol monomethacrylate) (PGMA) macro-CTA was chain extended *via* RAFT aqueous dispersion polymerisation of 2-hydroxypropyl methacrylate (HPMA) at 10 % w/w solids, to produce a series of spheres with mean diameters ranging from 26 nm to 105 nm. The same group reported that worms and vesicles could also be reproducibly prepared using the same PISA formulation.[41]

In the case of pure worms, soft free-standing gels are obtained at room temperature due to multiple inter-worm contacts. However, upon cooling to 5 °C a worm-to-sphere order-order transition is observed by transmission electron microscopy (TEM). This results in a loss of inter-worm contacts and hence degelation (see **Figure 2.2**).[42,43] Blanazs and co-workers used variable temperature ^{1}H NMR spectroscopy to show that the PHPMA core-forming block became significantly more hydrated on cooling; this is consistent with surface plasticisation of the PGMA-PHPMA worm cores, which leads to a reduction in the packing parameter and hence accounts for the observed worm-to-sphere transition.[44,45] This transition is fully reversible and enables sterilisation of the worms by cold ultra-filtration as the spheres are small (approximately 50 nm), whereas bacteria cells are much larger (typically > 500 nm).[43]

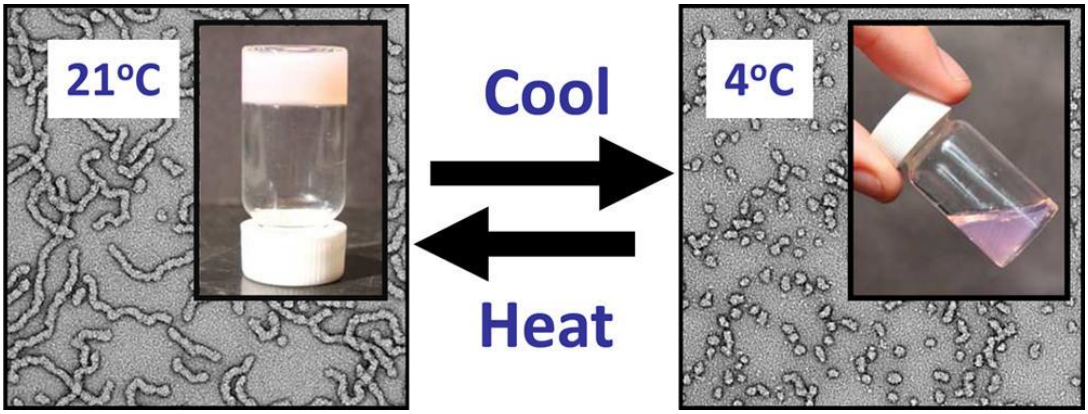

Figure 2.2 TEM and digital images (inset) obtained for a gel at 21 °C. Upon cooling to 4 °C these particles degel and TEM confirms a worm-to-sphere transition.[43]

Following this, Verber and co-workers extensively analysed a series of $PGMA_{54}$-$PHPMA_X$ diblock copolymer worms using oscillatory rheology.[42] An increase in storage modulus (G') or gel stiffness was observed as the PHPMA DP was increased from 130 to 170 (see **Figure 2.3a**). It is noteworthy that increasing the PHPMA block length beyond 170 results in the formation of turbid free-flowing vesicles. All these worm gels exhibited thermally-induced degelation on cooling to 5 °C as discussed above. However, the temperature this occurred, known as the critical gelation temperature (CGT), reduced with higher PHPMA DPs (see **Figure 2.3b**). This is because longer, more hydrophobic PHPMA blocks require a greater degree of surface plasticisation to induce a morphological transition (and degelation).

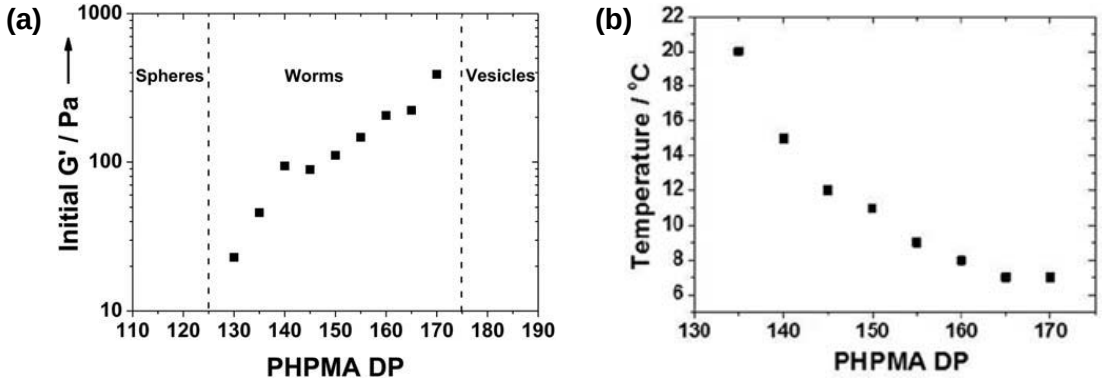

Figure 2.3 Variation of (a) G' at 25 °C and (b) the CGT for a series of $PGMA_{54}$-$PHPMA_X$ diblock copolymer worms measured using oscillatory rheology.[42]

In this Chapter we report that these predominately *non-ionic* PGMA-PHPMA diblock copolymer worms can also unexpectedly exhibit *pH-responsive* character when prepared with a carboxylic acid-functionalised CTA. In contrast, preparing diblock copolymers with an analogous non-ionic (ester) CTA yields pH-insensitive worms. Furthermore, fluorescently-labelled pH- and temperature-responsive worms are prepared by a post-polymerisation modification. This stimuli-responsive nature is monitored using fluorescence correlation spectroscopy (FCS).

2.2 Experimental Section

2.2.1 Materials

Glycerol monomethacrylate (GMA; 99.8 %) was donated by GEO Specialty Chemicals (Hythe, UK) and used without further purification. 2-Hydroxypropyl methacrylate (HPMA), 4,4'-azobis(4-cyanopentanoic acid) (ACVA; 99 %), 4-cyano-4-(phenylcarbonothioylthio) pentanoic acid (CPADB), 2-cyano-2-propyl dithiobenzoate (CPDB), dicyclohexylcarbodiimide (DCC), 4-(dimethylamino) pyridine (DMAP), ethanol (99 %, anhydrous grade), ethyl acetate, petroleum ether, methanol, dichloromethane and deuterated methanol were purchased from Sigma-Aldrich (UK) and were used as received. All solvents were of HPLC quality. 4-cyano-4-(2-phenylethanesulfanylthiocarbonyl)-sulfanylpentanoic acid (PETTC) was prepared and purified as reported elsewhere.[46]

2.2.2 Synthesis of poly(glycerol monomethacrylate) (HOOC-PGMA$_{56}$) macro-CTA using PETTC

GMA (10.0 g, 62.4 mmol), PETTC RAFT agent (0.303 g, 0.892 mmol; target DP = 70), and ACVA (0.050 g, 0.18 mmol; PETTC: ACVA molar ratio = 5.0) were weighed into a 100 ml round-bottomed flask. Anhydrous ethanol (previously purged with nitrogen for 1 h) was then added to produce a 40 % w/w solution. The mixture was placed in an ice bath and purged under nitrogen for a further 45 min at 0 °C. The

sealed flask was immersed in an oil bath set at 70 °C and stirred for 2 h. The polymerisation was then quenched at approximately 78 % conversion by simultaneous exposure to air and cooling to room temperature. Methanol (10 ml) was added to dilute the reaction solution, followed by precipitation into a ten-fold excess of dichloromethane in order to remove unreacted GMA monomer, RAFT agent and initiator. The precipitate was isolated *via* filtration and washed with excess dichloromethane before being dissolved in methanol (40 ml). This process was then repeated and the precipitate was then dissolved in water and freeze-dried overnight to afford a yellow solid. ^{1}H NMR studies indicated a DP of 56 *via* end-group analysis (by comparing aromatic peaks from the RAFT agent at 7.2 ppm to the polymer backbone signals between 0.5 to 2.5 ppm). DMF GPC studies (refractive index detector; calibrated against a series of near-monodisperse poly(methyl methacrylate) standards) indicated an M_n of 14,100 g mol^{-1} and an M_w/M_n of 1.17. ^{1}H NMR (400 MHz, CD_3OD, 25 °C): δ 0.77-1.24 (b, 3H, -$CH_2CR(C\mathbf{H_3})$-), 1.78-2.30 (b, 1.9H, -$\mathbf{CH_2}CR(CH_3)$-), 3.57-3.82 (b, 2H, -$C\mathbf{H_2}OH$), 3.82-4.24 (b, 3.3H, -$COO\mathbf{CH_2CH}(OH)$-).

2.2.3 Synthesis of HOOC-PGMA$_{56}$-PHPMA$_{155}$ diblock copolymer worms *via* RAFT aqueous dispersion polymerisation

A typical protocol for the chain extension of HOOC-PGMA$_{56}$ macro-CTA with 155 units of HPMA *via* RAFT aqueous dispersion polymerisation is as follows: PGMA$_{56}$ macro-CTA (0.208 g, 0.022 mmol), HPMA monomer (0.50 g, 3.4 mmol) ACVA (2.1 mg, 0.007 mmol; HOOC-PGMA$_{56}$ macro-CTA:ACVA molar ratio = 3.0) were added to a 25 ml round-bottomed flask, prior to addition of water to produce a 10 % w/w solution. The reaction solution was purged under nitrogen for 30 min at 20 °C prior to immersion into an oil bath set at 70 °C. The reaction mixture was stirred for 4 h to ensure almost complete conversion of the HPMA monomer (> 99 % as judged by disappearance of vinyl peaks at approximately 6.0 ppm by ^{1}H NMR analysis), and was quenched by simultaneous exposure to air and cooling to ambient temperature. The resulting worm gel was characterised by DLS, TEM and rheology without further purification. DMF GPC studies indicated an M_n of 36,600 g mol^{-1} and an M_w/M_n of 1.08. ^{1}H NMR (400 MHz, CD_3OD, 25 °C): δ 0.75-1.19 (b,

3H, -**CH$_3$** on polymer backbone), 1.19-1.36 (b, 2.4H, -**CH$_3$** in PHPMA), 1.54-2.23 (b, 2H, -**CH$_2$**- on polymer backbone), 3.53-3.72 (b, 0.8H, -**CH$_2$**OH in PGMA and –**CH**(OH)- in PHPMA), 3.72-4.21 (b, 2.8H, remaining pendent protons in PGMA and PHPMA).

2.2.4 Methylation of PETTC chain transfer agent

PETTC (0.20 g, 0.59 mmol) was dissolved in anhydrous dichloromethane (1.50 ml) in a 10 ml round-bottomed flask, which was cooled in an ice bath to 0 °C. DMAP (0.014 g, 0.12 mmol) and excess anhydrous methanol (0.10 g) were added to the stirred solution at 0 °C. DCC (0.14 g, 0.66 mmol) was added gradually over 5 min. This reaction mixture was allowed to warm up to 20 °C and stirred continuously for 16 h prior to filtration to remove the insoluble side-product (dicyclohexyl urea). The filtrate was then washed twice with acidic water (pH 3) and de-ionised water (pH 6) before being dried over magnesium sulphate. Finally, dichloromethane was removed under vacuum to produce an orange oil. ^{1}H NMR (400 MHz, CD_3OD, 25 °C): δ 1.89 (s, 3H, -(CN)C**H$_3$**), 2.39-2.70 (m, 4H, -C**H$_2$**C**H$_2$**-), 2.93-3.05 (m, 2H, -C**H$_2$**CH_2Ph), 3.61-3.68 (m, 2H, -CH_2C**H$_2$**Ph), 3.72 (s, 3H, -COOC**H$_3$**), 7.20-7.36 (m, 5H, -CH_2CH_2**Ph**). Elemental analysis calculated for $C_{16}H_{19}NO_2S_3$: C, 54.36 %; H, 5.42 %; N, 3.96 %; S, 27.21 %. Found: C, 54.32 %; H, 5.47 %; N, 4.19 %; S, 25.01 %. TOF MS ES$^+$ m/z = 354 (MH+).

2.2.5 Synthesis of poly(glycerol monomethacrylate) (H_3COOC-$PGMA_{59}$) macro-CTA using Me-PETTC

GMA (4.00 g, 25.0 mmol), Me-PETTC RAFT agent (0.126 g, 0.36 mmol; target DP = 70), and ACVA (0.020 g, 0.070 mmol; Me-PETTC:ACVA molar ratio = 5.0) were weighed into a 25 ml round-bottomed flask. Anhydrous ethanol (previously purged with nitrogen for 1 h) was then added to produce a 40 % w/w solution, which was placed in an ice bath and purged under nitrogen for 45 min at 0 °C. The sealed flask was immersed in an oil bath set at 70 °C and stirred for 2 h. The polymerisation was then quenched at approximately 72 % conversion by simultaneous exposure to air and cooling to room temperature. Methanol (5.0 ml)

was added to dilute the reaction solution, followed by precipitation into a ten-fold excess of dichloromethane in order to remove unreacted GMA monomer, RAFT agent and initiator. The precipitate was isolated *via* filtration and washed with excess dichloromethane before being dissolved in methanol (20 ml). This process was repeated and the precipitate was then dissolved in water and freeze-dried overnight to afford a yellow solid. ^{1}H NMR studies indicated a DP of 59 *via* end-group analysis (by comparing aromatic peaks from the RAFT agent at 7.2 ppm to the polymer backbone signals between 0.5 to 2.5 ppm). DMF GPC studies indicated an M_n of 15,600 g mol^{-1} and an M_w/M_n of 1.20. ^{1}H NMR (400 MHz, CD_3OD, 25 °C): δ 0.78-1.24 (b, 3H, -$CH_2CR(C\mathbf{H_3})$-), 1.76-2.27 (b, 2H, -$\mathbf{CH_2}CR(CH_3)$-), 3.53-3.83 (b, 2.1H, -$C\mathbf{H_2}OH$), 3.83-4.22 (b, 3.4H, -$COO\mathbf{CH_2CH}(OH)$-).

2.2.6 Synthesis of H_3COOC-$PGMA_{59}$-$PHPMA_{160}$ diblock copolymer worms *via* RAFT aqueous dispersion polymerisation

A typical protocol for the chain extension of H_3COOC-$PGMA_{56}$ macro-CTA with 160 units of HPMA *via* RAFT aqueous dispersion polymerisation is as follows: H_3COOC-$PGMA_{59}$ macro-CTA (0.167 g, 0.017 mmol), HPMA monomer (0.40 g, 2.8 mmol) ACVA (1.6 mg, 0.006 mmol; H_3COOC-$PGMA_{59}$ macro-CTA:ACVA molar ratio = 3.0) were added to a 25 ml round-bottomed flask, prior to addition of water to produce a 10 % w/w solution. The reaction solution was purged under nitrogen for 30 min at 20 °C prior to immersion into an oil bath set at 70 °C. The reaction mixture was stirred for 4 h to ensure almost complete conversion of the HPMA monomer (> 99 % as judged by disappearance of vinyl peaks at approximately 6.0 ppm by ^{1}H NMR analysis), and was quenched by simultaneous exposure to air and cooling to ambient temperature. The resulting worm gel was characterised by DLS, TEM and rheology without further purification. DMF GPC studies indicated an M_n of 35,000 g mol^{-1} and an M_w/M_n of 1.08. ^{1}H NMR (400 MHz, CD_3OD, 25 °C): δ 0.82-1.20 (b, 3H, -$\mathbf{CH_3}$ on polymer backbone), 1.20-1.35 (b, 2.6H, -$\mathbf{CH_3}$ in PHPMA), 1.80-2.27 (b, 1.9H, -$\mathbf{CH_2}$- on polymer backbone), 3.52-3.67 (b, 0.8H, -$\mathbf{CH_2}$OH in PGMA and –$\mathbf{CH}$(OH)- in PHPMA), 3.73-4.20 (b, 2.8H, remaining pendent protons in PGMA and PHPMA).

2.2.7 Synthesis of poly(glycerol monomethacrylate) (HOOC-PGMA$_{60}$) macro-CTA using CPADB

GMA monomer (38.44 g, 0.24 mol), CPADB RAFT agent (0.96 g, 3.43 mmol, target DP = 70) and anhydrous ethanol (59.4 g, 1.28 mol) were added to a round-bottomed flask. To this, ACVA initiator (0.19 g, 0.69 mmol, CPADB:ACVA molar ratio = 5.0) was added and the resulting pink solution was purged with N_2 for 20 min, before the sealed flask was immersed into an oil bath set at 70 °C. After 2.5 h the polymerisation was quenched by immersion of the flask in an ice bath and opening it to air. ^{1}H NMR indicated a conversion of 75 %. The polymerisation solution was then precipitated into a ten-fold excess of chloroform and washed three times in the precipitation solvent before being placed under high vacuum for three days at 40 °C. This purified PGMA macro-CTA was calculated to have a DP of 60 by ^{1}H NMR analysis. DMF GPC analysis indicated an M_n of 17,000 g mol^{-1} and M_w/M_n of 1.08. ^{1}H NMR (400 MHz, CD_3OD, 25 °C): δ 0.76-1.26 (b, 3H, -$CH_2CR(C\mathbf{H_3})$-), 1.79-2.25 (b, 2H, -$\mathbf{CH_2}CR(CH_3)$-), 3.55-3.82 (b, 2H, -$C\mathbf{H_2}OH$), 3.82-4.23 (b, 3.4H, -$COO\mathbf{CH_2CH}(OH)$-).

2.2.8 Synthesis of HOOC-PGMA$_{60}$-PHPMA$_{175}$ diblock copolymer worms *via* RAFT aqueous dispersion polymerisation

A typical protocol for the chain extension of HOOC-PGMA$_{60}$ macro-CTA with 175 units of HPMA *via* RAFT aqueous dispersion polymerisation is as follows: PGMA$_{60}$ macro-CTA (0.157 g, 0.016 mmol), HPMA monomer (0.40 g, 2.8 mmol) ACVA (1.5 mg, 0.005 mmol; HOOC-PGMA$_{60}$ macro-CTA:ACVA molar ratio = 3.0) were added to a 25 ml round-bottomed flask, prior to addition of water to produce a 10 % w/w solution. The reaction solution was purged under nitrogen for 30 min at 20 °C prior to immersion into an oil bath set at 70 °C. The reaction mixture was stirred for 4 h to ensure almost complete conversion of the HPMA monomer (> 99 % as judged by disappearance of vinyl peaks at approximately 6.0 ppm by ^{1}H NMR analysis), and was quenched by simultaneous exposure to air and cooling to ambient temperature. The resulting worm gel was characterised by DLS, TEM and rheology without further purification. DMF GPC studies indicated an M_n of 46,900 g

mol^{-1} and an M_w/M_n of 1.13. ^{1}H NMR (400 MHz, CD_3OD, 25 °C): δ 0.78-1.20 (b, 3H, **-CH$_3$** on polymer backbone), 1.20-1.34 (b, 2.4H, **-CH$_3$** in PHPMA), 1.72-2.30 (b, 1.8H, **-CH$_2$-** on polymer backbone), 3.58-3.72 (b, 0.7H, **-CH$_2$**OH in PGMA and –**CH**(OH)- in PHPMA), 3.73-4.20 (b, 2.2H, remaining pendent protons in PGMA and PHPMA).

2.2.9 Synthesis of poly(glycerol monomethacrylate) (Me-PGMA$_{57}$) macro-CTA using CPDB

GMA (40.0 g, 250 mmol), CPDB (1.105 g, 5.0 mmol; target DP = 50), and ACVA (0.280 g, 1.00 mmol; CPDB:ACVA molar ratio = 5.0) were weighed into a 250 mL round-bottomed flask. Anhydrous ethanol (previously purged with nitrogen for 1 h) was then added to produce a 40 % w/w solution. The mixture was placed in an ice bath and purged under nitrogen for 45 min at 0 °C. The sealed flask was immersed in an oil bath set at 70 °C and was left to stir for 2 h at this temperature. The polymerisation was quenched at approximately 76 % conversion (as judged by ^{1}H NMR) by simultaneous exposure to air and cooling the reaction mixture to room temperature. Methanol (20 mL) was added to dilute the reaction solution, followed by precipitation into a ten-fold excess of dichloromethane in order to remove unreacted GMA monomer. The precipitate was isolated by filtration and washed with excess dichloromethane before being dissolved in methanol (60 mL). This process was repeated and the precipitate was then dissolved in water and freeze-dried overnight to afford a pink solid. ^{1}H NMR studies indicated a DP of 57 *via* end-group analysis (by comparing aromatic peaks from the RAFT agent at 7.2 ppm to the polymer backbone signals between 0.5 to 2.5 ppm). DMF GPC studies indicated an M_n of 16,200 g mol^{-1} and an M_w/M_n of 1.16. ^{1}H NMR (400 MHz, CD_3OD, 25 °C): δ 0.73-1.23 (b, 3H, -$CH_2CR(CH_3)$-), 1.80-2.33 (b, 2H, **-CH$_2$**$CR(CH_3)$-), 3.46-3.82 (b, 2.1H, -C**H$_2$**OH), 3.84-4.28 (b, 3.4H, -COO**CH$_2$CH**(OH)-).

2.2.10 Synthesis of Me-PGMA$_{57}$-PHPMA$_{155}$ diblock copolymer worms *via* RAFT aqueous dispersion polymerisation

Me-PGMA$_{57}$-PHPMA$_{155}$ diblock copolymer worms were prepared by the following RAFT aqueous dispersion polymerisation formulation: Me-PGMA$_{57}$ macro-CTA (0.583 g, 0.063 mmol), HPMA monomer (1.40 g, 9.7 mmol) ACVA (5.9 mg, 0.021 mmol; Me-PGMA$_{57}$ macro-CTA:ACVA molar ratio = 3.0) were added to a 25 ml round-bottomed flask, followed by the addition of water to produce a 10% w/w aqueous solution. This reaction solution was purged with nitrogen gas for 30 min before immersion into an oil bath set at 70 °C. The reaction mixture was stirred for 4 h to ensure essentially complete conversion of the HPMA monomer (> 99 % as judged by disappearance of the vinyl signals in ^{1}H NMR) and was quenched by exposure to air, followed by cooling to ambient temperature. The resulting worm dispersion was characterised by DLS, TEM and rheology without further purification. DMF GPC studies indicated an M_n of 43,800 g mol^{-1} and an M_w/M_n of 1.14. ^{1}H NMR (400 MHz, CD_3OD, 25 °C): δ 0.82-1.20 (b, 3H, **-CH_3** on polymer backbone), 1.20-1.33 (b, 2.5H, **-CH_3** in PHPMA), 1.79-2.27 (b, 2H, **-CH_2-** on polymer backbone), 3.53-3.70 (b, 0.9H, **-CH_2**OH in PGMA and –**CH**(OH)- in PHPMA), 3.72-4.20 (b, 2.9H, remaining pendent protons in PGMA and PHPMA).

2.2.11 Synthesis of poly(glycerol monomethacrylate) (HOOC-PGMA$_{43}$) macro-CTA using PETTC

The HOOC-PGMA macro-CTA was prepared as described in **section 2.2.2**. ^{1}H NMR studies of the pure homopolymer indicated a DP of 43 *via* end-group analysis (by comparing aromatic peaks from the RAFT agent at 7.2 ppm to the polymer backbone between 0.5 to 2.5 ppm). DMF GPC studies (indicated an M_n of 15,700 g mol^{-1} and an M_w/M_n of 1.12. ^{1}H NMR (400 MHz, CD_3OD, 25 °C): δ 0.77-1.24 (b, 3H, -CH_2CR(C**H$_3$**)-), 1.75-2.24 (b, 2H, -**CH_2**CR(CH_3)-), 3.56-3.83 (b, 2.2H, -C**H$_2$**OH), 3.83-4.23 (b, 3.5H, -COO**CH_2CH**(OH)-).

2.2.12 Synthesis of HOOC-PGMA$_{43}$-block-P(HPMA$_{119}$-*stat*-GlyMA$_1$) diblock copolymer worms *via* RAFT aqueous dispersion copolymerisation

The protocol for the chain extension of HOOC-PGMA$_{43}$ macro-CTA *via* RAFT aqueous dispersion copolymerisation of 119 units of HPMA with 1 unit of GlyMA is as follows: HOOC-PGMA$_{43}$ macro-CTA (0.660 g, 0.087 mmol), HPMA monomer (1.500 g, 9.40 mmol), GlyMA monomer (0.012 g, 0.087 mmol), ACVA (8.20 mg, 0.026 mmol; HOOC-PGMA$_{43}$ macro-CTA:ACVA molar ratio = 3.0) were added to a 50 mL round-bottomed flask, prior to addition of water to produce a 10 % w/w solution. The reaction solution was purged under nitrogen for 30 min at 20 °C prior to immersion into an oil bath set at 70 °C. The reaction mixture was stirred for 4 h at this temperature to ensure almost complete conversion of the HPMA and GlyMA monomer (> 99 % by ^{1}H NMR analysis) and was quenched by simultaneous exposure to air and cooling to ambient temperature. The resulting copolymer worm gel was used without further purification and characterised by DLS, TEM and rheology. DMF GPC studies indicated a M_n of 43,800 g mol^{-1} and an M_w/M_n of 1.14. ^{1}H NMR (400 MHz, CD_3OD, 25 °C): δ 0.69-1.19 (b, 3H, **-CH$_3$** on polymer backbone), 1.19-1.36 (b, 2.7H, **-CH$_3$** in PHPMA), 1.53-2.20 (b, 2.1H, **-CH$_2$-** on polymer backbone), 2.72-3.06 (b, 0.1H, epoxy in PGlyMA), 3.54-3.73 (b, 0.9H, **-CH$_2$**OH in GMA and –**CH**(OH)- in PHPMA), 3.73-4.18 (b, 3.3H, remaining pendent protons in PGMA, PHPMA and PGlyMA).

2.2.13 Preparation of rhodamine B piperazine

Preparation of rhodamine B acid chloride

Rhodamine B (7.50 g, 16 mmol) was placed in a 50 mL single-neck round-bottomed flask under nitrogen and dissolved in thionyl chloride (7.50 mL, 12.3 g, 103 mmol). After stirring for 22 h, the thionyl chloride was removed *via* distillation at 100 °C. Once complete, the distillation head was removed and the solid was maintained under a flow of nitrogen overnight to remove residual thionyl chloride. The resulting solid was used without further purification and was stored in the dark in a freezer prior to use.

Reaction of rhodamine B acid chloride with piperazine

Piperazine (5.50 g, 64 mmol) was dissolved in dichloromethane (250 mL) and then rhodamine B acid chloride (4.00 g, 8.0 mmol) was added dropwise. The reaction mixture was stirred for 21 h and then the solvent was removed at 50 °C under reduced pressure. Diethyl ether (250 mL) was added to induce precipitation. The resulting solid was isolated by filtration, dissolved in water (200 mL) and acidified using 37 % w/w HCl. The aqueous phase was saturated with sodium chloride and extracted with 5 x 100 mL 1:2 dichloromethane/isopropanol mixture until colourless. The combined organic fractions were dried over anhydrous sodium sulphate, filtered, and the resultant liquor evaporated under vacuum. Finally, the crude rhodamine B piperazine was recrystallised in acetonitrile, filtered and dried under vacuum to give a purple solid. This reagent was used without further purification. TOF MS ES^+ m/z = 511 (MH+); ^{1}H NMR (400 MHz, CD_2CL_2): δ (ppm) = 0.5-1.6 (12H, CH_2-**CH_3**), 2.0-3.3 (7H, N-**CH_2**-**CH_2**-N). 3.3-4.2 (8H, N-**CH_2**-CH_3), 6.5-8.5 (10 H, aromatic,); ^{13}C NMR (400 MHz, JMOD, C_2D_6OS): δ (ppm) = 12 (CH_3, - polarity), 42-47 (CH_2, + polarity, 3 signals), 110-170 (aromatic, 13+ signals), 172 (C=O, + polarity). Note that TOF MS and NMR indicated traces of rhodamine B isopropanol impurity.

2.2.14 Reaction of HOOC-PGMA$_{43}$-P(HPMA$_{119}$-*stat*-GlyMA$_1$) with rhodamine B piperazine

A typical protocol for the preparation of rhodamine B piperazine-labelled HOOC-PGMA$_{43}$-P(HPMA$_{119}$-*stat*-GlyMA$_1$) is as follows: 5.00 g of a 10 % w/w HOOC-PGMA$_{43}$-P(HPMA$_{119}$-*stat*-GlyMA$_1$) worm gel (0.50 g copolymer, 20 µmol GlyMA) was weighed into a 20 mL vial equipped with a magnetic stirrer bar and was adjusted from approximately pH 3.5 to 8.0 using sodium hydroxide. This induces a worm-to-sphere transition, which in turn causes degelation. Rhodamine B piperazine (2.7 mg, 4.9 µmol; dye/epoxy molar ratio = 0.25) was added to the aqueous dispersion of spherical nanoparticles to give a dye label concentration of 1.0 mmol dm^{-3}. The reaction mixture was stirred overnight at 20°C. After 20 h, the fluorescently-labelled worm gel was dialysed against water for one week (with daily

changes of dialysate) so as to remove any unreacted dye. HPLC analysis of the unpurified labelled worms indicated that 90 % of the rhodamine B label was covalently grafted to the copolymer worms.

2.2.15 Instrumentation

^{1}H NMR spectra were recorded using a 500 MHz Bruker Avance-500 spectrometer (64 scans averaged per spectrum).

Gel Permeation Chromatography (GPC) was used to assess polymer molecular weight distributions. The DMF GPC set-up comprised of two Polymer Laboratories PL gel 5 μm Mixed-C columns connected in series to a Varian 390-LC multi-detector suite (refractive index detector) and a Varian 290-LC pump injection module operating at 60 °C. The GPC eluent was HPLC-grade DMF containing 10 mM LiBr at a flow rate of 1.0 mL min^{-1}. DMSO was used as a flow-rate marker. Calibration was conducted using a series of ten near-monodisperse poly(methyl methacrylate) standards (M_n = 625 to 2,480,000 g mol^{-1}). Chromatograms were analysed using Varian Cirrus GPC software (version 3.3).

Dynamic Light Scattering (DLS) studies were conducted using a Malvern Zetasizer NanoZS instrument at 25 °C. Measurements were performed on 0.10 % w/w aqueous in disposable cuvettes at a fixed back-scattering angle of 173^o. Intensity-average hydrodynamic diameters were calculated *via* the Stokes-Einstein equation. All data were averaged over three consecutive runs.

Aqueous electrophoresis measurements were conducted using a Malvern Zetasizer NanoZS instrument at 25 °C. Studies were performed on aqueous copolymer dispersions diluted to 0.10 % w/w containing 10^{-3} mol dm^{-3} KCl as background electrolyte. Zeta potentials were calculated from the Henry equation using the Smoluchowski approximation. All data were averaged over three consecutive runs.

Transmission Electron Microscopy (TEM) imaging was performed on a Phillips CM100 instrument at 100 kV, equipped with a Gatan 1 k CCD camera. Polymer dispersions were diluted 100-fold at 20 °C to generate 0.10 % w/w dispersions.

Images obtained at lower pH were prepared by diluting solutions in acidic water, which matched the pH of the concentrated dispersion (approximately pH 3.5). Copper/palladium TEM grids (Agar Scientific) were surface-coated in-house to yield a thin film of amorphous carbon. The grids were then plasma glow-discharged for 30 seconds to create a hydrophilic surface. Individual samples (0.10 % w/w, 12 μL) were adsorbed onto the freshly glow-discharged grids for one minute and then blotted with filter paper to remove excess solution. For contrast when imaging the aggregates, uranyl formate stain (0.75 % w/w, 9 μL) was placed on the sample-loaded grid for 20 s and then carefully blotted to remove excess stain. The grids were then dried using a vacuum hose.

Rheology studies were conducted using an AR-G2 stress controlled rheometer with a variable temperature Peltier plate. Storage moduli (G') were determined for the 10 % w/w HOOC-PGMA$_{56}$-HPMA$_{155}$ and CH_3OOC-PGMA$_{59}$-PHPMA$_{160}$ diblock copolymer worm gels at 25 °C at varying pH. Temperature dependent rheological studies were conducted from 25 °C to 4 °C to 25 °C with a temperature ramp rate of 0.5 °C min^{-1}. In all cases a cone-and-plate geometry (40 mm 2 ° aluminium cone) was used for these measurements at a fixed strain of 1.0 % and an angular frequency of 1.0 rad s^{-1} to allow comparisons between measurements.

High-Performance Liquid Chromatography (HPLC) chromatograms were acquired using a Shimadzu HPLC system consisting of an autosampler (Shimadzu SIL-20AXR), degasser (Shimadzu DGU-20A3), a solvent delivery module (Shimadzu CBM-20A), a diode array detector (Shimadzu SPD-M20A) and a 150 × 3.0 mm Jones chromatography Genesis C18 4 μ column. Samples were prepared as approximately 0.5 % solutions in methanol and 10 μL aliquots were injected. Conditions for measurements are as follows: initial eluent = 95:5 % v/v water/methanol mixture (initial aqueous phase containing 0.1 % trifluoroacetic acid); final eluent = 100 % methanol over 20 min, followed by equilibration for 10 min at the original initial eluent composition prior to injection of further samples. Absorbance was determined at a wavelength of 560 nm, which corresponds to the absorption maximum of the dye label.

Fluorescence Correlation Spectroscopy (FCS) measurements and analysis were conducted by Dr. C. Clarkson and Prof. M. Geoghegan (University of Sheffield). The data were acquired with an inverted LSM510 Meta confocal microscope with an attached ConFocor2 FCS module. The set-up was calibrated through the use of free Rhodamine B (RhB) dye, such that the pinhole dimensions, placement and the filters were optimised. Measurement of the diffusion time for RhB allowed for the calibration of the observation area. RhB is a standard fluorescent probe and as such has a well-known diffusion coefficient (see main text for further details). A Linkam FTIR600 stage with a T20 system controller was used to control temperature during FCS measurements when required. The sample was placed in a Ibidi μ-Dish$^{35mm, High}$ imaging dish. The temperature was cycled from room temperature down to the desired temperature for observation. The system was allowed to rest at this temperature for 5 min, the measurement was taken and the system was then returned to room temperature. For studies of the pH dependence, 400 μL of each solution was placed in a separate well of a Nunc Lab-Tek II 8 chamber slide. Once the sample is placed in the appropriate carrier, a 100 μL droplet of milliQ water was placed upon the objective lens and the carrier was mounted into the microscope with the standard microscope mounting. The objective was raised so that the focal volume could pass through the bottom of the carrier and into the bulk solution. Diffusion measurements were made in this position so that no interfaces were in the focal volume of the microscope. Each measurement was made for 6 s and repeated 150 times, with any measurements with count rates of less than 1 kHz being discarded. The LSM-FCS program provided by Carl Zeiss outputs the autocorrelation data as a plain text file. The data within this file were analysed using the software pro Fit (version 6.2, QuantumSoft). The data were then fitted to the autocorrelation function using the Levenberg-Marquardt algorithm. The diffusion time can then be used in conjunction with the focal volume dimensions to obtain the diffusion coefficient.

2.3 Results and Discussion

2.3.1 pH-responsive diblock copolymer worms due to RAFT end-groups

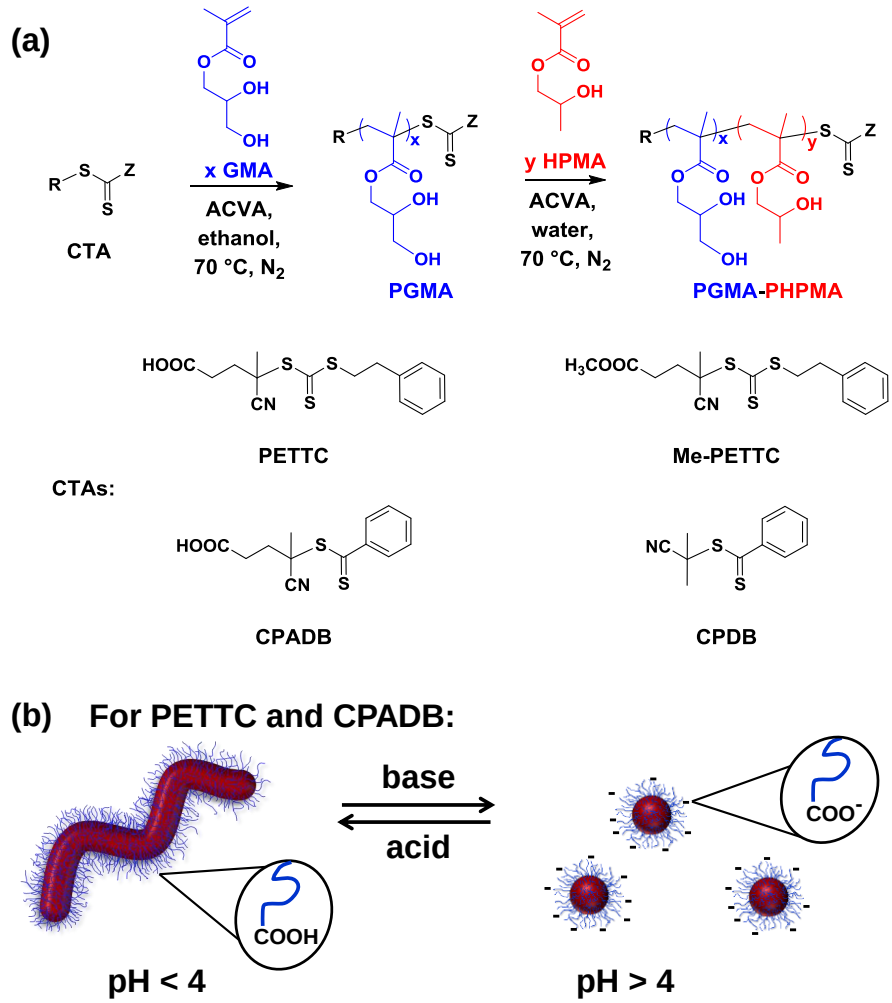

Figure 2.4 (a) A typical synthesis of a PGMA macro-CTA *via* RAFT solution polymerisation, and its subsequent chain extension with HPMA *via* RAFT aqueous dispersion polymerisation to form well-defined PGMA-PHPMA diblock copolymer nano-objects at pH 3.5. Such nano-objects demonstrate pH-responsive behaviour when a carboxylic acid-functionalised CTA is used (b) Illustration of the reversible worm-to-sphere transition that occurs when COOH-functionalised worms are subjected to a pH switch *via* addition of base.

Primarily, a $PGMA_{56}$ macro-CTA was prepared *via* RAFT solution polymerisation in ethanol using 4-cyano-4-(2-phenylethane sulfanylthiocarbonyl)

sulfanylpentanoic acid (PETTC) as a chain transfer agent (CTA), which possesses a terminal carboxylic acid group (**Figure 2.4a**). A typical ^{1}H NMR spectra of a PGMA macro-CTA is shown in **Figure 2.5a**. This near-monodisperse water-soluble macro-CTA was then chain-extended with HPMA *via* RAFT aqueous dispersion polymerisation (10 % w/w solids) at 70 °C and at approximately pH 3.5. Using the 'master phase diagram' previously shown in **Figure 1.25** (**section 1.7.2**), it is expected that chain-extending this macro-CTA with 155 units of HPMA will result in the formation of worms by PISA. The resulting $PGMA_{56}$-$PHPMA_{155}$ diblock copolymers produced an almost exclusive worm-like morphology, as expected. Very high (> 99 %) HPMA monomer conversions were observed by ^{1}H NMR analysis (see **Figure 2.5b**). Furthermore, DMF GPC analysis (see **Figure 2.6a**) indicated high blocking efficiency and a narrow molecular weight distribution (M_w/M_n < 1.20).

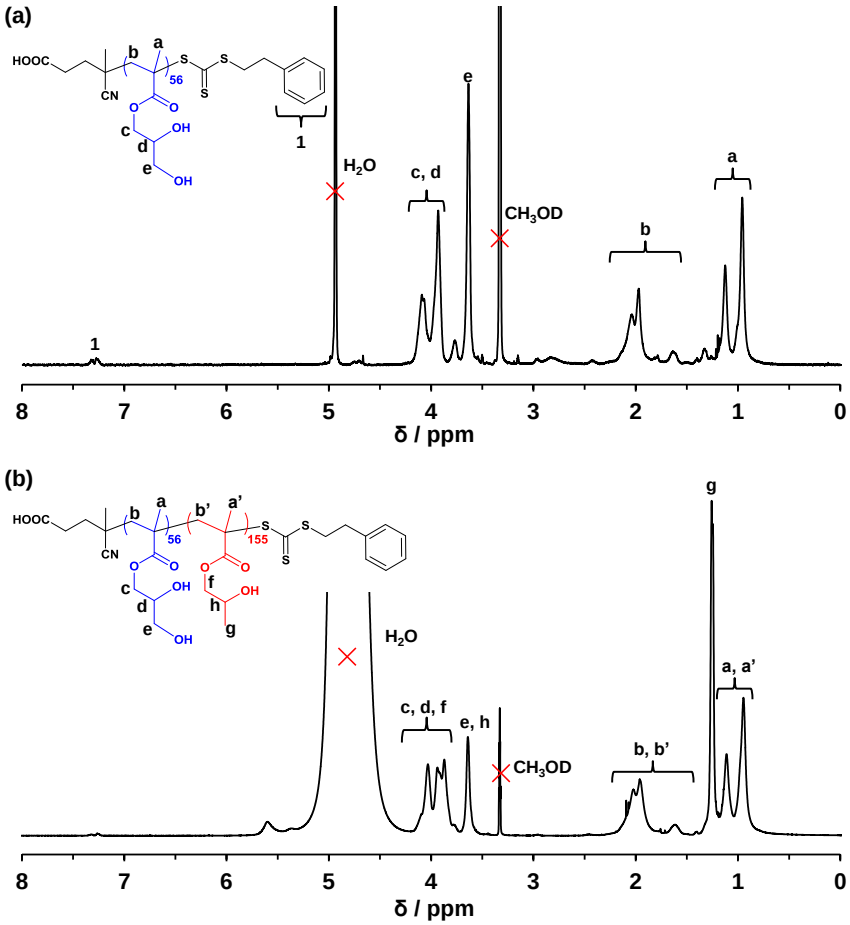

Figure 2.5 ^{1}H NMR spectra recorded in deuterated methanol for (a) freeze dried HOOC-$PGMA_{56}$ macro-CTA and (b) 10 % w/w HOOC-$PGMA_{56}$-$PHPMA_{155}$ diblock copolymer.

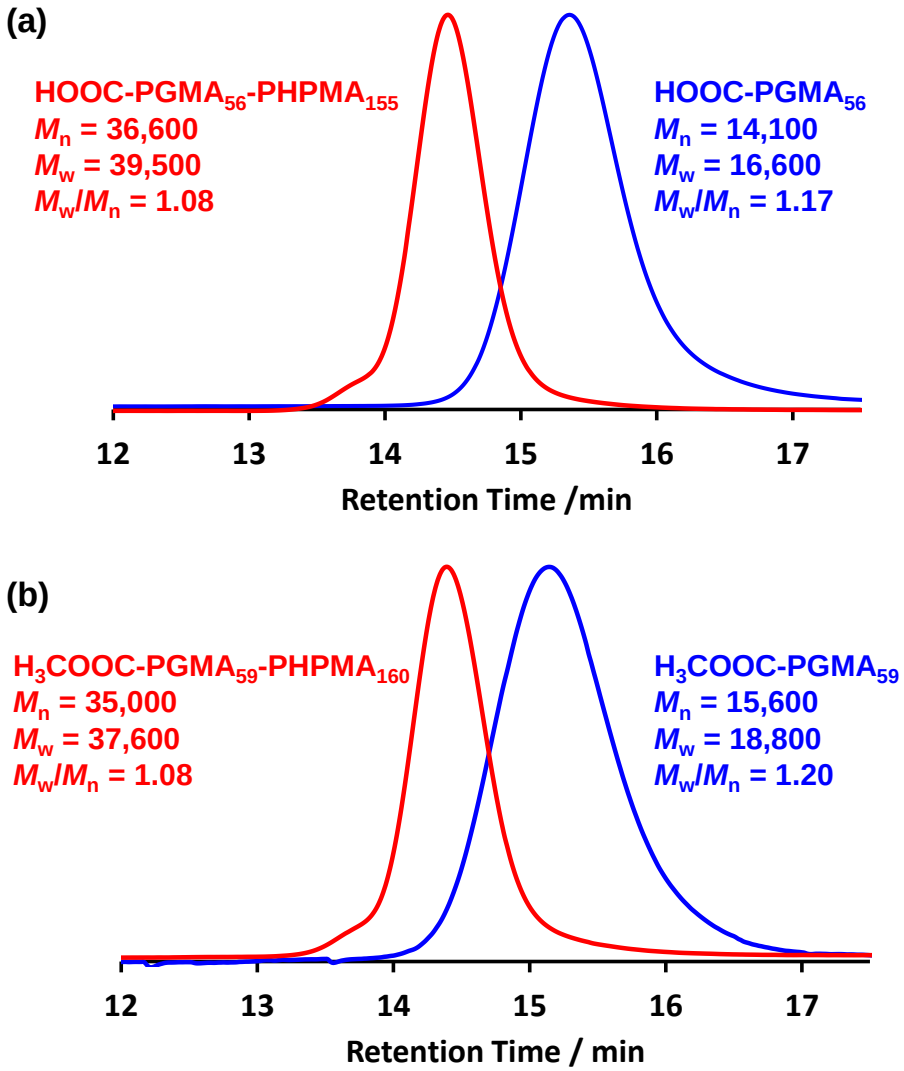

Figure 2.6 DMF gel permeation chromatographs obtained for (a) HOOC-PGMA$_{56}$ macro-CTA and the corresponding HOOC-PGMA$_{56}$-PHPMA$_{160}$ diblock copolymer and (b) H$_3$COOC-PGMA$_{59}$ macro-CTA and corresponding H$_3$COOC-PGMA$_{59}$-PHPMA$_{160}$ diblock copolymer. In both cases high blocking efficiencies and low final copolymer polydispersities were obtained.

TEM studies indicated a well-defined mean worm width of 21 nm, but the worm contour length was less well-controlled and ranged from 200 to 850 nm. The resulting HOOC-PGMA$_{56}$-PHPMA$_{155}$ diblock copolymer forms a soft, transparent worm gel at 10 % w/w solids in mildly acidic solution (pH < 4) due to multiple inter-worm contacts. Degelation occurs rapidly on cooling this gel. According to Blanazs *et al.*,[41] this is because the worms undergo an order-order transition to spheres as a

result of 'surface plasticisation' of the core-forming PHPMA block. It is thought this reduces the overall packing parameter, *p*, from the worm regime ($0.33 < p < 0.50$) to the sphere regime ($p < 0.33$), although these values were not calculated.[45] However, such non-ionic PGMA-PHPMA diblock copolymers also exhibit *pH-responsive behaviour*, with degelation being observed on increasing the solution pH from pH 3.5 to 6.0 using 0.1 M NaOH (**Figure 2.4b**, **Figure 2.7a** and **Figure 2.7b**). Furthermore, returning the solution pH to its original value using HCl resulted in reformation of the worms and hence regelation of the aqueous solution (see **Figure 2.7c** and **Figure 2.7d**). This reversible behaviour suggests that irreversible chemical degradation of the copolymer is an unlikely cause.

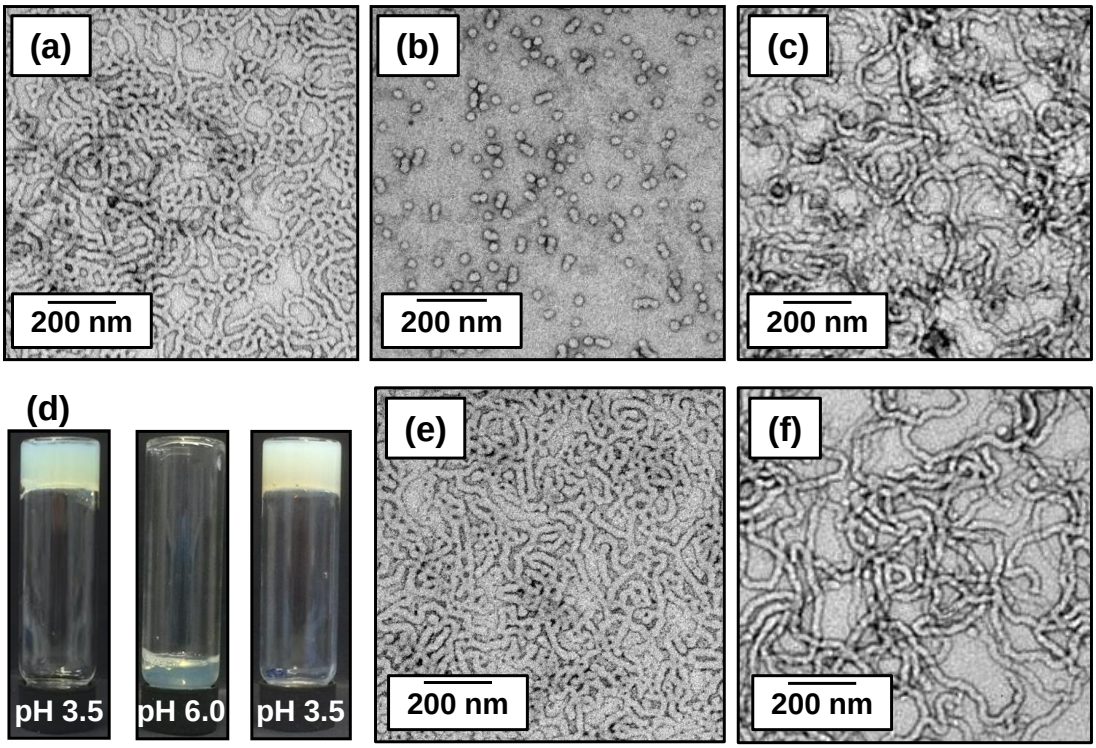

Figure 2.7 TEM images obtained from 0.1 % w/w dispersions of HOOC-$PGMA_{56}$-$PHPMA_{155}$ diblock copolymer nano-objects prepared using the carboxylic acid-functional PETTC RAFT agent for (a) pH 3.5 (initial worms); (b) pH 6.0 (spheres); (c) pH 3.5 (reformed worms after a pH cycle). (d) Digital images of the diblock copolymer nano-objects at 10 % w/w corresponding to images (a), (b) and (c) above. Control experiments: TEM images obtained for a H_3COOC-$PGMA_{59}$-$PHPMA_{160}$ diblock copolymer prepared using a *methylated* PETTC RAFT agent (Me-PETTC) at (e) pH 3.5 (worms) and (f) pH 6.0 (worms). Thus no worm-to-sphere transition is observed when the diblock copolymers are prepared using a non-ionic RAFT agent.

Acid titration studies of the HOOC-$PGMA_{56}$ macro-CTA in aqueous solution (see **Figure 2.8**) indicated that the pK_a of the terminal carboxylic acid group is approximately 4.7. Half of the acid residues are ionised when the solution pH is equal to this critical value. A small change in the solution pH around this value has a relatively large effect on the degree of ionisation. Therefore it was hypothesised that ionisation of the terminal carboxylic acid conferred by the PETTC CTA was the most likely explanation for the pH-responsive behaviour exhibited by the HOOC-$PGMA_{56}$-$PHPMA_{155}$ diblock copolymer. In order to further examine this hypothesis, control experiments were performed using a *methylated* PETTC RAFT agent (Me-PETTC) to prepare a PGMA macro-CTA with a mean DP of 59, which was subsequently chain-extended with HPMA to produce an analogous near-monodisperse H_3COOC-$PGMA_{59}$-$PHPMA_{160}$ diblock copolymer (see **Figure 2.6b**). Diblock copolymers of similar compositions were targeted so as to minimise any molecular weight effects of this pH-responsive phenomenon.

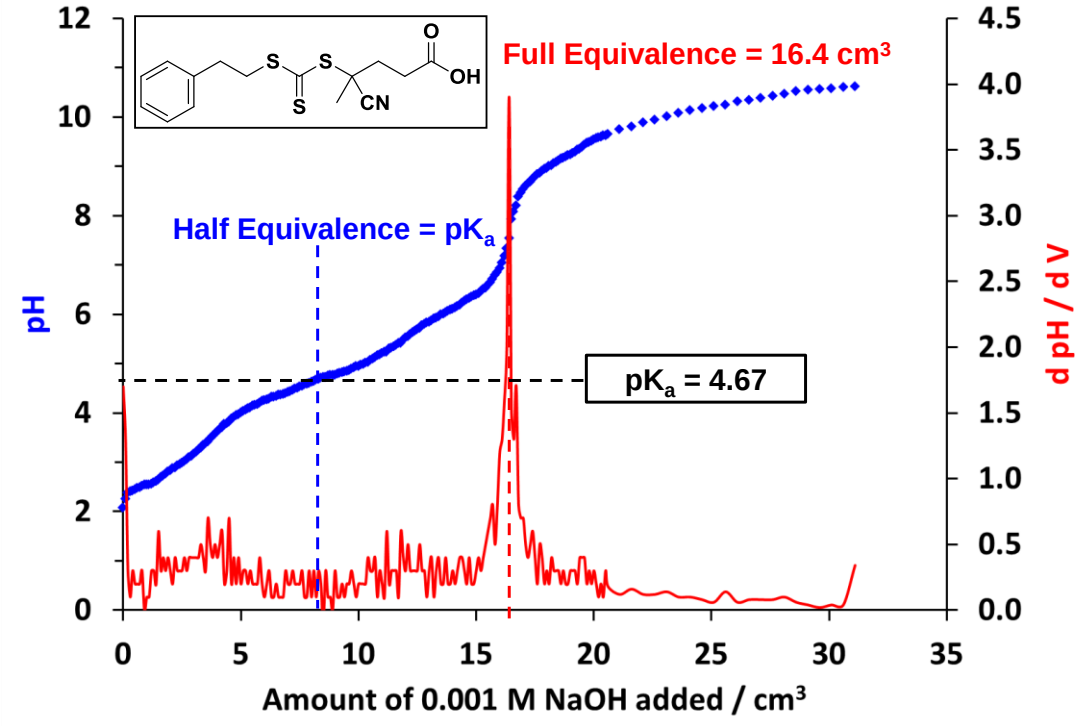

Figure 2.8 Acid titration curve obtained for the HOOC-$PGMA_{56}$ macro-CTA. The pK_a of 4.67 is consistent with that expected for an isolated carboxylic acid end-group.

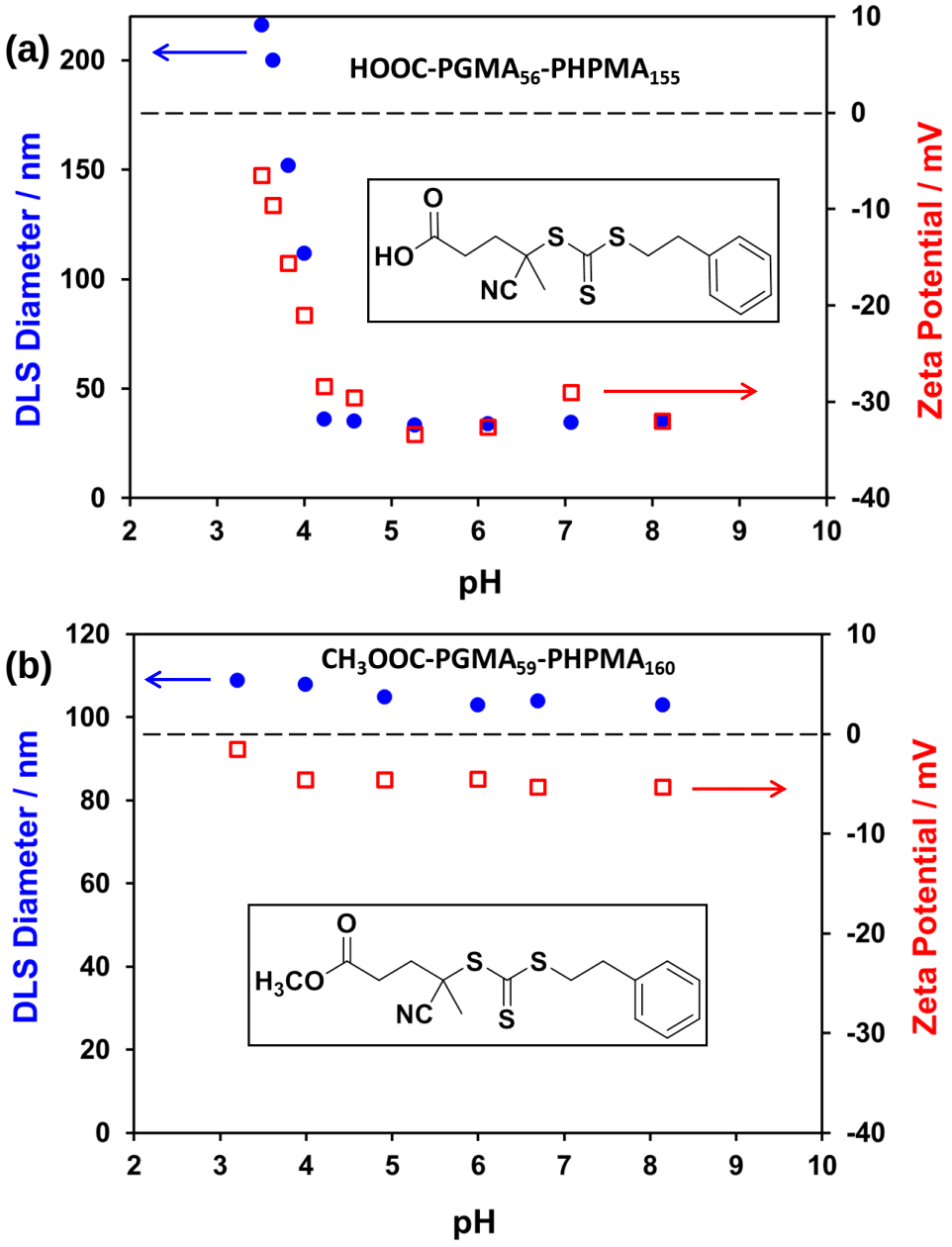

Figure 2.9 Variation of hydrodynamic particle diameter and zeta potential with solution pH recorded at 25 °C for 0.1 % w/w aqueous dispersions of: (a) HOOC-$PGMA_{56}$-$PHPMA_{155}$ pH-responsive worms and (b) H_3COOC-$PGMA_{59}$-$PHPMA_{160}$ pH-insensitive worms.

TEM studies of the H_3COOC-$PGMA_{59}$-$PHPMA_{160}$ diblock copolymer confirmed that the original worm copolymer morphology remained intact at 20 °C regardless of the solution pH (see **Figure 2.7e** and **Figure 2.7f**). In a further series of experiments, dynamic light scattering (DLS) and zeta potential studies were

conducted at varying dispersion pH values for the HOOC-$PGMA_{56}$-$PHPMA_{155}$ and H_3COOC-$PGMA_{59}$-$PHPMA_{160}$ diblock copolymer worms prepared using either the PETTC or Me-PETTC RAFT agents, respectively (**Figure 2.9**).

The significant reduction in apparent particle diameter from 220 nm to 40 nm observed on increasing the solution pH from pH 3.5 to pH 6.0 for HOOC-$PGMA_{56}$-$PHPMA_{155}$ provides good evidence for a worm-to-sphere transition (see **Figure 2.9a**) and was supported by TEM studies (see **Figure 2.7a** and **Figure 2.7b**). It is noteworthy that when analysing the initial copolymer worms, DLS only reports an apparent spherical-average diameter, rather than the actual mean worm length or width. Conversely, DLS provides a reliable estimate for the mean diameter of the copolymer spheres. The critical pH observed for the worm-to-sphere transition appears to be close to the pK_a of the terminal carboxylic acid. It is also emphasised that ionisation of this end-group leads to significantly greater anionic character for the nano-objects (from -5 mV for the original worms at pH 3.5 to around -30 mV for the spheres at pH 5-8). It is likely the significant charge, resulting from the ionisation of only a single carboxylic acid group at the end of each PGMA-PHPMA chain, increases the degree of hydrophilicity of the stabiliser block sufficiently and lowers the packing parameter, *p*, from the worm regime to the sphere regime.[45,47] Furthermore, electrostatic repulsion between the carboxylic acid end-groups is likely to cause an increase in surface curvature, which favours lower order morphologies. Hence, an order-order morphological transition is induced. This subtle end-group effect serves to illustrate the rather delicate hydrophilic-hydrophobic balance (or relatively narrow *p* range) that is required for the worm morphology. Further evidence to support this end-group ionisation effect was obtained by examining the effect of added salt on the pH-responsive behaviour. A HOOC-$PGMA_{56}$-$PHPMA_{155}$ gel synthesised in the presence of 100 mM KCl at pH 3.4 *remained* a gel on switching the solution pH to pH 7.5, as judged by the tube inversion test (see **Figure 2.10**). Electrophoresis and DLS studies indicate the presence of weakly anionic worms (apparent diameter = 212 nm; zeta potential ~ –5.7 mV at pH 7.5). Thus the anionic charge arising from ionisation of the terminal carboxylic acid group on each copolymer has been screened by adding salt. Hence, the worm-to-sphere transition is not observed under these conditions.

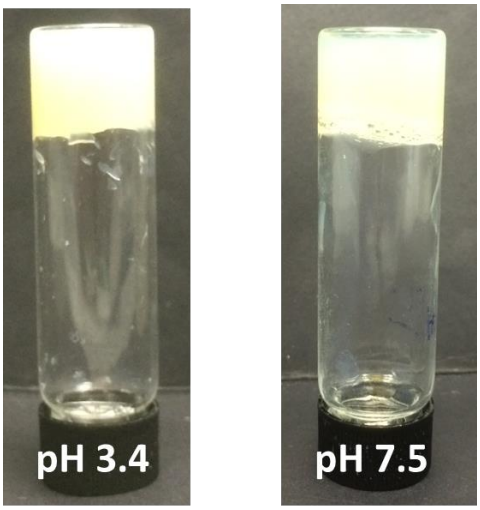

Figure 2.10 Digital images obtained for a HOOC-PGMA$_{56}$-PHPMA$_{155}$ worm gel synthesised in the presence of 100 mM KCl at an initial pH of 3.4 (left-hand image) and after adjusting the pH to 7.5 (right-hand image). The tube inversion test confirms that this sample remains a free-standing gel on increasing the pH, which indicates that no worm-to-sphere transition occurs in the presence of sufficient added salt.

As expected, DLS and aqueous electrophoresis studies of the analogous H_3COOC-PGMA$_{59}$-PHPMA$_{160}$ diblock copolymer worms prepared using the Me-PETTC RAFT agent over the same pH range exhibit minimal change in either particle size and zeta potential (see **Figure 2.9b**). This indicates that these worms are pH-insensitive, since they contain no terminal ionisable COOH group.

Rheology studies were conducted on 10 % w/w HOOC-PGMA$_{56}$-PHPMA$_{155}$ (blue data) and H_3COOC-PGMA$_{59}$-PHPMA$_{160}$ (red data) diblock copolymer dispersions at 25 °C as a function of solution pH (see **Figure 2.11**). Prior to this a strain sweep was conducted on the two worm gels at a fixed angular frequency of 1.0 rad s^{-1} to ensure the rheological conditions were in the linear viscoelastic regime (see Appendix for data). From this it was decided to conduct all subsequent rheological experiments at a fixed strain of 1.0 % and a fixed angular frequency of 1.0 rad s^{-1}. At around pH 3.7, both copolymers formed soft, free-standing worm gels with G' values of around 100 Pa, which is comparable to that reported by Blanazs *et al.* for a closely related PGMA$_{54}$-PHPMA$_{140}$ worm gel under similar rheological conditions.[42] Increasing the solution pH to 4.8 or above led to a dramatic reduction in G' for the HOOC-PGMA$_{56}$-PHPMA$_{155}$ diblock copolymer, in agreement with a gel to liquid

transition (see blue data). On returning to the original pH, regelation was observed and a G' comparable to the original value was obtained. In marked contrast, the G' of the H_3COOC-$PGMA_{59}$-$PHPMA_{160}$ diblock copolymer stayed reasonably constant from pH 4.1 to 7.5 and back to 3.4 (red data). Thus these gel rheology observations made at 10 % w/w solids are fully consistent with the TEM, DLS and aqueous electrophoresis studies of highly dilute (0.1 % w/w) copolymer dispersions. Furthermore, this further supports the hypothesis that end-group ionisation alone can be sufficient for non-ionic diblock copolymer nano-objects to exhibit to a reversible worm-to-sphere transition. Such observations, can be extended further to pH-sensitive vesicles based on non-ionic HOOC-$PGMA_{43}$-$PHPMA_{175\text{-}250}$ diblocks copolymers prepared with PETTC, which will discussed in more detail in Chapter 3.

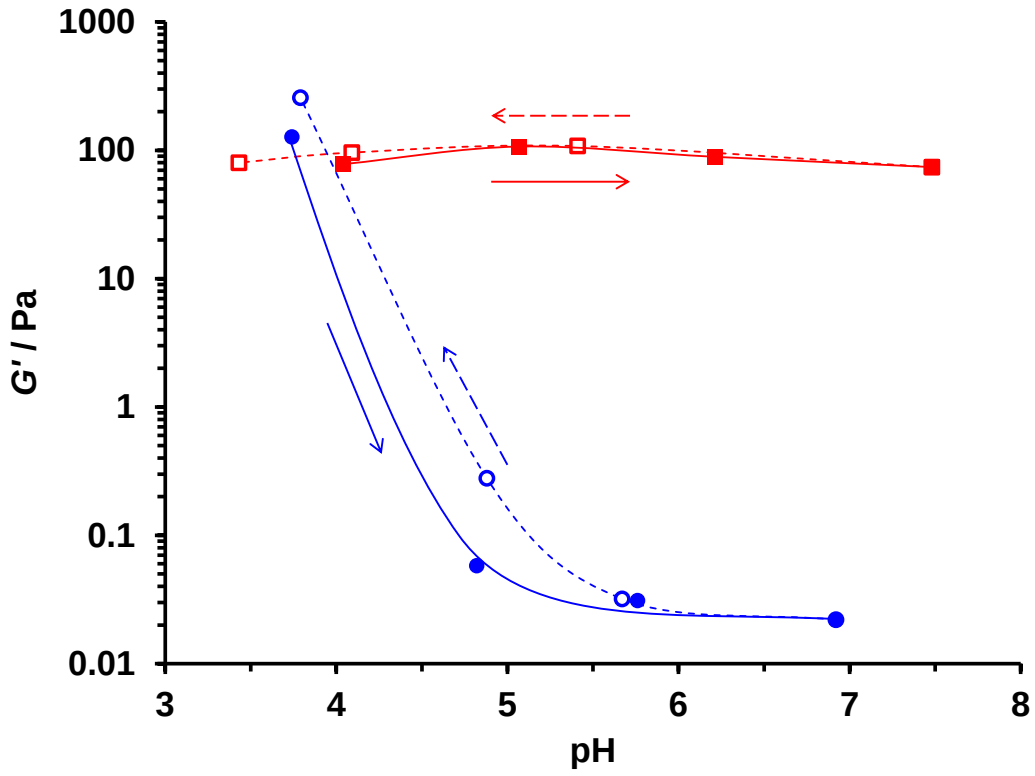

Figure 2.11 Variation in gel storage modulus (G') with solution pH from 3.7 to 6.9 at 25 °C for HOOC-$PGMA_{56}$-$PHPMA_{155}$ diblock copolymer worm/sphere dispersion at 10% w/w (closed blue circles), followed by a switch back to pH 3.8 (open blue circles). As a control experiment, a H_3COOC-$PGMA_{59}$-$PHPMA_{160}$ diblock copolymer worm gel showed essentially no change in the storage modulus, G', from pH 3.4 to 7.5 (red square data). In each case the solid lines represent increasing pH, while the dotted lines represent decreasing pH.

As discussed in the **section 2.1**, the thermo-responsive behaviour of PGMA-PHPMA diblock copolymer worm gels has previously been thoroughly studied.[42,43] Upon cooling PGMA-PHPMA diblock copolymer nano-objects undergo a worm-to-sphere order-order morphological transition due to 'surface plasticisation' of PHPMA core. This morphology transformation is also accompanied by de-gelation at lower temperatures, as confirmed by temperature dependant rheological studies.

As expected, the original HOOC-$PGMA_{56}$-$PHPMA_{155}$ and H_3COOC-$PGMA_{59}$-$PHPMA_{160}$ diblock copolymer worms display similar thermo-responsive behaviour at pH 3.5 (see **Figure 2.12a** and **d**). In both cases degelation is observed on cooling to 5 °C, as judged by the point where the loss modulus (G") exceeds G', known as CGT. After switching the solution pH from 3.5 to 6.0 for HOOC-$PGMA_{56}$-$PHPMA_{155}$, G' and G" reduce by 3 orders of magnitude. Furthermore, G" exceeds G' (indicating a free-flowing fluid) and remain relatively constant from 25 °C to 5 °C to 25 °C (see **Figure 2.12b**). On returning the pH to 3.5 from 6.0, HOOC-$PGMA_{56}$-$PHPMA_{155}$ diblock copolymer nano-objects re-gel and regain similar thermo-responsive behaviour to the original gel (see **Figure 2.12c**). Conversely, H_3COOC-$PGMA_{59}$-$PHPMA_{160}$ diblock copolymer worm-gels remain thermo-responsive irrespective of solution pH, as judged by the temperature sweeps conducted at pH 3.5 and 6.0 (see **Figure 2.12d** and **e**). However, a greater degree of hysteresis is observed, particularly at pH 6.0. It is emphasised that PGMA-PHPMA diblock copolymer worm gels prepared using an acid-functionalised RAFT agent are reversibly pH- and thermo-responsive. If the same diblock copolymer is prepared using a neutral RAFT only thermo-responsive behaviour is observed.

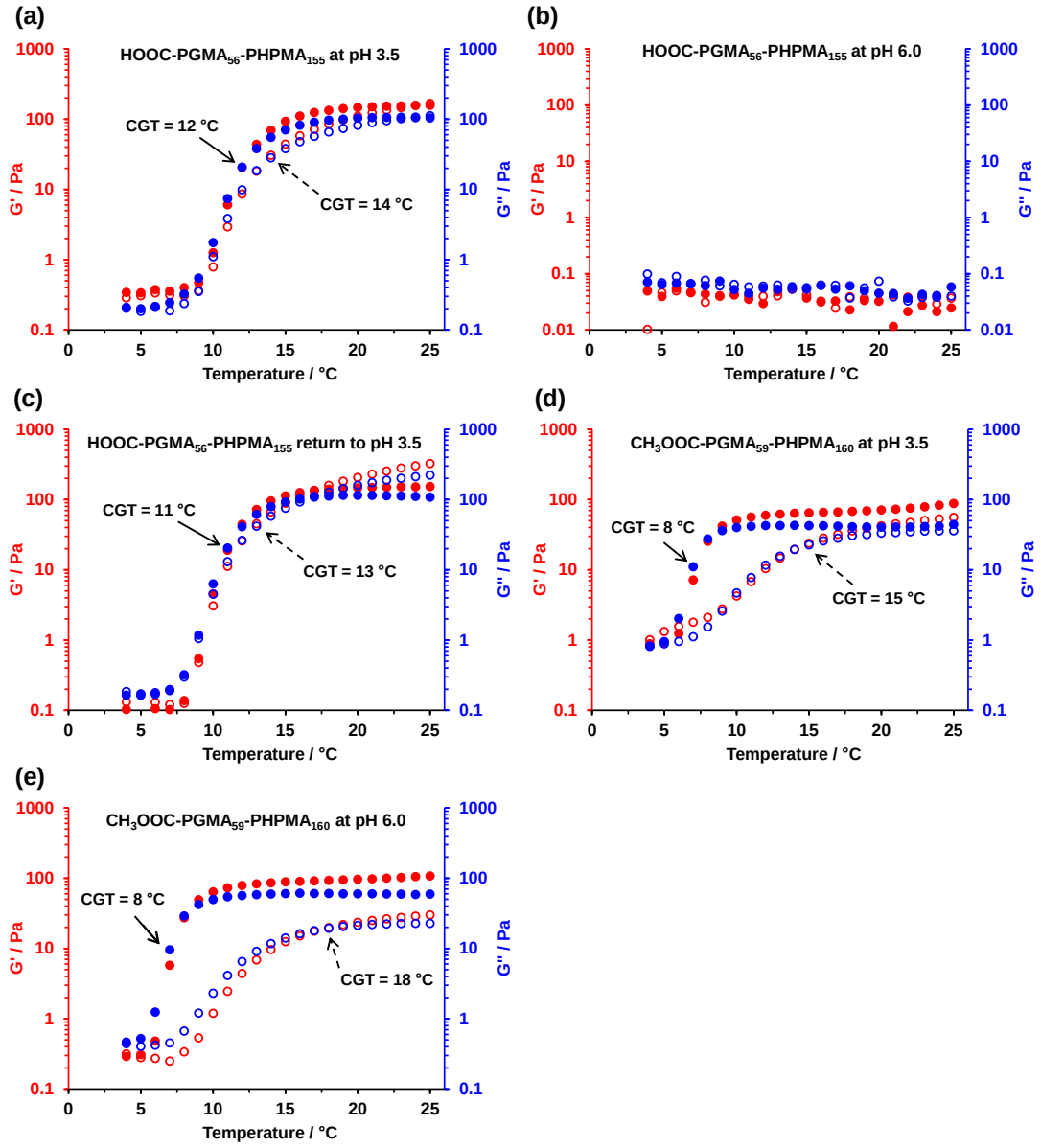

Figure 2.12 Temperature dependence of the storage modulus (G'; red data sets) and the loss modulus (G"; blue data sets) for a 10 % w/w aqueous dispersion of HOOC-$PGMA_{56}$-$PHPMA_{155}$ diblock copolymer nano-objects at (a) pH 3.5, (b) pH 6.0 and (c) after a pH cycle from 3.5 to 6.0 to 3.5 and H_3COOC-$PGMA_{59}$-$PHPMA_{160}$ diblock copolymer worms at (d) pH 3.5 and (e) pH 6.0. Closed circles denote the cooling cycle and the open cycles denote the heating cycle. Conditions: frequency = 1.0 rad s^{-1}; applied strain = 1.0 % and a heating/cooling rate of 0.5 °C min^{-1}. The cross-over of the G' and G" curves indicate the critical gelation temperature (CGT).

Similar pH-responsive behaviour is observed for PGMA-PHPMA diblock copolymer worms prepared using commercially available acid-functionalised and

neutral dithiobenzoate RAFT agents. More specifically, a HOOC-PGMA$_{60}$ macro-CTA and a Me-PGMA$_{57}$ macro-CTA have been prepared by RAFT solution polymerisation in ethanol using 4-cyano-4-(phenylcarbonothioylthio) pentanoic acid (CPADB) and 2-cyano-2-propyl dithiobenzoate (CPDB) CTAs, respectively. Both PGMA macro-CTAs were subsequently chain extended with HPMA by RAFT aqueous dispersion polymerisation to afford HOOC-PGMA$_{60}$-PHPMA$_{175}$ and Me-PGMA$_{57}$-PHPMA$_{155}$ diblock copolymer worms, which form free standing gels at room temperature. DMF GPC traces obtained for the PGMA macro-CTAs and the PGMA-PHPMA diblock copolymers indicate low polydispersities (M_w/M_n) and high blocking efficiencies (see **Figure 2.13**).

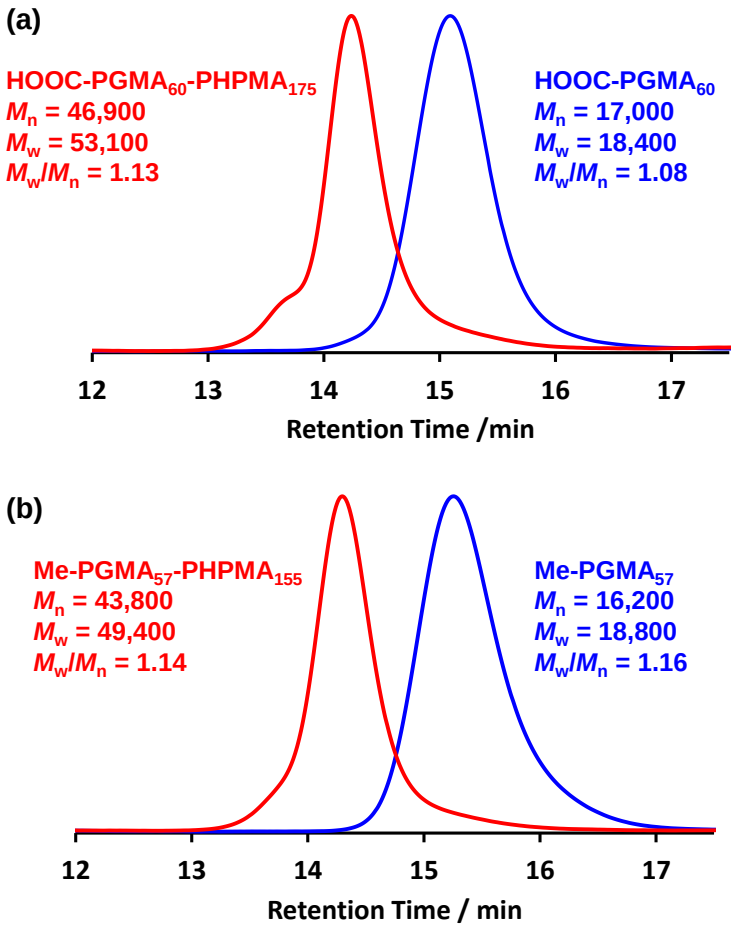

Figure 2.13 DMF GPC traces obtained for (a) HOOC-PGMA$_{60}$ macro-CTA prepared using CPADB and the corresponding HOOC-PGMA$_{60}$-PHPMA$_{175}$ diblock copolymer and (b) Me-PGMA$_{57}$ macro-CTA and corresponding Me-PGMA$_{57}$-PHPMA$_{155}$ diblock copolymer. In both cases high blocking efficiencies and low final copolymer polydispersities were obtained.

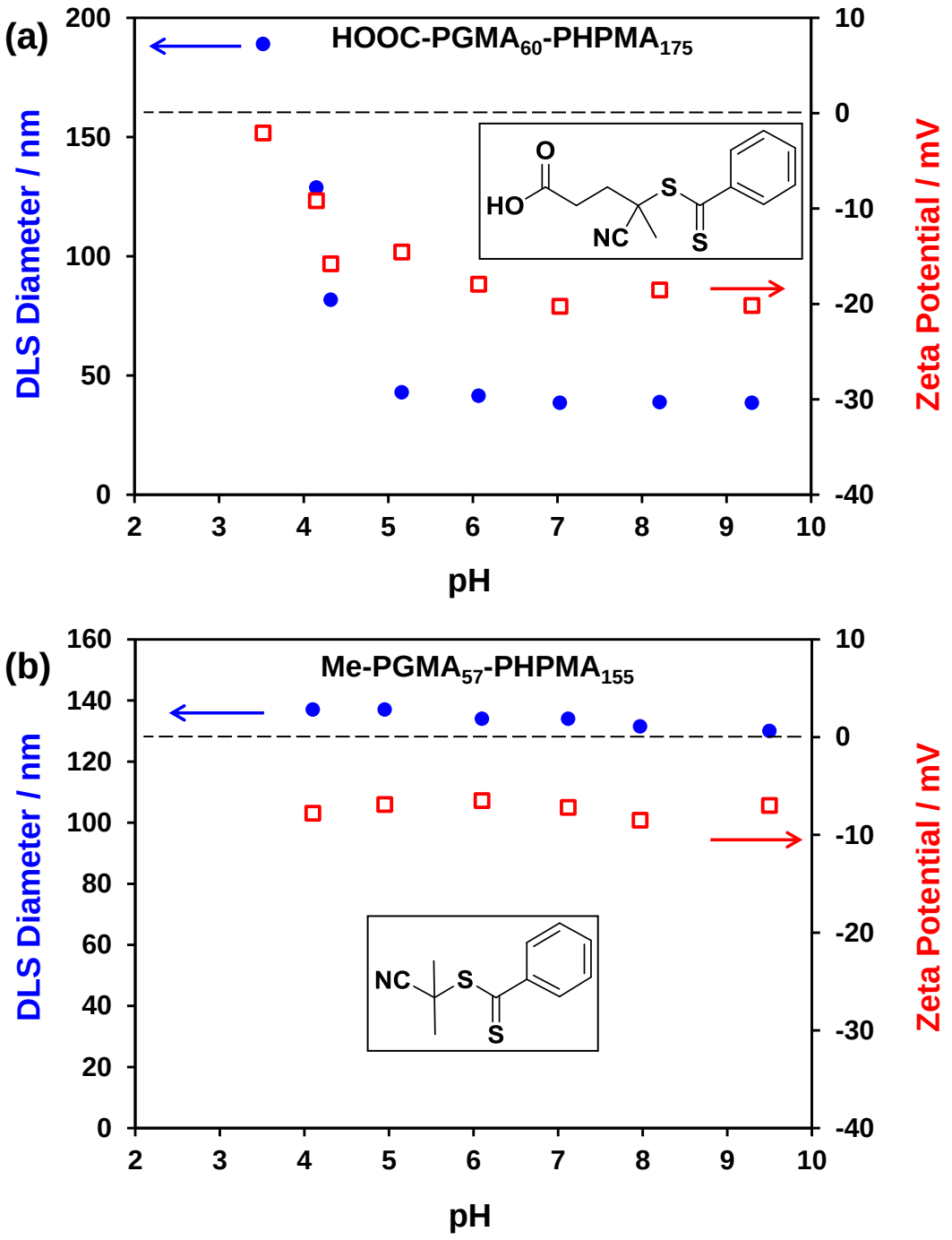

Figure 2.14 Variation of hydrodynamic particle diameter and zeta potential with solution pH recorded for 0.1% w/w aqueous dispersions of (a) HOOC-PGMA$_{60}$-PHPMA$_{175}$ pH-responsive worms and (b) Me-PGMA$_{57}$-PHPMA$_{155}$ pH-insensitive worms.

DLS studies conducted on dilute (0.1 % w/w) HOOC-PGMA$_{60}$-PHPMA$_{175}$ diblock copolymer worms at variable pH show a significant drop in diameter from 180 nm at pH 3.5 to 40 nm at pH 6.0, suggesting a worm-to-sphere transition (**Figure 2.14a**). TEM images obtained for HOOC-PGMA$_{60}$-PHPMA$_{175}$ diblock copolymers at pH 3.5 and pH 6.0 confirm the presence of worms and spheres, respectively (see **Figure 2.15a** and **b**). Furthermore, the order-order transition takes place at a similar pH to that of the pK_a of the terminal carboxylic acid, which in this case was measured to be 4.2. Similar to previous observations, aqueous electrophoretic studies of the HOOC-PGMA$_{60}$-PHPMA$_{175}$ diblock copolymer nano-objects confirm a reduction in the zeta potential from -2 mV at pH 3.5 to -20 mV at pH 6.0. This is likely to be due to the ionisation of the terminal COOH group on the PGMA stabiliser block. In contrast, the sphere equivalent hydrodynamic diameter of the neutral Me-PGMA$_{57}$-PHPMA$_{155}$ diblock copolymer worms remains at roughly 135 nm from pH 4.0 to pH 9.0 (see **Figure 2.14b**). Similarly, the zeta potential remains fixed at approximately -10 mV over the same pH range. Furthermore, TEM images obtained at pH 6.0 of Me-PGMA$_{57}$-PHPMA$_{155}$ confirm the presence of a predominantly worm-like morphology (**Figure 2.15c**).

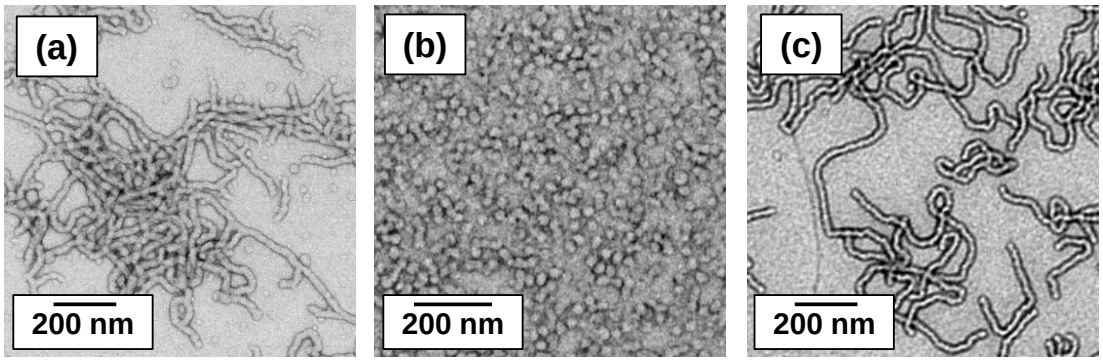

Figure 2.15 Representative TEM images obtained of HOOC-PGMA$_{60}$-PHPMA$_{175}$ diblock copolymer worms diluted to 0.1 % w/w in water at (a) pH 3.5 and (b) pH 6.0. (c) TEM image of Me-PGMA$_{57}$-PHPMA$_{155}$ diblock copolymer worms at pH 6.0.

2.3.2 Fluorescently-labelled pH- and thermo-responsive diblock copolymer worm gels

Fluorescently-labelled polymers and polymeric nano-objects are used for a wide range of applications such as visualisation of particles by confocal microscopy and determination of the fate of macromolecules in biological systems.[48,49] There have been many reports of the synthesis of fluorescently-labelled polymeric nanoparticles, but few have been conducted at high copolymer concentrations (i.e., 10 % w/w solids).[50]

In this study a fluorescently-labelled dual pH- and thermo-responsive diblock copolymer worm gel was prepared by covalently attaching rhodamine B piperazine dye to the core of the particles (**Figure 2.16**). More specifically, a HOOC-PGMA$_{43}$ macro-CTA was prepared by RAFT solution polymerisation in ethanol using PETTC as the CTA. PISA was utilised to produce a free-standing worm gel at 10 % w/w solids by chain-extending this HOOC-PGMA$_{43}$ macro-CTA with 119 units of HPMA and 1 unit of glycidyl methacrylate (GlyMA) *via* RAFT aqueous dispersion copolymerisation. The epoxy group in the GlyMA residues can be readily ring-opened by a reaction with primary or secondary amines.[51] Hence, an amine-functionalised rhodamine B piperazine was prepared (see **section 2.2.13** in the experimental section for this synthesis) and was added to the diblock copolymer worms at pH 8 (4:1 GlyMA/dye molar ratio, equivalent to a 1 mM rhodamine B concentration). This fluorescently-labelled HOOC-PGMA$_{43}$-P(HPMA$_{119}$-*stat*-GlyMA$_1$) was purified by dialysis, followed by freeze-drying and reconstitution to 10 % w/w solids in water at pH 3.9. High-performance liquid chromatography (HPLC) analysis of the rhodamine B piperazine-labelled P(HPMA$_{119}$-*stat*-GlyMA$_1$) copolymer before purification indicated that more than 90 % of the rhodamine dye was attached to the copolymer (see **Figure 2.17**).

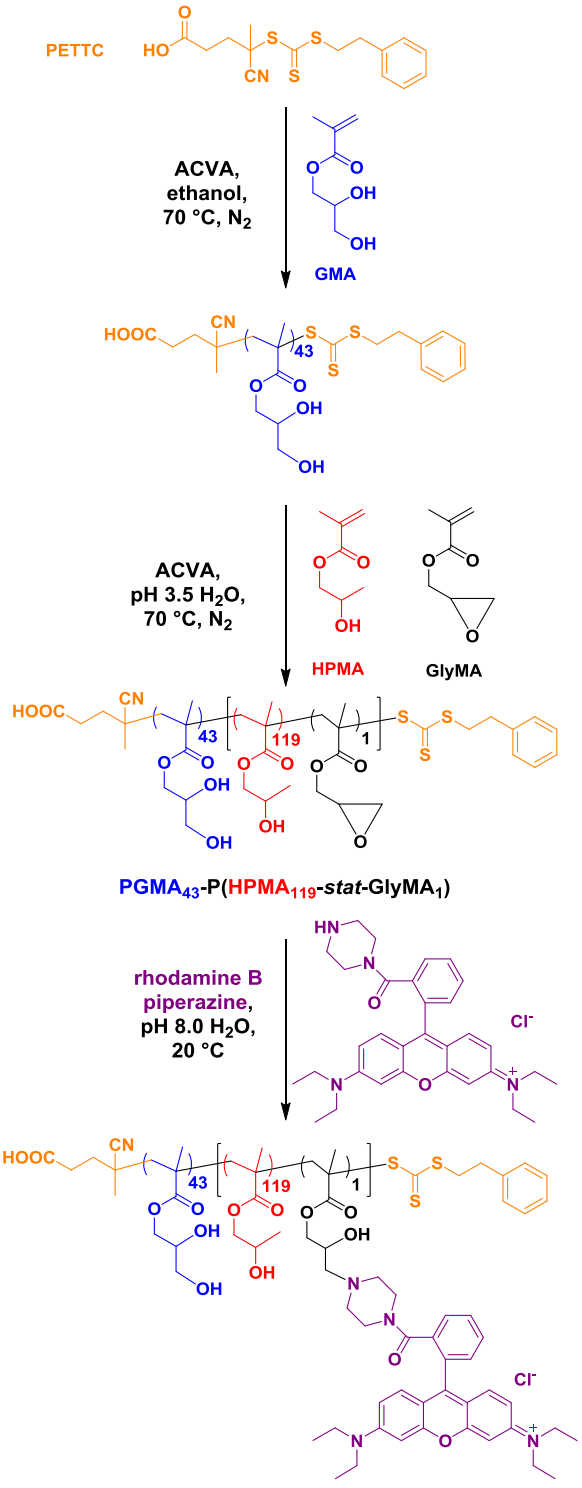

Figure 2.16 Synthesis of a $PGMA_{43}$ macro-CTA *via* RAFT solution polymerisation using PETTC as the RAFT agent, and its subsequent chain extension using 1 unit of GlyMA and 119 units HPMA *via* RAFT aqueous dispersion copolymerisation to form $PGMA_{43}$-P($HPMA_{119}$-*stat*-$GlyMA_1$) diblock copolymer worms at pH 3.5. The cores of these worms can be fluorescently-labelled by reacting rhodamine B piperazine with the pendent epoxy groups in the GlyMA residues.

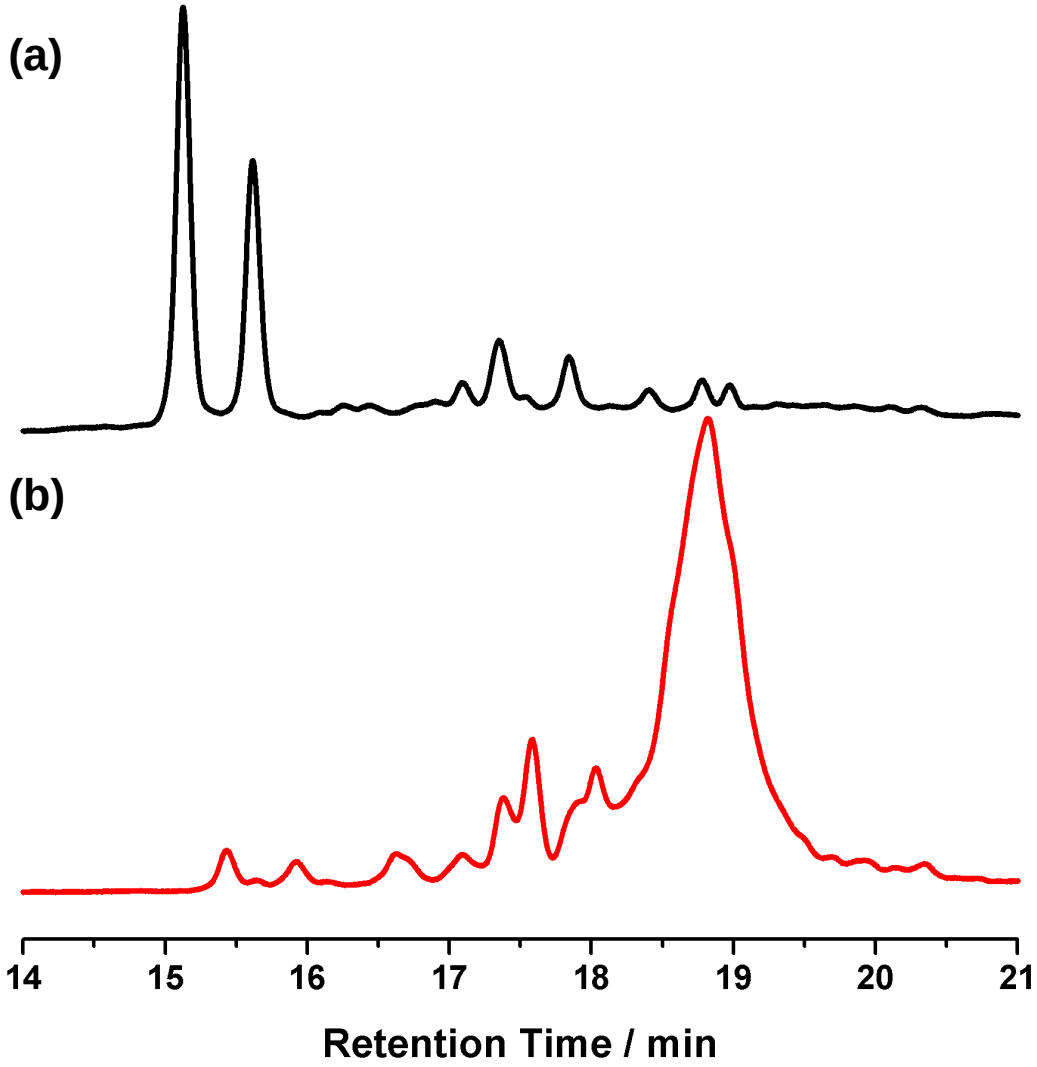

Figure 2.17 Chromatographs obtained by HPLC analysis (UV-visible detector operating at a wavelength of 560 nm) using a gradient eluent mixture (initially 95:5 % v/v water/methanol and finally pure methanol; initial aqueous phase contained 0.1 % trifluoroacetic acid) for: (a) rhodamine B piperazine dye precursor and (b) unpurified rhodamine B piperazine-labelled HOOC-PGMA$_{43}$-P(HPMA$_{119}$-*stat*-GlyMA$_1$) worm gel. This analytical protocol indicated that more than 90 % of the dye label was covalently grafted to the copolymer.

As discussed in **section 2.3.1**, dual pH- and thermo-responsive PGMA-PHPMA diblock copolymer worms can be prepared using a carboxylic acid-functionalised CTA. Upon increasing the solution pH from 3.5 to 6.0, or cooling from 20 to 5 °C, degelation is observed as a result of a worm-to-sphere transition. The former is due to ionisation of the terminal carboxylic acid group which increases

the hydrophilicity of the PGMA stabiliser (and likely some electrostatic repulsion), whereas cooling the worms results in surface plasticisation of the PHPMA core-forming block. It is noteworthy that replacing one unit of HPMA with GlyMA in the core does not affect the worm morphology, as judged by TEM images obtained from an acidic dilute dispersion (0.1 % w/w at pH 3.5) at 20 °C (see **Figure 2.18a**). Further TEM studies confirm that the HOOC-PGMA$_{43}$-P(HPMA$_{119}$-*stat*-GlyMA$_1$) diblock copolymer worms are both pH- and thermo-responsive as expected, undergoing a worm-to-sphere transition upon increasing the solution pH or cooling to 5 °C see **Figure 2.18b** and **c** respectively.

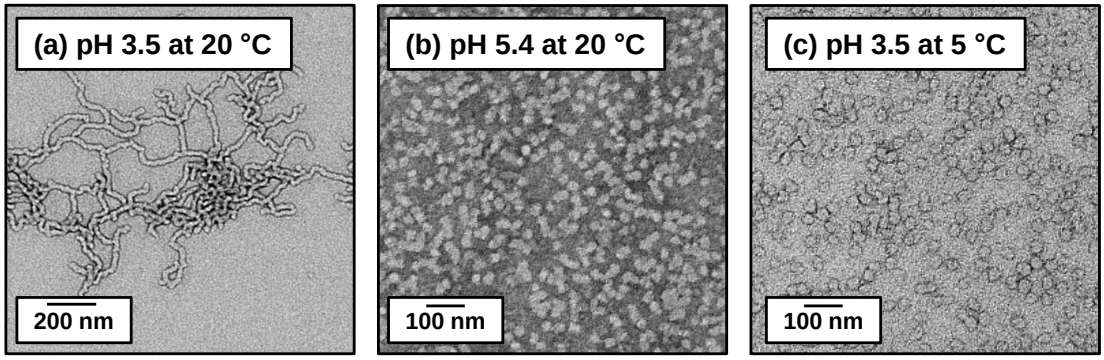

Figure 2.18 TEM images obtained for HOOC-PGMA$_{43}$-P(HPMA$_{119}$-*stat*-GlyMA$_1$) diblock copolymer nano-objects diluted to 0.1 % w/w at (a) pH 3.5 and 20 °C, (b) pH 5.4 at 20 °C and (c) pH 3.5 at 5 °C.

The worm-to-sphere transition of the HOOC-PGMA$_{43}$-P(HPMA$_{119}$-*stat*-GlyMA$_1$) diblock copolymer can be monitored by DLS as a function of pH or temperature (see **Figure 2.19**). As expected, a significant reduction in mean particle diameter is observed by either increasing the dispersion pH or reducing the temperature. Presumably, the apparent increase in particle diameter at low temperatures is due to the spheres dissociating to form unimers or weakly aggregated chains, since the derived count rates decrease by more than a factor of ten and the PDIs become significantly larger. Furthermore, previous small angle x-ray scattering studies conducted on PGMA$_{57}$-PHPMA$_{140}$ worms suggest dissolution to molecularly dissolved chains at low temperatures (-2 °C).[52]

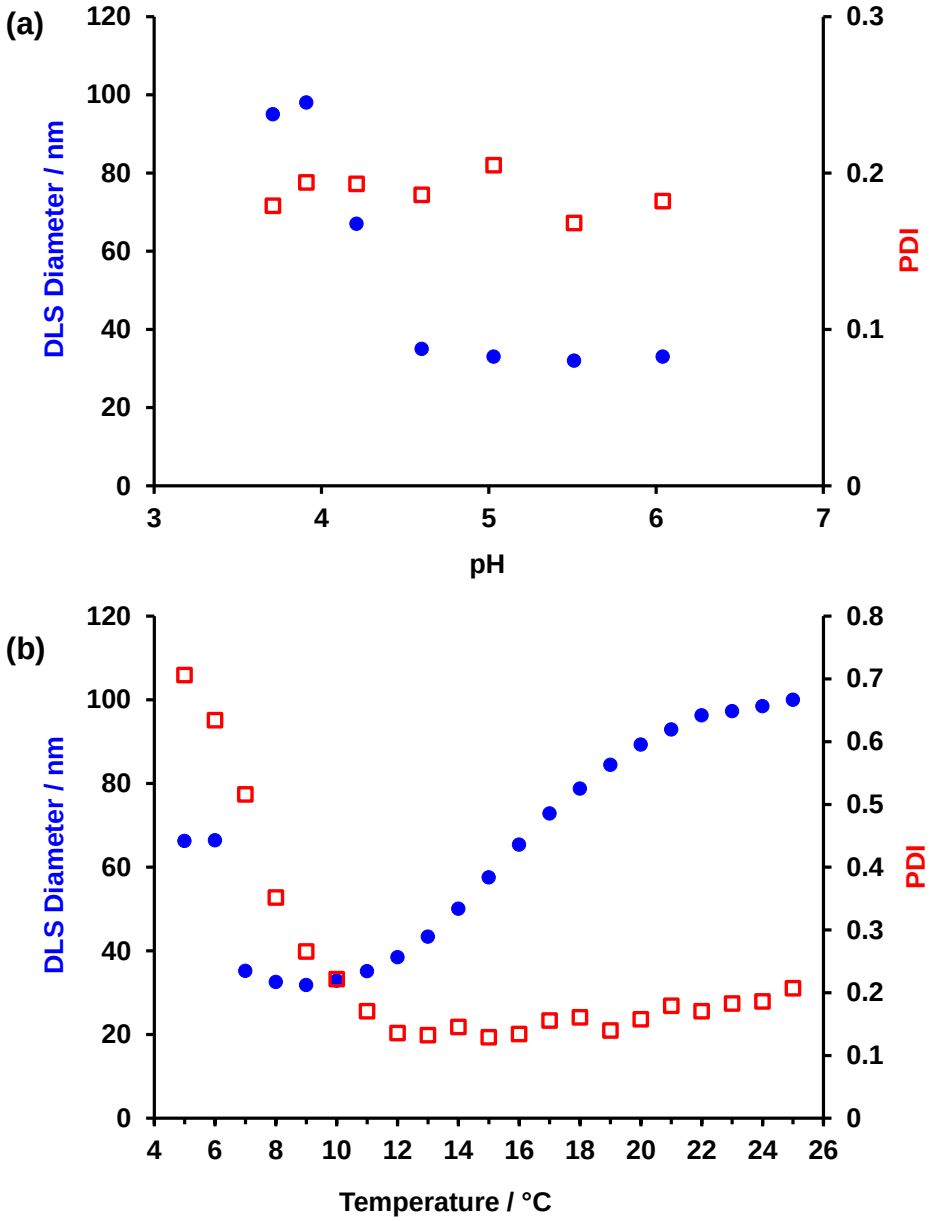

Figure 2.19 DLS diameter (blue closed circles) and polydispersity (PDI – red open squares) as a function of (a) solution pH at 25 °C and (b) temperature pH 3.5 for a 0.10 % w/w aqueous dispersion of HOOC-PGMA$_{43}$-P(HPMA$_{119}$-*stat*-GlyMA$_{1}$) diblock copolymer nano-objects.

Briefly, DLS involves determining the diffusion coefficient, *D*, of particles caused by Brownian motion by measuring fluctuations in light scattering. This diffusion coefficient can be used to calculate a sphere-equivalent diameter, *d*, using the Stokes-Einstein equation, which is given as follows:

$$D = \frac{k_B T}{3\pi\eta d} \quad (2.1)$$

Here K_b is the Boltzmann constant, T is the temperature and η is the solution viscosity and assumes that the particles are non-interacting. Therefore, measurements must be conducted on dilute dispersions (<< 1.0 % w/w). In contrast, fluorescence correlation spectroscopy (FCS) can be used to measure diffusion coefficients at relatively high copolymer concentrations by measuring fluctuations in fluorescence emission intensity. FCS is a powerful technique which makes use of a confocal experimental set-up to provide high spatial and temporal resolution. In collaboration with Dr. Clarkson and Prof. Geoghegan at the University of Sheffield, the pH- and temperature-induced worm-to-sphere transitions have been explored by FCS. Although I prepared the fluorescently-labelled worms, all FCS studies were conducted and analysed by these collaborators. In principle, the 10 % w/w HOOC-$PGMA_{43}$-P($HPMA_{119}$-*stat*-$GlyMA_1$) diblock copolymer worm gel should possess a relatively slow diffusion coefficient due to worm entanglements and/or multiple contacts, which prevent diffusion. Conversely, the equivalent spheres are free-flowing and diffuse much more freely. Unlike many fluorescence-based techniques (such as confocal microscopy), FCS requires very low fluorophore concentrations (10^{-6} – 10^{-9} M). This is because the technique is very sensitive to fluctuations in intensity and ideally only one dye molecule is present within the confocal volume at any given time. Therefore, the rhodamine B piperazine concentration is diluted to 10^{-9} M prior to analysis by FCS by mixing labelled and unlabelled HOOC-$PGMA_{43}$-P($HPMA_{119}$-*stat*-$GlyMA_1$) diblock copolymer worms together, whilst maintaining the copolymer concentration at 10 % w/w solids. As expected, inducing a worm-to-sphere transition by either raising the solution pH or decreasing the temperature results in higher diffusion coefficient (see **Figure 2.20**). More specifically, as the solution pH is increased above 4.0, the diffusion coefficient increases by eight-fold, indicating the worm-to-sphere transition (**Figure 2.20a**). Furthermore, the critical pH for this transition is in good agreement with previous findings (see **section 2.3.1**). Similarly, cooling the particles below 13 °C results in a four-fold increase in the

diffusion coefficient (**Figure 2.20b**). Moreover, temperature-dependent rheological studies (**Figure 2.21**) conducted on the 10 % w/w HOOC-PGMA$_{43}$-P(HPMA$_{119}$-*stat*-GlyMA$_1$) worm gel at pH 3.5 indicate a CGT of 13 °C, which is in excellent agreement with that indicated by the FCS studies.

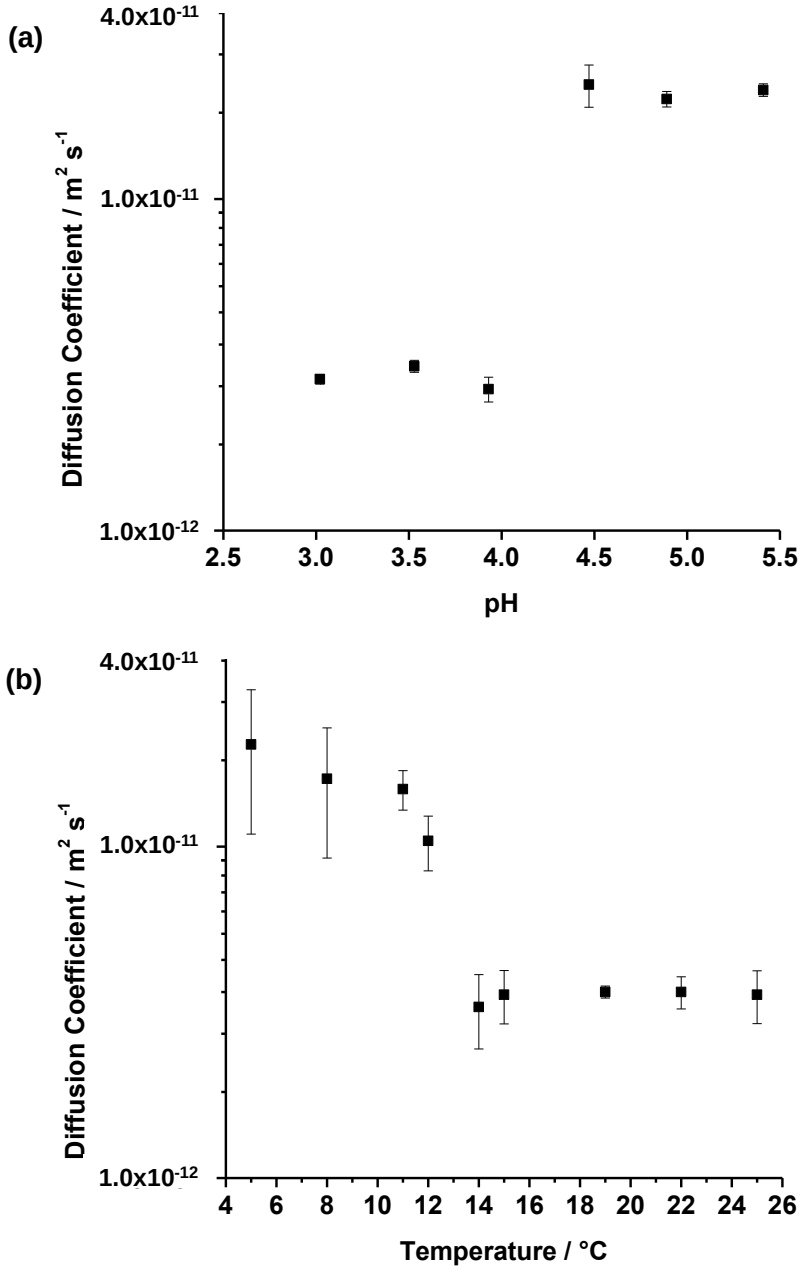

Figure 2.20 Diffusion coefficients determined by FCS for 10 % w/w dispersions of HOOC-PGMA$_{43}$-P(HPMA$_{119}$-*stat*-GlyMA$_1$) diblock copolymer nanoparticles as a function of (a) solution pH at 22 °C and (b) temperature at pH 3.5. The sharp transitions at approximately pH 4.2 and 13 °C, respectively, indicate the worm-to-sphere transition.

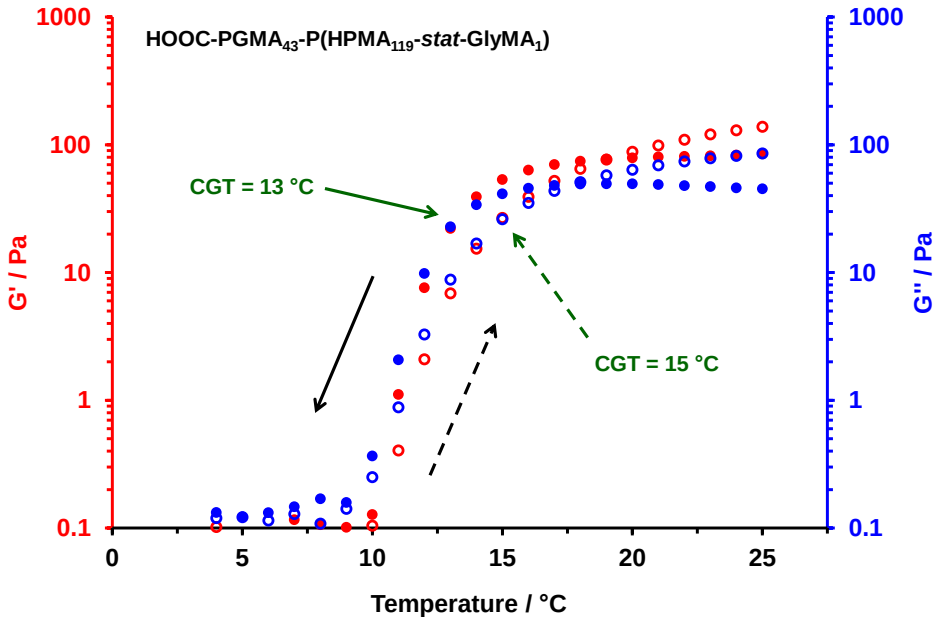

Figure 2.21 Variation in the storage modulus (G', red circles) and the loss modulus (G", blue circles) as a function of temperature for a 10 % w/w aqueous dispersion of HOOC-PGMA$_{43}$-P(HPMA$_{119}$-*stat*-GlyMA$_1$) worms. Closed circles denote a 25 °C to 5 °C temperature sweep and open circles denote a 5 °C to 25 °C temperature sweep. Conditions: Angular frequency of 1.0 rad s^{-1} at an applied strain of 1.0 % and a heating/cooling rate of 0.5 °C min^{-1}.

2.4 Conclusions

In this Chapter it is demonstrated that *non-ionic* diblock copolymer worms unexpectedly exhibit pH-responsive behaviour if prepared using a carboxylic acid-functionalised CTA. More specifically, PGMA-PHPMA diblock copolymer worm gels are converted into free-flowing spheres on increasing the solution pH. Such pH-responsive behaviour is reversible and is driven by ionisation of a *single carboxylic acid end-group* at the end of each PGMA stabiliser block, which serves to illustrate the remarkably subtle nature of the worm-to-sphere order-order transition. Moreover, unlike conventional poly electrolytes, these pH-responsive diblock copolymer nano-objects require *minimal* amounts of base (or acid) to induce a morphology transition. Conversely, preparing similar diblock copolymers with ester-based RAFT agents

yields pH-insensitive gels. Furthermore, these latter neutral worm gels undergo a worm-to-sphere (and degelation) upon cooling to 5 °C at both pH 3.5 and 6.0, due to surface plasticisation of the core-forming PHPMA block. However, the carboxylic acid-functionalised worms only exhibit similar thermo-responsive behaviour at pH 3.5 when the acid end-group is protonated. This work represents an important new paradigm for pH-induced morphological transitions exhibited by block copolymer nano-objects. Moreover, since this research was completed, a cationic morpholine-based CTA has been used to prepare pH-responsive PGMA-PHPMA nano-objects. In this case, a worm-to-sphere transition is observed on protonating the morpholine group when lowering the solution pH, which represents complementary pH-responsive behaviour.[53]

In collaboration with Prof. Mark Geoghegan, FCS has been utilised to probe order-order morphological transitions exhibited by HOOC-PGMA-PHPMA diblock copolymer worms at 10 % w/w solids by measuring nanoparticle diffusion coefficients as a function of temperature and solution pH. Thermo- and pH-responsive HOOC-PGMA$_{43}$-P(HPMA$_{119}$-*stat*-GlyMA$_{1}$) diblock copolymer worms were fluorescently-labelled by ring-opening the pendent epoxy groups in the GlyMA residues using rhodamine B piperazine. On cooling to 5 °C or raising the solution pH, the worm gels formed free-flowing spheres and the diffusion coefficients determined by FCS increased by factors of 4 and 8, respectively as a result. FCS is a complementary to DLS because it enables the worm-to-sphere transition to be monitored at much higher copolymer concentrations.

2.5 References

(1) Stuart, M. A.; Huck, W. T.; Genzer, J.; Muller, M.; Ober, C.; Stamm, M.; Sukhorukov, G. B.; Szleifer, I.; Tsukruk, V. V.; Urban, M.; Winnik, F.; Zauscher, S.; Luzinov, I.; Minko, S. *Nat. Mater.* **2010**, *9*, 101.

(2) Pelton, R. *Adv. Colloid Interface Sci.* **2000**, *85*, 1.

(3) Dimitrov, I.; Trzebicka, B.; Muller, A. H. E.; Dworak, A.; Tsvetanov, C. B. *Prog. Polym. Sci.* **2007**, *32*, 1275.

(4) Dai, S.; Ravi, P.; Tam, K. C. *Soft Matter* **2008**, *4*, 435.

(5) Bae, Y.; Fukushima, S.; Harada, A.; Kataoka, K. *Angew. Chem., Int. Ed.* **2003**, *42*, 4640.

(6) Bütün, V.; Liu, S.; Weaver, J. V. M.; Bories-Azeau, X.; Cai, Y.; Armes, S. P. *React. Funct. Polym.* **2006**, *66*, 157.

(7) Schmaljohann, D. *Adv. Drug Deliv. Rev.* **2006**, *58*, 1655.

(8) Brown, A. C.; Stabenfeldt, S. E.; Ahn, B.; Hannan, R. T.; Dhada, K. S.; Herman, E. S.; Stefanelli, V.; Guzzetta, N.; Alexeev, A.; Lam, W. A.; Lyon, L. A.; Barker, T. H. *Nat. Mater.* **2014**, *13*, 1108.

(9) Stayton, P. S.; Shimoboji, T.; Long, C.; Chilkoti, A.; Ghen, G.; Harris, J. M.; Hoffman, A. S. *Nature* **1995**, *378*, 472.

(10) Lomas, H.; Canton, I.; MacNeil, S.; Du, J.; Armes, S. P.; Ryan, A. J.; Lewis, A. L.; Battaglia, G. *Adv. Mater.* **2007**, *19*, 4238.

(11) Galaev, I. Y.; Mattiasson, B. *Trends Biotechnol.* **1999**, *17*, 335.

(12) Lee, K. Y.; Mooney, D. J. *Chem. Rev.* **2001**, *101*, 1869.

(13) Schmaljohann, D. *Adv. Drug. Deliv. Rev.* **2006**, *58*, 1655.

(14) Alarcon, C. D. H.; Pennadam, S.; Alexander, C. *Chem. Soc. Rev.* **2005**, *34*, 276.

(15) Tannock, I. F.; Rotin, D. *Cancer Res.* **1989**, *49*, 4373.

(16) Gerweck, L. E.; Seetharaman, K. *Cancer Res.* **1996**, *56*, 1194.

(17) Ko, J.; Park, K.; Kim, Y.-S.; Kim, M. S.; Han, J. K.; Kim, K.; Park, R.-W.; Kim, I.-S.; Song, H. K.; Lee, D. S.; Kwon, I. C. *J. Control. Release* **2007**, *123*, 109.

(18) Gao, Z. G.; Lee, D. H.; Kim, D. I.; Bae, Y. H. *J. Drug Target.* **2005**, *13*, 391.

(19) Schild, H. G. *Prog. Polym. Sci.* **1992**, *17*, 163.

(20) Hoffman, A. S. *J. Control. Release* **1987**, *6*, 297.

(21) Costioli, M. D.; Fisch, I.; Garret-Flaudy, F.; Hilbrig, F.; Freitag, R. *Biotechnology and Bioengineering* **2003**, *81*, 535.

(22) Yamato, M.; Akiyama, Y.; Kobayashi, J.; Yang, J.; Kikuchi, A.; Okano, T. *Prog. Polym. Sci.* **2007**, *32*, 1123.

(23) Idziak, I.; Avoce, D.; Lessard, D.; Gravel, D.; Zhu, X. X. *Macromolecules* **1999**, *32*, 1260.

(24) Malcolm, G. N.; Rowlinson, J. S. *Trans. Faraday Soc.* **1957**, *53*, 921.

(25) Horne, R. A.; Almeida, J. P.; Day, A. F.; Yu, N.-T. *J. Colloid Interface Sci.* **1971**, *35*, 77.

(26) Taylor, L. D.; Cerankowski, L. D. *J. Polym. Sci., Polym. Chem. Ed.* **1975**, *13*, 2551.

(27) Van Durme, K.; Verbrugghe, S.; Du Prez, F. E.; Van Mele, B. *Macromolecules* **2004**, *37*, 1054.

(28) Weaver, J. V. M.; Bannister, I.; Robinson, K. L.; Bories-Azeau, X.; Armes, S. P.; Smallridge, M.; McKenna, P. *Macromolecules* **2004**, *37*, 2395.

(29) Huang, G.; Gao, J.; Hu, Z.; St. John, J. V.; Ponder, B. C.; Moro, D. *J. Control. Release* **2004**, *94*, 303.

(30) Chung, J. E.; Yokoyama, M.; Aoyagi, T.; Sakurai, Y.; Okano, T. *J. Control. Release* **1998**, *53*, 119.

(31) Xia, Y.; Burke, N. A. D.; Stoever, H. D. H. *Macromolecules* **2006**, *39*, 2275.

(32) FitzGerald, P. A.; Gupta, S.; Wood, K.; Perrier, S.; Warr, G. G. *Langmuir* **2014**, *30*, 7986.

(33) Summers, M. J.; Phillips, D. J.; Gibson, M. I. *Chem. Commun.* **2013**, *49*, 4223.

(34) Moughton, A. O.; O'Reilly, R. K. *Chem. Commun.* **2010**, *46*, 1091.

(35) Liu, T.; Tian, W.; Zhu, Y.; Bai, Y.; Yan, H.; Du, J. *Polym. Chem.* **2014**, *5*, 5077.

(36) Vo, C.-D.; Rosselgong, J.; Armes, S. P.; Tirelli, N. *J. Polym. Sci., Part A: Polym. Chem.* **2010**, *48*, 2032.

(37) Murthy, N.; Campbell, J.; Fausto, N.; Hoffman, A. S.; Stayton, P. S. *Bioconjugate Chem.* **2003**, *14*, 412.

(38) Bajpai, A. K.; Shukla, S. K.; Bhanu, S.; Kankane, S. *Prog. Polym. Sci.* **2008**, *33*, 1088.

(39) Mano, J. F. *Adv. Eng. Mater.* **2008**, *10*, 515.

(40) Li, Y.; Armes, S. P. *Angew. Chem., Int. Ed.* **2010**, *49*, 4042.

(41) Blanazs, A.; Ryan, A. J.; Armes, S. P. *Macromolecules* **2012**, *45*, 5099.

(42) Verber, R.; Blanazs, A.; Armes, S. P. *Soft Matter* **2012**, *8*, 9915.

(43) Blanazs, A.; Verber, R.; Mykhaylyk, O. O.; Ryan, A. J.; Heath, J. Z.; Douglas, C. W. I.; Armes, S. P. *J. Am. Chem. Soc.* **2012**, *134*, 9741.

(44) Warren, N. J.; Armes, S. P. *J. Am. Chem. Soc.* **2014**, *136*, 10174.

(45) Blanazs, A.; Armes, S. P.; Ryan, A. J. *Macromol. Rapid Commun.* **2009**, *30*, 267.

(46) Jones, E. R.; Semsarilar, M.; Blanazs, A.; Armes, S. P. *Macromolecules* **2012**, *45*, 5091.

(47) Antonietti, M.; Förster, S. *Adv. Mater.* **2003**, *15*, 1323.

(48) Geng, Y.; Dalhaimer, P.; Cai, S.; Tsai, R.; Tewari, M.; Minko, T.; Discher, D. E. *Nat. Nanotechnol.* **2007**, *2*, 249.

(49) Taylor, D. L.; Wang, Y.-L. *Nature* **1980**, *284*, 405.

(50) Zhou, W.; Qu, Q.; Xu, Y.; An, Z. *ACS Macro Lett.* **2015**, *4*, 495.

(51) Clayden, J.; Greeves, N.; Warren, S.; Wothers, P. *Organic Chemistry*; Oxford University Press: New York, **2001**.

(52) Kocik, M. K.; Mykhaylyk, O. O.; Armes, S. P. *Soft Matter* **2014**, *10*, 3984.

(53) Penfold, N. J. W.; Lovett, J. R.; Warren, N. J.; Verstraete, P.; Smets, J.; Armes, S. P. *Polym. Chem.* **2016**, *7*, 79.

Chapter 3:

Order-Order Morphological Transitions for Dual Stimulus-Responsive Diblock Copolymer Vesicles

3.1 Introduction

Over the last fifty years or so, there have been many reports of block copolymer self-assembly in solvents that are selective for only one block.[1-14] In principle, varying the relative volume fractions of each block enables a wide range of morphologies to be obtained in dilute solution, including spherical micelles,[7,8] cylindrical micelles (e.g., rods or worms)[9-11] or vesicles.[12-14] Unlike spheres and worms, vesicles are formed from a polymeric bilayer with an internal void (or lumen) which consists of solvent. This makes aqueous based vesicles a potentially attractive vehicle for drug delivery[15-17] and diagnostic applications.[18,19] In principle, hydrophobic active ingredients can be loaded into the membrane,[15-19] whereas water-soluble active ingredients can be encapsulated within the vesicle lumen.[15,17,20] Therefore, biocompatible vesicles which are able to undergo order-order or order-disorder morphological transitions upon exposure to a physically-relevant stimulus are able to release their payloads on demand. Synthetic amphiphilic diblock copolymers offer opportunities in this context, as they can be tailored to respond to specific changes in external conditions such as pH,[21-24] temperature[21,25] or light[26,27] depending on the desired application.[6,17,28-30]

The self-assembly of such block copolymer vesicles is typically conducted using post-polymerisation techniques, such as a solvent- or pH-switch or thin film rehydration, which are usually conducted in dilute solutions (< 1 % w/w).[3,18,22-24] In contrast, polymerisation-induced self-assembly (PISA) allows the rational synthesis of vesicles at much higher copolymer concentrations (up to 25 % w/w) in aqueous media.[31-37] For example, Armes and co-workers chain-extended poly(glycerol monomethacrylate) (PGMA) with 2-hydroxypropyl methacrylate (HPMA) by reversible addition-fragmentation chain transfer (RAFT) aqueous dispersion polymerisation.[31-33] By varying the relative block DPs (and hence the relative volume fractions) and overall copolymer concentration, detailed phase diagrams have been constructed that enable the reproducible synthesis of pure spheres, worms or vesicles. Sampling the synthesis of a $PGMA_{47}$-$PHPMA_{200}$ diblock copolymer at regular time intervals and imaging the dried aliquots by transmission electron microscopy (TEM) revealed an evolution of the copolymer morphology from spheres to worms to

vesicles, *via* a jellyfish intermediate.[38] Furthermore, increasing the degree of polymerisation (DP) of the core-forming PHPMA block has minimal effect on the particle size, but simply yields vesicles with progressively thicker membranes (see **Figure 3.1**).[39] Therefore, the diblock copolymer composition can be judiciously chosen depending on whether such vesicles are to be used to encapsulate hydrophilic materials (with a large lumen volume being desirable) or hydrophobic materials (thicker membrane being desirable). Moreover, recently it has been demonstrated that either silica nanoparticles or globular proteins such as bovine serum albumin (BSA) can be encapsulated within the lumen of diblock copolymer vesicles during their PISA synthesis.[35,40] Presumably, such *in situ* encapsulation occurs during the jellyfish stage of the synthesis.

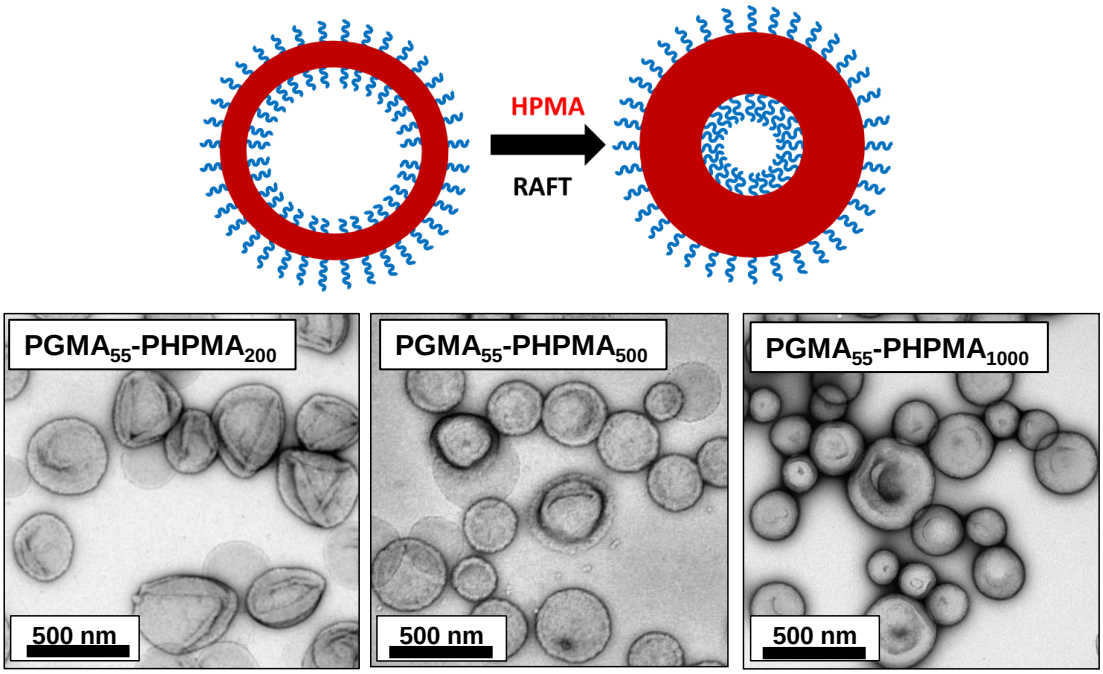

Figure 3.1 Schematic representation and TEM images obtained for $PGMA_{55}$-$PHPMA_X$ vesicles, indicating the increase in membrane thickness with PHPMA DP.[39]

In this Chapter, the pH-responsive end-group effects discussed in Chapter 2 are extended from worms to vesicles. It has been previously demonstrated that ionisation of a single carboxylic acid end-group on the stabiliser block is sufficient to drive a worm-to-sphere order-order morphology transition. A carboxylic acid-

functionalised RAFT agent is used to prepare a water-soluble HOOC-PGMA macro-CTA with a DP of 43. This macro-CTA is then chain-extended with HPMA to prepare four HOOC-$PGMA_{43}$-$PHPMA_X$ diblock copolymer vesicle dispersions (where X = 175, 200, 225 or 250) *via* PISA using RAFT aqueous dispersion polymerisation. The pH-responsive nature of these four diblock copolymers is explored in detail. Furthermore, it is well known that PGMA-PHPMA diblock copolymer worms undergo a worm-to-sphere transition upon cooling due to 'surface plasticisation' of the PHPMA core.[37,41,42] Although the temperature-responsive nature of such worms is well established, little research has been conducted on the temperature-dependent behaviour of the analogous vesicles until now. Finally, the effects of dual stimulus (i.e., changing the temperature and pH simultaneously) are explored.

3.2 Experimental Section

3.2.1 Materials

Glycerol monomethacrylate (GMA; 99.8 %) was donated by GEO Specialty Chemicals (Hythe, UK) and was used without further purification. 2-Hydroxypropyl methacrylate (HPMA) was purchased from Alfa Aesar (UK) and was used as received. 4,4'-Azobis(4-cyanopentanoic acid) (ACVA; V-501; 99 %), ethanol (99 %, anhydrous grade), methanol, dichloromethane and deuterated methanol were purchased from Sigma-Aldrich (UK) and were used as received. All solvents were of HPLC quality. 4-Cyano-4-(2-phenylethanesulfanylthiocarbonyl)sulfanylpentanoic acid (PETTC) was prepared and purified as reported elsewhere.[43]

3.2.2 Synthesis of poly(glycerol monomethacrylate) (HOOC-$PGMA_{43}$) macro-CTA

GMA (30.0 g, 187 mmol), PETTC (1.156 g, 3.4 mmol; target DP = 55), and ACVA (0.191 g, 0.68 mmol; PETTC: ACVA molar ratio = 5.0) were weighed into a

250 mL round-bottomed flask. Anhydrous ethanol (previously purged with nitrogen for 1 h) was then added to produce a 50 % w/w solution, which was placed in an ice bath and purged under nitrogen for 45 min at 0 °C. The sealed flask was immersed in an oil bath set at 70 °C to initiate the RAFT polymerisation of GMA and stirred for 2 h at this temperature. The polymerisation was then quenched at approximately 81 % conversion by simultaneous exposure to air and cooling the reaction mixture to room temperature. Methanol (20 mL) was added to dilute the reaction solution, followed by precipitation into a ten-fold excess of dichloromethane in order to remove unreacted GMA monomer. The precipitate was isolated *via* filtration and washed with excess dichloromethane before being dissolved in methanol (50 mL). This process was then repeated and the precipitate was then dissolved in water and freeze-dried overnight to afford a yellow solid. ^{1}H NMR studies indicated a mean degree of polymerisation of 43 *via* end-group analysis (the integrated aromatic RAFT end-group signals at 7.1-7.4 ppm were compared to polymer backbone signals at 0.5-2.5 ppm). DMF GPC studies indicated an M_n of 15,400 g mol^{-1} and an M_w/M_n of 1.20. ^{1}H NMR (400 MHz, CD_3OD, 25 °C): δ 0.77-1.24 (b, 3H, -$CH_2CR(CH_3)$-), 1.75-2.24 (b, 2H, -$CH_2CR(CH_3)$-), 3.56-3.81 (b, 2.2H, -CH_2OH), 3.82-4.23 (b, 3.5H, -$COOCH_2CH(OH)$-).

3.2.3 Synthesis of HOOC-PGMA$_{43}$-PHPMA$_X$ diblock copolymer vesicles *via* RAFT aqueous dispersion polymerisation of HPMA

A typical protocol for the chain extension of HOOC-PGMA$_{43}$ macro-CTA with 175 units of HPMA *via* RAFT aqueous dispersion polymerisation of HPMA is as follows: HOOC-PGMA$_{43}$ macro-CTA (0.143 g, 0.020 mmol), HPMA monomer (0.50 g, 3.5 mmol) ACVA (1.9 mg, 0.006 mmol; HOOC-PGMA$_{43}$ macro-CTA: ACVA molar ratio = 3.0) were added to a 25 ml round-bottomed flask, prior to addition of water to produce a 10 % w/w solution. This reaction solution was purged with nitrogen gas for 30 min at 20 °C prior to immersion into an oil bath set at 70 °C. The reaction mixture was stirred for 4 h to ensure essentially complete conversion of the HPMA monomer (> 99 % by ^{1}H NMR analysis) and was quenched by simultaneous exposure to air and cooling to ambient temperature. The resulting turbid free-flowing dispersion was characterised by DLS, TEM and rheology without

further purification. ^{1}H NMR (400 MHz, CD_3OD, 25 °C): δ 0.74-1.18 (b, 3H, **-CH_3** on polymer backbone), 1.18-1.39 (b, 2.8H, **-CH_3** in PHPMA), 1.47-2.24 (b, 1.6H, **-CH_2-** on polymer backbone), 3.55-3.73 (b, 0.4H, **-CH_2**OH in PGMA and –**CH**(OH)- in PHPMA), 3.73-4.20 (b, 1.9H, remaining pendent protons in PGMA and PHPMA).

3.2.4 Instrumentation

^{1}H NMR spectra were recorded using a 400 MHz Bruker Avance-500 spectrometer (64 scans averaged per spectrum).

Gel Permeation Chromatography (GPC) was used to assess polymer molecular weight distributions. The DMF GPC set-up comprised two Polymer Laboratories PL gel 5 μm Mixed-C columns connected in series to a Varian 390-LC multi-detector suite (refractive index detector) and a Varian 290-LC pump injection module operating at 60 °C. The GPC eluent was HPLC-grade DMF containing 10 mM LiBr at a flow rate of 1.0 mL min^{-1}. DMSO was used as a flow-rate marker. Calibration was conducted using a series of ten near-monodisperse poly(methyl methacrylate) standards (M_n = 625 to 2,480,000 g mol^{-1}). Chromatograms were analysed using Varian Cirrus GPC software (version 3.3).

Dynamic Light Scattering (DLS) analysis was conducted using a Malvern Zetasizer NanoZS instrument on 0.10 % w/w aqueous dispersions at 25 °C in disposable cuvettes at a fixed scattering angle of 173 °. The solution pH of the initially acidic copolymer dispersions was adjusted to the appropriate value using 0.1 M KOH. Intensity-average hydrodynamic diameters were calculated *via* the Stokes-Einstein equation. All data were averaged over three consecutive runs.

Aqueous electrophoresis measurements were conducted using a Malvern Zetasizer NanoZS instrument at 25 °C. Studies were performed on aqueous copolymer dispersions diluted to 0.10 % w/w containing 10^{-3} mol dm^{-3} KCl as background electrolyte. Zeta potentials were calculated from the Henry equation using the Smoluchowski approximation. All data were averaged over three consecutive runs.

Transmission Electron Microscopy (TEM) imaging was performed at 80 kV using a FEI Tecnai Spirit microscope equipped with a Gatan 1kMS600CW CCD camera. Solutions were diluted 100-fold at either 20 °C or 5 °C to generate 0.10 % w/w dispersions. Samples analysed under acidic conditions were prepared by diluting dispersions with water at the desired solution pH. Copper/palladium TEM grids (Agar Scientific, UK) were surface-coated in-house to yield a thin film of amorphous carbon. The grids were then plasma glow-discharged for 30 s to create a hydrophilic surface. Individual samples (0.10% w/w, 12 μL) were adsorbed onto the freshly glow-discharged grids for 60 s and then blotted with filter paper to remove excess solution. To stain the aggregates, a 9 μL drop of 0.75 % w/w uranyl formate solution was placed on the sample-loaded grid for 20 s and then carefully blotted to remove excess stain. The grids were then dried using a vacuum hose.

Rheology studies were conducted using an AR-G2 stress controlled rheometer with a variable temperature Peltier plate equipped with a cone-and-plate geometry (40 mm 2 ° aluminium cone). The temperature dependence on storage (G') and loss (G") moduli were determined between 25 °C and 4 °C for the HOOC-PGMA$_{43}$-HPMA$_{200}$ diblock copolymer dispersion after a pH switch from 3.5 to 6.0. Measurements were conducted at a fixed strain of 1.0 %, an angular frequency of 1.0 rad s^{-1} and a heating/cooling rate of 0.5 °C min^{-1}.

Visible absorption spectroscopy was used to measure changes in transmittance. Turbidimetry curves were recorded at 20 °C using a Perkin Elmer Lambda 25 instrument operating in time drive mode at a fixed wavelength of 450 nm for 20 h. Prior to analysis, the HOOC-PGMA$_{43}$-PHPMA$_X$ diblock copolymer vesicles were diluted to 0.10 % w/w in aqueous solution at pH 3.5. Measurements were recorded every minute immediately after this solution pH was increased to pH 9.0 using 0.1M KOH.

3.3 Results and Discussion

3.3.1 Diblock copolymer vesicle synthesis

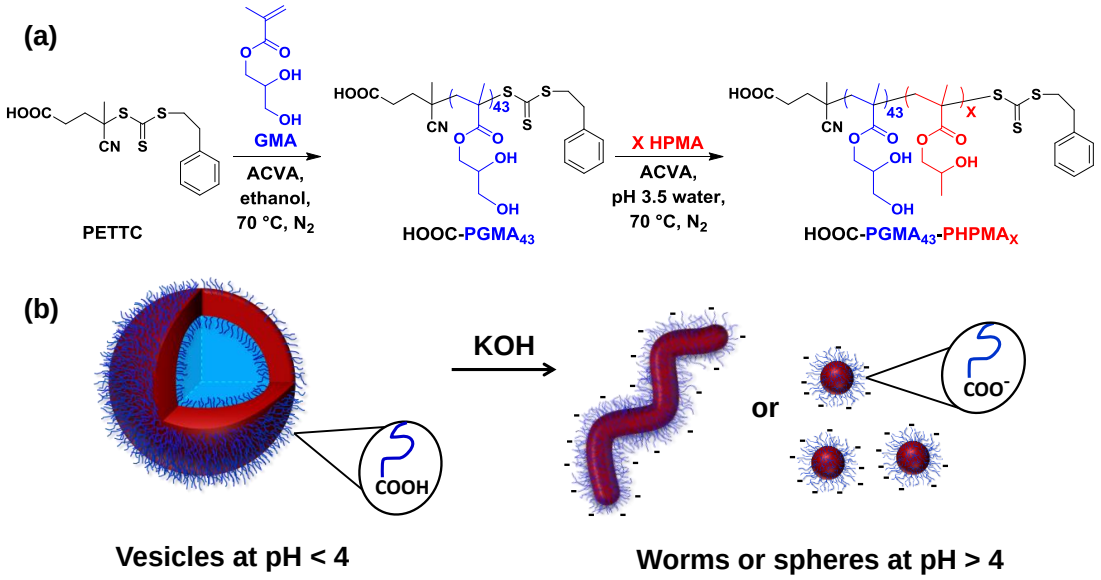

Figure 3.2 (a) Schematic of the synthesis of a HOOC-$PGMA_{43}$ macro-CTA using a PETTC CTA *via* RAFT solution polymerisation in ethanol at 70 °C. This HOOC-$PGMA_{43}$ macro-CTA is then chain extended with HPMA *via* RAFT aqueous dispersion polymerisation at pH 3.5 to prepare a series of HOOC-$PGMA_{43}$-$PHPMA_X$ diblock copolymer vesicles (where X = 175 - 250). (b) Illustration depicting the vesicle-to-sphere or vesicle-to-worm morphology transitions that occur when the terminal carboxylic acid on the PGMA stabiliser block becomes ionised as a result of a pH switch.

Firstly, a near-monodisperse water-soluble PGMA macro-CTA (M_w/M_n = 1.20) was prepared in ethanol at 70 °C by RAFT solution polymerisation of GMA using 4-cyano-4-(2-phenylethanesulfanylthiocarbonyl) sulfanylpentanoic acid (PETTC) (see **Figure 3.2a**). PETTC was judiciously selected to afford a macro-CTA with a terminal carboxylic acid. The crude HOOC-PGMA macro-CTA was purified by two precipitations into excess dichloromethane. ^{1}H NMR spectroscopy indicated a mean degree of polymerisation (DP) of 43 for this purified HOOC-PGMA macro-CTA by end-group analysis (**Figure 3.3a**). This macro-CTA was subsequently chain-extended with HPMA by RAFT aqueous dispersion polymerisation at 70 °C and 10

% w/w solids in water at pH 3.5. The target DP of the core-forming PHPMA block was systematically varied from 175 to 250 to produce a series of turbid, free-flowing vesicular dispersions. According to ^{1}H NMR analysis, all HPMA polymerisations reached near full conversion (> 99 % - see **Figure 3.3b**) after 4 hours. Furthermore, the absence of a peak due to the HOOC-PGMA$_{43}$ macro-CTA in the DMF GPC traces indicated high blocking efficiencies for all four block copolymers (see **Figure 3.4**). In addition, relatively narrow copolymer molecular weight distributions (M_w/M_n < 1.20) were observed, as expected based on previous reports.[31,38,39]

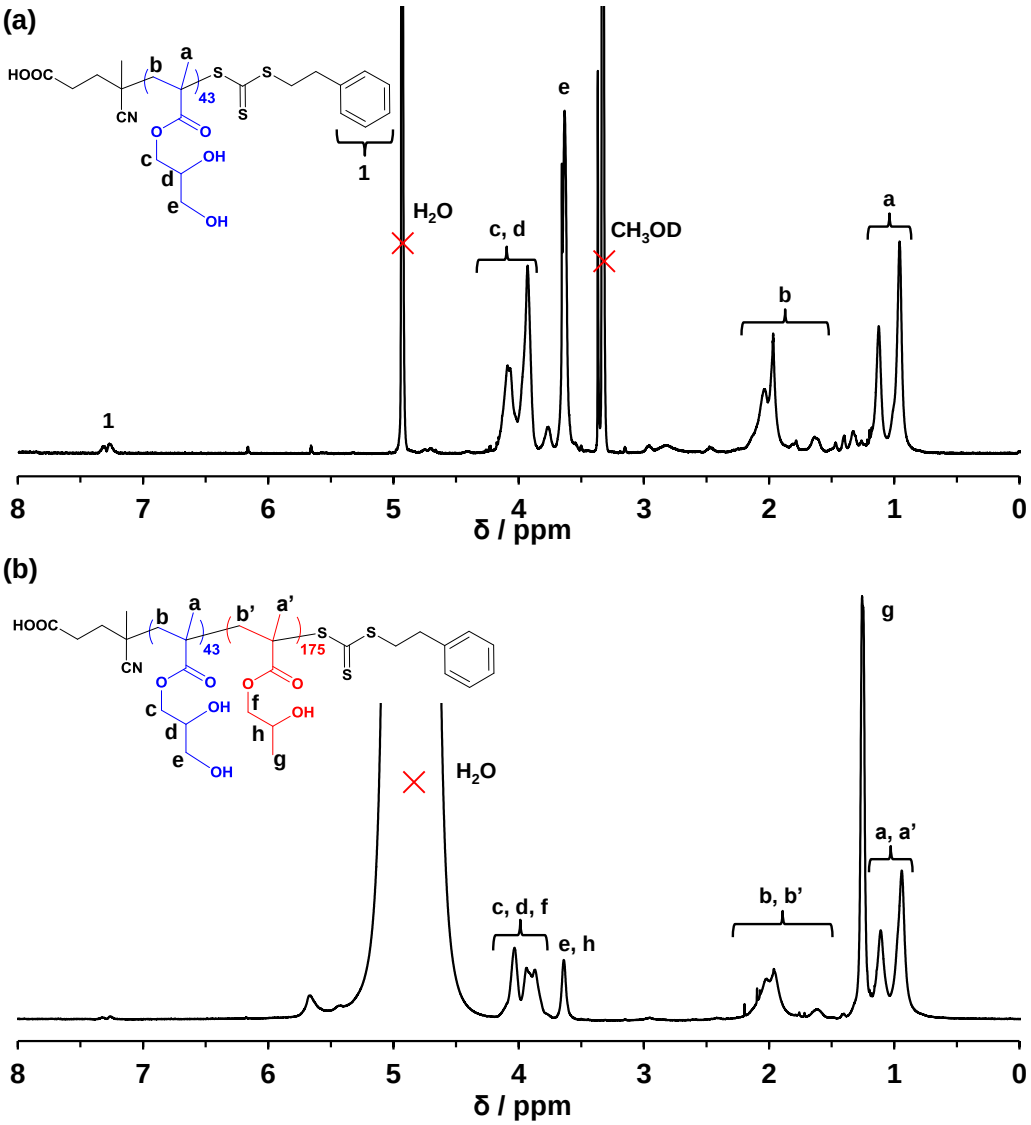

Figure 3.3 ^{1}H NMR spectra obtained in CD_3OD for (a) HOOC-PGMA$_{43}$ macro-CTA and (b) 10 % w/w solution of HOOC-PGMA$_{43}$-PHPMA$_{175}$ diblock copolymer

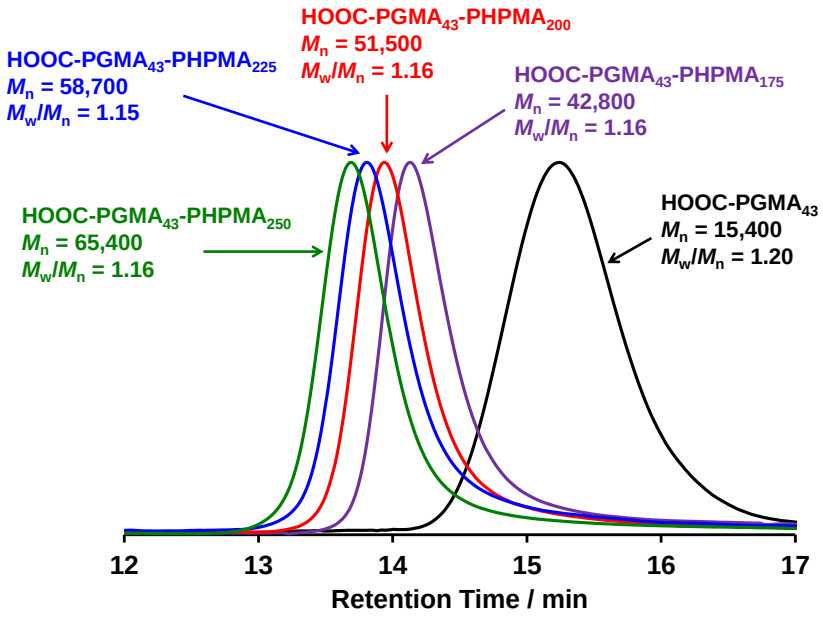

Figure 3.4 DMF GPC traces obtained for a HOOC-PGMA$_{43}$ macro-CTA (black curve) and the corresponding HOOC-PGMA$_{43}$-PHPMA$_X$ diblock copolymer vesicles (where X = 175 to 250).

Transmission electron microscopy (TEM) images obtained for the diblock copolymer dispersions (after dilution to 0.1 % w/w in water at pH 3.5) confirmed the presence of polydisperse vesicles of 150-500 nm in diameter in each case (see **Figure 3.5**). Furthermore, TEM studies also indicate a membrane thickness of around 10 to 15 nm, which is consistent with results reported by Warren *et al.* for a closely related series of PGMA$_{54}$-PHPMA$_X$ block copolymer vesicles (see **Figure 3.5**).[39]

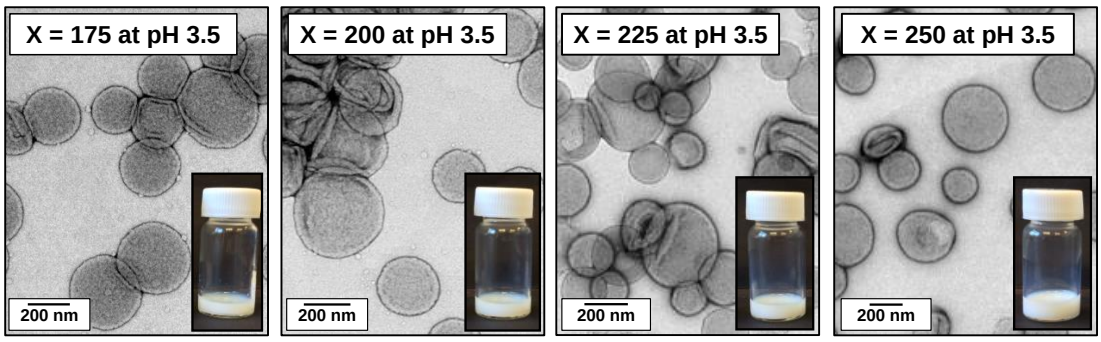

Figure 3.5 TEM images (recorded after dilution to 0.10 % w/w solids using an aqueous solution of pH 3.5) and corresponding digital photographs obtained for HOOC-PGMA$_{43}$-PHPMA$_X$ diblock copolymer vesicles at pH 3.5.

3.3.2 Order-order morphological transitions of vesicles due to pH-responsive end-groups

In theory, these HOOC-PGMA$_{43}$-PHPMA$_X$ diblock copolymer vesicles should exhibit similar pH-responsive behaviour to the previously reported HOOC-PGMA$_{56}$-PHPMA$_{155}$ worms in Chapter 2.[44] By increasing the solution pH above the pK_a of the terminal carboxylic acid (approximately 4.7) it becomes ionised and renders the PGMA stabiliser block more hydrophilic, which may induce a morphological transition. On increasing the solution pH of the HOOC-PGMA$_{43}$-PHPMA$_{175}$ copolymer vesicles dispersions from pH 3.5 to pH 6.0, a physical change from a turbid free-flowing dispersion to a transparent free-flowing dispersion was observed over approximately 12 hours. If the HOOC-PGMA$_{43}$-PHPMA$_{200}$ diblock copolymer vesicles are subjected to the same pH switch, a change from a turbid free-flowing dispersion to a translucent free-standing gel is observed. Furthermore, TEM studies conducted on the HOOC-PGMA$_{43}$-PHPMA$_{175}$ and HOOC-PGMA$_{43}$-PHPMA$_{200}$ diblock copolymers at pH 6.0 confirmed a vesicle-to-sphere and a vesicle-to-worm transition, respectively (see **Figure 3.6**). These order-order transitions are both due to the ionisation of the single terminal carboxylic acid group, which increases the volume fraction of the hydrophilic PGMA stabiliser block. Hence the packing parameter, *p*, is lowered below 0.5 (i.e., out of vesicle phase space) for the copolymer chains (as $p = v / a_0 l_c$).[6] In stark contrast, no physical change was observed for the HOOC-PGMA$_{43}$-PHPMA$_{225}$ or HOOC-PGMA$_{43}$-PHPMA$_{250}$ diblock copolymer vesicle dispersions when subjected to the same pH switch. In addition, TEM images obtained for the HOOC-PGMA$_{43}$-PHPMA$_{225}$ and HOOC-PGMA$_{43}$-PHPMA$_{250}$ diblock copolymers at pH 6.0 indicated no pH-responsive behaviour; the original vesicles are retained more or less intact. However, close inspection of the HOOC-PGMA$_{43}$-PHPMA$_{225}$ vesicles reveals some evidence for the presence of hemi-vesicles and possibly some degree of aggregation. Thus these preliminary studies suggest that there is a critical DP for the hydrophobic PHPMA block above which the vesicles no longer exhibit pH-responsive behaviour. This is reasonable, because increasing the PHPMA block DP is expected to increase the packing parameter such that *p* significantly exceeds 0.50, which leads to the formation of vesicles that are further removed from the vesicle/worm phase

boundary. Hence, the enhanced hydrophilic character gained by the PGMA stabiliser block as a result of ionisation of its terminal carboxylic acid group is no longer sufficient to induce an order-order transition.

In contrast, when shorter PHPMA DPs are targeted (175 or 200), the increased hydrophilicity gained for the PGMA stabiliser block (after a pH switch) is adequate to enable access to either worm ($0.33 < p < 0.50$) or sphere ($p < 0.33$) phase space. It is perhaps worth emphasising the subtle nature of the observations summarised in **Figure 3.5** and **Figure 3.6**: deprotonation of a single terminal carboxylic acid group on a diblock copolymer chain with a mean molecular weight of more than 35 000 g mol^{-1} is sufficient to induce a morphological transition. Moreover, it is noteworthy that this pH-response is *irreversible* in all cases. Adding acid to return the solution to its original pH of 6.0 merely produces an insoluble white paste, rather than a free-flowing turbid dispersion. This is believed to be because the worm phase constitutes a significant kinetic barrier to vesicle reformation at 20 °C. A worm-to-vesicle transition is well-documented for PGMA-PHPMA chains during PISA syntheses at 70 °C,[38] but in this case there is excess unreacted HPMA monomer present at intermediate monomer conversions to plasticise the hydrophobic PHPMA chains and hence ensure their high mobility.

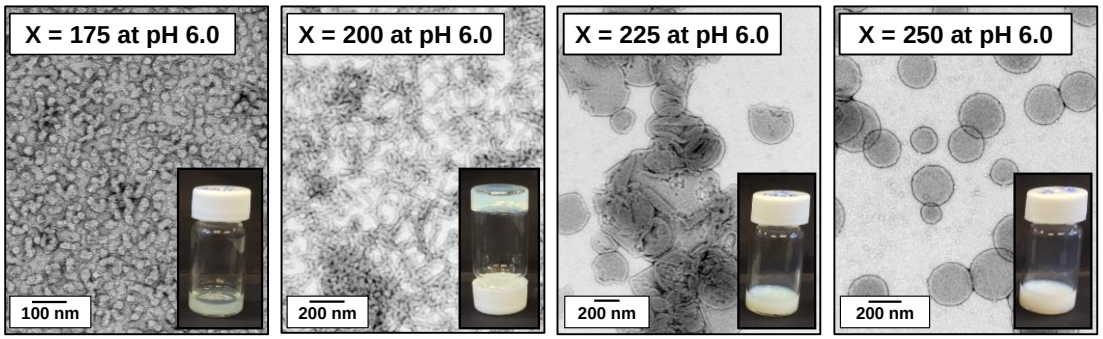

Figure 3.6 TEM images (recorded after dilution to 0.10 % w/w solids using an aqueous solution at pH 6.0) and corresponding digital photographs obtained for HOOC-$PGMA_{43}$-$PHPMA_X$ diblock copolymer nano-objects at pH 6.0.

To further examine these order-order morphological transitions, dynamic light scattering (DLS) and aqueous electrophoresis studies were conducted on 0.10 % w/w HOOC-$PGMA_{43}$-$PHPMA_{175-250}$ vesicle dispersions as a function of solution pH

(see **Figure 3.7**). In the case of the HOOC-$PGMA_{43}$-$PHPMA_{175}$ vesicles, a significant reduction in the mean particle diameter from 150 to 35 nm was observed on increasing the dispersion pH from 3.5 to 5.0, which provides good evidence for a vesicle-to-sphere transition (see **Figure 3.7a**). Moreover, this morphological transition occurs over a similar pH range to that previously reported for a worm-to-sphere transition.[44] A similar trend was observed for the HOOC-$PGMA_{43}$-$PHPMA_{200}$ diblock copolymer, which undergoes a vesicle-to-worm transition with a corresponding reduction in apparent particle diameter from 240 to 130 nm after the same pH switch (**Figure 3.7b**). In this latter case, it is noteworthy that DLS reports a 'sphere-equivalent' diameter for the final worm phase that corresponds to neither their mean length nor width. Conversely, the HOOC-$PGMA_{43}$-$PHPMA_{225}$ and HOOC-$PGMA_{43}$-$PHPMA_{250}$ diblock copolymer vesicles exhibit an *increase* in particle diameter over the same pH range, although the latter is less pronounced than the former (see **Figure 3.7c** and **d**). This is attributed to a more extended PGMA stabiliser layer when the terminal carboxylic acid groups become ionised, due to electrostatic repulsion. This suggests that these two types of vesicles do not undergo any morphological transition during a pH switch, which is corroborated by the TEM studies shown in **Figure 3.6**. In all cases, ionisation of the terminal carboxylic acid group above its pK_a results in greater anionic character for the nano-objects. This was confirmed by aqueous electrophoresis studies, where the zeta potential increases in each case from around -10 mV for the original vesicles at pH 3.5 to approximately -25 mV at pH 8.0 for the final diblock copolymer nano-objects.

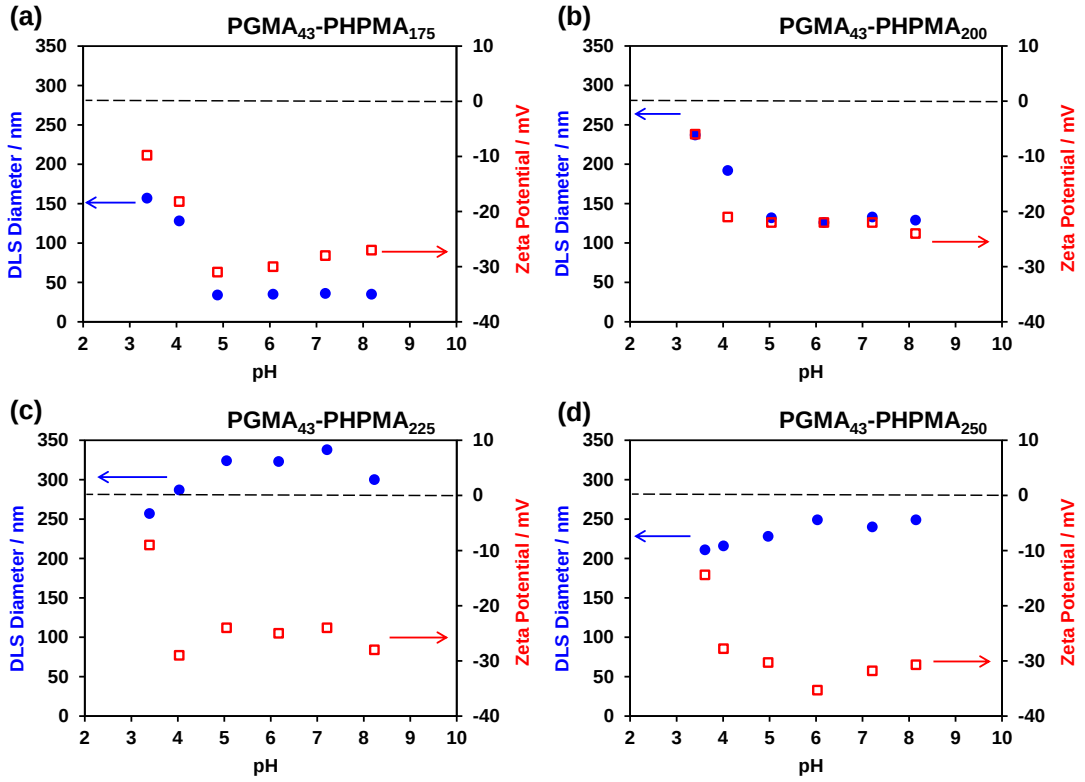

Figure 3.7 Variation of hydrodynamic particle diameter and zeta potential as a function of solution pH (starting at pH 3.5) recorded at 25 °C for 0.1 % w/w aqueous dispersions of (a) HOOC-$PGMA_{43}$-$PHPMA_{175}$ vesicles (b) HOOC-$PGMA_{43}$-$PHPMA_{200}$ vesicles (c) HOOC-$PGMA_{43}$-$PHPMA_{225}$ vesicles and (d) HOOC-$PGMA_{43}$-$PHPMA_{250}$ vesicles.

The worm-to-sphere order-order morphology transition discussed in Chapter 2 is relatively quick, occurring over a time scale of minutes.[44] In stark contrast, the vesicle-to-sphere and vesicle-to-worm transitions observed herein took place over much longer timescales (hours rather than minutes). Such changes in morphology from vesicles to worms or spheres are accompanied by a significant change in the visual appearance of the dispersions. More specifically, the initial vesicles are relatively large and hence scatter light strongly, resulting in turbid dispersions. On the other hand, the resulting worms or spheres are smaller and so scatter light much more weakly, leading to semi-transparent dispersions. In principle, this physical change can be utilised to probe the timescales of these morphological transitions by turbidimetry. However, such experiments must be conducted on relatively dilute dispersions (0.10 % w/w at pH 3.5), because 10 % w/w dispersions are much too

turbid to be analysed. The transmittance at a fixed wavelength of 450 nm was monitored for dilute copolymer dispersions over a 20 hour period after a pH switch from 3.5 to 9.0 using KOH (see **Figure 3.8**). As expected, no discernible change in transmittance was observed over 20 hours if the PHPMA DP is either 225 or 250. This is fully consistent with our TEM and DLS observations discussed earlier. Such vesicles cannot undergo an order-order morphological transition on ionisation of the carboxylic acid end-group on the PGMA stabiliser chains. Therefore, the particles remain as turbid dispersions. However, if the PHPMA DP is either 175 or 200, then a pH switch from pH 3.5 to pH 9.0 leads to a significant increase in transmittance being observed over time. These turbidimetry studies indicate that the vesicle-to-worm transition for the HOOC-$PGMA_{43}$-$PHPMA_{200}$ diblock copolymer is remarkably slow. According to these studies, the vesicle-to-worm transition is only complete only after approximately 15 hours. In contrast, the vesicle-to-sphere transformation observed for the HOOC-$PGMA_{43}$-$PHPMA_{175}$ diblock copolymer is complete within just 2 hours under the same conditions. It is not fully understood why such morphology transitions are so slow. However, it is hypothesized that the likely explanation is related to the varying DP of the membrane-forming PHPMA block. This parameter dictates how far the vesicles lie from the respective vesicle/worm and vesicle/sphere phase boundaries. Furthermore, longer PHPMA blocks should have more inter-chain entanglements, thus presenting a larger kinetic barrier to a stimulus-induced morphology transition.[45] Therefore, vesicles comprising longer PHPMA blocks respond more slowly to a pH switch.

It is noteworthy that such order-order morphological transitions are much slower compared to the characteristic time scale required for the acid-induced swelling of microgel particles reported in the literature.[46,47] However, this pronounced difference is perhaps not too surprising: the copolymer chains in a conventional pH-responsive microgel (or soluble polymer) typically undergo extensive protonation (or ionisation) during a pH switch to produce a highly hydrophilic polyelectrolyte. In contrast, the PHPMA block remains weakly hydrophobic both before and after the pH switch.

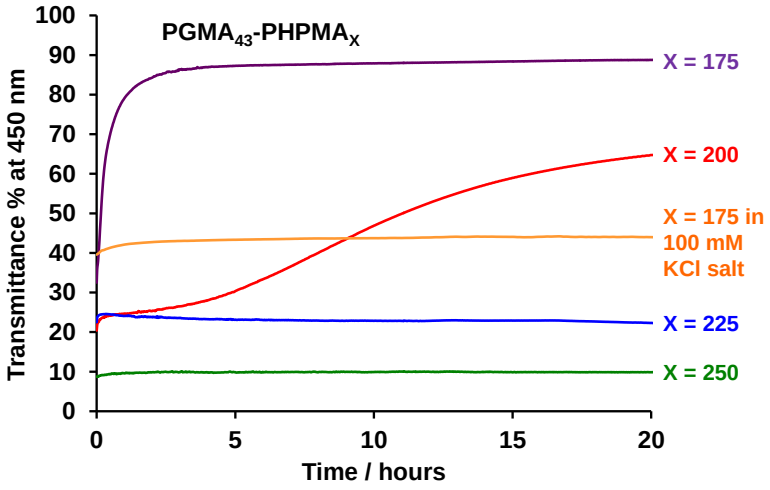

Figure 3.8 Change in transmittance % at a fixed wavelength of 450 nm for 0.10 % w/w aqueous dispersions of HOOC-PGMA$_{43}$-PHPMA$_{175\text{-}250}$ nano-objects over 20 hours at 20 °C after a pH switch from pH 3.5 to pH 9.0 using KOH.

If the same turbidimetry experiment is conducted on a 0.10 % w/w aqueous dispersion of HOOC-PGMA$_{43}$-PHPMA$_{175}$ vesicles prepared in the presence of 100 mM KCl, no significant increase in transmittance is observed over the same time period (see **Figure 3.8**). This suggests that added salt results in pH-insensitive vesicles. It is well documented that the behaviour of many pH-responsive polymers can be suppressed or altered upon addition of salt.[36,48-52] This behaviour might be expected as HOOC-PGMA$_{56}$-PHPMA$_{155}$ diblock copolymers, which undergo a worm-to-sphere transition (as discussed in Chapter 2), are also pH-insensitive in the presence of 100 mM KCl.[44] Moreover, DLS studies of HOOC-PGMA$_{43}$-PHPMA$_{175}$ vesicles in the presence of this electrolyte indicated a constant particle diameter of approximately 150 nm between pH 3.5 and 8.5 (see red data set in **Figure 3.9a**). TEM studies confirmed that the original vesicle morphology observed at pH 3.5 was *retained* at pH 8.5 (compare **Figure 3.9b** and **c**; N.B. the small dark crystals observed in these images are KCl nanocrystals). The corresponding data obtained for the same copolymer obtained under the same conditions in the *absence* of salt is included in **Figure 3.9d** and **e** as a reference. In summary, the addition of salt screens the additional solvation associated with the ionisation of the terminal carboxylic acid, and hence suppresses the vesicle-to-sphere transition.

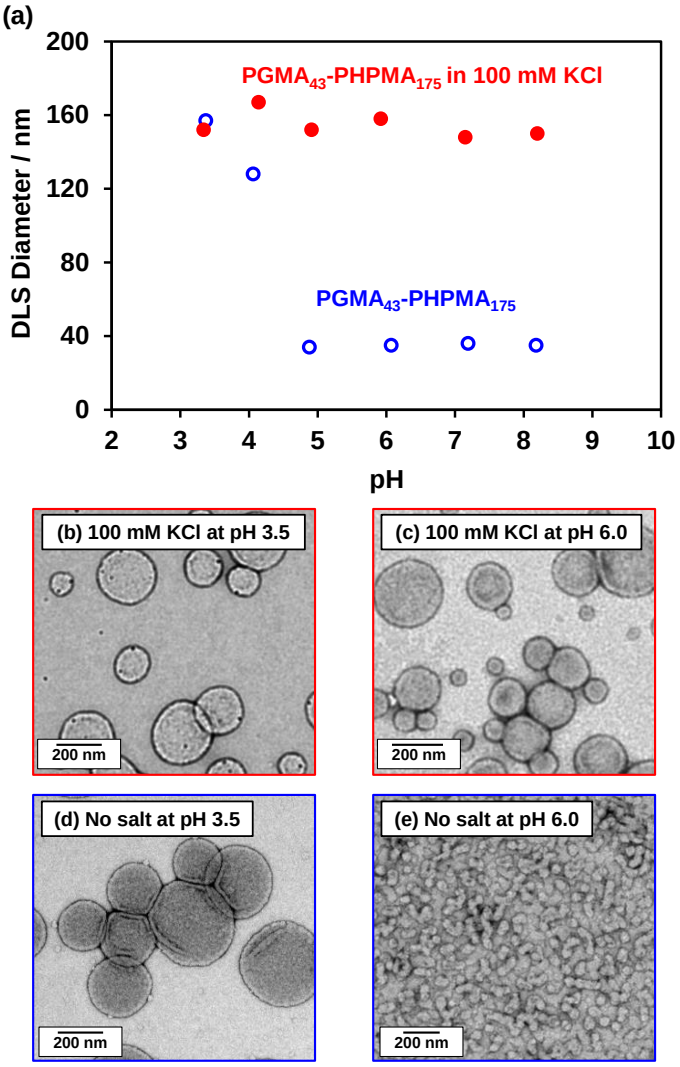

Figure 3.9 (a) Variation of the hydrodynamic particle diameter measured by dynamic light scattering with dispersion pH recorded for 0.1 % w/w aqueous dispersions of HOOC-PGMA$_{43}$-PHPMA$_{175}$ diblock copolymer vesicles starting at pH 3.5 in the absence of salt (open blue circles) and in the presence of 100 mM KCl (closed red circles). TEM images obtained for HOOC-PGMA$_{43}$-PHPMA$_{175}$ diblock copolymer nano-objects in the presence of 100 mM KCl salt at (b) pH 3.5 and (c) pH 6.0 and absence of salt at (d) pH 3.5 and (e) pH 6.0.

Of particular interest is the vesicle-to-worm transition observed for the HOOC-PGMA$_{43}$-PHPMA$_{200}$ diblock copolymer after a pH switch from 3.5 to 6.0. Unlike the relatively large phase space occupied by vesicles (and spheres), the worm phase space is typically very narrow.[31] Thus it is perhaps not surprising that a pure worm phase can only be obtained from a pure vesicle phase for a rather narrow range

of PHPMA DP (with a fixed PGMA DP). After end-group ionisation at pH 6.0, HOOC-$PGMA_{43}$-$PHPMA_{200}$ worms are believed to form a soft free-standing gel due to multiple inter-worm contacts. Rheological studies conducted on a 10 % w/w HOOC-$PGMA_{43}$-$PHPMA_{200}$ worm gel at pH 6.0 indicate a storage modulus (G') of approximately 60 Pa at 25 °C (see **Figure 3.10**). This is slightly lower than the moduli observed for the PGMA-PHPMA worm gels in Chapter 2. It is hypothesised that this is the result of electrostatic repulsion between the former *anionic* worms, resulting in weaker/fewer inter-worm contacts. Temperature-dependent rheological studies indicate that the HOOC-$PGMA_{43}$-$PHPMA_{200}$ worm gel undergoes degelation on cooling to approximately 4 °C. The critical gelation temperature (CGT) is defined as the temperature at which the loss modulus (G") exceeds the storage modulus (G'), indicating the formation of a viscoelastic fluid. For this HOOC-$PGMA_{43}$-$PHPMA_{200}$ worm gel at pH 6.0, the CGT was found to be approximately 5 °C. Verber and co-workers reported that the CGT values of their non-ionic $PGMA_{54}$-$PHPMA_X$ diblock copolymer worm gels decreased monotonically from 20 °C to 7 °C as the PHPMA DP (X) was increased from 135 to 170.[42] This is due to longer PHPMA DPs requiring a greater degree of hydration to induce a worm-to-sphere transition. Thus it might be expected that the HOOC-$PGMA_{43}$-$PHPMA_{200}$ worm gel possesses a lower CGT due to the higher PHPMA DP.

In Chapter 2, temperature-dependent oscillatory rheology studies indicated that the temperature-induced worm-to-sphere transition was fully reversible (although some degree of hysteresis was observed). In contrast, rheological studies of the HOOC-$PGMA_{43}$-$PHPMA_{200}$ worm gel formed from vesicles after a pH switch suggests *irreversible* thermo-responsive behaviour for this system, at least on the time scale of this experiment. More specifically, after cooling to 5 °C and returning to 25 °C, regelation does not occur: the loss modulus remains larger than the storage modulus (see red data on **Figure 3.10**), which is characteristic of free-flowing spherical micelles. It is hypothesised that these anionic micelles are mutually repulsive (zeta potential ~ -25 mV), and hence are unable to undergo the multiple fusion events required for worm reconstitution. Moreover, if the HOOC-$PGMA_{43}$-$PHPMA_{200}$ nano-objects are returned to pH 3.5 after a 25 °C - 5 °C - 25 °C thermal cycle then a white insoluble paste is produced, rather than the original colloidally

stable vesicles. Again, it appears that the worm phase provides an effective kinetic barrier to vesicle reformation.

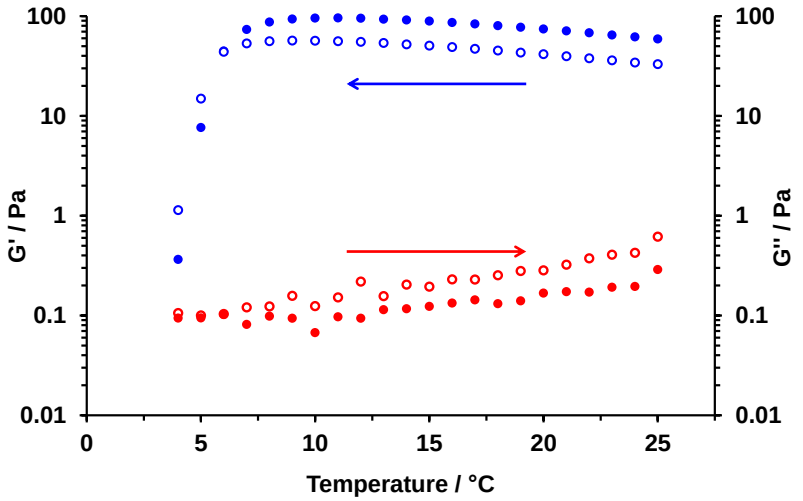

Figure 3.10 Variation of the storage modulus (G' – denoted by full circles) and loss modulus (G'' – denoted by open circles) for a 10 % w/w aqueous dispersion of HOOC-PGMA$_{43}$-PHPMA$_{200}$ diblock copolymer nano-objects as a function of temperature, after a pH switch from 3.5 to 6.0 to induce a vesicle-to-worm transition. In each case the blue data represent decreasing temperature and the red data represent increasing temperature. Conditions: 1.0 rad s^{-1} angular frequency at an applied strain of 1.0 %.

3.3.3 Order-order morphological transitions of vesicles due to thermo-responsive PHPMA core-forming block

The thermo-responsive behaviour of PGMA-PHPMA diblock copolymer worms has been studied in some detail.[41,42] However, to date there have been no analogous studies of PGMA-PHPMA diblock copolymer vesicles. Thus the four HOOC-PGMA$_{43}$-PHPMA$_{175\text{-}250}$ diblock copolymer vesicles were studied to examine the effect of varying the PHPMA DP on their thermo-responsive behaviour. As mentioned above Verber and co-workers reported that PGMA$_{54}$-PHPMA$_X$ worms exhibited lower CGTs when targeting higher X values, as judged by temperature dependent rheological studies.[42] This was attributed to the longer (and hence more hydrophobic) PHPMA blocks requiring a higher degree of hydration (which causes surface plasticisation) to induce a worm-to-sphere transition, which can only be attained at lower temperatures. By analogy, PGMA-PHPMA diblock copolymer

vesicles prepared using a sufficiently high PHPMA DP might be expected to possess no thermo-responsive behaviour. Moreover, Kocik *et al*. used SAXS to show that $PGMA_{57}$-$PHPMA_{140}$ worms underwent a worm-to-sphere transition at around 5 °C, but further cooling to -2 °C resulted in near-molecular dissolution of the spheres to form molecularly dissolved chains.[53] In view of these observations, the lower limit temperature in the present study was restricted to 5 °C. Perhaps surprisingly, only the *shortest* HOOC-$PGMA_{43}$-$PHPMA_{175}$ diblock copolymer switched from a turbid, free-flowing dispersion (at pH 3.5) to a translucent, free-standing gel on cooling to 5 °C (see **Figure 3.11**). Moreover, this thermal transition was irreversible: an insoluble white paste was obtained on returning to 25 °C. TEM studies on grids prepared at 5 °C using 0.10 % w/w copolymer dispersions at pH 3.5 are consistent with a vesicle-to-worm transition (see **Figure 3.11**). In contrast, representative TEM images obtained at 5 °C for the other three diblock copolymers suggested that their original vesicular morphologies remained unchanged. At first sight it is perhaps surprising that ionisation of a *single* terminal carboxylic acid group leads to pH-responsive behaviour for HOOC-$PGMA_{43}$-$PHPMA_{200}$, yet the same copolymer exhibits no thermo-responsive behaviour (at pH 3.5). On reflection, this discrepancy is not unreasonable: carboxylic acid group ionisation makes the relatively short PGMA stabiliser significantly more hydrophilic, whereas lowering the temperature leads to greater hydration (i.e., more weakly hydrophobic character) for the relatively long PHPMA core-forming block. In the latter case, if the PHPMA DP is too high then this effect is negated.

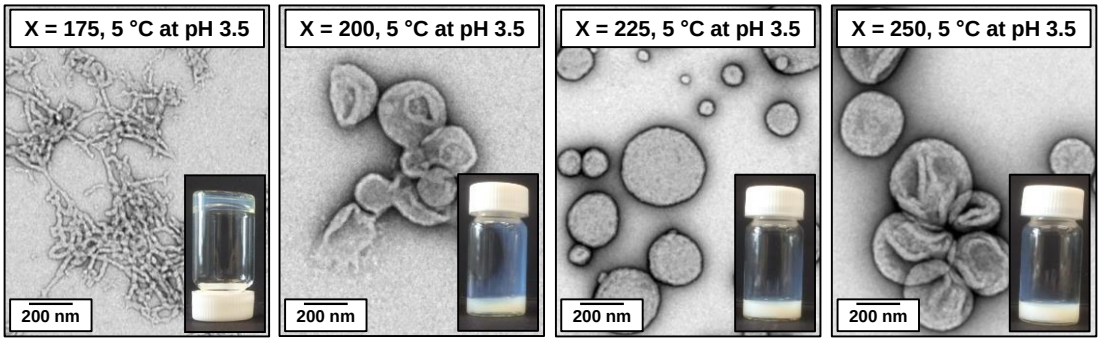

Figure 3.11 TEM images (for grids prepared at 5 °C after dilution to 0.10 % w/w copolymer at pH 3.5) and corresponding digital photographs obtained for HOOC-$PGMA_{43}$-$PHPMA_X$ diblock copolymer nano-objects for X = 175, 200, 225 or 250.

3.3.4 Investigation into the dual responsive nature of PGMA-PHPMA vesicles

The stimuli-responsive nature of the four HOOC-PGMA$_{43}$-PHPMA$_X$ diblock copolymer vesicles was investigated further by subjecting them to a pH switch from 3.5 to 6.0, followed by immediate cooling to 5 °C. In all cases a morphological order-order transition was observed. The original dispersions become significantly less turbid, while remaining free-flowing dispersions (see **Figure 3.12**). TEM studies conducted on the HOOC-PGMA$_{43}$-PHPMA$_X$ nano-objects after this dual stimulus confirmed that the vesicles are transformed into a mixture of spheres and 'spherical dimers',[41] with mean particle width dimensions estimated to be 21 to 30 nm (based on analysis of at least 100 particles in each case). Similarly, DLS studies conducted at 5 °C on the final copolymer dispersions reported a mean hydrodynamic diameter of approximately 40 nm at pH 6.0, which is substantially lower than that of the original vesicles.

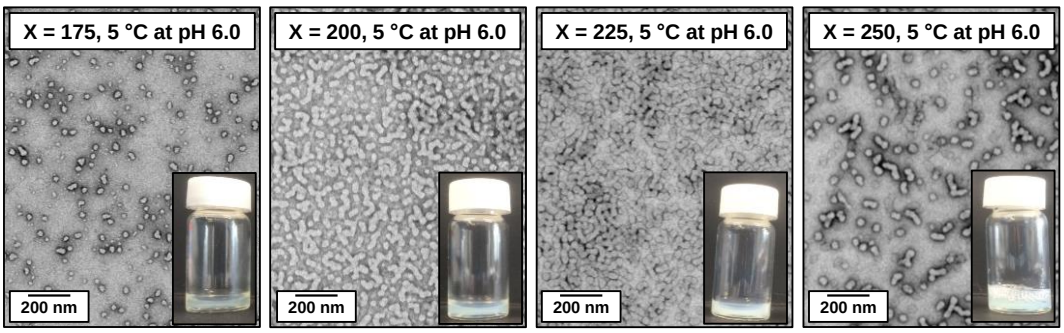

Figure 3.12 Representative TEM images for HOOC-PGMA$_{43}$-PHPMA$_X$ dispersions obtained at 5 °C after dilution to 0.10 % w/w copolymer at pH 6.5 and (inset) the corresponding digital photographs of their visual appearance at 10 % w/w copolymer.

It is perhaps worth emphasising that the HOOC-PGMA$_{43}$-PHPMA$_{250}$ diblock copolymer vesicles only undergo a morphological transition when subjected to *both* a pH switch *and* a temperature switch. Otherwise exposure to either stimulus *alone* results in no morphological transition and the nano-objects remain as vesicles. However, regardless of the route taken to return to the original conditions (i.e., heating followed by a pH switch, or vice versa), these order-order morphological transitions always proved to be irreversible. TEM images obtained after dilution of

the insoluble white paste revealed a mixed phase of vesicles and worms (see **Figure 3.13**).

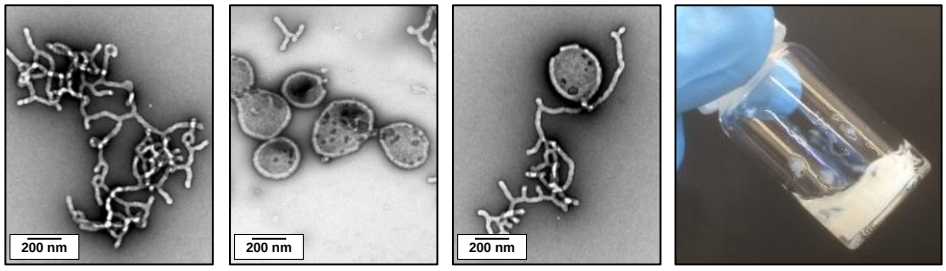

Figure 3.13 Representative TEM images obtained for a 0.1 % w/w aqueous dispersion of HOOC-$PGMA_{43}$-$PHPMA_{250}$ diblock copolymer vesicles after cycling from pH 3.5 at 25 °C to pH 6.0 at 5 °C to pH 3.5 at 25 °C. The final dispersion contains a mixture of worms and vesicles and is no longer colloidally stable, indicating irreversible changes in the copolymer morphology

3.3.5 Summary of stimuli-responsive nature of HOOC-$PGMA_{43}$-$PHPMA_X$ vesicles

Despite only relative small changes in the core PHPMA DP (175-250), the stimulus-responsive nature of the four HOOC-$PGMA_{43}$-$PHPMA_x$ vesicles is unexpectedly complex and their overall behaviour is summarised in **Table 3.1**. For X = 225 or 250, no pH-responsive behaviour is observed on raising the pH from pH 3.5 to pH 6.0. On the other hand, a vesicle-to-worm transition is observed after a pH switch for X = 200, while a vesicle-to-sphere (plus spherical dimers) transition is found for X = 175. Only the latter vesicles exhibit a thermally-triggered transition, which produces a free-standing worm gel at 5 °C. However, all four HOOC-$PGMA_{43}$-$PHPMA_{175-250}$ vesicles undergo morphological transitions to give a mixture of spheres and spherical dimers when subjected to a dual stimulus (i.e., a pH switch followed by immediate cooling to 5 °C). In all cases these morphological transitions proved to be irreversible. This is believed to be because the worm phase acts as an effective kinetic barrier that prevents the original vesicle morphology from being reformed.

.

PHPMA DP	M_n / g mol^{-1} (a)	M_w/M_n (a)	Particle diameter at pH 3.5 and 25 °C / nm (b)	PDI (b)	pH responsive? (c)	Morphology after 3.5 to 6.0 pH Switch (c)	Temperature responsive? (c)	Morphology after 20 to 5 °C temperature Switch (c)	Dual responsive? (c)	Morphology after temperature and pH Switch (c)
175	42,800	1.16	157	0.218	Yes	Spheres and spherical dimers	Yes	Worms	Yes	Spheres and spherical dimers
200	51,500	1.16	237	0.264	Yes	Worms	No	Vesicles	Yes	Spheres and spherical dimers
225	58,700	1.15	232	0.108	No	Vesicles	No	Vesicles	Yes	Spheres and spherical dimers
300	65,400	1.16	211	0.058	No	Vesicles	No	Vesicles	Yes	Spheres and spherical dimers

(a) Measured using DMF GPC versus near-monodisperse PMMA calibration standards

(b) Measured using dynamic light scattering (DLS)

(c) Determined by TEM

Table 3.1 Summary of data obtained for HOOC-PGMA$_{43}$-HPMA$_X$ diblock copolymer vesicles illustrating their pH- and thermo-responsive behaviour.

There are many literature examples of the use of pH- or thermo-responsive vesicles for potential biomedical applications such as drug delivery.[2,8,42-46] In principle, the vesicle lumen can be loaded *in situ* during their preparation *via* PISA,[35,40] with exposure to an external stimulus resulting in an order-order morphological transition, loss of the membrane structure and hence subsequent release of the payload. Furthermore, vesicles that only undergo a morphological transition when exposed to two or more stimuli may offer greater control in terms of specificity compared to vesicles that can respond to just one stimulus. These possibilities will be examined in future studies. However, in this context it is noteworthy that the weakly hydrated nature of the PHPMA membrane-forming block suggests that PGMA-PHPMA vesicles are unlikely to retain water-soluble small molecules over long time periods.[39] Given this limitation, it may be more fruitful to focus on the encapsulation of organic nano particles such as globular proteins (e.g., enzymes, antibodies etc.).

3.4 Conclusions

In summary, it has been demonstrated that PGMA-PHPMA diblock copolymer vesicles prepared using a carboxylic acid-functionalised RAFT agent exhibit complex stimulus-responsive behaviour in aqueous solution. By fixing the DP of the PGMA stabiliser block at 43, vesicles can be prepared by targeting PHPMA block DPs of 175, 200, 225 or 250. Switching the solution pH from 3.5 to 6.0 induces ionisation of the terminal carboxylic acid on the PGMA stabiliser block, which increases its hydrophilic character. This results in a vesicle-to-sphere transition for HOOC-PGMA$_{43}$-PHPMA$_{175}$ and a vesicle-to-worm transition for HOOC-PGMA$_{43}$-PHPMA$_{200}$, respectively. However, if the DP of the PHPMA block is longer (either 225 or 250) no morphological transformation is observed by TEM and DLS. In this case, the vesicles lie further from the vesicle/worm phase boundary. Therefore, the increased hydrophilicity gained from the ionised carboxylic acid is insufficient to enable a morphology transition. Turbidimetry studies conducted on dilute vesicle dispersions indicate that these vesicle-to-sphere and vesicle-to-worm

transitions are relatively slow, requiring time scales of hours at 20 °C. However, if the original vesicles were subjected to the same pH switch in the presence of added salt, charge screening resulted in no order-order transition being observed. Only the HOOC-$PGMA_{43}$-$PHPMA_{175}$ vesicles undergo an order-order transition to form worms simply on cooling to 5 °C. However, subjecting the HOOC-$PGMA_{43}$-$PHPMA_X$ vesicles to *both* a pH switch *and* a temperature switch causes a vesicle-to-sphere transition in each case, as judged by TEM and DLS studies. In summary, the stimulus-responsive behaviour of HOOC-$PGMA_{43}$-$PHPMA_X$ vesicles is unexpectedly complex and critically depends on the DP of the core-forming PHPMA block.

3.5 References

(1) Jain, S.; Bates, F. S. *Science* **2003**, *300*, 460.

(2) Charleux, B.; Delaittre, G.; Rieger, J.; D'Agosto, F. *Macromolecules* **2012**, *45*, 6753.

(3) Zhang, L.; Eisenberg, A. *Polym. Adv. Tech.* **1998**, *9*, 677.

(4) Hayward, R. C.; Pochan, D. J. *Macromolecules* **2010**, *43*, 3577.

(5) Chu, B. *Langmuir* **1995**, *11*, 414.

(6) Blanazs, A.; Armes, S. P.; Ryan, A. J. *Macromol. Rapid Commun.* **2009**, *30*, 267.

(7) Zhang, L.; Eisenberg, A. *Science* **1995**, *268*, 1728.

(8) Tuzar, Z.; Kratochvíl, P. *Adv. Colloid Interface Sci.* **1976**, *6*, 201.

(9) Won, Y.-Y.; Davis, H. T.; Bates, F. S. *Science* **1999**, *283*, 960.

(10) Wang, X.; Guerin, G.; Wang, H.; Wang, Y.; Manners, I.; Winnik, M. A. *Science* **2007**, *317*, 644.

(11) Cui, H.; Chen, Z.; Zhong, S.; Wooley, K. L.; Pochan, D. J. *Science* **2007**, *317*, 647.

(12) Antonietti, M.; Förster, S. *Adv. Mater.* **2003**, *15*, 1323.

(13) Discher, D. E.; Eisenberg, A. *Science* **2002**, *297*, 967.

(14) Lim Soo, P.; Eisenberg, A. *J. Polym. Sci. Part B Polym. Phys* **2004**, *42*, 923.

(15) Ahmed, F.; Pakunlu, R. I.; Srinivas, G.; Brannan, A.; Bates, F.; Klein, M. L.; Minko, T.; Discher, D. E. *Mol. Pharm.* **2006**, *3*, 340.

(16) Sanson, C.; Schatz, C.; Le Meins, J.-F.; Soum, A.; Thévenot, J.; Garanger, E.; Lecommandoux, S. *J. Control. Release* **2010**, *147*, 428.

(17) Christian, D. A.; Cai, S.; Bowen, D. M.; Kim, Y.; Pajerowski, J. D.; Discher, D. E. *Eur. J. Pharm. Biopharm.* **2009**, *71*, 463.

(18) Ghoroghchian, P. P.; Frail, P. R.; Susumu, K.; Park, T.-H.; Wu, S. P.; Uyeda, H. T.; Hammer, D. A.; Therien, M. J. *J. Am. Chem. Soc.* **2005**, *127*, 15388.

(19) Christian, N. A.; Milone, M. C.; Ranka, S. S.; Li, G.; Frail, P. R.; Davis, K. P.; Bates, F. S.; Therien, M. J.; Ghoroghchian, P. P.; June, C. H.; Hammer, D. A. *Bioconjugate Chem.* **2007**, *18*, 31.

(20) Meng, F.; Engbers, G. H. M.; Feijen, J. *J. Control. Release* **2005**, *101*, 187.

(21) He, C. L.; Zhuang, X. L.; Tang, Z. H.; Tian, H. Y.; Chen, X. S. *Adv. Healthc. Mater.* **2012**, *1*, 48.

(22) Pegoraro, C.; Cecchin, D.; Gracia, L. S.; Warren, N.; Madsen, J.; Armes, S. P.; Lewis, A.; MacNeil, S.; Battaglia, G. *Cancer Lett.* **2013**, *334*, 328.

(23) Bellomo, E. G.; Wyrsta, M. D.; Pakstis, L.; Pochan, D. J.; Deming, T. J. *Nat. Mater.* **2004**, *3*, 244.

(24) Du, J.; Tang, Y.; Lewis, A. L.; Armes, S. P. *J. Am. Chem. Soc.* **2005**, *127*, 17982.

(25) Qin, S.; Geng, Y.; Discher, D. E.; Yang, S. *Adv. Mater.* **2006**, *18*, 2905.

(26) Kros, A.; Jansen, J. A.; Holder, S. J.; Nolte, R. J. M.; Sommerdijk, N. A. J. M. *J. Adhes. Sci. Technol.* **2002**, *16*, 143.

(27) Liu, G.; Wang, X.; Hu, J.; Zhang, G.; Liu, S. *J. Am. Chem. Soc.* **2014**, *136*, 7492.

(28) Blum, A. P.; Kammeyer, J. K.; Rush, A. M.; Callmann, C. E.; Hahn, M. E.; Gianneschi, N. C. *J. Am. Chem. Soc.* **2015**, *137*, 2140.

(29) Bajpai, A. K.; Shukla, S. K.; Bhanu, S.; Kankane, S. *Prog. Polym. Sci.* **2008**, *33*, 1088.

(30) Meng, F.; Zhong, Z.; Feijen, J. *Biomacromolecules* **2009**, *10*, 197.

(31) Blanazs, A.; Ryan, A. J.; Armes, S. P. *Macromolecules* **2012**, *45*, 5099.

(32) Sugihara, S.; Blanazs, A.; Armes, S. P.; Ryan, A. J.; Lewis, A. L. *J. Am. Chem. Soc.* **2011**, *133*, 15707.

(33) Warren, N. J.; Mykhaylyk, O. O.; Mahmood, D.; Ryan, A. J.; Armes, S. P. *J. Am. Chem. Soc.* **2014**, *136*, 1023.

(34) Figg, C. A.; Simula, A.; Gebre, K. A.; Tucker, B. S.; Haddleton, D. M.; Sumerlin, B. S. *Chem. Sci.* **2015**, *6*, 1230.

(35) Tan, J.; Sun, H.; Yu, M.; Sumerlin, B. S.; Zhang, L. *ACS Macro Lett.* **2015**, *4*, 1249.

(36) Boissé, S.; Rieger, J.; Pembouong, G.; Beaunier, P.; Charleux, B. *J. Polym. Sci. A Polym. Chem.* **2011**, *49*, 3346.

(37) Warren, N. J.; Armes, S. P. *J. Am. Chem. Soc.* **2014**, *136*, 10174.

(38) Blanazs, A.; Madsen, J.; Battaglia, G.; Ryan, A. J.; Armes, S. P. *J. Am. Chem. Soc.* **2011**, *133*, 16581.

(39) Warren, N. J.; Mykhaylyk, O. O.; Ryan, A. J.; Williams, M.; Doussineau, T.; Dugourd, P.; Antoine, R.; Portale, G.; Armes, S. P. *J. Am. Chem. Soc.* **2015**, *137*, 1929.

(40) Mable, C. J.; Gibson, R. R.; Prevost, S.; McKenzie, B. E.; Mykhaylyk, O. O.; Armes, S. P. *J. Am. Chem. Soc.* **2015**, *137*, 16098.

(41) Blanazs, A.; Verber, R.; Mykhaylyk, O. O.; Ryan, A. J.; Heath, J. Z.; Douglas, C. W. I.; Armes, S. P. *J. Am. Chem. Soc.* **2012**, *134*, 9741.

(42) Verber, R.; Blanazs, A.; Armes, S. P. *Soft Matter* **2012**, *8*, 9915.

(43) Jones, E. R.; Semsarilar, M.; Blanazs, A.; Armes, S. P. *Macromolecules* **2012**, *45*, 5091.

(44) Lovett, J. R.; Warren, N. J.; Ratcliffe, L. P.; Kocik, M. K.; Armes, S. P. *Angew. Chem., Int. Ed.* **2015**, *54*, 1279.

(45) Battaglia, G.; Ryan, A. J. *J. Am. Chem. Soc.* **2005**, *127*, 8757.

(46) Dupin, D.; Rosselgong, J.; Armes, S. P.; Routh, A. F. *Langmuir* **2007**, *23*, 4035.

(47) Morse, A. J.; Armes, S. P.; Mills, P.; Swart, R. *Langmuir* **2013**, *29*, 15209.

(48) Lee, A. S.; Buetuen, V.; Vamvakaki, M.; Armes, S. P.; Pople, J. A.; Gast, A. P. *Macromolecules* **2002**, *35*, 8540.

(49) Geng, Y.; Ahmed, F.; Bhasin, N.; Discher, D. E. *J. Phys. Chem. B* **2005**, *109*, 3772.

(50) An, S. W.; Thirtle, P. N.; Thomas, R. K.; Baines, F. L.; Billingham, N. C.; Armes, S. P.; Penfold, J. *Macromolecules* **1999**, *32*, 2731.

(51) Fujii, S.; Dupin, D.; Araki, T.; Armes, S. P.; Ade, H. *Langmuir* **2009**, *25*, 2588.

(52) Zhang, L.; Eisenberg, A. *Macromolecules* **1996**, *29*, 8805.

(53) Kocik, M. K.; Mykhaylyk, O. O.; Armes, S. P. *Soft Matter* **2014**, *10*, 3984.

Chapter 4

Preparation of Acid-Responsive Worms, Vesicles and Spheres

4.1 Introduction

It is well documented that stimuli-responsive polymers have a wide range of potential biomedical applications.[1-6] In particular, pH-responsive polymers have been widely studied as their properties can change significantly in aqueous solution. More specifically, certain polymers can undergo a globule-to-coil conformational change upon ionisation or protonation in aqueous solution.[7,8] Broadly, there are two types of pH-responsive polymers, polyacids and polybases. The former typically contain carboxylic acid groups (such as poly(acrylic acid) (PAA) and poly(methacrylic acid) (PMAA)), which can become anionic on increasing the solution pH above its pK_a. In contrast, polybases become cationic at solution pH values below their pK_a as a result of protonation. Examples include poly(2-diisopropylaminoethyl methacrylate) (PDPA) and poly(2-(dimethylamino)ethyl methacrylate) (PDEA). Small changes in the solution pH around their pK_a value have relatively large effects on the degree of ionisation and, in some cases, solubility. Therefore, appropriate polymers must be carefully selected depending on the desired application and pH response.

Adding a chemical cross-linker during the synthesis of a pH-responsive polymer can result in the formation of a microgel or hydrogel.[9-12] However, more relevant to thesis is the incorporation of a pH-responsive block into amphiphilic diblock copolymers, which are well known to undergo self-assembly in aqueous solution.[13-16] Such nano-objects may undergo either order-order or order-disorder transitions by adjusting the solution pH to charge up the pH-responsive block.[17-38] For example, Webber *et al*. used anionic polymerisation to prepare a poly(2-vinylpyridine)-poly(ethylene oxide) (PVP-PEO) diblock copolymer in THF.[25] When transferred into aqueous solution, this diblock copolymer underwent self-assembly to give spherical nanoparticles above pH 5.0 where the PVP units are deprotonated and hydrophobic. Here the PEO block acts as a steric stabiliser. Lowering the solution pH below pH 5.0 protonates the PVP block and produces a double-hydrophilic diblock copolymer, resulting in micellar dissociation to form molecularly dissolved cationic chains (i.e., an order-disorder transition – see **Figure 4.1**). Similarly, Armes and co-workers prepared poly(2-(methacryloyloxy)ethyl phosphorylcholine)-poly(2-(diisopropylamino) ethyl methacrylate) (PMPC-PDPA) diblock copolymers *via* atom

transfer radical polymerisation (ATRP).[26,27] These diblock copolymers formed spheres or vesicles after transfer into aqueous solution above pH 6.0, since the PDPA block is deprotonated and hydrophobic at this pH. However, when its tertiary amine groups become protonated below 6.0, the PDPA block becomes hydrophilic. This causes an order-disorder transition. PMPC-PDPA vesicles have been evaluated for the encapsulation and release of either DNA or doxorubicin (a water-soluble anti-cancer drug) by this mechanism.[39,40] In contrast, McCormick's group prepared poly(2-acrylamido-2-methyl propanesulfonate)-poly(2-acrylamido-2-methyl propane butanoate) (PAMPS-PAMBA) diblock copolymers by reversible addition-fragmentation chain transfer (RAFT) polymerisation in aqueous solution at pH 8.0.[28] At this solution pH the PAMBA block is ionised and hydrophilic, thus the diblock copolymer is molecularly dissolved as an ionic polyelectrolyte. Below pH 5.5 the pendent carboxylic acid groups in PAMBA become protonated, rendering the PAMBA block sufficiently hydrophobic to induce self-assembly to form spherical nanoparticles.

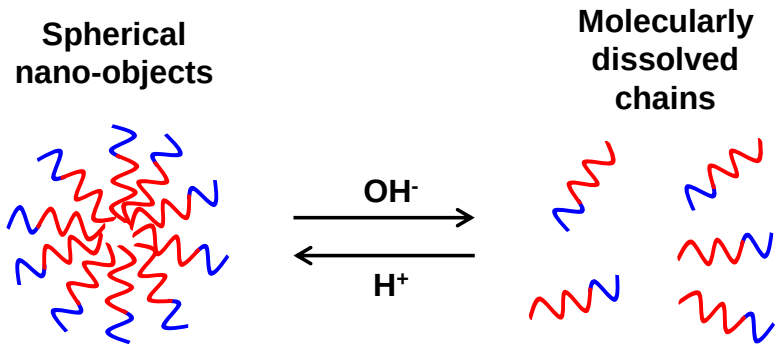

Figure 4.1 Schematic illustration of an order-disorder transition from spheres-to-molecularly dissolved chains. In this case deprotonation results in molecularly dissolved chains.

Elsewhere, Doncom and co-workers prepared a poly(methyl acrylate)-poly(2-(*N*,*N*-diisopropylamino)ethyl acrylamide) (PMA-PDPAEAM) diblock copolymer with a quaternary amine end-group by RAFT polymerisation followed by post-polymerisation modification.[29] When transferred from DMF into water at pH 7.4, (where the PDPAEAM residues are neutral), such doubly-hydrophobic diblock copolymers spontaneously self-assemble to form vesicles. Presumably the cationic

charge conferred by the end-group ensures colloidal stability rather than phase separation. However, the PDMAEAM block is protonated at pH 3.0, resulting in a vesicle-to-sphere transition, which was found to reversible on returning the pH (see **Figure 4.2**). More recently, Dhara *et al*. prepared a poly((ethylene glycol) monomethyl ether acrylate)-poly(Boc-L-tryptophan acryloyloxy ethyl ester) by RAFT polymerisation in DMF.[30] After removal of the Boc protecting group to give an amine, this diblock copolymer was transferred into water at pH 7.4, which resulted in vesicle formation. However, lowering the solution below pH 5.2 resulted in a vesicle-to-sphere transition.

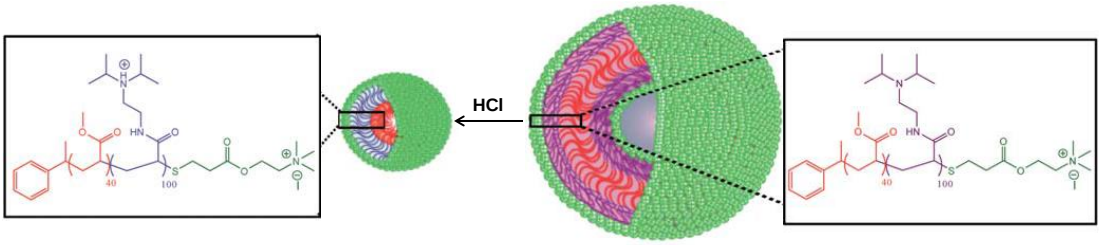

Figure 4.2 Graphical illustration of the sphere-to-vesicle order-order transition observed for PMA-PDPAEAM diblock copolymers on protonation of the tertiary amine groups in DPAEAM units.[29]

Armes *et al.* and others have used 'schizophrenic' diblock copolymers to induce an order-order transition depending on solution pH.[31-36] Here a zwitterionic diblock copolymer is prepared that comprises both a polyacid and a polybase. Under acidic conditions the polyacid is hydrophobic and can act as the core-forming block, whereas the polybase is protonated, hydrophilic and forms the stabiliser block. Switching to basic pH ionises the polyacid block and deprotonates the polybase, thus the blocks switch roles as the stabiliser and core-forming block. One example is the synthesis of zwitterionic poly(4-vinylbenzoic acid)-poly(2-(diethylamino)ethyl methacrylate) (PVBA-PDEA) diblock copolymers by ATRP using protecting group chemistry and subsequent hydrolysis.[33] These diblock copolymers form spheres with a PVBA core at pH 2, whereas at pH 10 they form spheres with a PDEA core (see **Figure 4.3**). Similarly, Lecommandoux and Rodriguez-Hernández reported the synthesis of 'schizophrenic' zwitterionic poly(L-glutamic acid)-poly(L-lysine) diblock copolymer *vesicles*, which switch morphology by a similar mechanism.[37]

Similar order-disorder and order-order transitions have also been made for triblock copolymers consisting of pH-responsive blocks.[41-45]

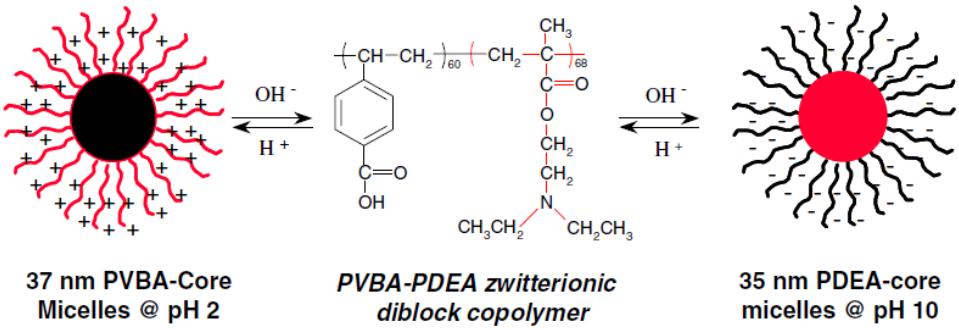

Figure 4.3 Graphical representation of the micellar self-assembly of the 'schizophrenic' zwitterionic PVBA-PDEA diblock copolymers at pH 2 and at pH 10.[33,34]

As discussed in Chapter 1, there are many examples of diblock copolymer nano-objects synthesised by polymerisation-induced self-assembly (PISA) in water.[46-58] However, there appear to be no reports of diblock copolymer nano-objects prepared by a *wholly aqueous* RAFT PISA formulation that undergo a pH induced morphology transition. An and co-workers reported the chain extension of a PDMAEMA macro-CTA with 1,6-hexanediol diacrylate, in an 1:1 *ethanol/water* mixture by RAFT dispersion polymerisation to prepare core cross-linked micelles.[59] After purification by repeated ultrafiltration in aqueous solution, these particles acted as efficient dodecane-in-water Pickering emulsifiers at low pH. However, deprotonating the tertiary amines of the PDMAEMA block causes the cross-linked micelles to aggregate, leading to demulsification.

In this Chapter, a poly(glycerol monomethacrylate) (PGMA) macro-CTA is chain-extended *via* a statistical copolymerisation mixture of 2-hydroxypropyl methacrylate (HPMA) and DPA by RAFT aqueous dispersion polymerisation. A series of $PGMA_{56}$-P($HPMA_y$-*stat*-DPA_z) diblock copolymer worms, vesicles and spheres were prepared by PISA and their pH-responsive behaviour was analysed by various techniques. In contrast to Chapters 2 and 3, the pH-responsive component is

a tertiary amine and is located within the core, rather than at the periphery of the stabiliser block.

4.2 Experimental Section

4.2.1 Materials

Glycerol monomethacrylate (GMA; 99.8 %) was donated by GEO Specialty Chemicals (Hythe, UK) and used without further purification. 2-Hydroxypropyl methacrylate (HPMA) was purchased from Alfa Aesar (UK) and used as received. 2-(Diisopropylamino)ethyl methacrylate (DPA, > 98 %) was purchased from Scientific Polymer Products Inc. (USA) and passed through a basic alumina column prior to use. 2-Cyano-2-propyl dithiobenzoate (CPDB), 4,4'-azobis(4-cyanopentanoic acid) (ACVA; V-501; 99 %), deuterated methanol, DCl, ethanol (99 %, anhydrous grade), methanol and dichloromethane were purchased from Sigma-Aldrich (UK) and were used as received. All solvents were of HPLC quality.

4.2.2 Synthesis of poly(glycerol monomethacrylate) ($PGMA_{56}$) macro-CTA

A typical protocol for the synthesis of $PGMA_{56}$ macro-CTA was as follows: GMA (203.0 g, 1.268 mol), CPDB (6.03 g, 0.020 mol; target DP = 63), ACVA (1.14 g, 4.07 mmol; CPDB: ACVA molar ratio = 5.0) and anhydrous ethanol (156.0 g, 3.38 mol) were added to a round-bottomed flask to afford a 55 % w/w solution. The resulting pink solution was purged with N_2 for 40 min, before the sealed flask was immersed into an oil bath set at 70 °C. After 140 min (69 % conversion as judged by ^{1}H NMR) the polymerisation was quenched by immersion of the flask into an ice bath and exposing the reaction mixture to air. The crude polymer was then precipitated into a ten-fold excess of dichloromethane and washed three times using this non-solvent to remove residual unreacted GMA monomer before being dried under high vacuum for three days at 40 °C. ^{1}H NMR studies indicated a mean degree of polymerisation of 56 *via* end-group analysis (the integrated aromatic RAFT end-

group signals at 7.1-7.4 ppm were compared to polymer backbone signals between 0.5 to 2.5 ppm). Taking into account the target DP of 63 and the GMA conversion of 69 %, this indicated a CTA efficiency of 76 %. DMF GPC studies indicated an M_n of 15,000 g mol^{-1} and an M_w/M_n of 1.11. ^{1}H NMR (400 MHz, CD_3OD, 25 °C): δ 0.73-1.26 (b, 3H, -$CH_2CR(CH_3)$-), 1.55-2.32 (b, 2.2H, -$CH_2CR(CH_3)$-), 3.50-3.83 (b, 2.4H, -CH_2OH), 3.84-4.25 (b, 3.1H, -COOCH_2CH(OH)-).

4.2.3 Synthesis of $PGMA_{56}$-$PHPMA_x$ diblock copolymer nano-objects *via* RAFT aqueous dispersion polymerisation

A typical protocol for the chain extension of $PGMA_{56}$ macro-CTA with 140 units of HPMA *via* RAFT aqueous dispersion polymerisation is as follows: $PGMA_{56}$ macro-CTA (0.319 g, 0.035 mmol), HPMA monomer (0.70 g, 4.9 mmol), ACVA (3.2 mg, 0.012 mmol; $PGMA_{56}$ macro-CTA: ACVA molar ratio = 3.0) were added to a 25 ml round-bottomed flask, prior to addition of water to produce a 15 % w/w solution. The reaction solution was purged under nitrogen for 30 min at 20 °C prior to immersion into an oil bath set at 70 °C. The reaction mixture was stirred for 4 h to ensure almost complete conversion of the HPMA monomer (> 99 % by ^{1}H NMR analysis) and was quenched by exposure to air and cooling to ambient temperature. The copolymer dispersion was characterised by DLS, TEM and rheology without further purification. ^{1}H NMR (400 MHz, 96: 4 CD_3OD/DCl, 25 °C): δ 0.73-1.19 (b, 3H, -CH_3 on polymer backbone), 1.19-1.39 (b, 2.3H, -CH_3 in PHPMA), 1.48-2.31 (b, 2.1H, -CH_2- on polymer backbone), 3.53-3.71 (b, 0.8H, -CH_2OH in PGMA and –CH(OH)- in HPMA), 3.71-4.95 (b, 2.8H, remaining pendent protons in PGMA and PHPMA).

4.2.4 RAFT synthesis of $PGMA_{56}$-$P(HPMA_y$-*stat*-$DPA_z)$ diblock copolymer worms

A typical protocol for the chain extension of $PGMA_{56}$ macro-CTA with 130 units of HPMA and 10 units of DPA *via* RAFT polymerisation in water is as follows: $PGMA_{56}$ macro-CTA (0.393 g, 0.043 mmol), HPMA monomer (0.80 g, 5.5 mmol), ACVA (4.0 mg, 0.014 mmol; $PGMA_{56}$ macro-CTA: ACVA molar ratio = 3.0) were

added to a 25 ml round-bottomed flask, prior to addition of water to produce a 15 % w/w solution. The reaction solution was purged under nitrogen for 10 min at 20 °C. Degassed DPA (32 mg, 0.16 mmol) was added to this reaction mixture and the pH of the solution was adjusted to approximately 7.5-8.0. The reaction solution was then degassed further for 20 min prior to immersion into an oil bath set at 70 °C. The reaction mixture was stirred for 4 h to ensure almost complete conversion of the HPMA monomer (> 99 % by ^{1}H NMR analysis) and a high DPA monomer conversion (93 % by ^{1}H NMR analysis). Finally the reaction was quenched by exposure to air and cooling to ambient temperature. The resulting free-standing gel was characterised by DLS, TEM and rheology without further purification. ^{1}H NMR (400 MHz, 96: 4 CD_3OD/DCl, 25 °C): δ 0.72-1.19 (b, 3H, **-CH_3** on polymer backbone), 1.20-1.36 (b, 2.4H, **-CH**OH in PHPMA), 1.45-1.56 (b, 0.5H, **-CH_3** in PDPA), 1.56-2.30 (b, 2.1H, **-CH_2-** on polymer backbone), 3.50-3.72 (b, 1.1H, -**CH_2**OH in PGMA and –**CH**(OH)- in PHPMA), 3.73-4.90 (b, 2.8H, remaining pendent protons in PGMA, PHPMA and PDPA).

4.2.5 RAFT synthesis of $PGMA_{56}$-P($HPMA_y$-*stat*-DPA_z) diblock copolymer vesicles

A typical protocol for the chain extension of $PGMA_{56}$ macro-CTA with 240 units of HPMA and 10 units of DPA *via* RAFT polymerisation in water is as follows: $PGMA_{56}$ macro-CTA (0.213 g, 0.023 mmol), HPMA monomer (0.80 g, 5.5 mmol), ACVA (2.2 mg, 0.008 mmol; $PGMA_{56}$ macro-CTA: ACVA molar ratio = 3.0) were added to a 25 ml round-bottomed flask, prior to addition of water to produce a 15 % w/w solution. The reaction solution was purged under nitrogen for 10 min at 20 °C. Degassed DPA (49 mg, 0.23 mmol) was added to this reaction mixture and the pH of the solution was adjusted to approximately 7.5-8.0. The reaction solution was then degassed further for 20 min prior to immersion into an oil bath set at 70 °C. The reaction mixture was stirred for 4 h to ensure almost complete conversion of the HPMA monomer (> 99 % by ^{1}H NMR analysis) and a high DPA monomer conversion (91 % by ^{1}H NMR analysis). Finally the reaction was quenched by exposure to air, following by cooling to ambient temperature. The resulting turbid free-flowing dispersion was characterised by DLS, TEM and visible spectroscopy

without further purification. ^{1}H NMR (400 MHz, 96: 4 CD_3OD/DCl, 25 °C): δ 0.79-1.20 (b, 3H, **-CH_3** on polymer backbone), 1.20-1.35 (b, 2.6H, -**CH**OH in PHPMA), 1.46-1.56 (b, 0.3H, **-CH_3** in PDPA), 1.56-2.23 (b, 2H, **-CH_2-** on polymer backbone), 3.52-3.73 (b, 0.9H, **-CH_2**OH in PGMA and –**CH**(OH)- in PHPMA), 3.73-4.86 (b, 2.7H, remaining pendent protons in PGMA, PHPMA and PDPA).

4.2.6 RAFT synthesis of $PGMA_{56}$-$P(HPMA_y$-*stat*-$DPA_z)$ diblock copolymer spheres

A typical protocol for the chain extension of $PGMA_{56}$ macro-CTA with 90 units of HPMA and 10 units of DPA *via* RAFT polymerisation in water is as follows: $PGMA_{56}$ macro-CTA (0.1347 g, 0.015 mmol), HPMA monomer (0.19 g, 1.3 mmol), ACVA (1.4 mg, 0.005 mmol; $PGMA_{56}$ macro-CTA: ACVA molar ratio = 3.0) were added to a 10 ml round-bottomed flask, prior to addition of water to produce a 15 % w/w solution. The reaction solution was purged under nitrogen for 10 min at 20 °C. Degassed DPA (31 mg, 0.15 mmol) was added to this reaction mixture and the pH of the solution was adjusted to approximately 7.5-8.0. The reaction solution was then degassed for a further 15 min prior to immersion into an oil bath set at 70 °C. The reaction mixture was stirred for 4 h to ensure near complete conversion of the HPMA monomer (> 99 % by ^{1}H NMR analysis) and a high DPA monomer conversion (91 % by ^{1}H NMR analysis). Finally, the reaction was quenched by exposure to air and cooling to ambient temperature. The resulting free-flowing dispersion was characterised by DLS and TEM without further purification. ^{1}H NMR (400 MHz, 96: 4 CD_3OD/DCl, 25 °C): δ 0.72-1.19 (b, 3H, **-CH_3** on polymer backbone), 1.18-1.38 (b, 2.3H, -**CH**OH in PHPMA), 1.46-1.57 (b, 0.6H, **-CH_3** in PDPA), 1.57-2.23 (b, 2H, **-CH_2-** on polymer backbone), 3.52-3.71 (b, 1.2H, **-CH_2**OH in PGMA and –**CH**(OH)- in PHPMA), 3.74-4.86 (b, 2.8H, remaining pendent protons in PGMA, PHPMA and PDPA).

4.2.7 Synthesis of $PGMA_{56}$-$PDPA_{140}$ diblock copolymer spheres *via* RAFT aqueous emulsion polymerisation

A typical protocol for the chain extension of $PGMA_{56}$ macro-CTA with 140 units of DPA *via* RAFT aqueous emulsion polymerisation is as follows: $PGMA_{56}$ macro-CTA (0.249 g, 0.027 mmol), DPA monomer (0.80 g, 3.8 mmol), ACVA (2.5 mg, 0.009 mmol; $PGMA_{56}$ macro-CTA: ACVA molar ratio = 3.0) were added to a 25 ml round-bottomed flask, prior to addition of water to produce a 15 % w/w solution. The pH of the solution was adjusted to approximately 7.5-8.0. Then the reaction solution was purged under nitrogen for 30 min at 20 °C prior to immersion into an oil bath set at 70 °C. The reaction mixture was stirred for 8 h before being quenched by exposure to air and cooling to ambient temperature. ^{1}H NMR analysis indicated DPA monomer conversions of 85 %. ^{1}H NMR (400 MHz, 96: 4 CD_3OD/DCl, 25 °C): δ 0.76-1.25 (b, 3H, **-CH_3** on polymer backbone), 1.37-1.62 (b, 10.6H, **-CH_3** in PDPA), 1.74-2.54 (b, 2H, **-CH_2-** on polymer backbone), 3.41-4.61 (b, 4.9H, remaining pendent protons in PGMA and PDPA).

4.2.8 Instrumentation

^{1}H NMR spectra were recorded using a 500 MHz Bruker Avance-500 spectrometer (64 scans averaged per spectrum).

Gel Permeation Chromatography (GPC) was used to assess polymer molecular weight distributions. The DMF GPC set-up comprised two Polymer Laboratories PL gel 5 μm Mixed-C columns connected in series to a Varian 390-LC multi-detector suite (refractive index detector) and a Varian 290-LC pump injection module operating at 60 °C. The GPC eluent was HPLC-grade DMF containing 10 mM LiBr at a flow rate of 1.0 mL min^{-1}. DMSO was used as a flow-rate marker. Calibration was conducted using a series of ten near-monodisperse poly(methyl methacrylate) standards (M_n = 625 to 2,480,000 g mol^{-1}). Chromatograms were analysed using Varian Cirrus GPC software (version 3.3). The molecular weight distribution of the $PGMA_{56}$-$PDPA_{140}$ copolymer was assessed by GPC using THF eluent. Prior to analysis, the copolymer was modified with benzoic anhydride to ensure copolymer

solubility in THF using a previously described protocol.[60] The THF GPC system was equipped with two 5 μm (30 cm) Mixed-C columns and a WellChrom K-2301 refractive index detector operating at 950 ± 30 nm. The mobile phase contained 2.0 % v/v triethylamine and 0.05 % w/v butylhydroxytoluene (BHT) with a toluene flow rate marker and the flow rate was fixed at 1.0 mL min-1. A series of ten near-monodisperse poly(methyl methacrylate) standards (M_n values ranging from 645 to 2,480,000 g mol^{-1}) were used for calibration.

Dynamic Light Scattering (DLS) studies were conducted using a Malvern Zetasizer NanoZS instrument at 25 °C. Measurements were performed on 0.10 % w/w aqueous dispersions in disposable cuvettes at a fixed back-scattering angle of 173°. Intensity-average hydrodynamic diameters were calculated *via* the Stokes-Einstein equation. All data were averaged over three consecutive runs. The 15 % w/w aqueous copolymer dispersion was diluted to 0.1 % in aqueous solution at pH 8.5. The solution pH was manually adjusted to the desired pH using HCl.

Aqueous electrophoresis measurements were conducted using a Malvern Zetasizer NanoZS instrument at 25 °C. Studies were performed on aqueous copolymer dispersions diluted to 0.10 % w/w containing 10^{-3} mol dm^{-3} KCl as background electrolyte. The solution pH was manually adjusted to the desired pH value using HCl starting from pH 8.5. Zeta potentials were calculated from the Henry equation using the Smoluchowski approximation. All data were averaged over three consecutive runs.

Transmission Electron Microscopy (TEM) imaging was performed on FEI Tecnai Spirit microscope fitted with a Gatan 1kMS600CW CCD camera operating at 80 kV. Copolymer dispersions were diluted at 20 °C to produce 0.10 % w/w dispersions at either pH 8.5 or pH 3.5. Copper/palladium TEM grids (Agar Scientific, UK) were surface-coated in-house to yield a thin film of amorphous carbon. The grids were then plasma glow-discharged for 30 s to create a hydrophilic surface. Individual samples (0.10 % w/w, 12 μL) were adsorbed onto the freshly glow-discharged grids for one minute and then blotted with filter paper to remove excess solution. For improved contrast when imaging, copolymer dispersions containing a low DPA contents (3 ≤ units), uranyl formate stain (0.75 % w/w, 9 μL) was placed on the

sample-loaded grid for 20 s and then carefully blotted to remove excess stain. Phosphotungstic acid (1.00 % w/w, 9 μL) was used to stain copolymer dispersions consisting of 5 or more DPA units, but was left on the grid for 4 s. The grids were then carefully dried using a vacuum hose.

Rheology studies were conducted using an AR-G2 stress controlled rheometer with a variable temperature Peltier plate. Storage moduli (G') were determined for the $PGMA_{56}$-P($HPMA_y$-*stat*-DPA_z) diblock copolymer worm gels at 25 °C at varying solution pH. After the dispersions were adjusted to the desired pH, they were left for one hour prior to measurements. Storage (G') and loss (G") moduli were determined by temperature-dependent rheological studies from 25 °C to 4 °C to 25 °C with a cooling/heating rate of 0.5 °C min^{-1}. In all cases a cone-and-plate geometry (40 mm 2 ° aluminium cone) was used for these measurements at a fixed strain of 1.0 % and an angular frequency of 1.0 rad s^{-1}.

Visible absorption spectroscopy was used to monitor changes in transmittance. Turbidimetry curves were recorded at 20 °C using a Shimadzu UV-1800 instrument operating in time drive mode at a fixed wavelength of 450 nm for 15 hours. Prior to analysis, the $PGMA_{56}$-P($HPMA_y$-*stat*-DPA_z) diblock copolymer vesicles were diluted to 0.10 % w/w aqueous dispersions at pH 8.5. Measurements were recorded every minute for $PGMA_{56}$-$PHPMA_{250}$ and $PGMA_{56}$-P($HPMA_{249}$-*stat*-DPA_1) vesicles and every 6 seconds for $PGMA_{56}$-P($HPMA_{245}$-*stat*-DPA_5) and $PGMA_{56}$-P($HPMA_{240}$-*stat*-DPA_{10}) vesicles immediately after this solution pH was reduced to pH 3.0 using 0.5 M HCl.

4.3 Results and Discussion

In Chapters 2 and 3 PGMA-PHPMA diblock copolymers prepared using a carboxylic acid-functionalised RAFT agent afforded pH-sensitive worms and vesicles (providing that a sufficiently low PHPMA core DP was targeted). Such nano-objects undergo order-order morphological transitions as a result of ionisation of the terminal acid group on the stabiliser block. Similarly, PGMA-PHPMA diblock

copolymer nano-objects can be prepared with a morpholine functionalised-CTA that undergo similar transformations when protonated.[61] In this Chapter, the effect of adding tertiary amine methacrylate groups to the *core* (or membrane) of similar diblock copolymer worms, vesicles and spheres (rather than the *periphery* of such particles) is explored. Therefore, a non-ionic CTA was used to eliminate the possibility of pH-responsive behaviour due to end-group effects. Furthermore, the amount number of amine units incorporated into the core of the nano-objects is systematically varied (see **Figure 4.4**).

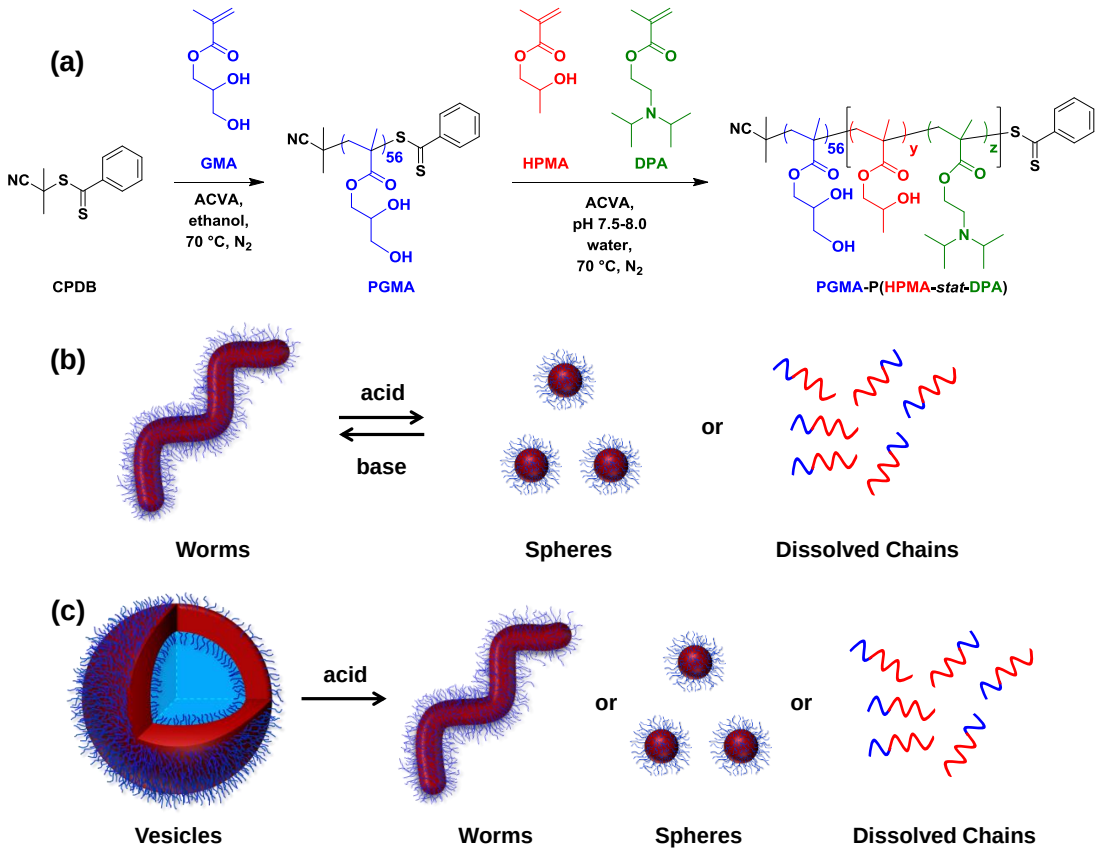

Figure 4.4 (a) Synthesis of a $PGMA_{56}$ macro-CTA *via* RAFT solution polymerisation of GMA in ethanol using CPDB, and its subsequent chain extension with a mixture of HPMA and DPA *via* RAFT aqueous dispersion polymerisation to prepare a series of $PGMA_{56}$-P($HPMA_y$-*stat*-DPA_z) diblock copolymer worms, vesicles or spheres. Illustrations of the (b) worms and (c) vesicles and their response to a pH switch by addition of either HCl or KOH.

A near-monodisperse (M_w/M_n = 1.15) PGMA macro-CTA was prepared by reversible-addition fragmentation chain transfer (RAFT) solution polymerisation in ethanol using 2-cyano-2-propyl dithiobenzoate (CPDB) as a non-ionic CTA. End-group analysis of the PGMA macro-CTA by ^{1}H NMR indicated a DP of 56 (see **Figure 4.5a**). The $PGMA_{56}$ macro-CTA was chain-extended with varying amounts of HPMA and DPA *via* RAFT dispersion copolymerisation in water at pH 8.0 to afford three series of $PGMA_{56}$-P($HPMA_y$-*stat*-DPA_z) diblock copolymers. PISA afforded either worms, vesicles or spheres depending on the target block composition.

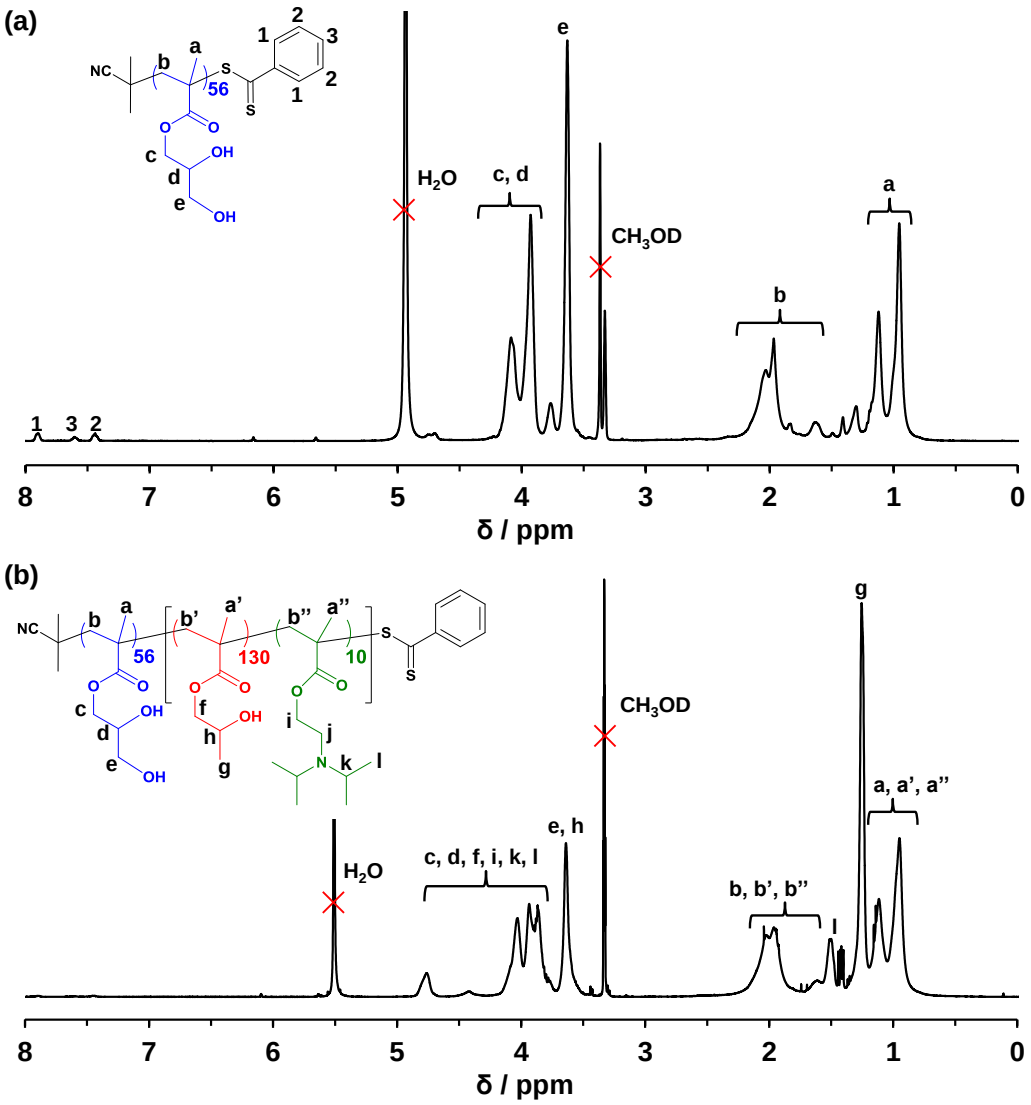

Figure 4.5 ^{1}H NMR spectra obtained for (a) purified $PGMA_{56}$ macro-CTA in CD_3OD and (b) $PGMA_{56}$-P($HPMA_{130}$-*stat*-DPA_{10}) in a 96:4 CD_3OD/DCl mixture.

It is noteworthy that preparation of $PGMA_{56}$-$PDPA_{140}$ diblock copolymers at pH 8.0 by RAFT aqueous emulsion polymerisation led to only spherical nanoparticles, as judged by TEM (see **Figure 4.6a**). This observation is consistent with several other PISA by RAFT aqueous emulsion formulations.[62-64] Although these nanoparticles proved to be pH-responsive, the final monomer conversion only reached approximately 85 % and some precipitation was observed. Moreover, after modification of the PGMA block with excess benzoic anhydride, THF GPC indicated that the polymerisations were only poorly controlled (M_w/M_n = 2.17), see **Figure 4.6b**). Hence a statistical core-forming copolymer comprising DPA and HPMA was selected to produce worms and vesicles.

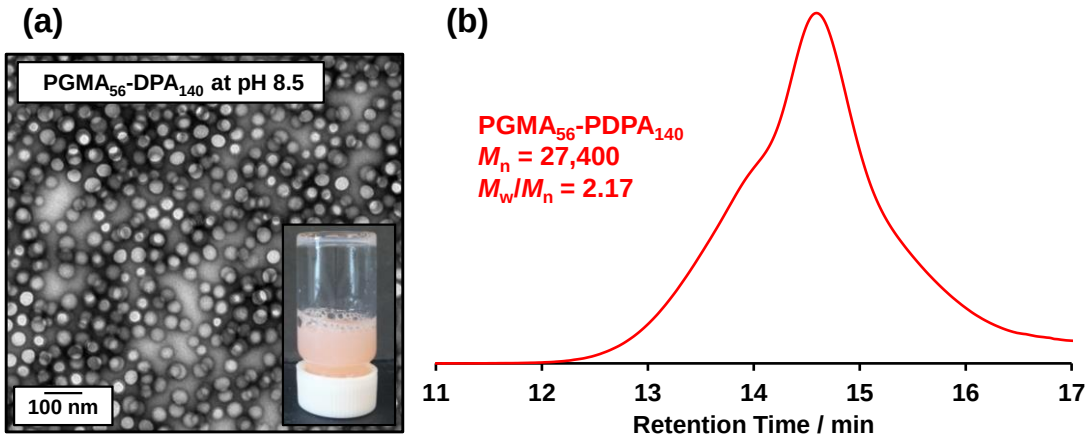

Figure 4.6 (a) TEM image recorded at pH 8.5 for dilute 0.1 % w/w aqueous copolymer dispersion and the corresponding digital image obtained at 15 % w/w solids at pH 8.5 for $PGMA_{56}$-$PDPA_{140}$ diblock copolymer spheres. (b) THF GPC trace obtained for $PGMA_{56}$-$PDPA_{140}$ diblock copolymer.

A typical ^{1}H NMR spectra recorded for $PGMA_{56}$-P($HPMA_{130}$-*stat*-DPA_{10}) diblock copolymer chains dissolved in a 96: 4 CD_3OD/DCl mixture is shown in **Figure 4.5b**. DPA comonomer was selected in order to introduce pH-responsive character into the core-forming block of the particles. Furthermore, DPA has previously been successfully polymerised by RAFT chemistry and offers complementary pH-responsive behaviour to that reported in the two previous Chapters.[17,18,65,66] More specifically, at relatively high solution pH values (> 7.0) the tertiary amine groups in DPA residues are mainly deprotonated and hence

hydrophobic. When the solution pH is lowered, the tertiary amine groups become protonated and the P(HPMA-*stat*-DPA) block should become cationic and hence more water-soluble. It is hoped that such switches in pH may induce morphology transitions. Acid titration studies indicated that the pK_a of this tertiary amine is approximately 7.2. Therefore, it is hoped such pH-responsive morphology transitions may be useful for biological applications in the future (such as encapsulation and delivery of payloads). This is because the extracellular fluid is typically approximately pH 7.4, whereas the pH inside a lysosome (an organelle within a cell that breaks down biomolecules and cellular debris) is approximately pH 4.5.[2]

^{1}H NMR analysis of the chain extension of $PGMA_{56}$ with 140 units of HPMA in water at 15 % w/w solids indicated that high monomer conversion (> 99 %) was reached after 2 h at 70 °C (**Figure 4.7a**). Three separate rate regimes were observed. Initially, HPMA monomer was consumed slowly, which may indicate some degree of retardation.[67] After 30 min, a modest increase in rate is observed in the semi-logarithmic plot (see blue data). At approximately 50 min, the rate of polymerisation is enhanced by a factor of three. This is likely to be the result of micellar nucleation, which causes unreacted HPMA monomer to migrate into the cores of the nascent particles, thus causing an increase in the local concentration.[68] The reaction was complete after approximately 90 min. In contrast, ^{1}H NMR kinetic studies of the PISA synthesis of $PGMA_{56}$-P($HPMA_{130}$-*stat*-DPA_{10}) in water at 15 % w/w solids indicated that HPMA monomer reached almost full conversion (> 99 %) after 60 min at 70 °C (see red data in **Figure 4.7b**), whereas DPA monomer only reached 84 % conversion after 90 min (see green data). After 240 min only a slight increase in DPA conversion (86 %) was observed. Like the $PGMA_{56}$-$PHPMA_{140}$ diblock copolymer synthesis, the initial rate of copolymerisation was quite slow. However, after only 30 min the rate of copolymerisation increases significantly by a factor of approximately seven, presumably as a result of nucleation and subsequent migration of HPMA and DPA monomers into the cores. Surprisingly, the DPA monomer initially polymerises faster than HPMA. Previous work by Ratcliffe and co-workers suggest that this is probably due to HPMA being consumed *via* dispersion polymerisation, whereas DPA is consumed by emulsion polymerisation, which has been shown to proceed faster.[69] In light of these findings, each diblock copolymer

was allowed to react for 4 h at 70 °C to ensure as high a final conversion as possible was obtained.

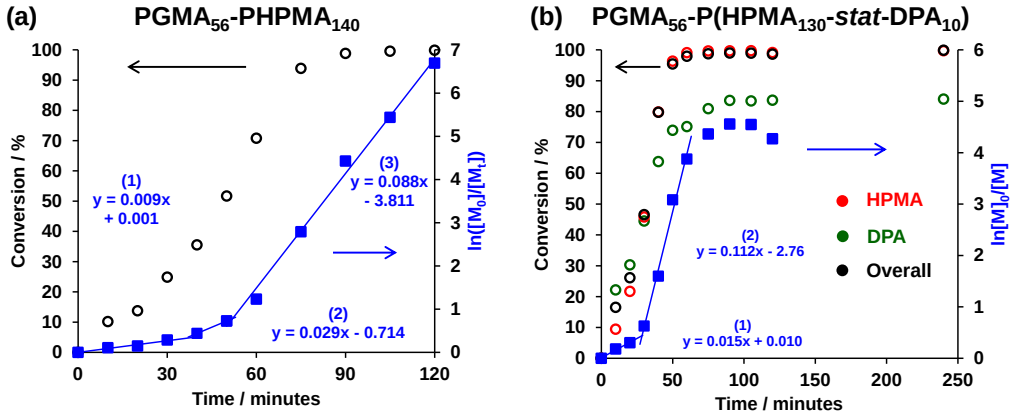

Figure 4.7 Monomer conversion versus time curves determined by ^{1}H NMR analysis versus time for the chain extension of a $PGMA_{56}$ macro-CTA with (a) 140 units of HPMA and (b) a statistical comonomer mixture of 130 units of HPMA (red circles) and 10 units of DPA (green circles). The semi-logarithmic plot of the overall monomer conversion is shown by the blue squares.

4.3.1 Acid-responsive $PGMA_{56}$-P($HPMA_y$-*stat*-DPA_z) diblock copolymer worms

Six $PGMA_{56}$-P($HPMA_y$-*stat*-DPA_z) diblock copolymer worms with varying core compositions were prepared by PISA *via* RAFT aqueous dispersion statistical copolymerisation of HPMA and DPA at 70 °C and 15 % w/w copolymer solids. In all cases a total DP of 140 was targeted for the core block (i.e., y + z = 140), but the number of DPA units was varied from 0 to 15. ^{1}H NMR analysis indicated that very high HPMA conversions (> 99 %) and fairly high DPA conversions (> 90 %) were achieved after 4 h at 70 °C in all cases. It is noteworthy that target compositions will be quoted throughout this Chapter for brevity. DMF GPC studies indicated that all diblock copolymers possessed similar number-average molecular weights (M_n) and high blocking efficiencies relative to $PGMA_{56}$ macro-CTA (**Figure 4.8**). However, increasing the amount of DPA in the core block produced a pronounced high molecular weight shoulder (at lower retention times) and broader molecular weight distributions. This may indicate some degree of chain transfer to the isopropyl groups

on the DPA units, which may cause light branching.[70,71] Furthermore, DPA monomer might conceivably contain dimethacrylate impurity which could also cause chain branching.[52,69] Nevertheless, fairly good control is still achieved even at relatively high DPA contents, and the formation of nano-objects by PISA appears to be unaffected.

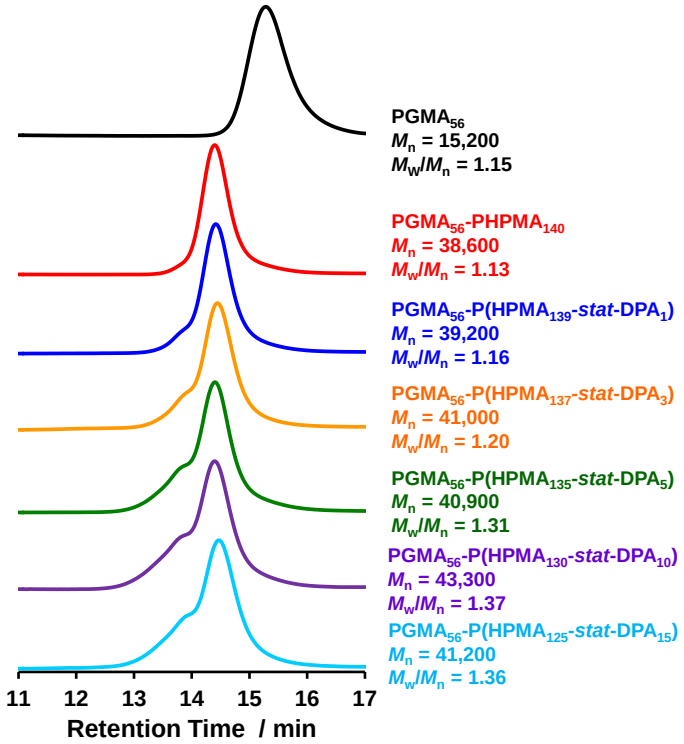

Figure 4.8 DMF GPC traces obtained for a $PGMA_{56}$ macro-CTA (black curve) and a series of six $PGMA_{56}$-P($HPMA_y$-*stat*-DPA_z) diblock copolymers where y + z =140. In all cases high blocking efficiencies are observed.

As expected, all six $PGMA_{56}$-P($HPMA_y$-*stat*-DPA_z) diblock copolymers form free-standing gels at 15 % w/w solids, as judged by the tube inversion test (see insets in **Figure 4.9**). However, TEM studies conducted on dilute aqueous dispersions (0.1 % w/w) at pH 8.5 suggested that pure worm phases are only obtained if the core-forming block consists of 3 DPA units or less (i.e., $z \leq 3$) (see **Figure 4.9a-c**). Conversely, TEM images obtained for the $PGMA_{56}$-P($HPMA_{135}$-*stat*-DPA_5) diblock dispersion suggested a mixed phase of branched worms with a small fraction of vesicles is formed (**Figure 4.9d**). Similarly, $PGMA_{56}$-P($HPMA_{130}$-*stat*-DPA_{10}) diblock copolymers yielded a mixture of vesicles and branched worms (**Figure 4.9e**).

In the latter two cases, turbid gels were obtained, presumably due to the presence of the (larger) vesicles. This morphology evolution (i.e., from worms to branched worms to vesicles) is similar to that previously reported by Verber *et al.* for a series of $PGMA_{54}$-$PHPMA_X$ diblock copolymers of increasing PHPMA DP.[68] Surprisingly, in the case of $PGMA_{56}$-P($HPMA_{125}$-*stat*-DPA_{15}) diblock copolymers, no vesicles were observed by TEM, but instead a mixed phase of worms and spheres was obtained (**Figure 4.9f**). Increasing the DPA content in the copolymers afforded more hydrophobic core-forming blocks. Thus it seems that more hydrophobic blocks drive assembly into higher order morphologies. However, adding too much water-immiscible DPA to the formulation favours RAFT *emulsion* rather than *dispersion* polymerisation. Thus self-assembly into lower order morphologies occurs. This is reasonable, because using DPA as the sole core-forming monomer leads to exclusively spherical PGMA-PDPA nano-objects, as discussed above. Similar kinetically-trapped spheres have been reported for various other RAFT aqueous emulsion polymerisation formulations.[62-64]

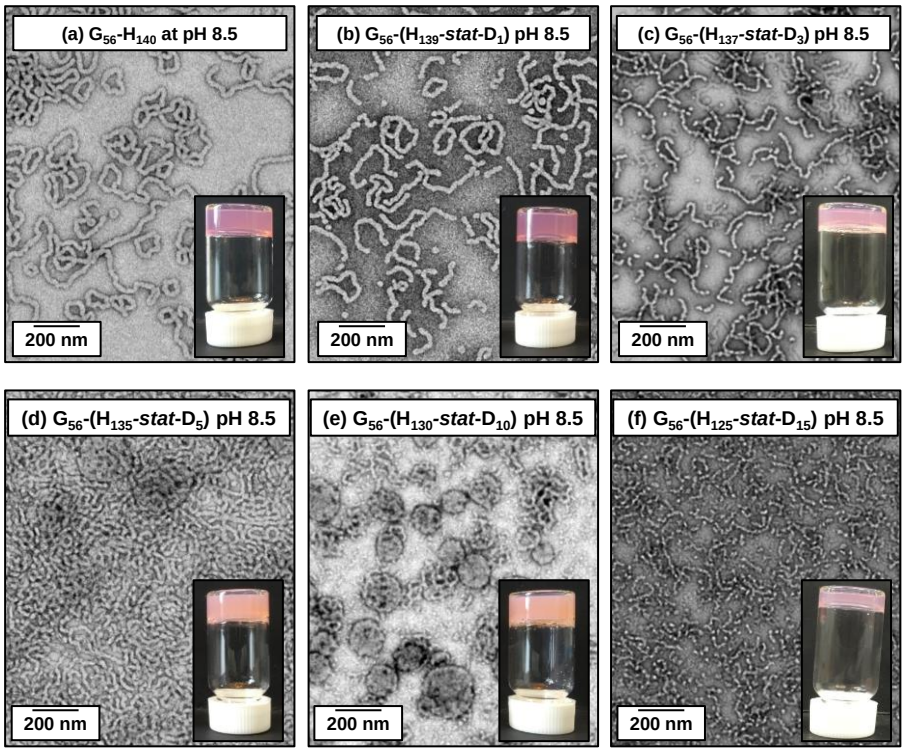

Figure 4.9 TEM images recorded at pH 8.5 for dilute 0.1 % w/w aqueous copolymer dispersion and the corresponding digital images obtained at 15 % w/w at pH 8.5 for a series of $PGMA_{56}$-P($HPMA_y$-*stat*-DPA_z) diblock copolymer nano-objects, where y + z =140. These copolymers are denoted as G_{56}-(H_y-*stat*-D_z) for brevity.

Since these $PGMA_{56}$-P($HPMA_y$-*stat*-DPA_z) diblock copolymer nano-objects were prepared at pH 8.0, the tertiary amine groups in the DPA units are deprotonated and uncharged. However, when the pH is adjusted to 3.5, these amines become protonated and cationic, since the pK_a of the DPA units is approximately 7.2. As expected, the non-ionic $PGMA_{56}$-$PHPMA_{140}$ diblock copolymer worms exhibit no pH-responsive behaviour and remain as a pure worm phase at pH 3.5, as judged by TEM (**Figure 4.10a**). Similarly, $PGMA_{56}$-P($HPMA_{139}$-*stat*-DPA_1) worms appear pH-insensitive as judged by TEM images obtained at pH 3.5 (**Figure 4.10b**). This behaviour is in stark contrast to that observed for HOOC-$PGMA_{56}$-$PHPMA_{155}$ diblock copolymer worms prepared in Chapter 2, whereby ionisation of a *single* carboxylic acid end-group on the PGMA stabiliser block is sufficient to induce an order-order morphological transition.[72] Although protonation of an amine rather than ionisation of a carboxylic acid is being explored here, it nevertheless appears that the spatial location of the charge can influence whether pH-responsive behaviour is observed. More specifically, placing (cationic) charge in the core rather than (anionic) charge at the periphery of the particles yields nano-objects that are less pH-sensitive. In contrast, order-order or order-disorder morphological transitions were observed on switching from pH 8.5 to pH 3.5 when three or more DPA units were present in the core-forming block. These morphology transitions were accompanied by rapid degelation, since multiple inter-worm contacts are no longer possible (see inset of **Figure 4.10c-d**). For example, TEM studies indicated $PGMA_{56}$-P($HPMA_{137}$-*stat*-DPA_3) and $PGMA_{56}$-P($HPMA_{135}$-*stat*-DPA_5) diblock copolymers form ill-defined mixtures of spheres and spherical dimers at pH 3.5 (see **Figure 4.10c** and **d**). In contrast, no particles were observed for $PGMA_{56}$-P($HPMA_{130}$-*stat*-DPA_{10}) and $PGMA_{56}$-P($HPMA_{125}$-*stat*-DPA_{15}), suggesting a transition to molecularly dissolved chains in these two cases (**Figure 4.10e** and **f**). These latter transitions are believed to occur because the larger number of cationic DPA residues renders the core-forming block sufficiently hydrophilic.

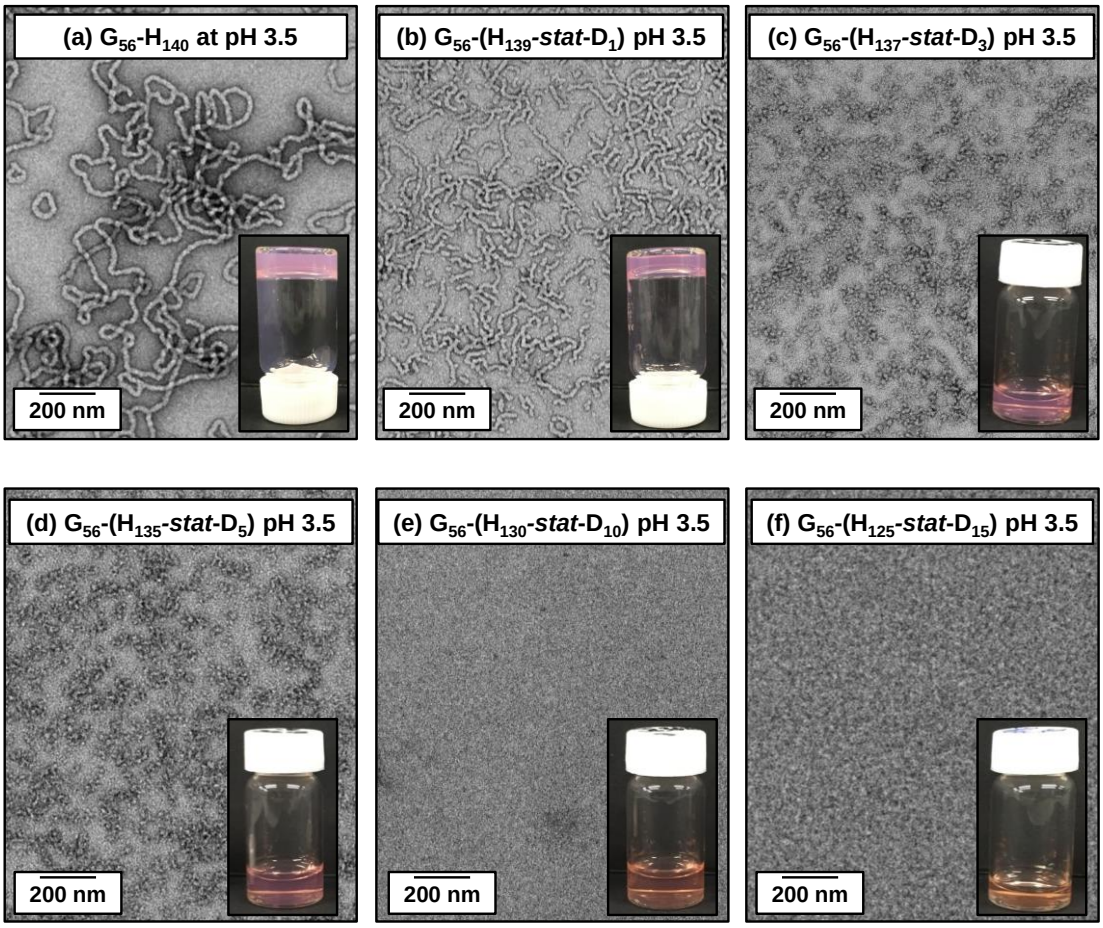

Figure 4.10 TEM images recorded at pH 3.5 (from a dilute 0.1 % w/w aqueous dispersion) and the corresponding digital photographs obtained at 15 % w/w solids at pH 3.5 for a series of $PGMA_{56}$-P($HPMA_y$-*stat*-DPA_z) diblock copolymers, where y + z = 140. These copolymers are denoted as G_{56}-(H_y-*stat*-D_z) for brevity.

The worm-to-sphere morphological transition observed for $PGMA_{56}$-P($HPMA_{137}$-*stat*-DPA_3) and $PGMA_{56}$-P($HPMA_{135}$-*stat*-DPA_5) diblock copolymers is more complex and not yet fully understood. If the P($HPMA_y$-*stat*-DPA_z) core was truly statistical, then a worm-to-vesicle (or to a higher order morphology) transformation might be expected on protonation of the DPA units at low pH. This is because the volume of the core segment should increase due to a combination of electrostatic repulsion between cationic DPA units and greater water solubility of the core-forming block. Therefore, the packing parameter should increase (as $p = v / a_0 l_c$) and so favour higher order morphologies, such as vesicles. However, DPA is initially consumed significantly faster than HPMA (as judged by ^{1}H NMR studies,

see **Figure 4.7**), thus the copolymer residues near the block junction point with the PGMA stabiliser block become DPA-enriched. Thus the protonated cationic DPA residues near the block junction increases the effective volume of the stabiliser block compared to that of the core-forming block (see **Figure 4.11**). Furthermore, electrostatic repulsion between weakly cationic chains at the junction point also favours formation of spheres (or lower order morphologies).[73]

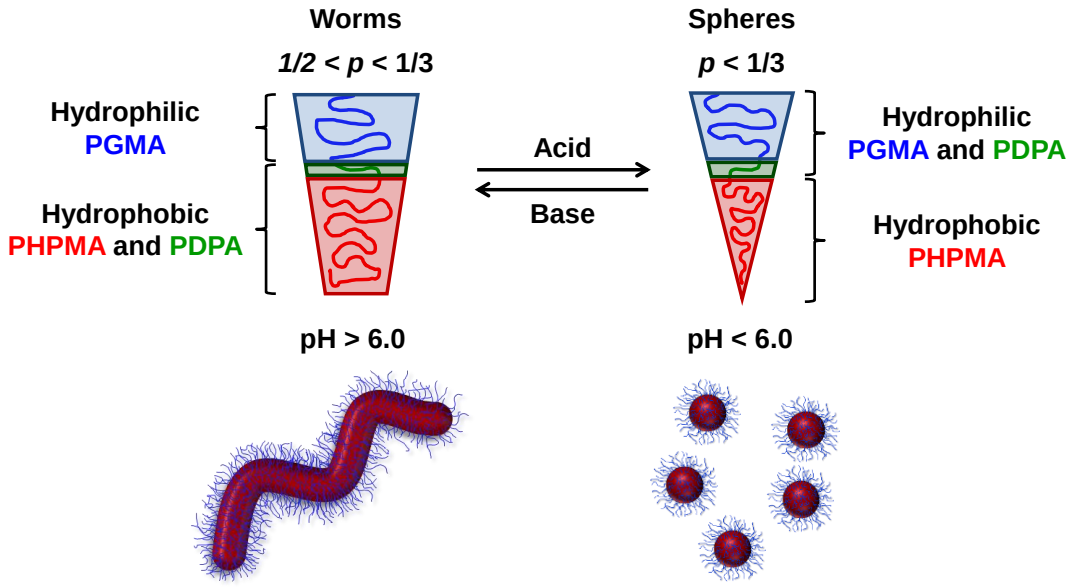

Figure 4.11 Graphical representation of the change in packing parameter and the associated worm-to-sphere transition for P(HPMA$_{137}$-*stat*-DPA$_3$) and PGMA$_{56}$-P(HPMA$_{135}$-*stat*-DPA$_5$) diblock copolymer nano-objects after a pH switch.

The pH-responsive nature of these particles was also examined by dynamic light scattering (DLS) studies performed on dilute aqueous dispersions (0.1 % w/w) between pH 8.5 and 3.0 at 25 °C. DLS reports sphere-equivalent diameters, rather than lengths or widths of the worm particles. Nevertheless, this technique can provide useful information regarding changes in apparent diameter with pH. Furthermore, monitoring derived count rates from these measurements can give a good indication of certain morphological transitions, in particular dissolution into molecularly-dissolved unimers. This is because the intensity of the scattered light is related to the derived count rate, and larger particles scatter more light. It is important that these studies are conducted at 25 °C, as PGMA-PHPMA particles are

known to undergo a worm-to-sphere transition on cooling below 10 °C.[74,75] As expected, both the apparent diameter and count rate for the neutral $PGMA_{56}$-$PHPMA_{140}$ diblock copolymer worm remained fairly constant on varying the solution pH (**Figure 4.12a**). The slight noticeable upturn in diameter at pH 3-4 is most likely due to protonation of some carboxylic acid end-groups derived from the ACVA initiator used in the synthesis of the PGMA macro-CTA. Furthermore ACVA is used in the PISA synthesis of the nano-objects. Remarkably, $PGMA_{56}$-P($HPMA_{139}$-*stat*-DPA_1) diblock copolymer worms undergo a significant reduction in diameter from 70 nm at pH 8.5 to 30 nm at pH 3.0, despite appearing to be pH-insensitive by TEM (**Figure 4.12b**). Furthermore, the derived count rate was reduced from 40,000 kcps to 6,000 kcps, which suggests a morphology transition. This apparent change in diameter is anomalous and warrants further investigation in the future. Similar trends were also observed for DLS studies of $PGMA_{56}$-P($HPMA_{137}$-*stat*-DPA_3) and $PGMA_{56}$-P($HPMA_{135}$-*stat*-DPA_5) diblock copolymer worms on lowering the solution pH from 8.5 to 3.0 using HCl (**Figure 4.12c** and **d**). The apparent diameter reduction for these DPA-containing copolymers occurred between pH 7.0 and 6.0 (i.e., close to the pK_a value of PDPA). This suggests that nearly all the tertiary amines are required to be protonated to induce a morphology transition. The increase in particle diameter observed between pH 8.5 and 7.0, is believed to be due to partial protonation of the amine groups leading to swelling. In contrast, DLS studies of $PGMA_{56}$-P($HPMA_{130}$-*stat*-DPA_{10}) and $PGMA_{56}$-P($HPMA_{125}$-*stat*-DPA_{15}) diblock copolymer nano-objects suggest molecular dissolution as the derived count rates were reduced from 40,000 kcps at pH 8.5 to below 1,000 kcps at pH 3.5 (**Figure 4.12e** and **f**).[76] It is noteworthy DLS is not well-suited for the characterisation of molecularly-dissolved chains as they scatter little light. Hence unreliable values for diameters are often obtained.

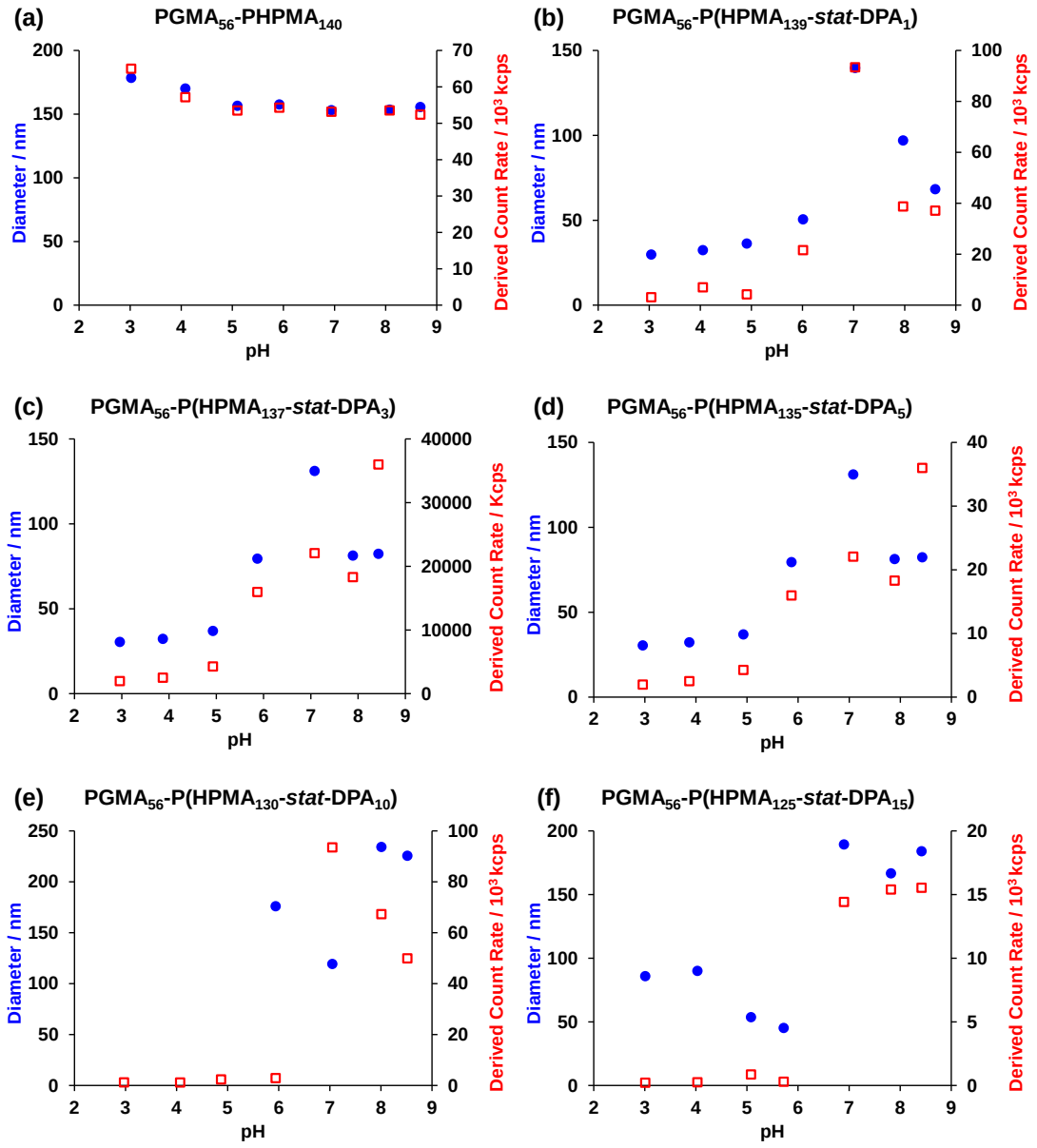

Figure 4.12 pH-dependent hydrodynamic diameter and derived count rate determined by dynamic light scattering (DLS) at 25 °C for 0.1 % w/w aqueous dispersions of (a) $PGMA_{56}$-$PHPMA_{140}$, (b) $PGMA_{56}$-P($HPMA_{139}$-*stat*-DPA_1), (c) $PGMA_{56}$-P($HPMA_{137}$-*stat*-DPA_3), (d) $PGMA_{56}$-P($HPMA_{135}$-*stat*-DPA_5), (e) $PGMA_{56}$-P($HPMA_{130}$-*stat*-DPA_{10}) and (f) $PGMA_{56}$-P($HPMA_{125}$-*stat*-DPA_{15}) diblock copolymer nano-objects. The dispersions were adjusted from pH 8.5 to pH 3.0 using HCl.

Aqueous electrophoresis studies were conducted on the six $PGMA_{56}$-P($HPMA_y$-*stat*-DPA_z) diblock copolymers diluted to 0.1 % w/w solids at varying solution pH to assess the surface charge (zeta potential) associated with such

particles (**Figure 4.13**). At high pH, all six diblock copolymer nano-objects possessed slightly negative character (-5 mV to -10 mV), which is most likely due to deprotonated ACVA initiator used for the synthesis of the particles and perhaps the presence of some methacrylic acid residues due to hydrolysis. Furthermore, a small fraction of the PGMA stabiliser chains will have carboxylic acid end-groups as ACVA initiator was utilised for the synthesis of the macro-CTA. As expected, $PGMA_{56}$-$PHPMA_{140}$ diblock copolymer worms remain slightly anionic between pH 8.5 and 3.0 as they do not contain any DPA units. Conversely, all $PGMA_{56}$-P($HPMA_y$-*stat*-DPA_z) diblock copolymers containing at least one DPA residue in the core-forming block exhibit cationic character at pH 3.0 (with zeta potentials ranging from + 5 mV to + 20 mV). Moreover, their isoelectric points are between pH 5.0 and 7.0 which is in reasonable agreement with the pK_a of PDPA (approximately 7.2).

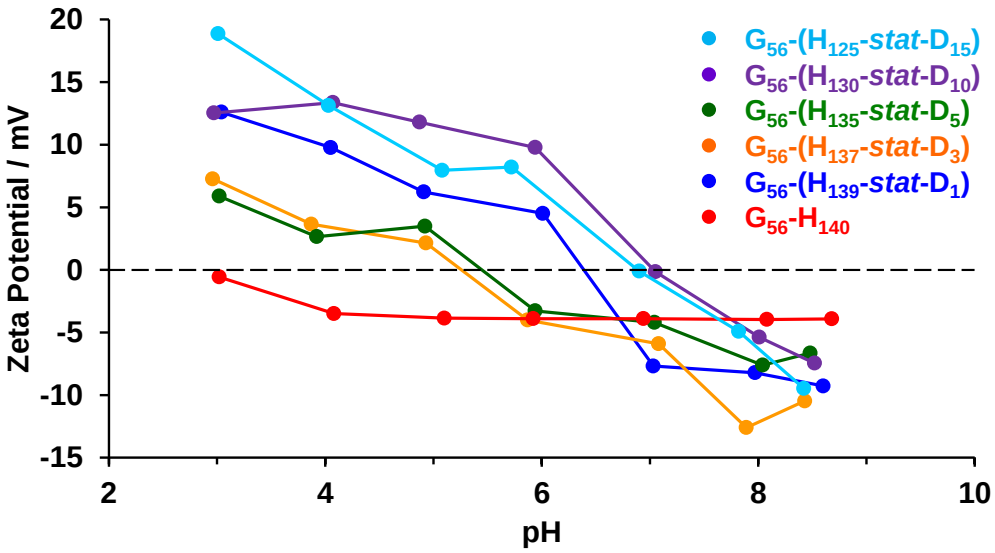

Figure 4.13 Zeta potential vs. pH curves for a series of $PGMA_{56}$-P($HPMA_y$-*stat*-DPA_z) diblock copolymer nano-objects diluted to 0.1 % w/w at 25 °C. These copolymers are denoted as G_{56}-(H_y-*stat*-D_z) for brevity.

15 % w/w aqueous dispersions of $PGMA_{56}$-$PHPMA_{140}$, $PGMA_{56}$-P($HPMA_{139}$-*stat*-DPA_1), $PGMA_{56}$-P($HPMA_{135}$-*stat*-DPA_5) and $PGMA_{56}$-P($HPMA_{130}$-*stat*-DPA_{10}) were characterised by pH-dependent oscillatory rheological studies conducted at 25 °C (**Figure 4.14**). As mentioned above, these diblock copolymers form free-standing gels at pH 8.5, as judged by the tube inversion test.

Strain sweeps were conducted at 25 °C on the four 15 % w/w diblock gels at a fixed angular frequency of 1.0 rad s^{-1} to ensure the rheological conditions were in the linear viscoelastic regime at pH 8.5 (see Appendix for data). From this it was decided to conduct all subsequent rheological experiments at a fixed strain of 1.0 % and a fixed angular frequency of 1.0 rad s^{-1}. Interestingly, increasing the number of DPA units from 0 to 10 results in the formation of stiffer gels at pH 8.5, as judged by an increase in the storage modulus (G' – see **Figure 4.14**). This observation is consistent with previous studies rheological studies conducted by Verber and co-workers on a series of 10 % w/w $PGMA_{54}$-$PHPMA_X$ diblock copolymer worms.[74] In this prior study, it was shown that increasing the core PHPMA DP (or X) from 130 to 170 resulted in a morphology evolution from linear worms to branched worms to worm clusters, combined with an increase in gel stiffness by an order of magnitude. The greater gel strength is thought to be the result of more branching, which leads to more inter-worm contacts being formed. In the present study, a similar morphology evolution (see **Figure 4.9** for TEM images) and increase in gel stiffness are observed for $PGMA_{56}$-P($HPMA_y$-*stat*-DPA_z) diblock copolymers as the target number of DPA units is increased from 0 to 10.

No significant change in G' is observed when the solution pH of $PGMA_{56}$-$PHPMA_{140}$ diblock copolymer worms prepared using CPDB is adjusted from pH 8.5 to 3.0 to 8.5, as expected (see red data in **Figure 4.14**). However, incorporating just one DPA unit into the core-forming block (blue data set) results in G' being lowered from 260 Pa to 90 Pa as the pH is adjusted from 8.5 to 3.0, thus forming a weaker gel. This suggests that protonation of the amine residues leads to the formation of worms closer to the worm-sphere boundary, which are known to form weaker gels. A sharp reduction in G' is observed between pH 7.0 and 6.0 as the DPA residues become protonated. Furthermore, this process is reversible, since the original gel strength is more or less regained on increasing the solution pH from 3.0 to 8.5, although some hysteresis is observed. Switching the dispersion pH from 8.5 to 3.0 for the $PGMA_{56}$-P($HPMA_{135}$-*stat*-DPA_5) and $PGMA_{56}$-P($HPMA_{130}$-*stat*-DPA_{10}) diblock copolymer nano-objects (see green and blue data sets in **Figure 4.14** respectively) results in G' being reduced by more than four orders of magnitude. This dramatic drop in G' is fully consistent with a transformation from a soft gel to a

free-flowing liquid (either spheres or dissolved chains – see insets for **Figure 4.10d** and **e**). On returning to the original dispersion pH, regelation was observed and a G' comparable to the original value was recorded in both cases. Furthermore, all of the 15 % w/w dispersions reformed free-standing gels after a pH cycle from 8.5 to 3.0 to 8.5, as judged by the tube inversion test (see insets in **Figure 4.15**).

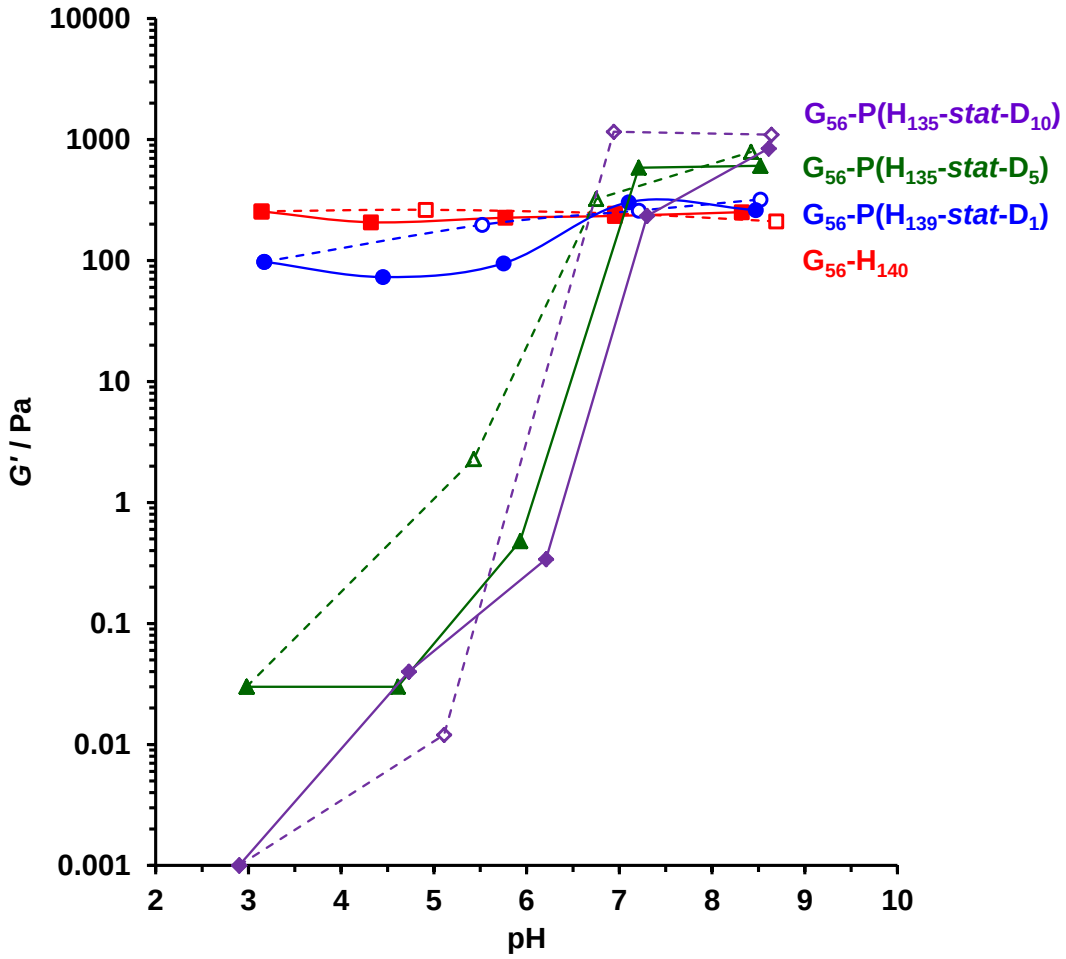

Figure 4.14 Variation in gel storage modulus (G') as a function of pH for 15 % w/w aqueous dispersions of $PGMA_{56}$-$PHPMA_{140}$ (red squares), $PGMA_{56}$-P($HPMA_{139}$-*stat*-DPA_1) (blue circles), $PGMA_{56}$-P($HPMA_{135}$-*stat*-DPA_5) (green triangles) and $PGMA_{56}$-P($HPMA_{130}$-*stat*-DPA_{10}) (purple diamonds) diblock copolymer nano-objects at 25 °C. These copolymers are denoted as G_{56}-(H_y-*stat*-D_z) for brevity. The initial pH was adjusted from 8.5 to 3.0 (closed circles and solid lines) and the pH subsequently returned from 3.0 to 8.5 (open circles and dotted lines). The dispersion pH was adjusted using 0.5 M HCl and 0.5 M KOH. Measurements were recorded at a fixed strain of 1.0 % and an angular frequency of 1.0 rad s^{-1}.

Clearly, the gel stiffness of these $PGMA_{56}$-P($HPMA_y$-*stat*-DPA_z) diblock copolymers can be finely tuned by changing the DPA content of the core-forming block while subtly adjusting the solution pH. The importance of tuning the stiffness/elasticity of gels was beautifully established in ground-breaking research by Discher *et al.*[77] More specifically, these workers demonstrated that the fate of stem cells was highly dependent on the elasticity of their environment. In related work, Tanaka and co-workers demonstrated that mouse myoblast cells adhered strongly to $PDPA_{50}$-$PMPC_{250}$-$PDPA_{50}$ ABA triblock hydrogel films at pH 8.0, which forms a relatively stiff substrate (G' ~ 40 kPa) when the PDPA is neutral.[78] However, the same cells adhere less strongly when the solution pH was lowered to 7.0, which was attributed to the softer hydrogel (G' ~ 1 kPa) formed when the PDPA blocks became partially protonated. Clearly, the ability to tune the stiffness of the $PGMA_{56}$-P($HPMA_y$-*stat*-DPA_z) diblock copolymer gels in this study could be of vital importance for controlling cell adhesion and will be explored in the future. Furthermore, PGMA and PGMA-PHPMA diblock copolymer worms have previously been demonstrated to be biocompatible.[75,79] Therefore, it is highly likely that the $PGMA_{56}$-P($HPMA_y$-*stat*-DPA_z) nano-objects reported herein are also biocompatible.

To further explore the reversibility of pH-mediated changes in particle morphology, TEM studies were conducted on the $PGMA_{56}$-P($HPMA_y$-*stat*-DPA_z) diblock copolymers after a pH cycle (from 8.5 to 3.0 to 8.5) and subsequent dilution to 0.1 % w/w at pH 8.5 (see **Figure 4.15**). Diblock copolymers with target amounts of 0, 1, 3 or 15 DPA units all reverted to their original morphology. However, TEM images obtained for $PGMA_{56}$-P($HPMA_{135}$-*stat*-DPA_5) and $PGMA_{56}$-P($HPMA_{130}$-*stat*-DPA_{10}) diblock copolymers after this pH cycle suggest that a branched worm phase was formed (see **Figure 4.15d** and **e**). This is perhaps surprising, since prior to the pH cycle both dispersions contained vesicles. However, for molecularly-dissolved chains or spheres to form vesicles they must pass through a worm phase.[68] This may act as a significant kinetic barrier to the reformation of vesicles (as seen in Chapter 3).

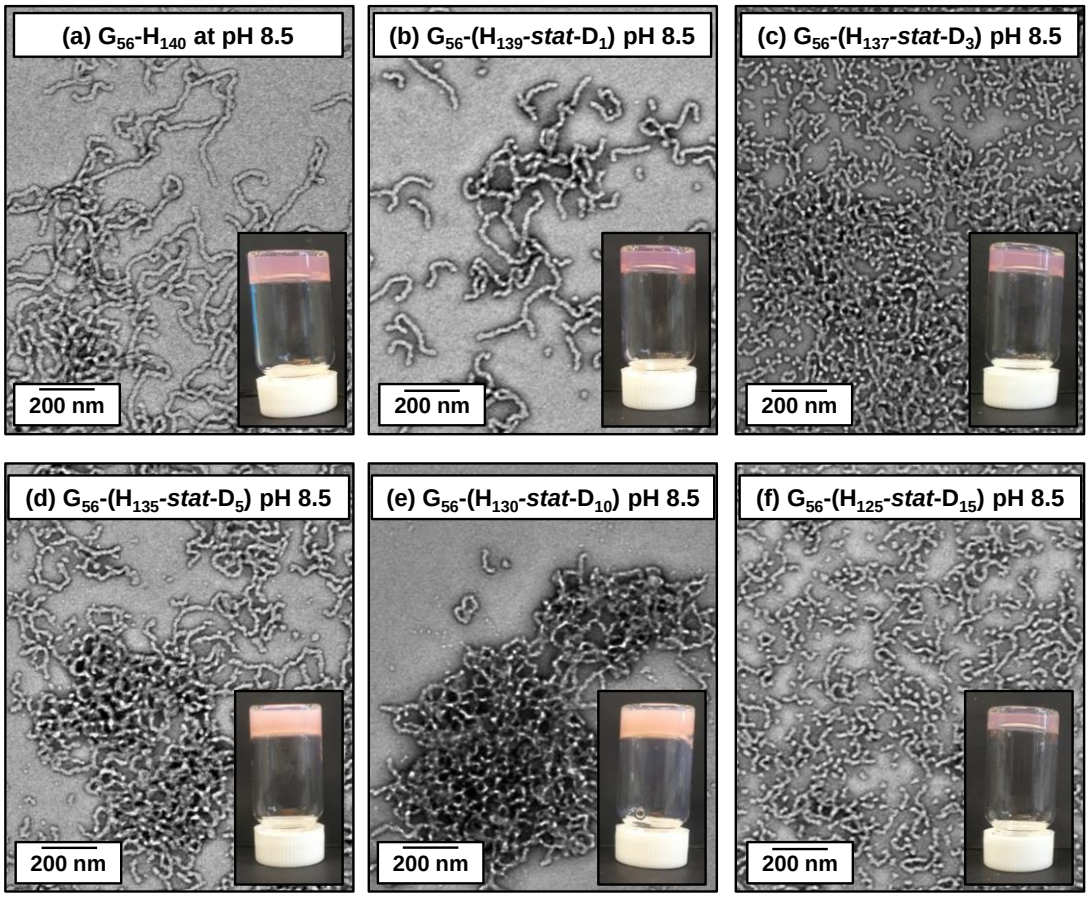

Figure 4.15 TEM images recorded for 0.1 % w/w aqueous dispersions at pH 8.5 for a series of $PGMA_{56}$-P($HPMA_y$-*stat*-DPA_z) diblock copolymer nano-objects (where y + z = 140) after a pH cycle from pH 8.5 to 3.5 to 8.5. The inset shows the corresponding digital photographs obtained for the same diblock copolymer nano-objects at 15 % w/w after a pH cycle from pH 8.5 to 3.5 to 8.5. These copolymers are denoted as G_{56}-(H_y-*stat*-D_z) for brevity.

As previously mentioned, PGMA-PHPMA diblock copolymers worms are known to be thermo-responsive.[74,75] This stimulus-responsive nature has been discussed in detail in Chapters 2 and 3. Briefly, cooling the particles to 5 °C results in a worm-to-sphere transition (and degelation) due to surface plasticisation of the PHPMA core-forming block at lower temperatures. This results in a reduction in the packing parameter *p* thus inducing an order-order transition.[74,75] Temperature-dependent oscillatory rheological studies conducted from 25 to 5 to 25 °C for the 15 % w/w $PGMA_{56}$-$PHPMA_{140}$ diblock copolymer worms confirm its thermo-responsive behaviour (see **Figure 4.16a**). This worm gel possesses a critical gelation

temperature (CGT) of 14 °C on cooling, as judged by the cross-over point of the storage modulus (red data) and loss modulus (G" – blue data). Moreover, G' is reduced by two orders of magnitude at 5 °C, suggesting a free-flowing fluid rather than a visco-elastic gel. Very similar G' and G" values are obtained for the same dispersion at pH 3.5 and at pH 8.5 after a pH cycle (i.e., pH 8.5 to 3.5 to 8.5), when exposed to an identical temperature sweep (see **Figure 4.16b** and **c**). This is expected, since this diblock copolymer does not undergo a pH-induced morphological transition.

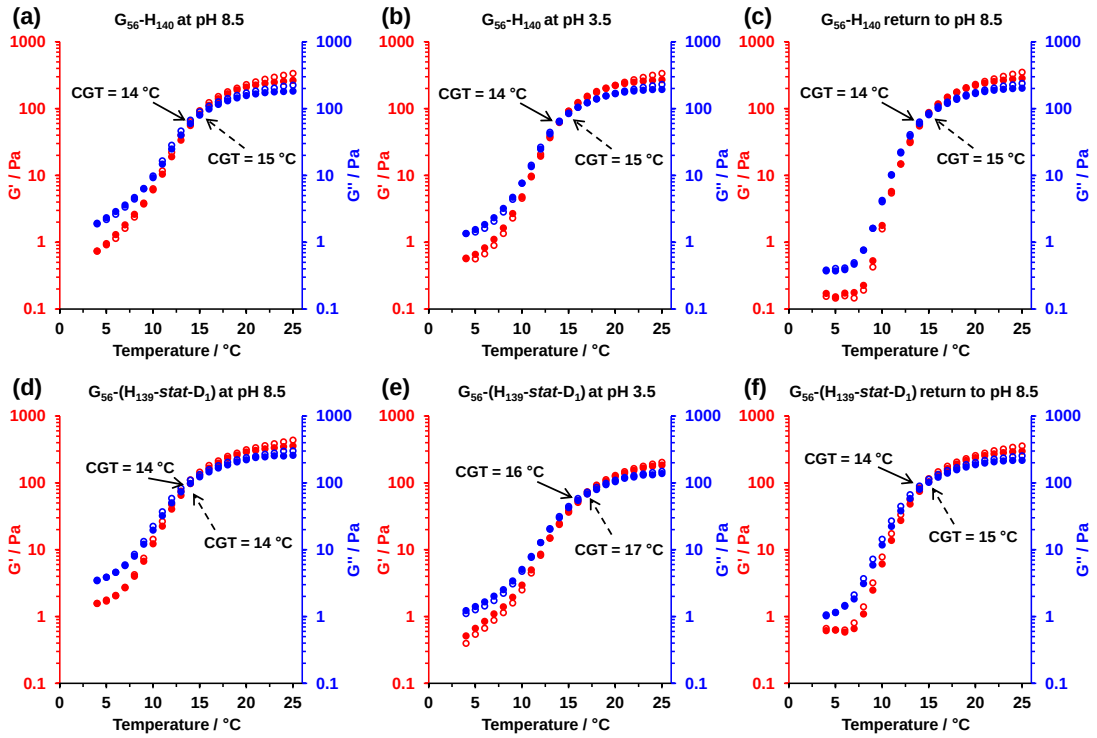

Figure 4.16 Temperature dependence of the storage modulus (G'; red data sets) and the loss modulus (G"; blue data sets) for 15 % w/w aqueous dispersions of $PGMA_{56}$-$PHPMA_{140}$ gel at (a) pH 8.5, (b) pH 3.5 and (c) pH 8.5 after a pH cycle and for $PGMA_{56}$-P($HPMA_{139}$-*stat*-DPA_1) gel at (d) pH 8.5, (e) pH 3.5 and (f) pH 8.5 after a pH cycle. Closed circles denote a 25 °C to 5 °C temperature sweep and open circles denote a 5 °C to 25 °C temperature sweep. Conditions: frequency = 1.0 rad s^{-1}; applied strain = 1.0 % and a heating/cooling rate of 0.5 °C min^{-1}. These copolymers are denoted as G_{56}-(H_y-*stat*-D_z) for brevity.

Temperature-dependent rheological studies of the 15 % w/w $PGMA_{56}$-P($HPMA_{139}$-*stat*-DPA_1) worm gel at pH 8.5 suggest that it has similar CGT and G'

values to that of the neutral $PGMA_{56}$-$PHPMA_{140}$ worm gel (see **Figure 4.16d**). However, lowering the solution pH of the 15 % $PGMA_{56}$-P($HPMA_{139}$-*stat*-DPA_1) diblock copolymer worm gel to pH 3.5 results in a reduction in G' at 25 °C, as discussed above. Moreover, the rheology studies indicated that the CGT increased to 16 °C after a pH switch to pH 3.5 (see **Figure 4.16e**). This is most likely to be due to an increase in the hydrophilic character of the core when the DPA residues are protonated. Therefore, smaller reductions in temperature (i.e., higher temperatures) are required to drive the worm-to-sphere morphological transition and hence degelation. On returning this copolymer solution pH back to pH 8.5, the G' and CGT are comparable to the original gel prior to the pH cycle (see **Figure 4.16f**). Hence the CGT for this copolymer can be altered merely by adjusting the solution pH.

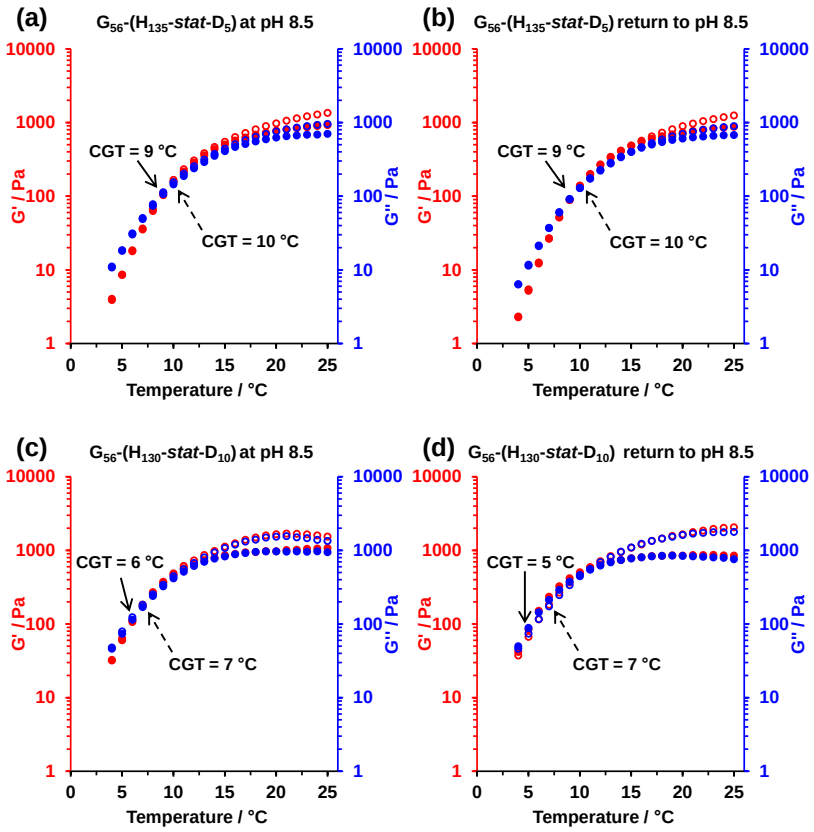

Figure 4.17 Temperature dependence of the storage modulus (G'; red data sets) and the loss modulus (G"; blue data sets) for 15 % w/w aqueous dispersions of $PGMA_{56}$-P($HPMA_{135}$-*stat*-DPA_5) gel at (a) pH 8.5 and (b) pH 8.5 after a pH cycle and $PGMA_{56}$-P($HPMA_{130}$-*stat*-DPA_{10}) gel at (c) pH 8.5 and (d) pH 8.5 after a pH cycle. Conditions: frequency = 1.0 rad s^{-1}; applied strain = 1.0 % and a heating/cooling rate of 0.5 °C min^{-1}. These copolymers are denoted as G_{56}-(H_y-*stat*-D_z) for brevity.

When the DPA content in the core is increased to 5 or 10 units, a systematic reduction in the CGT is observed to 9 °C or 6 °C, respectively (see **Figure 4.17a** and **c**). This is most likely a combination of three factors. (i) The initial section of the core-forming block is enriched with DPA units, which relatively is hydrophobic compared to the same number of HPMA units. Therefore, lower temperatures are required to plasticise sufficient core-forming block units to induce a worm-to-sphere transition and degelation. (ii) Increasing the DPA content of the core causes a change in morphology to branched worms or vesicles, which most likely requires lower temperatures to form spheres and hence degel. (iii) DMF GPC suggests a slight increase in the degree of light branching with higher DPA content, which may resist dissociation to form spheres. After subjecting both diblock copolymers to a pH cycle from pH 8.5 to 3.5 to 8.5, their rheological properties are almost identical to the original gels (**Figure 4.17b** to **d**). However, greater hysteresis is observed for the $PGMA_{56}$-P($HPMA_{130}$-*stat*-DPA_{10}) diblock copolymer nano-objects. This may be a result of the formation of a pure branched worm phase after a pH cycle, rather than the vesicle/worm mixed phase that is originally produced.

4.3.2 Acid-responsive $PGMA_{56}$-P($HPMA_y$-*stat*-DPA_z) diblock copolymer vesicles

Four $PGMA_{56}$-P($HPMA_y$-*stat*-DPA_z) diblock copolymer vesicles were prepared using the same water-soluble $PGMA_{56}$ macro-CTA by PISA *via* RAFT polymerisation at 15 % w/w solids in water. The reaction solutions were left four 4 h at 70 °C. In this series a total core DP of 250 was targeted (i.e., y + z = 250), where the number of DPA units is 0, 1, 5 or 10. ^{1}H NMR analysis suggested that HPMA monomer attained almost full conversion (> 99 %) while the DPA monomer reached 90 % conversion in all cases. After 4 h, the 15 % w/w dispersions formed turbid free-flowing fluids (see inset in **Figure 4.18**), which suggested vesicle formation. TEM studies conducted on the $PGMA_{56}$-P($HPMA_y$-*stat*-DPA_z) diblock copolymers after dilution to 0.1 % w/w at pH 8.5 confirmed the presence of vesicles in all cases (see **Figure 4.18**).

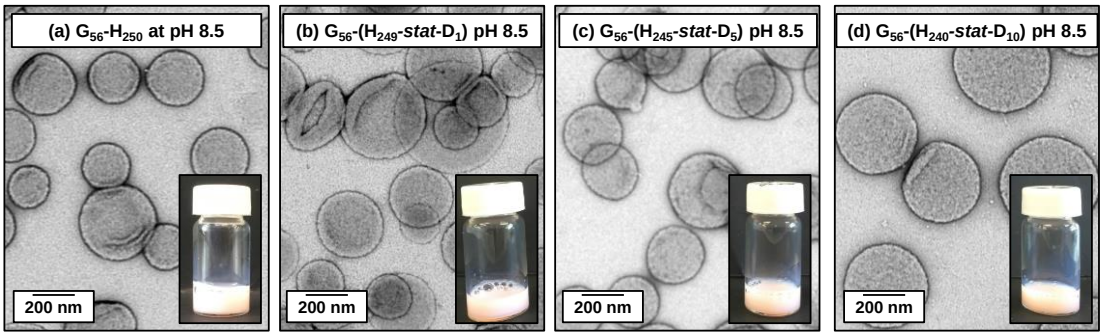

Figure 4.18 TEM images recorded at pH 8.5 (from a dilute 0.1 % w/w aqueous dispersion) and the corresponding digital images obtained at 15 % w/w solids and pH 8.5 for a series of $PGMA_{56}$-P($HPMA_y$-*stat*-DPA_z) diblock copolymer vesicles, where y + z = 250. These copolymers are denoted as G_{56}-(H_y-*stat*-D_z) for brevity.

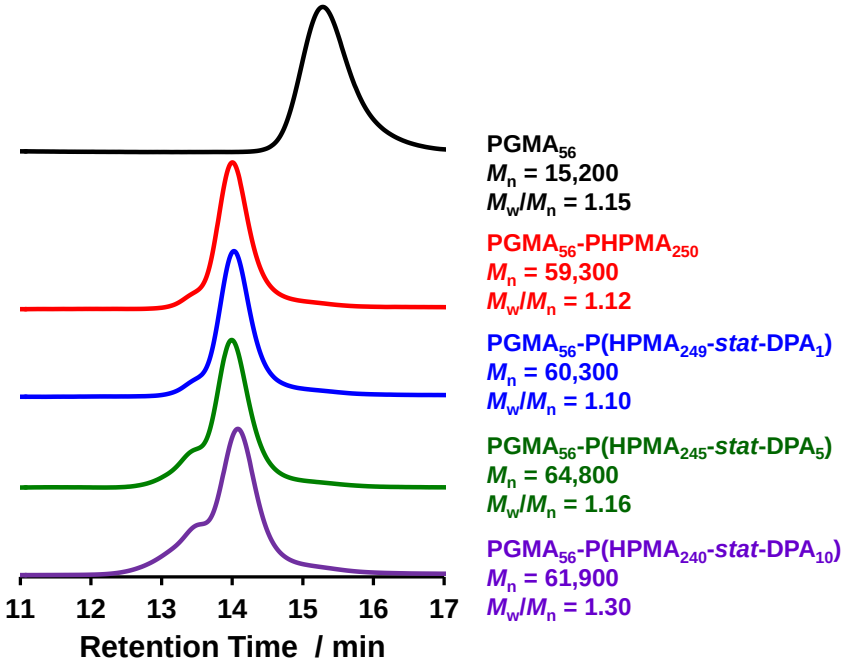

Figure 4.19 DMF GPC traces obtained for a $PGMA_{56}$ macro-CTA (black curve) and a series of $PGMA_{56}$-P($HPMA_y$-*stat*-DPA_z) diblock copolymer vesicles where y + z =250. In all cases high blocking efficiencies are observed.

DMF GPC studies conducted on the four $PGMA_{56}$-P($HPMA_y$-*stat*-DPA_z) diblock copolymers indicated high blocking efficiencies relative to the $PGMA_{56}$ macro-CTA (**Figure 4.19**). Furthermore, similar number-average molecular weights (M_n) and narrow molecular weight distributions (M_w/M_n) were obtained for all

diblock copolymers. However, increasing the amount of DPA in these particles leads to a more pronounced high molecular weight shoulder (at lower retention times), as observed in the worm series reported in **section 4.3.1**. Again, this is likely to be due to a combination of chain transfer to copolymerised DPA residues and/or dimethacrylate impurities in DPA, either of which would result in light branching.

On lowering the solution pH for the 15 % w/w $PGMA_{56}$-$PHPMA_{250}$ vesicular dispersions from pH 8.0 to pH 3.5, no apparent physical change from an initial turbid free-flowing dispersion is observed. Moreover, TEM studies conducted on this diblock copolymer dried at pH 3.5 confirm that the vesicles remained unchanged after this pH switch, as expected (see **Figure 4.20a**). In contrast, incorporating DPA residues into the core-forming block should yield pH-responsive vesicles. Below pH 6.0, the tertiary amine group in the DPA residues becomes protonated, resulting in a more hydrophilic core-forming block. As discussed in **section 4.3.1**, the relatively high concentration of DPA units next to the block junction means that order-order transitions to lower order morphologies are preferred. However, 15 % w/w $PGMA_{56}$-P($HPMA_{249}$-*stat*-DPA_1) diblock copolymer nano-objects remain as a turbid, free-flowing dispersion at pH 3.5. Interestingly, TEM studies of this diblock copolymer conducted at pH 3.5 suggest that some vesicles partially dissociate to give jellyfish (see **Figure 4.20b**). As previously discussed, such jellyfish morphologies were observed by Blanazs *et al.* during an investigation of the morphological evolution of vesicles during PISA, and were found to be a key intermediate between the worm and vesicle phases.[68] In contrast, lowering the solution pH from 8.5 to 3.5 for the $PGMA_{56}$-P($HPMA_{245}$-*stat*-DPA_5) diblock copolymer vesicles, results in the formation of a turbid free-standing gel. TEM images obtained on diluting this gel to 0.1 % w/w at pH 3.5 suggest that ill-defined spheres/short worms are obtained rather than pure worms (**Figure 4.20c**). Finally, $PGMA_{56}$-P($HPMA_{240}$-*stat*-DPA_{10}) diblock copolymers form a weakly turbid free-flowing dispersion at pH 3.5, which suggests spheres. TEM images obtained for 0.1 % w/w $PGMA_{56}$-P($HPMA_{240}$-*stat*-DPA_{10}) dispersion at pH 3.5 indicate a vesicle-to-sphere transition, albeit with somewhat ill-defined spheres/aggregates (**Figure 4.20d**).

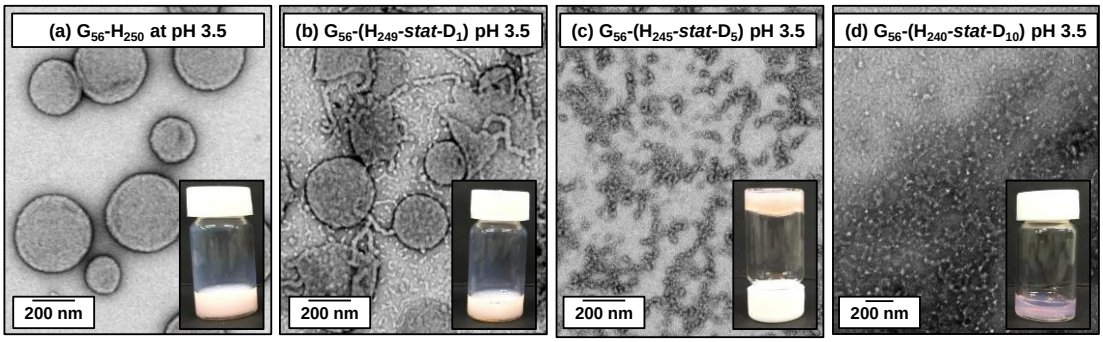

Figure 4.20 TEM images recorded on drying a dilute 0.1 % w/w aqueous dispersion at pH 3.5 and the corresponding digital photographs obtained at 15 % w/w solids for a series of $PGMA_{56}$-P($HPMA_y$-*stat*-DPA_z) diblock copolymer nano-objects at pH 3.5, where y + z = 250. These copolymers are denoted as G_{56}-(H_y-*stat*-D_z) for brevity.

The pH-responsive nature of these diblock copolymer vesicles was further examined by DLS studies conducted as a function of pH on 0.1 % w/w dispersion. As expected, the hydrodynamic diameter (260 nm) and count rates of the neutral $PGMA_{56}$-$PHPMA_{250}$ diblock copolymer vesicles do not change significantly between pH 8.5 and pH 3.0 as these nano-objects are not pH-responsive (see **Figure 4.21a**). In the case of $PGMA_{56}$-P($HPMA_{99}$-*stat*-DPA_1) diblock copolymer vesicles, only a slight increase in particle diameter from 225 nm to 250 nm is observed between pH 7.0 and pH 5.0 according to DLS studies (see **Figure 4.21b**). In contrast, pH-dependent studies conducted on $PGMA_{56}$-P($HPMA_{245}$-*stat*-DPA_5) diblock copolymers show a dramatic reduction in particle diameter from 280 nm at pH 8.5 to 40 nm at pH 3.0. Likewise, the derived count rates decrease from 110,000 kcps to 12,000 kcps over the same pH range. This suggests a vesicle-to-sphere transition (as observed by TEM) rather than a vesicle-to-worm transition (as suggested by physical inspection and the tube inversion test). Clearly this paradox warrants further research in the future. Similarly, the apparent diameter of $PGMA_{56}$-P($HPMA_{240}$-*stat*-DPA_{10}) diblock copolymer vesicles dramatically decreases to 30 nm as the PDPA becomes protonated (see **Figure 4.21**). This is accompanied with a reduction in count rate from 110,000 kcps to 8,000 kcps, indicating a vesicle-to-sphere transition. Moreover, this change in particle diameter and derived count rate for the two latter samples

occurs between pH 7.0 and 5.0. This again suggests that nearly all the tertiary amines are required to be protonated to induce a morphology transition since the $pK_a \approx 7.2$.

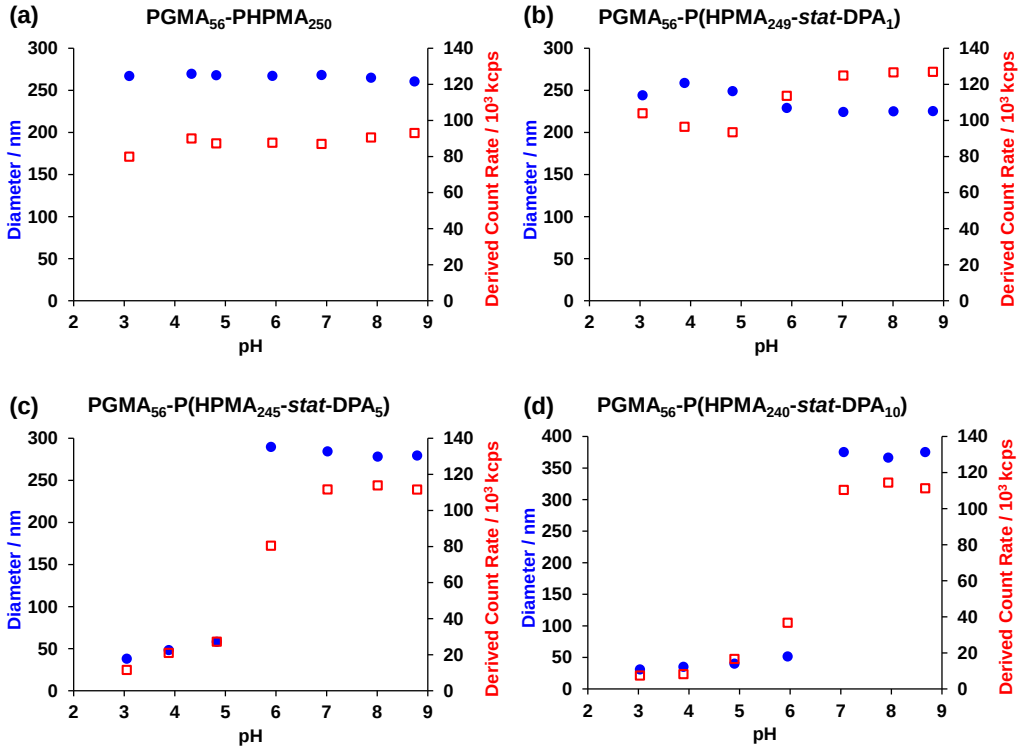

Figure 4.21 pH-dependent intensity-average hydrodynamic diameter and derived count rate determined by DLS at 25 °C for 0.1 % w/w aqueous dispersions of (a) $PGMA_{56}$-$PHPMA_{250}$, (b) $PGMA_{56}$-P($HPMA_{99}$-*stat*-DPA_1), (c) $PGMA_{56}$-P($HPMA_{245}$-*stat*-DPA_5) and (d) $PGMA_{56}$-P($HPMA_{240}$-*stat*-DPA_{10}) diblock copolymer nano-objects. These dispersions were adjusted from pH 8.5 using HCl.

Aqueous electrophoresis studies conducted on these for four 0.1 % w/w $PGMA_{56}$-P($HPMA_y$-*stat*-DPA_z) vesicles revealed similar behaviour to the worm series discussed in **section 4.3.1**. All four vesicles possess anionic character (-10 mV to -15 mV) at pH 8.5, presumably due to some deprotonated carboxylic acid end-groups on the PGMA stabiliser derived from the ACVA initiator used during its synthesis. Furthermore it could be due to carboxylic acid groups derived from ACVA in the synthesis of the nano-objects. Lowering the dispersion pH of the diblock copolymer nano-objects containing 1, 5 or 10 DPA units in the core-forming block, results in a change in zeta potential (see **Figure 4.22**). More specifically, they switch from anionic to cationic between pH 5.0 and 7.0. Furthermore, these three DPA-

based diblock copolymers possess zeta potentials of approximately + 12 mV at pH 3.0. In contrast, $PGMA_{56}$-$PHPMA_{250}$ diblock copolymer vesicles (i.e., zero DPA content) remain weakly anionic over the entire pH range, as expected (see red data in **Figure 4.22**).

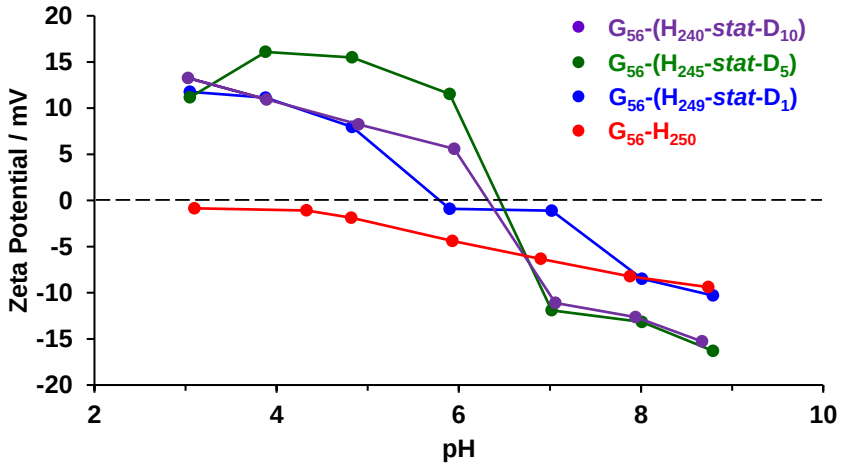

Figure 4.22 Zeta potential vs. pH curves obtained for a series of $PGMA_{56}$-$P(HPMA_y$-*stat*-$DPA_z)$ diblock copolymer nano-objects diluted to 0.1 % w/w at 25 °C. These copolymers are denoted as G_{56}-(H_y-*stat*-D_z) for brevity.

In the case of the 15 % w/w $PGMA_{56}$-$P(HPMA_{240}$-*stat*-$DPA_{10})$ diblock copolymer dispersions, a significant reduction in turbidity was observed after the solution pH was adjusted from 8.5 to 3.0. This is because the initial large vesicles at pH 8.5 are very efficient at scattering light, whereas the relatively small spheres form at pH 3.5 are weak light scatters. Unlike the vesicle-to-worm (and vesicle-to-sphere) transition reported in Chapter 3, which is caused by end-group ionisation of a terminal carboxylic acid, this morphology transformation occurs much more quickly (within minutes rather than hours). In contrast, the physical appearance of 15 % w/w $PGMA_{56}$-$PHPMA_{250}$ and $PGMA_{56}$-$P(HPMA_{249}$-*stat*-$DPA_1)$ diblock copolymers remain unchanged after the same pH switch, as judged by visual inspection. Therefore, these differences in turbidity can be used to monitor the time scales of the order-order morphology transitions. However, these experiments must be conducted on 0.1 % $PGMA_{56}$-$P(HPMA_y$-*stat*-$DPA_z)$ diblock copolymer vesicles, because the 15 % w/w dispersions are too turbid for analysis. The transmittance of 0.1 % w/w $PGMA_{56}$-$P(HPMA_y$-*stat*-$DPA_z)$ diblock copolymer dispersions was measured at 450

nm for a fixed period of time after a pH switch from 8.5 to 3.0 using HCl (see **Figure 4.23**). As expected, no significant changes in transmittance were recorded for the $PGMA_{56}$-$PHPMA_{250}$ and $PGMA_{56}$-P($HPMA_{249}$-*stat*-DPA_1) diblock copolymer dispersions over 15 h (see **Figure 4.23a** and **b**). The former diblock copolymer remains as vesicles and does not undergo a morphology transition after a pH switch, hence minimal changes in the transmittance of this dispersion are observed. In the case of the $PGMA_{56}$-P($HPMA_{249}$-*stat*-DPA_1) diblock copolymer vesicles, an initial modest increase in transmittance is observed after the pH switch, but no significant changes observed from thereafter. According to TEM studies, this diblock copolymer undergoes a partial morphology transition to vesicles/jellyfish after a pH switch from 8.5 to 3.0 (**Figure 4.20b**). However, the particles before and after this pH switch both strongly scatter light, hence no significant changes in transmittance were recorded.

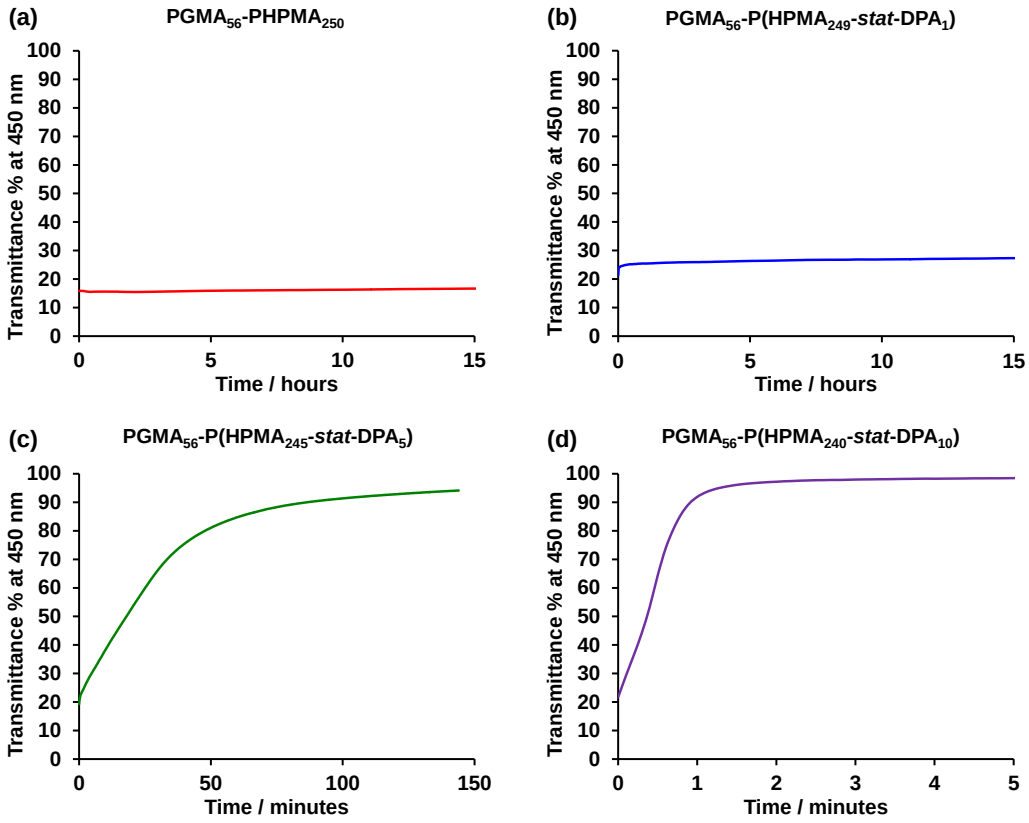

Figure 4.23 Change in % transmittance at a fixed wavelength of 450 nm for 0.10 % w/w aqueous dispersions of (a) $PGMA_{56}$-$PHPMA_{250}$, (b) $PGMA_{56}$-P($HPMA_{249}$-*stat*-DPA_1), (c) $PGMA_{56}$-P($HPMA_{245}$-*stat*-DPA_5) and (d) $PGMA_{56}$-P($HPMA_{240}$-*stat*-DPA_{10}) vesicles after a pH switch from pH 8.5 to pH 3.0 using 0.5 M HCl. Note the differences in time scale on the x-axis.

In contrast, turbidimetry studies of the $PGMA_{56}$-P($HPMA_{245}$-*stat*-DPA_5) and $PGMA_{56}$-P($HPMA_{240}$-*stat*-DPA_{10}) diblock copolymer vesicles indicate a significant increase in the transmittance (**Figure 4.23c** and **d**). These studies suggest that the former is complete after approximately 1 h and the latter after only 1 minute. Furthermore, the magnitude of the increase in transmittance is consistent with the vesicle-to-sphere morphology transition observed by TEM. Not surprisingly, increasing the DPA content in the core-forming block yields vesicles which undergo faster morphological transitions and more pronounced changes in copolymer morphology after a pH switch.

As expected, the $PGMA_{56}$-$PHPMA_{250}$ diblock copolymer vesicles remained intact after adjusting the solution pH back to 8.5, as judged by TEM studies (see **Figure 4.24a**). Moreover, the 15 % w/w dispersion remained as a turbid free-flowing fluid, which is characteristic of vesicles. Conversely, the $PGMA_{56}$-P($HPMA_{245}$-*stat*-DPA_5) and $PGMA_{56}$-P($HPMA_{240}$-*stat*-DPA_{10}) diblock copolymer nano-objects formed insoluble solid pastes after a pH cycle from 8.5 to 3.0 to 8.5 at 15 % w/w solids, rather than turbid free-flowing dispersions. TEM studies conducted on these diluted pastes at 0.1 % w/w at pH suggest that ill-defined aggregates were formed (see **Figure 4.24c** and **d**). This is not really surprising as similar observations were for the order-order pH- and thermo-responsive HOOC-$PGMA_{43}$-$PHPMA_{175}$ diblock copolymer vesicles (as discussed in Chapter 3). This was attributed to particles becoming kinetically-trapped in the worm phase, which constitutes a significant barrier to vesicle reformation. Remarkably, TEM images obtained for the $PGMA_{56}$-P($HPMA_{249}$-*stat*-DPA_1) diblock copolymer after a pH cycle from 8.5 to 3.0 to 8.5 suggest that a pure vesicle phase is reformed. At pH 3.0, such particles actually form a vesicle/jellyfish mixed phase rather than a worm phase according to TEM (**Figure 4.20b**). Hence, on switching the solution pH back to 8.5 the $PGMA_{56}$-P($HPMA_{249}$-*stat*-DPA_1) diblock copolymers do not have to overcome the worm phase and are able to reform vesicles. Such morphology transitions may offer some potential for post-polymerisation encapsulation and release of payloads.[80,81]

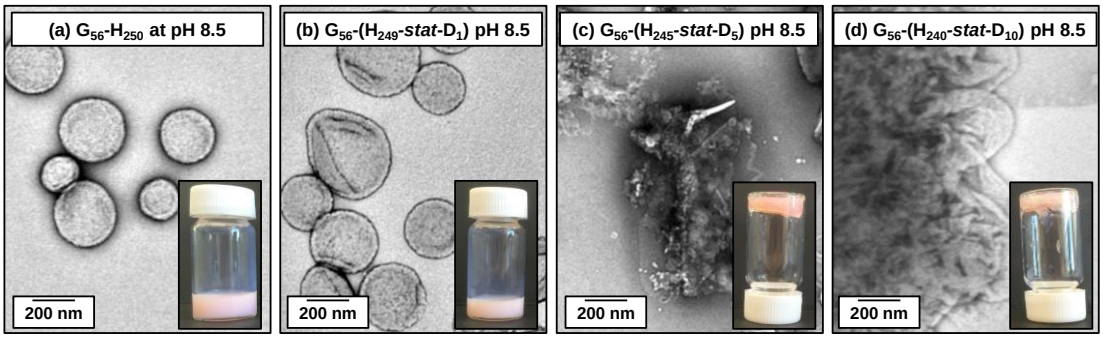

Figure 4.24 TEM images recorded at pH 8.5 (from a dilute 0.1 % w/w aqueous dispersion) for a series of $PGMA_{56}$-P($HPMA_y$-*stat*-DPA_z) diblock copolymer nano-objects (where y + z = 250) after a pH cycle from pH 8.5 to 3.5 to 8.5. The inset shows the corresponding digital photographs for the same diblock copolymer nano-objects at 15 % w/w solids after a pH cycle from pH 8.5 to 3.5 to 8.5. These copolymers are denoted as G_{56}-(H_y-*stat*-D_z) for brevity.

4.3.3 Acid-responsive $PGMA_{56}$-P($HPMA_y$-*stat*-DPA_z) diblock copolymer spheres

Finally, a series of four $PGMA_{56}$-P($HPMA_y$-*stat*-DPA_z) diblock copolymer spheres were prepared by PISA *via* RAFT copolymerisation of HPMA and DPA at 15 % w/w in water at pH 8.0. More specifically, block compositions of $PGMA_{56}$-$PHPMA_{100}$, $PGMA_{56}$-P($HPMA_{99}$-*stat*-DPA_1), $PGMA_{56}$-P($HPMA_{95}$-*stat*-DPA_5) and $PGMA_{56}$-P($HPMA_{90}$-*stat*-DPA_{10}) were targeted. ^{1}H NMR analysis after 4 hours at 70 °C indicated that HPMA reached almost full conversion (> 99 %), and DPA reached conversions > 90 % in all cases. DMF GPC traces obtained for these four diblock copolymers indicated that they each had similar number-average molecular weights (see **Figure 4.25**). Furthermore, comparison of the diblock copolymer traces to the $PGMA_{56}$ macro-CTA suggests high blocking efficiencies were obtained. $PGMA_{56}$-$PHPMA_{100}$ and $PGMA_{56}$-P($HPMA_{99}$-*stat*-DPA_1) possess relatively narrow molecular weight distributions (M_w/M_n < 1.15). However, targeting either 5 or 10 DPA units in the core-forming block, the molecular weight distribution significantly broadens (M_w/M_n > 1.20). This is due to a significant increase in a high molecular weight shoulder. It is likely that this is a result of chain transfer to copolymerised DPA residues (and/or dimethacrylate impurity in the DPA monomer) causing some branching.

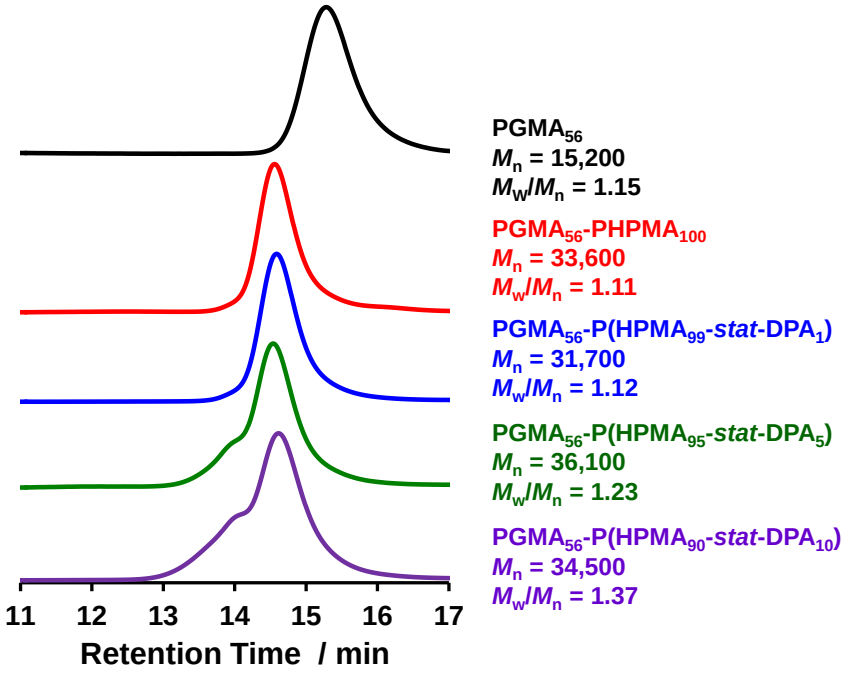

Figure 4.25 DMF GPC traces obtained for a $PGMA_{56}$ macro-CTA (black curve) and a series of $PGMA_{56}$-P($HPMA_y$-*stat*-DPA_z) diblock copolymer spheres (where y + z = 100). High blocking efficiencies are observed in all cases.

All four $PGMA_{56}$-P($HPMA_y$-*stat*-DPA_z) diblock copolymers form weakly turbid free-flowing dispersions, which is characteristic for spheres (see inset in **Figure 4.26**). TEM studies conducted at pH 8.5 of the four diblock copolymers confirm that all form spheres except $PGMA_{56}$-P($HPMA_{95}$-*stat*-DPA_5), which forms a mixture of spheres and short worms (**Figure 4.26**).

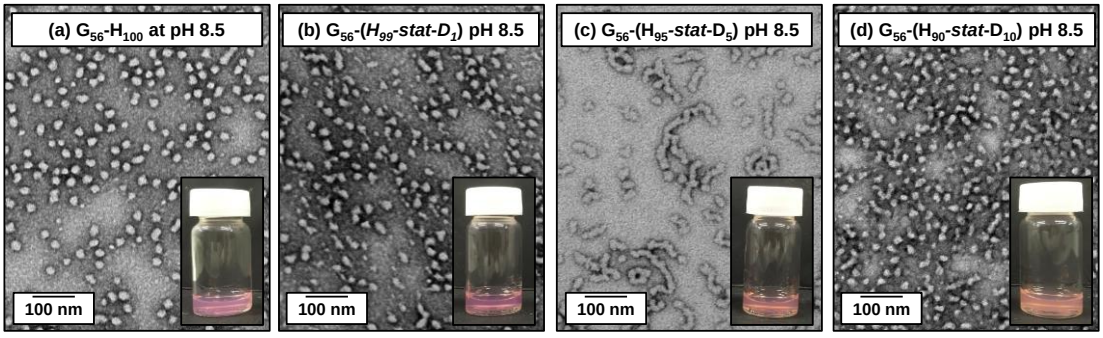

Figure 4.26 TEM images recorded at pH 8.5 after drying 0.1 % w/w aqueous dispersions and the corresponding digital photographs obtained at 15 % w/w at pH 8.5 for a series of $PGMA_{56}$-P($HPMA_y$-*stat*-DPA_z) diblock copolymer spheres, where y + z = 100. These copolymers are denoted as G_{56}-(H_y-*stat*-D_z) for brevity.

Similar to observations made in **section 4.3.1**, increasing the DPA content of such copolymers yields a more hydrophobic core-forming block. This leads to the formation of higher order morphologies. However, increasing the amount of water-immiscible DPA in the formulation also favours RAFT *emulsion* polymerisation, which in the case of DPA preferentially yields spheres.

Lowering the solution pH of these diblock copolymers to pH 3.5 results in protonation of the tertiary amine in the copolymerised DPA residues, generating a more hydrophilic core. $PGMA_{56}$-$PHPMA_{100}$ and $PGMA_{56}$-P($HPMA_{99}$-*stat*-DPA_1) remain weakly turbid free-flowing dispersions on lowering the solution pH from 8.5 to 3.0 using HCl. Furthermore, TEM images obtained for 0.1 % w/w diblock copolymers at pH 3.5 (see **Figure 4.27a** and **b)** confirm the presence of spheres (albeit ill-defined spheres for $PGMA_{56}$-P($HPMA_{99}$-*stat*-DPA_1)). Thus the greater hydrophilic character gained from one protonated DPA unit in the core is insufficient to drive a morphology transition. On the other hand, the 15 % w/w $PGMA_{56}$-P($HPMA_{95}$-*stat*-DPA_5) and $PGMA_{56}$-P($HPMA_{90}$-*stat*-DPA_{10}) diblock copolymer dispersions lose their initial weak turbidity after the same pH switch. Moreover, no particles were observed by TEM studies conducted on dilute dispersions dried at pH 3.5 (see **Figure 4.27c** and **d**). This is because protonation of the relatively high DPA content in the copolymer significantly increases the hydrophilicity of the core-forming block, resulting in molecular dissolution (i.e., an order-disorder transition).

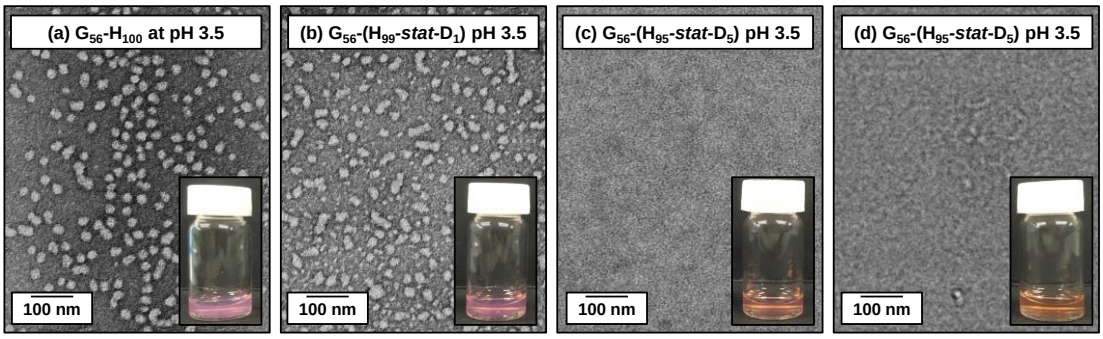

Figure 4.27 TEM images recorded at pH 3.5 after drying 0.1 % w/w aqueous dispersions and the corresponding digital photographs images obtained at 15 % w/w solids for a series of $PGMA_{56}$-P($HPMA_y$-*stat*-DPA_z) diblock copolymer dispersions at pH 3.5, where y + z = 100. These copolymers are denoted as G_{56}-(H_y-*stat*-D_z) for brevity.

DLS studies conducted on $PGMA_{56}$-$PHPMA_{100}$ and $PGMA_{56}$-P($HPMA_{99}$-*stat*-DPA_1) diblock copolymer spheres as a function of pH also indicate that no morphological transition occurs on lowering the solution pH (see **Figure 4.28a** and **b**). More specifically, the mean hydrodynamic diameters (approximately 35 nm in both cases) and derived count rate do not change significantly on lowering the solution pH from 8.5 to 3.0.

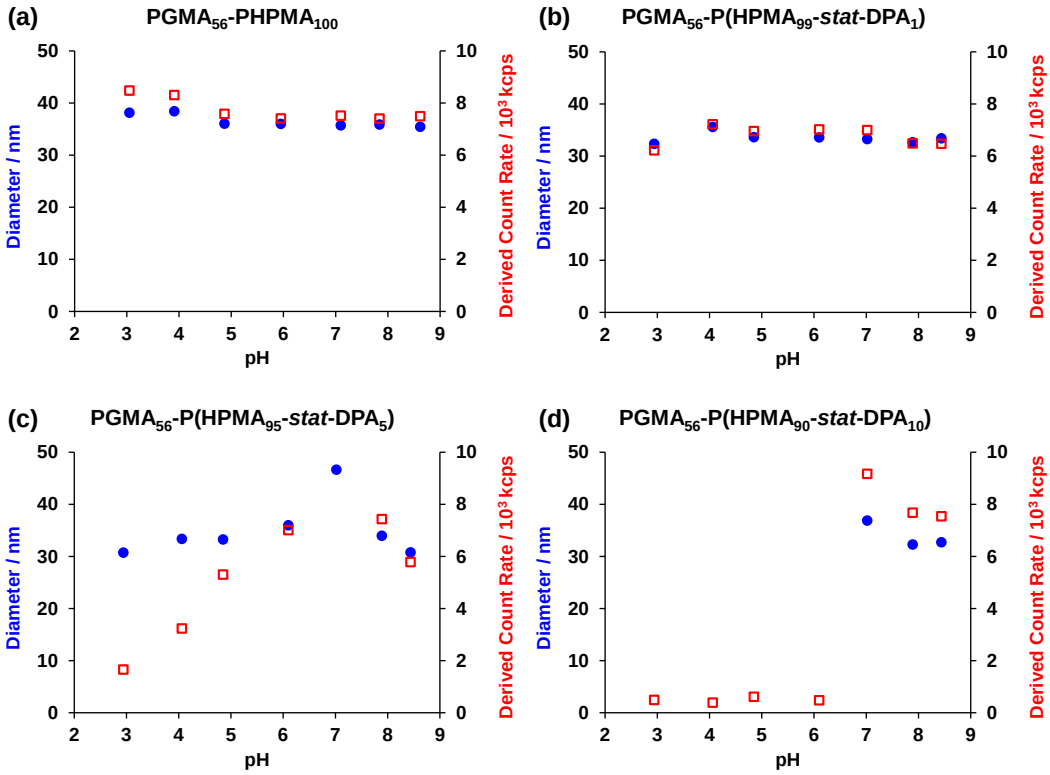

Figure 4.28 pH-dependent hydrodynamic diameter and derived count rate measured by dynamic light scattering (DLS) at 25 °C for 0.1 % w/w aqueous dispersions of (a) $PGMA_{56}$-$PHPMA_{100}$, (b) $PGMA_{56}$-P($HPMA_{99}$-*stat*-DPA_1), (c) $PGMA_{56}$-P($HPMA_{95}$-*stat*-DPA_5) and (d) $PGMA_{56}$-P($HPMA_{90}$-*stat*-DPA_{10}) diblock copolymer nano-objects. The dispersions were adjusted from pH 8.5 using HCl.

Similar studies carried out for the $PGMA_{56}$-P($HPMA_{95}$-*stat*-DPA_5) diblock copolymers at pH 8.5 and 3.0 suggested that the particle diameter were both approximately 30 nm, despite no apparent evidence for particles as judged by TEM (see **Figure 4.28c**). However, the derived count rates decrease from 6,000 kcps to 1,600 kcps between pH 6.0 and pH 3.0, signalling significant particle dissolution. The increase in particle diameter at pH 7.0 is likely to be the result of swelling due to

partially protonated DPA residues. Finally, pH-dependent DLS studies conducted on the $PGMA_{56}$-P($HPMA_{90}$-*stat*-DPA_{10}) nanoparticles suggest their molecular dissolution below pH 7.0, since the derived count rates dropped to approximately 400 kcps (**Figure 4.28**).

Aqueous electrophoresis data recorded for the four $PGMA_{56}$-P($HPMA_y$-*stat*-DPA_z) diblock copolymer spheres between pH 8.5 and pH 3.0 demonstrate similar behaviour to the worm and vesicle series discussed in **sections 4.3.1** and **4.3.2**, respectively. Neutral $PGMA_{56}$-$PHPMA_{100}$ spheres display no cationic behaviour between pH 8.5 and pH 3.0, as expected (**Figure 4.29**). In contrast, $PGMA_{56}$-P($HPMA_{99}$-*stat*-DPA_1), $PGMA_{56}$-P($HPMA_{95}$-*stat*-DPA_5) and $PGMA_{56}$-P($HPMA_{90}$-*stat*-DPA_{10}) diblock copolymers confer weakly cationic character (+ 3 mV to + 15 mV) at pH 3.0 as a result of protonation of the amine groups in the copolymerised DPA residues.

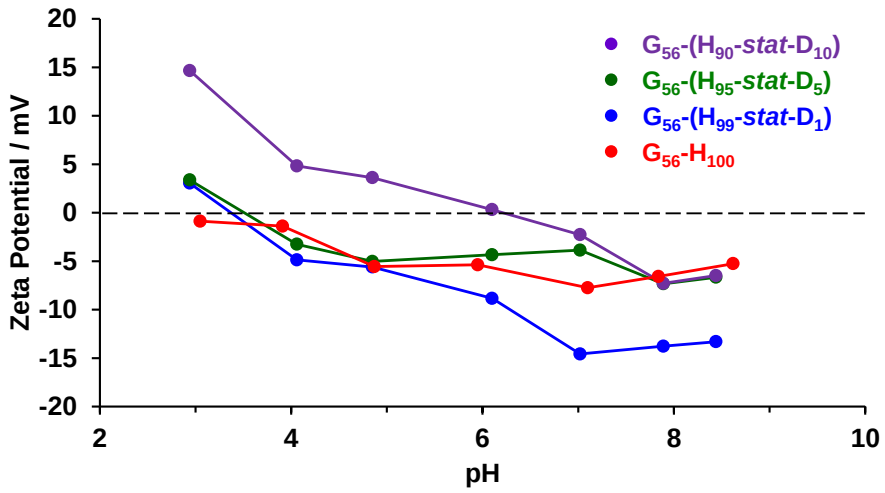

Figure 4.29 Zeta potential with vs. pH curves obtained for a series of $PGMA_{56}$-P($HPMA_y$-*stat*-DPA_z) diblock copolymer nano-objects diluted to 0.1 % w/w at 25 °C. These copolymers are denoted as G_{56}-(H_y-*stat*-D_z) for brevity.

On returning the solution pH of the 15 % w/w $PGMA_{56}$-P($HPMA_y$-*stat*-DPA_z) diblock copolymers to pH 8.5, weakly turbid free-flowing dispersions were obtained in each case. Furthermore, TEM analysis of these diblock copolymers after a pH cycle from 8.5 to 3.0 to 8.5 conducted after drying at 0.1 % w/w at pH 8.5

confirm the presence of spheres (see **Figure 4.30**). In the case of the $PGMA_{56}$-$P(HPMA_{95}$-*stat*-$DPA_5)$, a mixture of spheres and short worms were observed, which is similar to the original particles (i.e., prior to any pH switch). Thus $PGMA_{56}$-$P(HPMA_{95}$-*stat*-$DPA_5)$ and $PGMA_{56}$-$P(HPMA_{90}$-*stat*-$DPA_{10})$ diblock copolymer nano-objects exhibit reversible order-disorder transitions on switching the dispersion pH from 8.5 to 3.0.

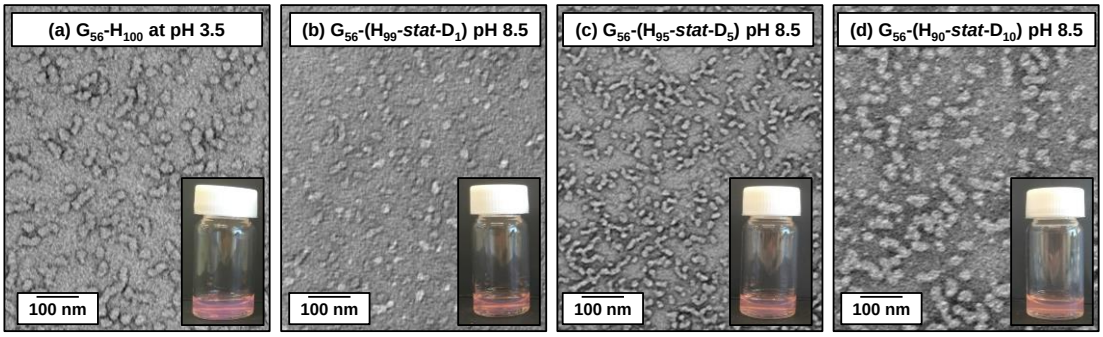

Figure 4.30 TEM images recorded at pH 8.5 (for dilute 0.1 % w/w aqueous copolymer dispersions) for a series of $PGMA_{56}$-$P(HPMA_y$-*stat*-$DPA_z)$ diblock copolymer nano-objects (where y + z = 100) after a pH cycle from pH 8.5 to 3.5 to 8.5. The inset shows the corresponding digital photographs obtained for the same diblock copolymer nano-objects at 15 % w/w solids after a pH cycle from pH 8.5 to 3.5 to 8.5. These copolymers are denoted as G_{56}-$(H_y$-*stat*-$D_z)$ for brevity.

4.4 Conclusions

In summary, a series of $PGMA_{56}$-$P(HPMA_y$-*stat*-$DPA_z)$ diblock copolymer worms, vesicles and spheres with varying DPA contents have been prepared by PISA. $PGMA_{56}$-$PHPMA_y$ nano-objects display *no* pH-responsive behaviour, as expected. However, statistically copolymerising HPMA with DPA in the core-forming block yields pH-responsive nano-objects. More specifically, order-order or order-disorder transitions can occur after a pH switch from 8.5 to 3.0 provided that the PDPA content is sufficiently high, as judged by TEM and DLS. Furthermore, all $PGMA_{56}$-$P(HPMA_y$-*stat*-$DPA_z)$ diblock copolymers containing DPA in the core exhibit cationic character at pH 3.0 according to aqueous electrophoresis studies.

Order-disorder transitions (i.e., formation of molecularly dissolved chains) occur when the protonated DPA residues cause the core-forming block to become water-soluble. ^{1}H NMR kinetic studies indicate that DPA is initially consumed much faster than HPMA, since the former comonomer is consumed *via* emulsion polymerisation, rather than dispersion polymerisation. Consequently, the block junction becomes enriched in DPA units compared to the rest of the core-forming block. Thus protonation at low pH results in order-order transitions to produce lower order morphologies (e.g. worm-to-sphere) as the stabiliser volume fraction increases relative to the core volume fraction. Not surprisingly, turbidimetry experiments of 0.1 % w/w PGMA$_{56}$-P(HPMA$_y$-*stat*-DPA$_z$) vesicles suggest that increasing the DPA content yields a faster pH-response. TEM studies conducted on the PGMA$_{56}$-P(HPMA$_y$-*stat*-DPA$_z$) diblock copolymer spheres and worms after a pH cycle from 8.5 to 3.0 to 8.5 indicated good reversibility in all cases. Conversely, PGMA$_{56}$-P(HPMA$_{245}$-*stat*-DPA$_5$) and PGMA$_{56}$-P(HPMA$_{240}$-*stat*-DPA$_{10}$) diblock copolymer vesicles formed solid pastes after a similar pH cycle, rather than turbid free-flowing solutions. Presumably the highly viscous worm phase acts as an efficient kinetic barrier to vesicle reformation. Only PGMA$_{56}$-P(HPMA$_{249}$-*stat*-DPA$_1$) vesicles exhibit reversibility because they only undergo a partial transition to produce vesicles and jellyfish, so they do not have to overcome the worm phase barrier. This particular composition offers some potential for post-polymerisation encapsulation and release by pH cycling.

Remarkably, increasing the DPA content in the PGMA$_{56}$-P(HPMA$_y$-*stat*-DPA$_z$) worms results in a subtle shift in morphology from worms to branched worms to a worm/vesicle mixed phase. This is accompanied by an increase in gel strength (G') according to rheological analysis. Further rheological studies conducted on the 15 % w/w PGMA$_{56}$-P(HPMA$_y$-*stat*-DPA$_z$) diblock copolymer worm gels as a function of pH confirm weaker gels are formed (and degelation in some cases) on lowering the solution pH from pH 8.0 to pH 6.0, which is consistent with the protonation of DPA residues. Such fine control over gel strength may be a useful parameter for cell biology studies. Furthermore, temperature-dependent rheological studies conducted on the 15 % w/w PGMA$_{56}$-P(HPMA$_y$-*stat*-DPA$_z$) diblock copolymer worms indicates that all such gels are thermo-responsive. This is caused

by surface plasticisation of the core-forming block resulting in a worm-to-sphere transition and hence degelation. Interestingly, the CGT decreases as the DPA content is increased because DPA is not thermo-responsive. Therefore lower temperatures are required for effective surface plasticisation of core-forming blocks.

4.5 References

(1) Meng, F.; Zhong, Z.; Feijen, J. *Biomacromolecules* **2009**, *10*, 197.

(2) Schmaljohann, D. *Adv. Drug Deliv. Rev.* **2006**, *58*, 1655.

(3) Bajpai, A. K.; Shukla, S. K.; Bhanu, S.; Kankane, S. *Prog. Polym. Sci.* **2008**, *33*, 1088.

(4) Stuart, M. A.; Huck, W. T.; Genzer, J.; Muller, M.; Ober, C.; Stamm, M.; Sukhorukov, G. B.; Szleifer, I.; Tsukruk, V. V.; Urban, M.; Winnik, F.; Zauscher, S.; Luzinov, I.; Minko, S. *Nat. Mater.* **2010**, *9*, 101.

(5) Alarcon, C. D. H.; Pennadam, S.; Alexander, C. *Chem. Soc. Rev.* **2005**, *34*, 276.

(6) Mendes, P. M. *Chem. Soc. Rev.* **2008**, *37*, 2512.

(7) Dai, S.; Ravi, P.; Tam, K. C. *Soft Matter* **2008**, *4*, 435.

(8) Hudson, E. S. G. a. S. M. *Prog. Polym. Sci.* **2004**, *29*, 1173.

(9) Khokhlov, A. R.; Starodubtsev, S. G.; Vasilevskaya, V. V. *Adv. Polym. Sci.* **1993**, *109*, 123.

(10) Philippova, O. E.; Hourdet, D.; Audebert, R.; Khokhlov, A. R. *Macromolecules* **1997**, *30*, 8278.

(11) Tokarev, I.; Minko, S. *Soft Matter* **2009**, *5*, 511.

(12) Dupin, D.; Fujii, S.; Armes, S. P.; Reeve, P.; Baxter, S. M. *Langmuir* **2006**, *22*, 3381.

(13) Chen, W.-Y.; Alexandridis, P.; Su, C.-K.; Patrickios, C. S.; Hertler, W. R.; Hatton, T. A. *Macromolecules* **1995**, *28*, 8604.

(14) Jain, S.; Bates, F. S. *Science* **2003**, *300*, 460.

(15) Zhang, L.; Eisenberg, A. *Polym. Adv. Tech.* **1998**, *9*, 677.

(16) Blanazs, A.; Armes, S. P.; Ryan, A. J. *Macromol. Rapid Commun.* **2009**, *30*, 267.

(17) Hu, Y. Q.; Kim, M. S.; Kim, B. S.; Lee, D. S. *J. Polym. Sci. A Polym. Chem.* **2008**, *46*, 3740.

(18) Hu, Y. Q.; Kim, M. S.; Kim, B. S.; Lee, D. S. *Polymer* **2007**, *48*, 3437.

(19) Gohy, J.-F.; Creutz, S.; Garcia, M.; Mahltig, B.; Stamm, M.; Jerome, R. *Macromolecules* **2000**, *33*, 6378.

(20) Gohy, J.-F.; Antoun, S.; Jérôme, R. *Macromolecules* **2001**, *34*, 7435.

(21) Schilli, C. M.; Zhang, M.; Rizzardo, E.; Thang, S. H.; Chong, Y. K.; Edwards, K.; Karlsson, G.; Müller, A. H. E. *Macromolecules* **2004**, *37*, 7861.

(22) Tan, J. F.; Ravi, P.; Too, H. P.; Hatton, T. A.; Tam, K. C. *Biomacromolecules* **2005**, *6*, 498.

(23) Xu, Y.; Shi, L.; Ma, R.; Zhang, W.; An, Y.; Zhu, X. X. *Polymer* **2007**, *48*, 1711.

(24) Mendrek, S.; Mendrek, A.; Adler, H.-J.; Dworak, A.; Kuckling, D. *J. Polym. Sci., Part A: Polym. Chem.* **2009**, *47*, 1782.

(25) Martin, T. J.; Procházka, K.; Munk, P.; Webber, S. E. *Macromolecules* **1996**, *29*, 6071.

(26) Ma, Y.; Tang, Y.; Billingham, N. C.; Armes, S. P.; Lewis, A. L.; Lloyd, A. W.; Salvage, J. P. *Macromolecules* **2003**, *36*, 3475.

(27) Du, J.; Tang, Y.; Lewis, A. L.; Armes, S. P. *J. Am. Chem. Soc.* **2005**, *127*, 17982.

(28) Sumerlin, B. S.; Lowe, A. B.; Thomas, D. B.; McCormick, C. L. *Macromolecules* **2003**, *36*, 5982.

(29) Doncom, K. E. B.; Hansell, C. F.; Theato, P.; O'Reilly, R. K. *Polym. Chem.* **2012**, *3*, 3007.

(30) Maiti, C.; Banerjee, R.; Maiti, S.; Dhara, D. *Langmuir* **2015**, *31*, 32.

(31) Bories-Azeau, X.; Armes, S. P.; van den Haak, H. J. W. *Macromolecules* **2004**, *37*, 2348.

(32) Dai, S.; Ravi, P.; Tam, K. C.; Mao, B. W.; Gan, L. H. *Langmuir* **2003**, *19*, 5175.

(33) Liu, S.; Armes, S. P. *Angew. Chem., Int. Ed.* **2002**, *41*, 1413.

(34) Bütün, V.; Liu, S.; Weaver, J. V. M.; Bories-Azeau, X.; Cai, Y.; Armes, S. P. *React. Funct. Polym* **2006**, *66*, 157.

(35) Bo, Q.; Zhao, Y. *J. Polym. Sci., Part A: Polym. Chem.* **2006**, *44*, 1734.

(36) Xin, X.; Wang, Y.; Liu, W. *Eur. Polym. J.* **2005**, *41*, 1539.

(37) Rodríguez-Hernández, J.; Lecommandoux, S. *J. Am. Chem. Soc.* **2005**, *127*, 2026.

(38) Chen, L.; Chen, T.; Fang, W.; Wen, Y.; Lin, S.; Lin, J.; Cai, C. *Biomacromolecules* **2013**, *14*, 4320.

(39) Lomas, H.; Canton, I.; MacNeil, S.; Du, J.; Armes, S. P.; Ryan, A. J.; Lewis, A. L.; Battaglia, G. *Adv. Mater.* **2007**, *19*, 4238.

(40) Pegoraro, C.; Cecchin, D.; Gracia, L. S.; Warren, N.; Madsen, J.; Armes, S. P.; Lewis, A.; MacNeil, S.; Battaglia, G. *Cancer Lett.* **2013**, *334*, 328.

(41) Qian, J.; Berkland, C. *Polym. Chem.* **2015**, *6*, 3472.

(42) Betthausen, E.; Drechsler, M.; Fortsch, M.; Schacher, F. H.; Muller, A. H. E. *Soft Matter* **2011**, *7*, 8880.

(43) Luo, C.; Liu, Y.; Li, Z. *Soft Matter* **2012**, *8*, 2618.

(44) Cai, Y.; Armes, S. P. *Macromolecules* **2004**, *37*, 7116.

(45) Zhang, W.; Shi, L.; Ma, R.; An, Y.; Xu, Y.; Wu, K. *Macromolecules* **2005**, *38*, 8850.

(46) Chaduc, I.; Crepet, A.; Boyron, O.; Charleux, B.; D'Agosto, F.; Lansalot, M. *Macromolecules* **2013**, *46*, 6013.

(47) Ferguson, C. J.; Hughes, R. J.; Pham, B. T. T.; Hawkett, B. S.; Gilbert, R. G.; Serelis, A. K.; Such, C. H. *Macromolecules* **2002**, *35*, 9243.

(48) Zhang, X.; Boissé, S.; Zhang, W.; Beaunier, P.; D'Agosto, F.; Rieger, J.; Charleux, B. *Macromolecules* **2011**, *44*, 4149.

(49) Chaduc, I.; Girod, M.; Antoine, R.; Charleux, B.; D'Agosto, F.; Lansalot, M. *Macromolecules* **2012**, *45*, 5881.

(50) An, Z.; Shi, Q.; Tang, W.; Tsung, C.-K.; Hawker, C. J.; Stucky, G. D. *J. Am. Chem. Soc.* **2007**, *129*, 14493.

(51) Rieger, J.; Grazon, C.; Charleux, B.; Alaimo, D.; Jerome, C. *J. Polym. Sci., Part A: Polym. Chem.* **2009**, *47*, 2373.

(52) Li, Y.; Armes, S. P. *Angew. Chem., Int. Ed.* **2010**, *49*, 4042.

(53) Liu, G.; Qiu, Q.; Shen, W.; An, Z. *Macromolecules* **2011**, *44*, 5237.

(54) Sugihara, S.; Blanazs, A.; Armes, S. P.; Ryan, A. J.; Lewis, A. L. *J. Am. Chem. Soc.* **2011**, *133*, 15707.

(55) Blanazs, A.; Ryan, A. J.; Armes, S. P. *Macromolecules* **2012**, *45*, 5099.

(56) Warren, N. J.; Armes, S. P. *J. Am. Chem. Soc.* **2014**, *136*, 10174.

(57) Doncom, K. E. B.; Warren, N. J.; Armes, S. P. *Polym. Chem.* **2015**, *6*, 7264.

(58) Zhou, W.; Qu, Q.; Xu, Y.; An, Z. *ACS Macro Lett.* **2015**, *4*, 495.

(59) Chen, Q.; Cao, X.; Liu, H.; Zhou, W.; Qin, L.; An, Z. *Polym. Chem.* **2013**, *4*, 4092.

(60) Save, M.; Weaver, J. V. M.; Armes, S. P.; McKenna, P. *Macromolecules* **2002**, *35*, 1152.

(61) Penfold, N. J. W.; Lovett, J. R.; Warren, N. J.; Verstraete, P.; Smets, J.; Armes, S. P. *Polym. Chem.* **2016**, *7*, 79.

(62) Rieger, J.; Zhang, W.; Stoffelbach, F.; Charleux, B. *Macromolecules* **2010**, *43*, 6302.

(63) Cunningham, V. J.; Alswieleh, A. M.; Thompson, K. L.; Williams, M.; Leggett, G. J.; Armes, S. P.; Musa, O. M. *Macromolecules* **2014**, *47*, 5613.

(64) Truong, N. P.; Dussert, M. V.; Whittaker, M. R.; Quinn, J. F.; Davis, T. P. *Polym. Chem.* **2015**, *6*, 3865.

(65) Tang, M.; Yang, Z.; Feng, Z.; Zhou, J.; Liu, J.; Liu, J.; Wang, W.; Zhao, J.; Dong, A.; Deng, L. *Polym. Chem.* **2015**, *6*, 6671.

(66) Jager, A.; Jager, E.; Surman, F.; Hocherl, A.; Angelov, B.; Ulbrich, K.; Drechsler, M.; Garamus, V. M.; Rodriguez-Emmenegger, C.; Nallet, F.; Stepanek, P. *Polym. Chem.* **2015**, *6*, 4946.

(67) Barner-Kowollik, C.; Buback, M.; Charleux, B.; Coote, M. L.; Drache, M.; Fukuda, T.; Goto, A.; Klumperman, B.; Lowe, A. B.; McLeary, J. B.; Moad, G.; Monteiro, M. J.; Sanderson, R. D.; Tonge, M. P.; Vana, P. *J. Polym. Sci., Part A: Polym. Chem.* **2006**, *44*, 5809.

(68) Blanazs, A.; Madsen, J.; Battaglia, G.; Ryan, A. J.; Armes, S. P. *J. Am. Chem. Soc.* **2011**, *133*, 16581.

(69) Ratcliffe, L. P. D.; Blanazs, A.; Williams, C. N.; Brown, S. L.; Armes, S. P. *Polym. Chem.* **2014**, *5*, 3643.

(70) Guha, S.; Mandal, B. M. *J. Colloid Interface Sci.* **2004**, *271*, 55.

(71) Liu, Z.; Rimmer, S. *Macromolecules* **2002**, *35*, 1200.

(72) Lovett, J. R.; Warren, N. J.; Ratcliffe, L. P.; Kocik, M. K.; Armes, S. P. *Angew. Chem., Int. Ed.* **2015**, *54*, 1279.

(73) Semsarilar, M.; Ladmiral, V.; Blanazs, A.; Armes, S. P. *Langmuir* **2013**, *29*, 7416.

(74) Verber, R.; Blanazs, A.; Armes, S. P. *Soft Matter* **2012**, *8*, 9915.

(75) Blanazs, A.; Verber, R.; Mykhaylyk, O. O.; Ryan, A. J.; Heath, J. Z.; Douglas, C. W. I.; Armes, S. P. *J. Am. Chem. Soc.* **2012**, *134*, 9741.

(76) Chambon, P.; Blanazs, A.; Battaglia, G.; Armes, S. P. *Langmuir* **2012**, *28*, 1196.

(77) Engler, A. J.; Sen, S.; Sweeney, H. L.; Discher, D. E. *Cell* **2006**, *126*, 677.

(78) Yoshikawa, H. Y.; Rossetti, F. F.; Kaufmann, S.; Kaindl, T.; Madsen, J.; Engel, U.; Lewis, A. L.; Armes, S. P.; Tanaka, M. *J. Am. Chem. Soc.* **2011**, *133*, 1367.

(79) Rimmer, S.; Wilshaw, S.-P.; Pickavance, P.; Ingham, E. *Biomaterials* **2009**, *30*, 2468.

(80) Mable, C. J.; Gibson, R. R.; Prevost, S.; McKenzie, B. E.; Mykhaylyk, O. O.; Armes, S. P. *J. Am. Chem. Soc.* **2015**, *137*, 16098.

(81) Tan, J.; Sun, H.; Yu, M.; Sumerlin, B. S.; Zhang, L. *ACS Macro Lett.* **2015**, *4*, 1249.

Chapter 5:

Preparation of Core Cross-Linked Worms

5.1 Introduction

Over the last fifty years or so, block copolymer self-assembly has become a well-recognised and widely adopted route for the production of organic nanoparticles in a wide range of solvents. Many copolymer morphologies have been reported in the literature.[1-5] However, there have been relatively few studies of block copolymer worms, cylinders or rods *via* traditional post-polymerisation processing routes, such as a solvent switch in dilute solution.[5-13] This is presumably because such highly anisotropic morphologies typically occupy relatively little phase space, which means that the range of required block compositions tends to be rather narrow (see **Figure 5.1**). In contrast, polymerisation-induced self-assembly (PISA) has recently enabled the *rational* synthesis of block copolymer worms in the form of highly concentrated dispersions in a wide range of polar and non-polar solvents.[14-32]

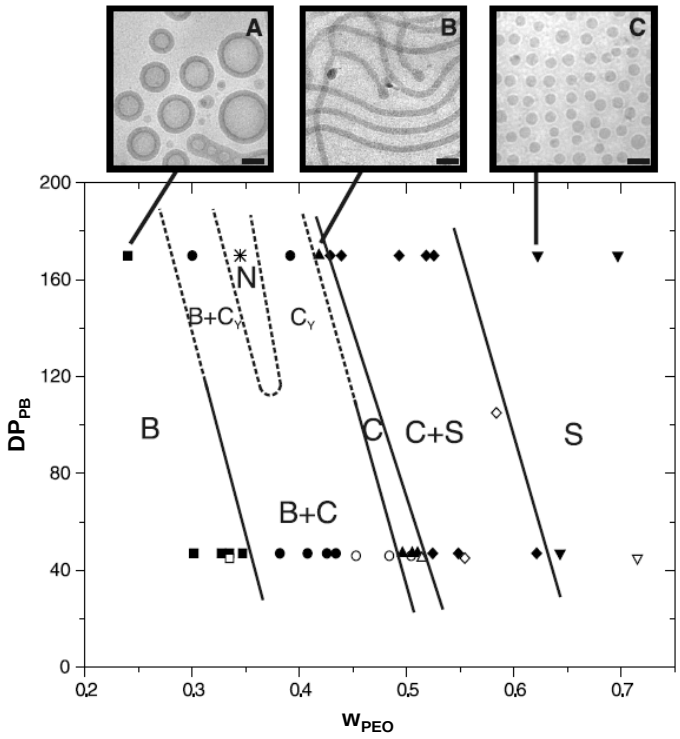

Figure 5.1 Phase diagram constructed by Bates and co-workers for poly(1,2-butadiene)-poly(ethylene oxide) (PB-PEO) diblock copolymers at 1 % w/w solids at varying degrees of polymerisation (DP) of PB and varying weight fraction (W) of the PEO block. Here S stands for spheres, C stands for cylinders, C_Y represents branched cylinders, B stands for bilayers and N indicates macroscopic phase separation. Transmission electron microscopy images of pure phases are shown above.[5]

The worm morphology is particularly interesting for various potential applications. Discher and co-workers have shown that poly(ethylene oxide)-poly(caprolactone) diblock copolymer worms exhibit substantially extended *in vivo* circulation times compared to the equivalent spherical morphology.[9] Armes and co-workers have recently demonstrated the advantages offered by highly anisotropic worms when deployed as Pickering emulsifiers:[33] they are much more strongly adsorbed at the oil-water interface compared to the equivalent spheres, yet retain a relatively high specific surface area.[34,35] Several research groups have studied the rheological properties of block copolymer worms,[31,32,36-40] with thermo-reversible gelation being observed in aqueous solution,[14,31] polar solvents such as ethanol[41] and non-polar solvents such as *n*-alkanes.[19,32,42]

Many strategies have been explored for the covalent stabilisation of block copolymer nano-objects. Core cross-linked spherical micelles have been reported by various groups,[43-46] while Wooley[47-51] and Armes[52-55] have worked extensively on shell cross-linked micelles. Both Antonietti *et al*.[56] and Bates and co-workers[7,37] have cross-linked polybutadiene-based block copolymer worms in dilute solution using gamma radiation or redox chemistry, respectively. In contrast, Liu's group has developed various photochemical strategies based on cinnamoyl side-groups.[57,58]

In the context of PISA formulations, cross-linked block copolymer spheres, worms and vesicles have been reported by copolymerising small amounts of divinyl comonomers such as ethylene glycol di(meth)acrylate or poly(ethylene glycol) diacrylate.[32,34,59-62] However, this strategy is somewhat problematic for the worm morphology, since small perturbations in the block composition can result in the formation of mixed phases, rather than pure worms. An alternative post-polymerisation approach was reported by Chambon *et al*. for cross-linked block copolymer vesicles, whereby pendent epoxy groups on glycidyl methacrylate (GlyMA) were reacted with small molecule or oligomeric diamines (see **Figure 5.2**).[63] Similarly An and co-workers prepared poly(poly(ethylene oxide) methyl ether methacrylate)-poly(2-(acetoacetoxy)ethyl methacrylate) (PPEOMA-PAEMA) diblock copolymer vesicles (and spheres) using PISA by RAFT dispersion polymerisation in ethanol.[64] These nano-objects were subsequently cross-linked

using O,O′-1,3-propanediylbisoxylamine dihydrochloride, which reacted with ketone groups in the PAEMA core-forming block.

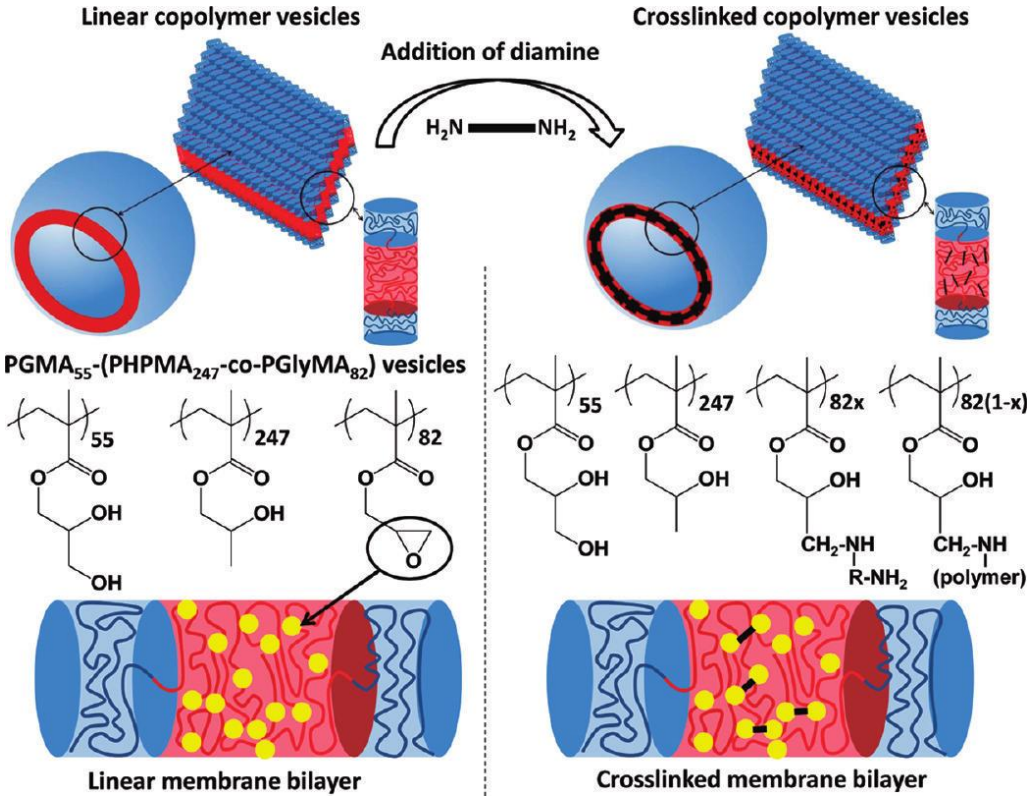

Figure 5.2 Schematic representation of the preparation of cross-linked of GMA_{55}-($PHPMA_{247}$-*stat*-$PGlyMA_{82}$) vesicles using a diamine.[63]

Generally speaking, there are relatively few literature reports describing the synthesis and cross-linking of diblock copolymer worms.[6-8,57,65-68] Herein the facile preparation of core cross-linked diblock copolymer worms is reported. More specifically, a series of hydroxyl-functional methacrylic diblock copolymer worms containing varying amounts of GlyMA in the core-forming block are prepared in aqueous solution *via* PISA. Such worms are then covalently stabilised by cross-linking of the core-forming block using 3-aminopropyl triethoxysilane (APTES). The physical properties of aqueous dispersions of these cross-linked worms are compared to those of the linear worm precursors using various characterisation techniques, including transmission electron microscopy (TEM), dynamic light scattering (DLS) and oscillatory rheology.

5.2 Experimental Section

5.2.1 Materials

Glycerol monomethacrylate (GMA; 99.8 % purity) was kindly donated by GEO Specialty Chemicals (Hythe, UK) and used without further purification. 2-Hydroxypropyl methacrylate (HPMA) was purchased from Alfa Aesar (UK) and used as received. 2,2'-Azobis[2-(2-imidazolin-2-yl)propane]dihydrochloride (VA-044) was purchased from Wako Pure Chemical Industries (Japan) and used as received. Glycidyl methacrylate (GlyMA), 2-cyano-2-propyl dithiobenzoate (CPDB), 4,4'-azobis(4-cyanopentanoic acid) (ACVA; 99 %), 3-aminopropyl triethoxysilane (APTES), d_4-sodium trimethylsilyl propanoate (TMSP), sodium dodecyl sulfate (SDS), deuterated methanol-D_4, ethanol (99 %, anhydrous grade), methanol and dichloromethane were purchased from Sigma-Aldrich (UK) and were used as received. All solvents were of HPLC-grade quality.

5.2.2 Synthesis of poly(glycerol monomethacrylate) ($PGMA_{56}$) macro-CTA *via* RAFT solution polymerisation in ethanol

A typical protocol for the synthesis of $PGMA_{56}$ macro-CTA was as follows: GMA (203.0 g, 1.268 mol), CPDB (6.03 g, 0.020 mol; target DP = 63), ACVA (1.14 g, 4.07 mmol; CPDB: ACVA molar ratio = 5.0) and anhydrous ethanol (156.0 g, 3.38 mol) were added to a round-bottomed flask to afford a 55 % w/w solution. The resulting pink solution was purged with N_2 for 40 min, before the sealed flask was immersed into an oil bath set at 70 °C. After 140 min (69 % conversion as judged by ^{1}H NMR) the polymerisation was quenched by immersion of the flask into an ice bath and exposing the reaction mixture to air. The crude polymer was then precipitated into a ten-fold excess of dichloromethane and washed three times using this non-solvent to remove residual unreacted GMA monomer before being dried under high vacuum for three days at 40 °C. ^{1}H NMR studies indicated a mean degree of polymerisation of 56 *via* end-group analysis (the integrated aromatic RAFT end-group signals at 7.1-7.4 ppm were compared to polymer backbone signals between

0.5 to 2.5 ppm). Taking into account the target DP of 63 and the GMA conversion of 69 %, this indicated a CTA efficiency of 76 %. GPC studies indicated an M_n of 15,000 g mol^{-1} and an M_w/M_n of 1.11. ^{1}H NMR (400 MHz, CD_3OD, 25 °C): δ 0.73-1.26 (b, 3H, -$CH_2CR(CH_3)$-), 1.55-2.32 (b, 2.2H, -$CH_2CR(CH_3)$-), 3.50-3.83 (b, 2.4H, -CH_2OH), 3.84-4.25 (b, 3.1H, -COOCH_2CH(OH)-).

5.2.3 Synthesis of $PGMA_{56}$-$PHPMA_{144}$ diblock copolymer worms *via* RAFT aqueous dispersion polymerisation

A typical protocol for the chain extension of $PGMA_{56}$ macro-CTA with 144 units of HPMA *via* RAFT aqueous dispersion polymerisation was as follows. $PGMA_{56}$ macro-CTA (0.399 g, 0.043 mmol), HPMA monomer (0.90 g, 6.0 mmol), VA-044 (3.50 mg, 0.011 mmol; $PGMA_{56}$ macro-CTA: VA-044 molar ratio = 4.0) were added to a 25 ml round-bottomed flask, prior to addition of water to produce a 15 % w/w aqueous solution. The reaction solution was purged under nitrogen for 30 min at 20 °C prior to immersion into an oil bath set at 50 °C. The reaction mixture was stirred for 105 min to ensure almost complete conversion of the HPMA monomer (> 99 % by ^{1}H NMR analysis), and was quenched by simultaneous exposure to air and cooling to ambient temperature. The resulting dispersion was diluted with deionised water to give a free-standing 7.5 % w/w worm gel that was characterised by DLS, TEM and rheology without further purification. ^{1}H NMR (400 MHz, CD_3OD, 25 °C): δ 0.79-1.19 (b, 3H, -CH_3 on polymer backbone), 1.19-1.38 (b, 2.7H, -CH_3 in PHPMA), 1.54-2.23 (b, 2.2H, -CH_2- on polymer backbone), 3.53-3.71 (b, 0.9H, -CH_2OH in PGMA and –CH(OH)- in PHPMA), 3.72-4.20 (b, 2.9H, remaining pendent protons in PGMA and PHPMA).

5.2.4 Synthesis of $PGMA_{56}$-$P(HPMA_y$-stat-$GlyMA_z)$ diblock copolymer worms *via* RAFT aqueous emulsion/dispersion polymerisation

A typical protocol for chain extension of $PGMA_{56}$ macro-CTA with 122 units of HPMA and 22 units of GlyMA *via* RAFT aqueous dispersion/emulsion polymerisation was as follows: $PGMA_{56}$ macro-CTA (0.418 g, 0.046 mmol), HPMA monomer (0.800 g, 5.5 mmol), GlyMA monomer (0.140 g, 1.0 mmol), VA-044 (3.70

mg, 0.011 mmol; $PGMA_{56}$ macro-CTA: VA-044 molar ratio = 4.0) were added to a 25 ml round-bottomed flask, prior to addition of sufficient water to afford a 15 % w/w aqueous solution. This reaction solution was purged under nitrogen for 30 min at 20 °C prior to immersion into an oil bath set at 50 °C. The reaction mixture was stirred for 105 min to ensure almost complete conversion of the HPMA and GlyMA comonomers (> 99 % by ^{1}H NMR analysis). Then the copolymerisation was quenched by simultaneous exposure to air and cooling to ambient temperature. The resulting dispersion was immediately diluted with deionised water to 7.5 % w/w solids, yielding a free-standing worm gel that was characterised by DLS, TEM and rheology without further purification. ^{1}H NMR (400 MHz, CD_3OD, 25 °C): δ 0.73-1.19 (b, 3H, **-CH_3** on polymer backbone), 1.19-1.39 (b, 2.3H, **-CH_3** in PHPMA), 1.55-2.28 (b, 2.2H, **-CH_2-** on polymer backbone), 2.72-3.06 (b, 0.4H, epoxy in PGlyMA), 3.52-3.73 (b, 0.9H, **-CH_2**OH in GMA and –**CH**(OH)- in PHPMA), 3.73-4.20 (b, 2.9H, remaining pendent protons in PGMA, PHPMA and PGlyMA).

5.2.5 Post-polymerisation cross-linking of a 7.5 % w/w aqueous dispersion of $PGMA_{56}$-P($HPMA_y$-*stat*-$GlyMA_z$) worm gel using APTES

A typical protocol for the covalent cross-linking of $PGMA_{56}$-P($HPMA_{122}$-*stat*-$GlyMA_{22}$) diblock copolymer worm gel at 7.5 % w/w solids using APTES was as follows. APTES (0.111 g, 0.5 mmol, APTES: GlyMA molar ratio = 1.0) was added to 9.1 g of a 7.5 % w/w aqueous dispersion of $PGMA_{56}$-P($HPMA_{122}$-*stat*-$GlyMA_{22}$) diblock copolymer worms and the epoxy-amine reaction was allowed to proceed for 24 h at 20 °C with continuous stirring of the shear-thinning worm gels.

5.2.6 Instrumentation

^{1}H NMR spectra were recorded using a 500 MHz Bruker Avance-500 spectrometer (64 scans averaged per spectrum).

Gel Permeation Chromatography (GPC) was used to assess polymer molecular weight distributions. The DMF GPC set-up comprised two Polymer Laboratories PL gel 5 μm Mixed-C columns connected in series to a Varian 390-LC multi-detector

suite (refractive index detector) and a Varian 290-LC pump injection module operating at 60 °C. The GPC eluent was HPLC-grade DMF containing 10 mM LiBr at a flow rate of 1.0 mL min^{-1}. DMSO was used as a flow-rate marker. Calibration was conducted using a series of ten near-monodisperse poly(methyl methacrylate) standards (M_n = 625 to 2,480,000 g mol^{-1}). Chromatograms were analysed using Varian Cirrus GPC software (version 3.3).

Dynamic Light Scattering (DLS) studies were conducted using a Malvern Zetasizer NanoZS instrument at 25 °C. Measurements were performed on 0.10 % w/w aqueous in disposable cuvettes at a fixed back-scattering angle of 173°. Intensity-average hydrodynamic diameters were calculated *via* the Stokes-Einstein equation. All data were averaged over three consecutive runs.

Aqueous electrophoresis measurements were conducted using a Malvern Zetasizer NanoZS instrument at 25 °C. Studies were performed on aqueous copolymer dispersions diluted to 0.10 % w/w containing 10^{-3} mol dm^{-3} KCl as background electrolyte. Zeta potentials were calculated from the Henry equation using the Smoluchowski approximation. All data were averaged over three consecutive runs.

Transmission Electron Microscopy (TEM) Imaging was performed using a FEI Tecnai Spirit microscope fitted with a Gatan 1kMS600CW CCD camera operating at 80 kV. Copolymer dispersions were diluted 150-fold at 20 °C in either methanol or water to generate 0.10 % w/w dispersions. Copper/palladium TEM grids (Agar Scientific, UK) were surface-coated in-house to yield a thin film of amorphous carbon. The grids were then plasma glow-discharged for 30 s to create a hydrophilic surface. A micropipette was used to place droplets (12 μL) of aqueous copolymer dispersions onto freshly glow-discharged grids for one minute, followed by careful blotting with filter paper to remove excess sample. To stain the aggregates, a 0.75% w/w uranyl formate solution (9 μL) was added on the sample-loaded grid for 20 s and then carefully blotted to remove excess stain. Each grid was then carefully dried using a vacuum hose.

Rheology studies were conducted using an AR-G2 stress controlled rheometer with a variable temperature Peltier plate equipped with a cone-and-plate geometry (40 mm

2 ° aluminium cone). Storage (G') and loss (G") moduli were determined between 4 °C and 25 °C for diblock copolymer worm gels both before and after covalent cross-linking at a fixed strain of 1.0 % and an angular frequency of 1.0 rad s^{-1}. A cone-and-plate geometry (40 mm 2 ° aluminium cone) was used for these measurements.

5.3 Results and Discussion

A well-defined near-monodisperse poly(glycerol monomethacrylate) (PGMA) macro-CTA was prepared *via* reversible addition-fragmentation chain transfer (RAFT) solution polymerisation of GMA in ethanol at 70 °C using 2-cyano-2-propyl dithiobenzoate (CPDB) as the chain transfer agent (CTA).[69,70] ^{1}H NMR spectroscopy studies suggested a mean degree of polymerisation (DP) of 56, as judged by end-group analysis (**Figure 5.3a**). Moreover, gel permeation chromatography (GPC) studies conducted in DMF against near-monodisperse poly(methyl methacrylate) (PMMA) standards indicated that the $PGMA_{56}$ macro-CTA possessed a relatively narrow molecular weight distribution (M_n = 15,000 g mol^{-1} and M_w/M_n = 1.11).

This homopolymer precursor was then chain-extended *via* statistical copolymerisation of 0, 5, 10, 15 or 20 mol % of glycidyl methacrylate (GlyMA) with 2-hydroxypropyl methacrylate (HPMA) at 15 % w/w solids using a polymerisation-induced self-assembly (PISA) formulation (see **Figure 5.4**). This protocol produced a series of free-standing copolymer worm gels after cooling to room temperature. For each $PGMA_{56}$-P($HPMA_y$-*stat*-$GlyMA_z$) diblock copolymer synthesis, a mean DP of 144 was targeted for the core-forming block (i.e., y + z = 144). High monomer conversions (99 %) were achieved in all cases as judged by the disappearance of monomer vinyl signals between 5.9 and 6.1 ppm in the ^{1}H NMR spectra (see **Figure 5.3b**).

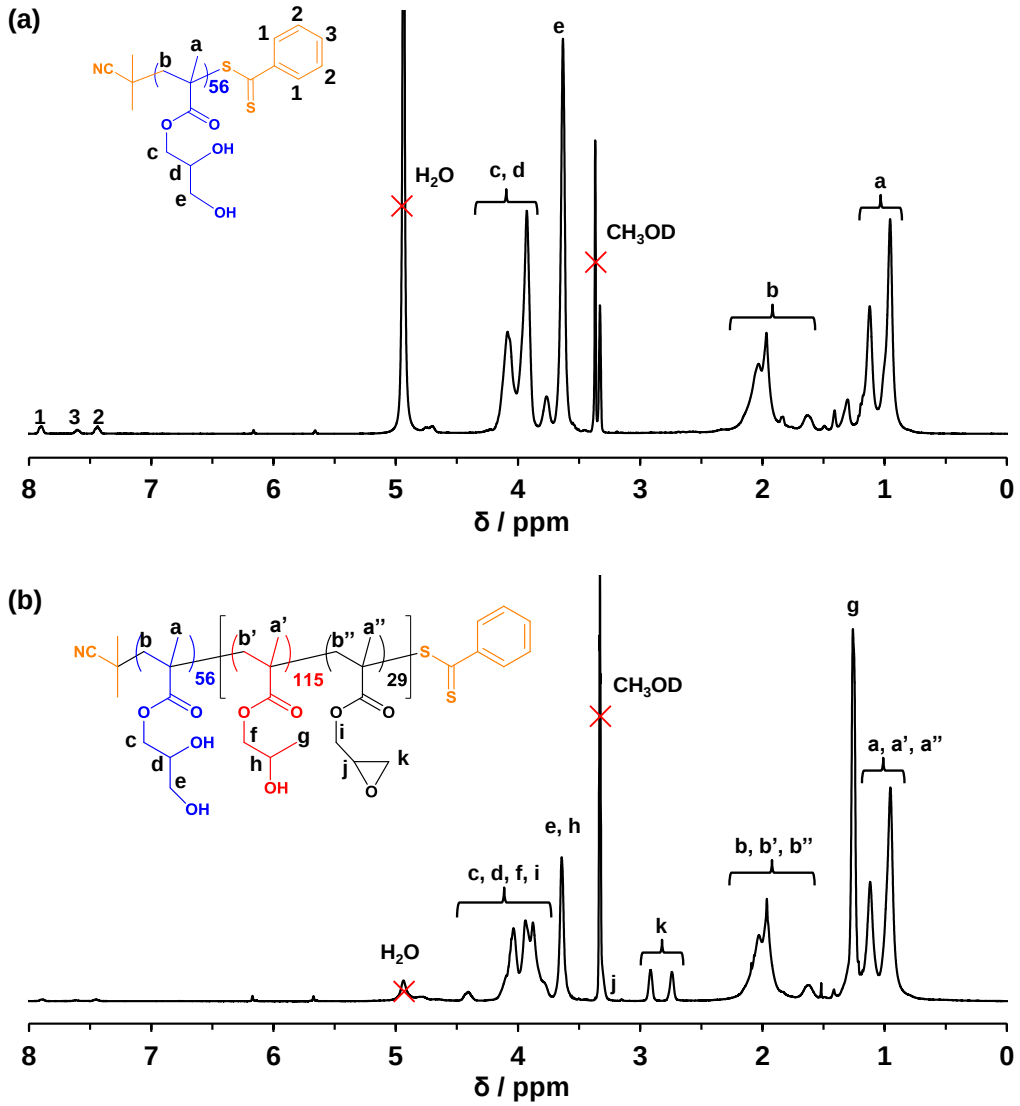

Figure 5.3 ^{1}H NMR spectra recorded in deuterated methanol for (a) $PGMA_{56}$ macro-CTA and (b) $PGMA_{56}$-P($HPMA_{115}$-*stat*-$GlyMA_{29}$) diblock copolymer.

The as-prepared 15 % w/w aqueous dispersions of block copolymer worms described above were diluted to 7.5 % w/w solids to allow efficient stirring when conducting post-polymerisation derivatisation reactions using 3-aminopropyl triethoxysilane (APTES), see **Figure 5.4**. The primary amine group on this siloxane reagent reacts with the pendent epoxide groups[71] located within the core-forming blocks, with APTES ingress aided by the partially hydrated nature of the HPMA-rich worm cores.[14] In principle, the triethoxysilane component of the grafted APTES molecules should then undergo hydrolysis-condensation reactions, both with each other and also with the pendent secondary (and primary) hydroxyl groups on the

HPMA residues, resulting in core cross-linked worms.[72] Post-polymerisation cross-linking was undertaken in order to minimise the possibility of *in situ* cross-linking during PISA, which might otherwise prevent the formation of worms, or perhaps cause inter-worm aggregation. After cross-linking at 7.5 % w/w solids, the diblock copolymer worm gels were expected to be dispersible in a good solvent for both blocks (e.g., methanol) and also possess enhanced resistance towards the presence of ionic surfactants, which are known to cause rapid dissociation of closely-related PGMA-PHPMA *linear* diblock copolymer nano-objects.[63] Furthermore, the rheological properties of the worm gels were investigated both before and after cross-linking.

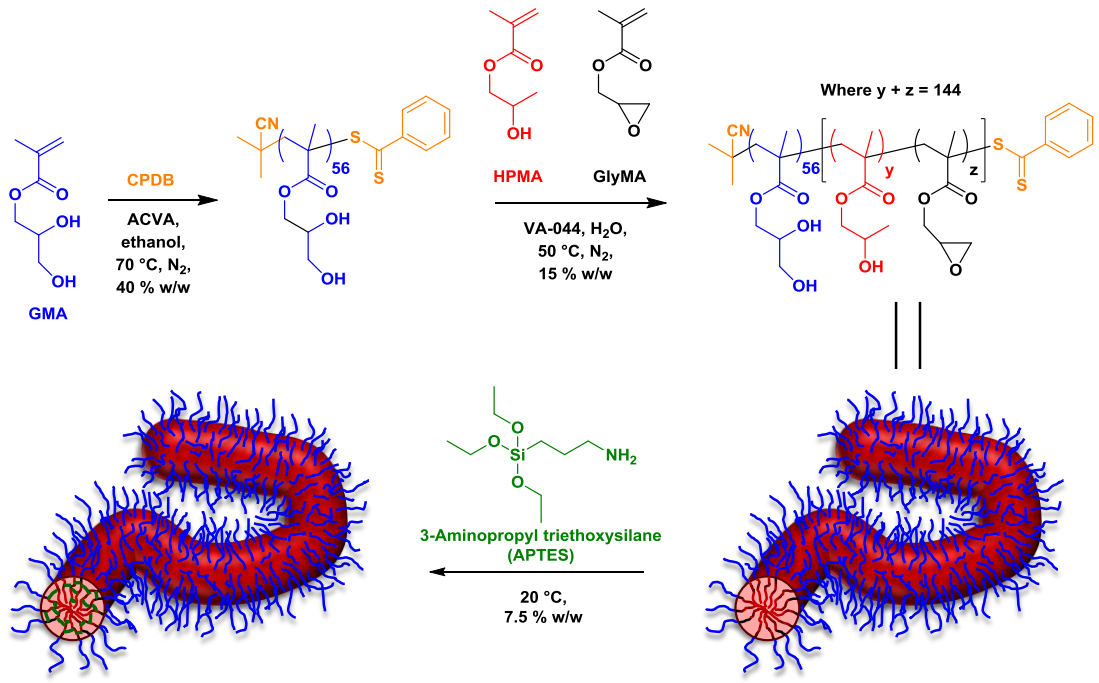

Figure 5.4 Synthesis of a $PGMA_{56}$ macro-CTA *via* RAFT solution polymerisation of GMA in ethanol using a CPDB RAFT agent, and its subsequent chain extension *via* statistical copolymerisation of varying molar ratios of HPMA and GlyMA to form diblock copolymer worms in aqueous solution *via* polymerisation-induced self-assembly (PISA). Such worms are then cross-linked using APTES in a two-step post-polymerisation process involving (i) an epoxy-amine reaction with the GlyMA residues and (ii) hydrolysis-condensation reaction with the hydroxyl groups on the HPMA residues.

In Chapter 2 it was demonstrated that PGMA-PHPMA diblock copolymer worms prepared using a carboxylic acid-based RAFT CTA undergo worm-to-sphere transitions upon a pH switch as a result of end-group ionisation.[73] Thus it was important to employ a *non-ionic* CTA in the present study in order to prevent such order-order morphological transitions on addition of the strongly basic APTES reagent.

5.3.1 Synthesis and characterisation of PGMA-P(HPMA$_y$-*stat*-GlyMA$_z$) diblock copolymer worms

Previous syntheses of similar PGMA$_{55}$-P(HPMA$_{247}$-*stat*-GlyMA$_{82}$) diblock copolymer vesicles were conducted by Chambon *et al.*, with full conversion being attained after 4 h at 70 °C.[63] According to ^{1}H NMR studies, around 90 % of the epoxide groups on the GlyMA residues survived these conditions, with 10% undergoing hydrolysis with water (to afford GMA residues) and/or pendent hydroxyl groups in HPMA resulting in partial *in situ* cross-linking. In the present study, diblock copolymer syntheses were conducted at 50 °C for 105 min in order to minimise such side reactions. ^{1}H NMR studies confirmed the success of this modified protocol, with approximately 98 % of epoxide groups surviving at full comonomer conversion. The (co)polymerisation kinetics for the synthesis of PGMA$_{56}$-PHPMA$_{144}$, PGMA$_{56}$-P(HPMA$_{130}$-*stat*-GlyMA$_{14}$) and PGMA$_{56}$-P(HPMA$_{115}$-*stat*-GlyMA$_{29}$) at 50 °C were monitored by ^{1}H NMR (see **Figure 5.5**). Aliquots of reaction mixtures were extracted at regular time intervals and diluted prior to NMR analysis using CD_3OD, which is a good solvent for all monomeric and copolymer species.

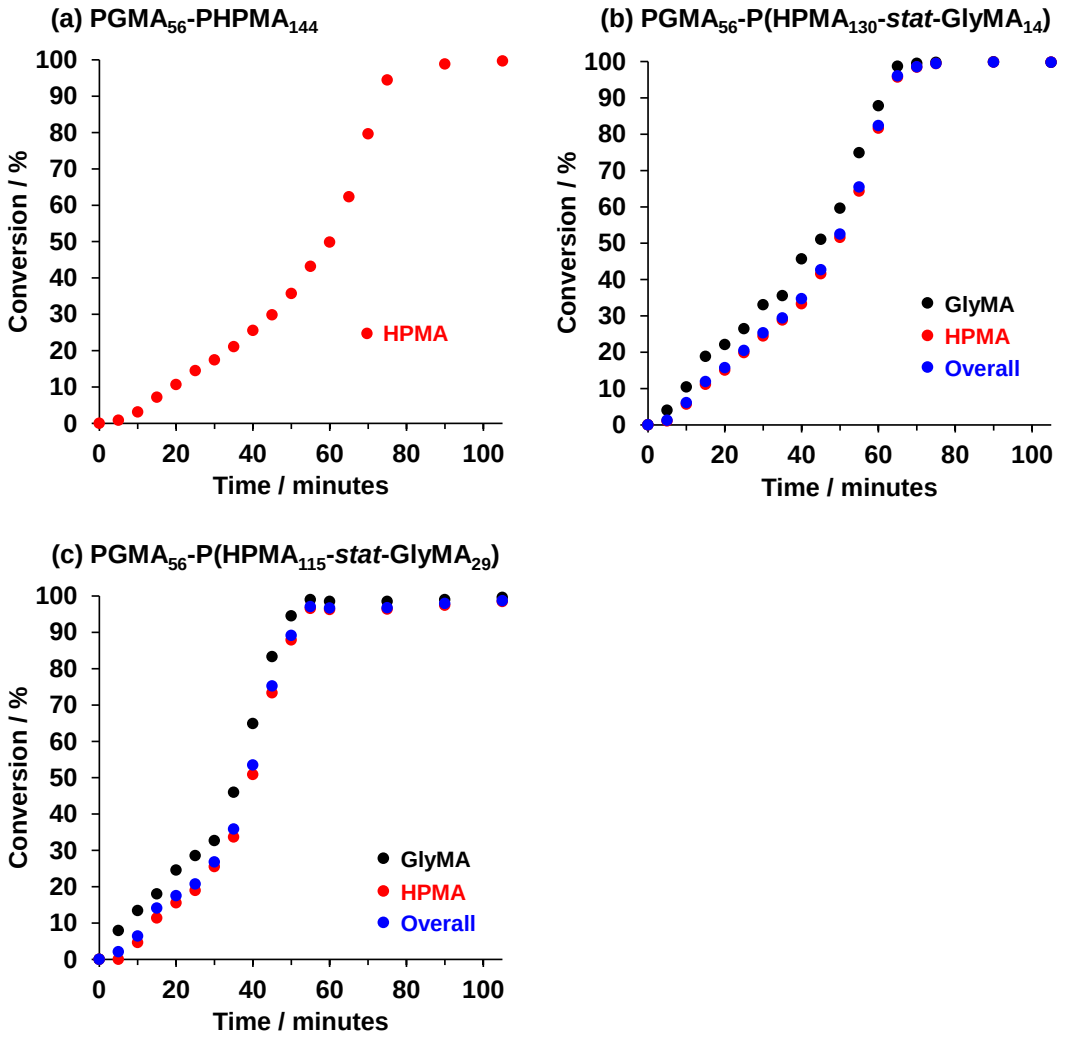

Figure 5.5 Conversion vs. time curves obtained by ^{1}H NMR for the (co)polymerisation of HPMA (red circles), GlyMA (black circles), and the overall comonomer mixture (blue circles) at 50 °C using a $PGMA_{56}$ macro-CTA when targeting diblock copolymer compositions of: (a) $PGMA_{56}$-$PHPMA_{144}$; (b) $PGMA_{56}$-P($HPMA_{130}$-*stat*-$GlyMA_{14}$) and (c) $PGMA_{56}$-P($HPMA_{115}$-*stat*-$GlyMA_{29}$). All syntheses were conducted at 15 % w/w solids.

Kinetic studies of the $PGMA_{56}$-$PHPMA_{144}$ diblock copolymer formulation indicated that full conversion was achieved after 90 min. After a brief induction period, consumption of the water-miscible HPMA monomer was relatively slow for 35 min. This may be the result of mild retardation, which is not fully understood.[74] After 65 min (or 62 % conversion, which corresponds to a PHPMA DP of 89), the rate of polymerisation increases by an order of magnitude (see **Figure 5.6a**). This is

the result of micellar nucleation, which heralds a switch from RAFT solution polymerisation to RAFT aqueous dispersion polymerisation, as judged by both visual inspection and dynamic light scattering (DLS), see **Figure 5.6d**. According to Blanazs and co-workers, unreacted HPMA migrates into the micelle cores, increasing the local monomer concentration and hence leading to a faster rate of polymerisation.[75]

A similar rate enhancement is also observed when HPMA is partially replaced by GlyMA (see **Figure 5.6b** and **c**). However, in this case the water-immiscible GlyMA comonomer is consumed *via* aqueous *emulsion* polymerisation. ^{1}H NMR studies indicate significantly faster initial consumption of GlyMA compared to HPMA. For example in the case of $PGMA_{56}$-P($HPMA_{115}$-*stat*-$GlyMA_{29}$), 13 % GlyMA was consumed after 10 min whereas only 5 % HPMA had reacted on the same time scale. Similar observations have been recently reported by Ratcliffe and co-workers for the RAFT statistical copolymerisation of *water-immiscible* 4-hydroxybutyl methacrylate (HBMA) with *water-miscible* 2-hydroxyethyl methacrylate (HEMA) in aqueous solution.[76] Moreover, similar observations were made in Chapter 4 when a PGMA macro-CTA was chain-extended with a mixture of HPMA and 2-(diisopropylamino)ethyl methacrylate (DPA). In the present study, this situation leads to a GlyMA-enriched (HPMA-depleted) segment of the core-forming block at the junction point with the PGMA stabiliser block. This is important, because it has a significant effect on the physical properties of the resulting worm gel, as discussed in more detail below. Visual inspection of the reaction mixture indicates that a homogeneous solution is obtained within 10 min, which suggests that the remaining GlyMA concentration becomes sufficiently low for the statistical copolymerisation to proceed as an aqueous dispersion polymerisation before micellar nucleation occurs. This is consistent with the temperature-dependent water solubility of GlyMA reported by Ratcliffe and co-workers.[77]

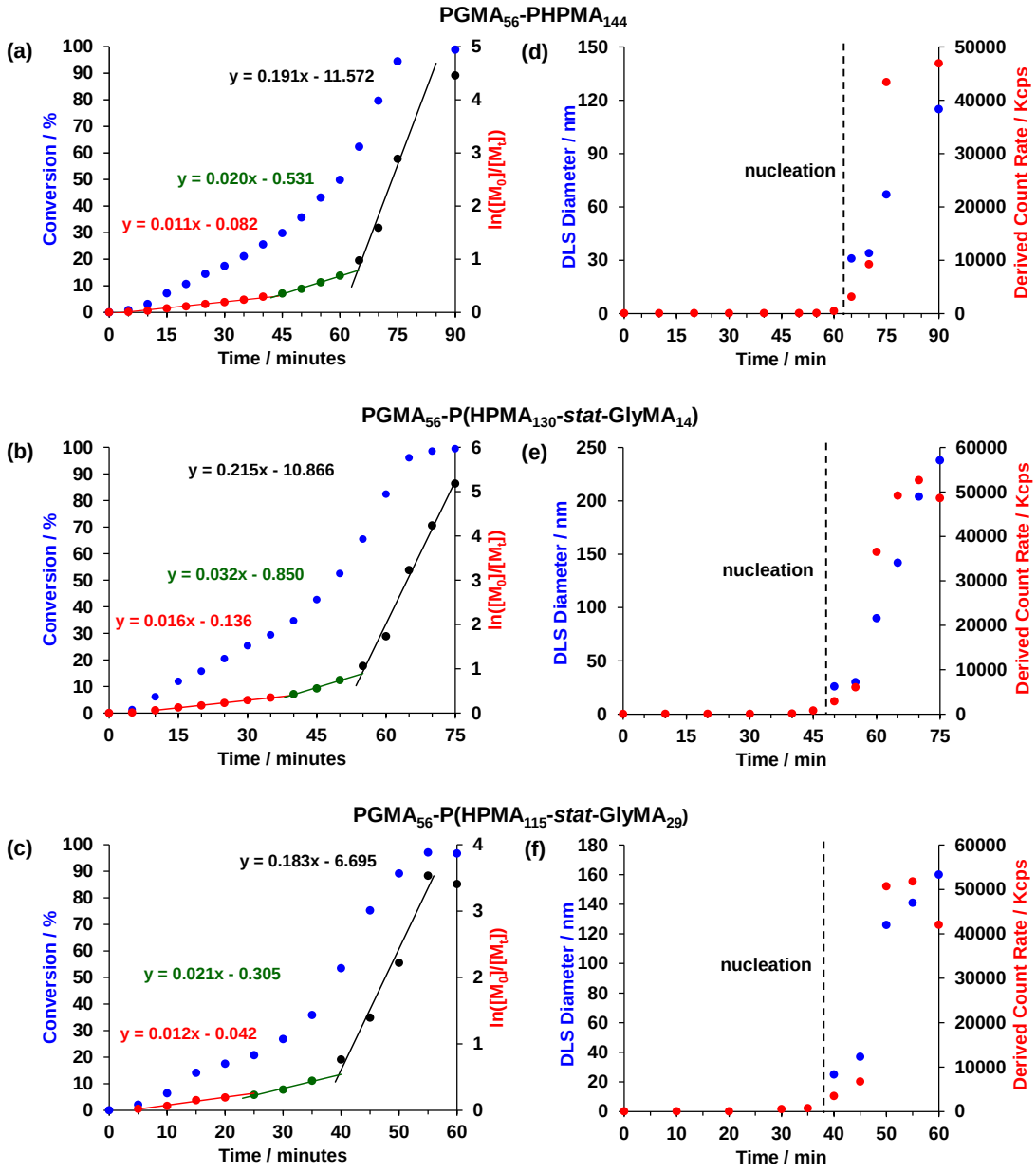

Figure 5.6 Conversion (calculated by ^{1}H NMR) and semi-logarithmic plots versus time for the chain extension of a $PGMA_{56}$ macro-CTA with varying amounts of HPMA and GlyMA at 70 °C and at 15 % w/w solids for (a) $PGMA_{56}$-$PHPMA_{144}$; (b) $PGMA_{56}$-P($HPMA_{130}$-*stat*-$GlyMA_{14}$) and (c) $PGMA_{56}$-P($HPMA_{115}$-*stat*-$GlyMA_{29}$). The DLS diameters and derived count rate versus time for the same diblock copolymers are shown in (d), (e) and (f) respectively. The onset of micellar nucleation (see dashed lines) was arbitrarily judged to be when the derived count rate lifted from the base line (which equated to above 2500 kcps). This time point is in good agreement with the ten-fold rate enhancement indicated by the semi-logarithmic plots. DLS diameters (blue data) are only shown after micellar nucleation.

As expected, partial replacement of HPMA with increasing amounts of GlyMA within the core-forming block induces micellar nucleation at shorter reaction times (see **Figures 5.6e** and **f**). For example, nucleation occurs after approximately 55 min when targeting $PGMA_{56}$-P($HPMA_{130}$-*stat*-$GlyMA_{14}$) but after only 40 min when targeting $PGMA_{56}$-P($HPMA_{115}$-*stat*-$GlyMA_{29}$).

The enhanced rate of copolymerisation achieved under heterogeneous conditions leads to essentially full monomer conversion within relatively short time scales. More specifically, the synthesis of $PGMA_{56}$-P($HPMA_{130}$-*stat*-$GlyMA_{14}$) was complete after 75 min, while more than 99 % conversion was observed for $PGMA_{56}$-P($HPMA_{115}$-*stat*-$GlyMA_{29}$) after only 60 min. In view of these kinetic data, it was decided to conduct these diblock copolymer syntheses for 105 min at 50 °C. These conditions were chosen to ensure very high (> 99 %) comonomer conversions while minimising loss of pendent epoxide groups to side reactions, as discussed above.

At the end of each copolymerisation, each of the five $PGMA_{56}$-P($HPMA_y$-*stat*-$GlyMA_z$) diblock copolymer dispersions were immediately diluted to 7.5 % w/w solids to aid efficient mixing of the APTES cross-linker. Once fully dispersed, these 7.5 % w/w dispersions were split into two batches. The first batch was used to determine the physical properties of the linear worms obtained prior to cross-linking, while the second batch was used to examine worm core cross-linking with APTES. DMF GPC analysis of these five diblock copolymers prior to addition of the APTES cross-linker suggested minimal intrinsic cross-linking occurred during their synthesis, since no high molecular weight shoulder was observed at shorter retention times (see **Figure 5.7**). This was not unexpected, since the reaction of epoxy groups with the (mainly) secondary hydroxyl groups on the HPMA residues should be negligible at 50 °C. Furthermore, these GPC studies indicated relatively high blocking efficiencies, narrow molecular weight distributions and similar number-average molecular weights (M_n) for all five diblock copolymers. In striking contrast, DMF GPC analysis of $PGMA_{55}$-P($HPMA_{247}$-*stat*-$GlyMA_{82}$) *vesicles* prepared at 70 °C for 4 h performed by Chambon *et al*. indicated relatively high polydispersities and a prominent high molecular weight shoulder.[63] This suggests that epoxide-based cross-linking occurs when such statistical copolymerisations are conducted over

longer reaction times at elevated temperatures, although in principle differences in the levels of dimethacrylate impurity in the HPMA comonomer could be an alternative explanation.[59,75]

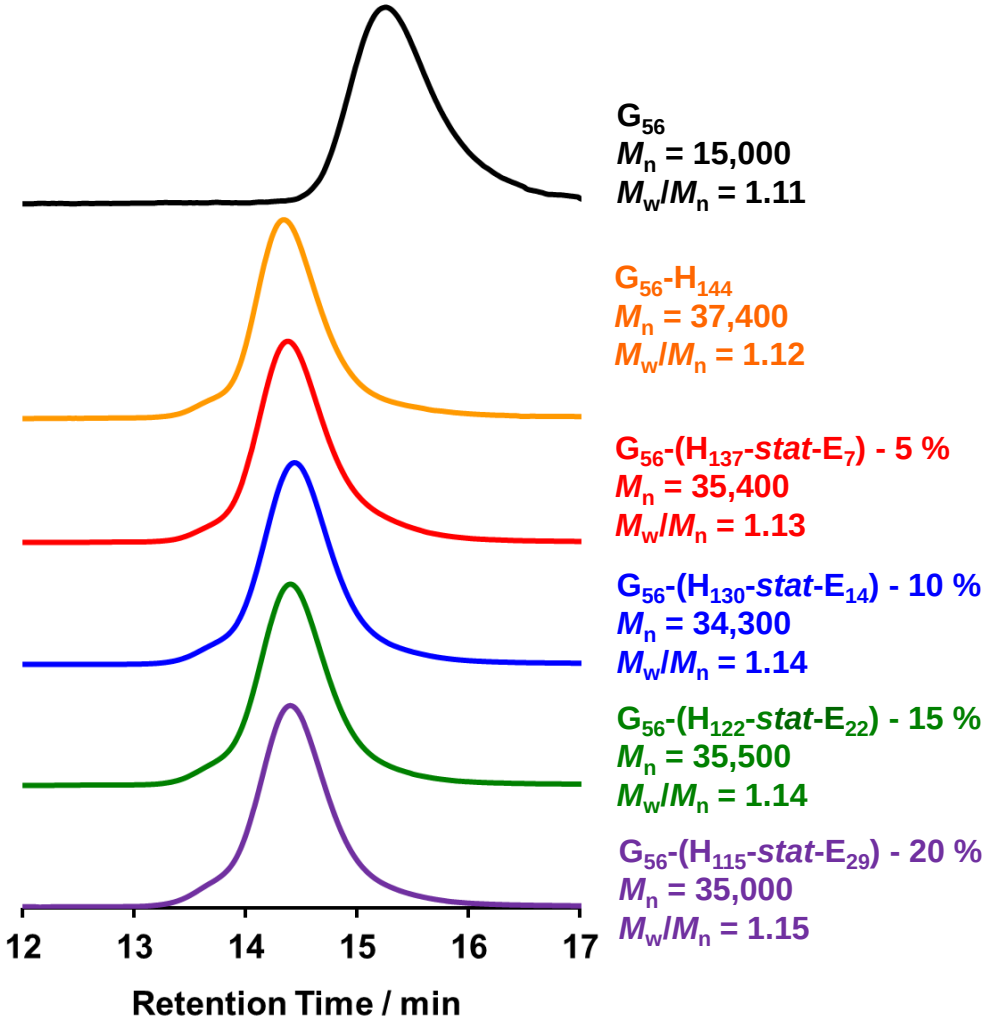

Figure 5.7 DMF GPC curves obtained for $PGMA_{56}$ macro-CTA (black curve) and the corresponding traces for four $PGMA_{56}$-P($HPMA_y$-*stat*-$GlyMA_z$) (where y + z = 144; these copolymers are denoted as G_{56}-(H_y-*stat*-E_z) for brevity) diblock copolymers prepared at 50 °C. Molecular weights are expressed relative to a series of near monodisperse poly(methyl methacrylate) calibration standards.

DLS and transmission electron microscopy (TEM) studies were conducted on dilute (0.1 % w/w) dispersions of the five diblock copolymer worms prior to cross-linking in order to assess their colloidal stability in both water and methanol. DLS

studies of dilute aqueous dispersions indicate that these worms possessed sphere-equivalent hydrodynamic diameters of 100 to 210 nm and relatively high polydispersities (> 0.20), which compares well with literature data reported for such nano-objects.[14,73] Moreover, relatively intense light scattering (derived count rates exceeding 30,000 kcps) were recorded in all cases, which is consistent with the presence of nano-objects (see **Table 5.1**). TEM images obtained for dried aqueous copolymer dispersions confirmed the presence of highly anisotropic worms in all cases (see **Figure 5.8**). In contrast, TEM studies of the same diblock copolymer dispersions diluted using methanol prior to drying confirmed the absence of any well-defined nano-objects (see **Figure 5.9**) while only very weak light scattering (< 300 kcps) was observed by DLS. Both observations are consistent with *molecular dissolution* of copolymer chains in methanol, which is a good solvent for both blocks.[72,78]

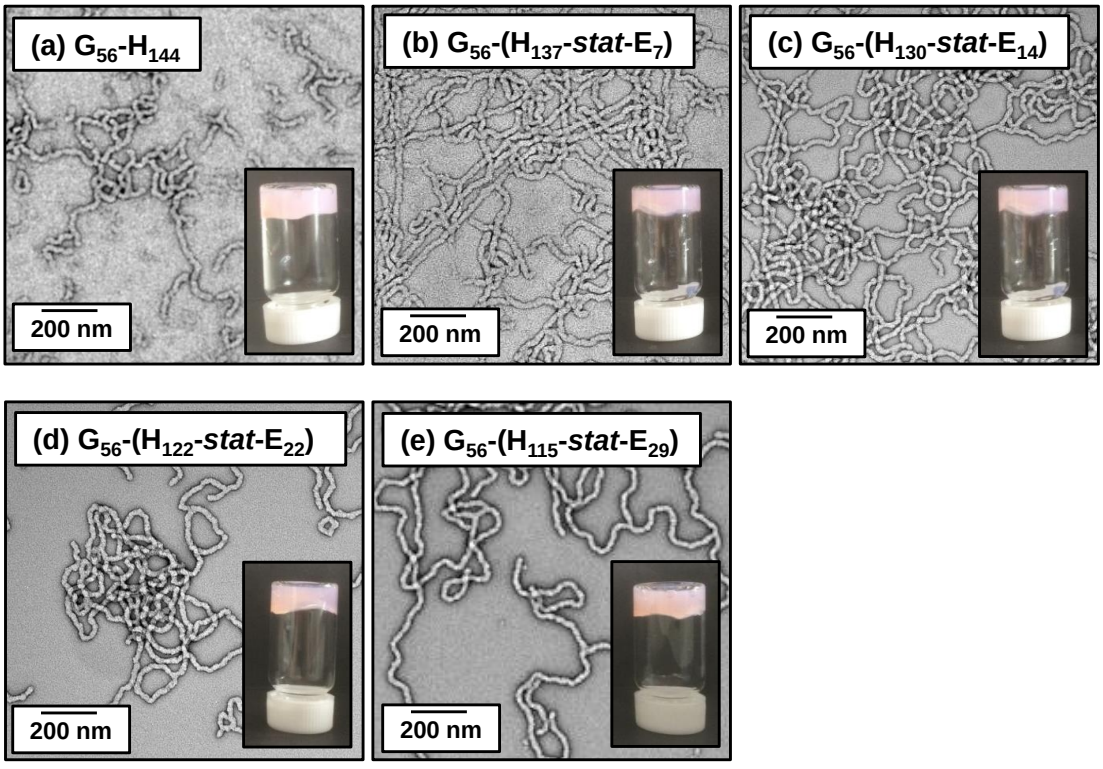

Figure 5.8 Representative TEM images obtained for dried 0.1 % w/w aqueous dispersions of $PGMA_{56}$-P($HPMA_y$-*stat*-$GlyMA_z$) linear diblock copolymers prior to cross-linking (where y + z = 144; these copolymers are denoted as G_{56}-(H_y-*stat*-E_z) for brevity). Digital photographic images of the corresponding free-standing gels recorded at 7.5 % w/w solids are shown as insets.

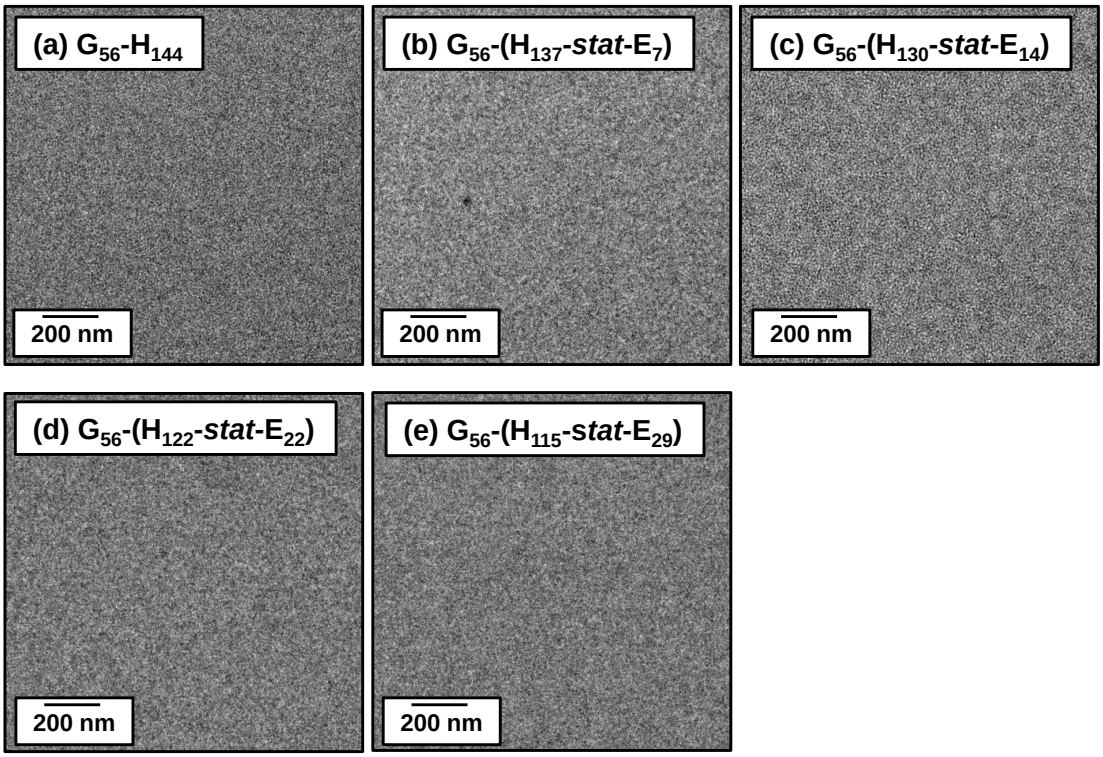

Figure 5.9 Representative TEM images obtained for $PGMA_{56}$-P($HPMA_y$-*stat*-$GlyMA_z$) diblock copolymers after dilution to 0.1 % w/w in methanol prior to cross-linking (where y + z = 144; these copolymers are denoted as G_{56}-(H_y-*stat*-E_z) for brevity). These featureless images confirm molecular dissolution of the copolymer chains under these conditions.

As discussed in previous Chapters, PGMA-PHPMA diblock copolymer worm gels undergo degelation on cooling to 5 °C.[14,36] TEM studies confirmed that this is the result of a worm-to-sphere order-order morphological transition. Similar temperature-dependent rheological studies were conducted on these gels. Before these studies were carried out, a strain sweep was conducted at 25 °C on the 5 worm gels prior to cross-linking at a fixed angular frequency of 1.0 rad s^{-1} to ensure the rheological conditions were in the linear viscoelastic regime (see Appendix for data). From this it was decided to conduct all subsequent rheological experiments at a fixed strain of 1.0 % and a fixed angular frequency of 1.0 rad s^{-1}. As expected, the linear $PGMA_{56}$-$PHPMA_{144}$ diblock copolymer worm gel prepared in this study is similarly thermo-responsive. Its critical gelation temperature (CGT) was determined to be 13 °C on cooling to 5 °C, as judged by the point of cross-over of the storage modulus (G') and loss modulus (G") curves in temperature dependent rheological studies (see

Figure 5.10a). $PGMA_{56}$-P($HPMA_y$-*stat*-$GlyMA_z$) diblock copolymer worm gels possess similar thermo-responsive degelation when up to 15 mol % GlyMA (z = 22) is incorporated into the core-forming block, as judged by rheology (see **Figure 5.10d-e**). However, increasing the GlyMA content suppresses the thermo-responsive behaviour of the diblock copolymer worm gels, with lower CGTs being observed. In contrast, $PGMA_{56}$-P($HPMA_{115}$-*stat*-$GlyMA_{29}$) diblock copolymer worms exhibit no thermo-responsive behaviour under the same rheological conditions (**Figure 5.10e**). As previously discussed, GlyMA is consumed faster than HPMA during the RAFT statistical copolymerisation of these two comonomers. This results in a GlyMA-enriched block junction. However, as GlyMA residues are more hydrophobic than HPMA residues, progressively lower temperatures are required for the surface plasticisation necessary to induce a worm-to-sphere transition (and hence degelation). This is shown by a systematic decrease in the CGT from 13 °C to 6 °C as the GlyMA content in the core is increased from 0 to 15 mol % (similar to observations made in Chapter 4). Furthermore, more pronounced hysteresis is observed on returning to 25 °C.

These rheological studies also indicate a reduction in storage modulus (G') from 86 Pa to 11 Pa at 25 °C on increasing the GlyMA content in the core-forming block from 0 mol % to 20 mol %. Rheological studies of $PGMA_{54}$-$PHPMA_y$ diblock copolymer worms reported by Verber and co-workers for a range of y values indicate that block compositions closer to the worm/sphere phase boundary form weaker gels.[36] Thus it seems likely that incorporating more GlyMA into the core-forming statistical block shifts the worm morphology towards this phase boundary.

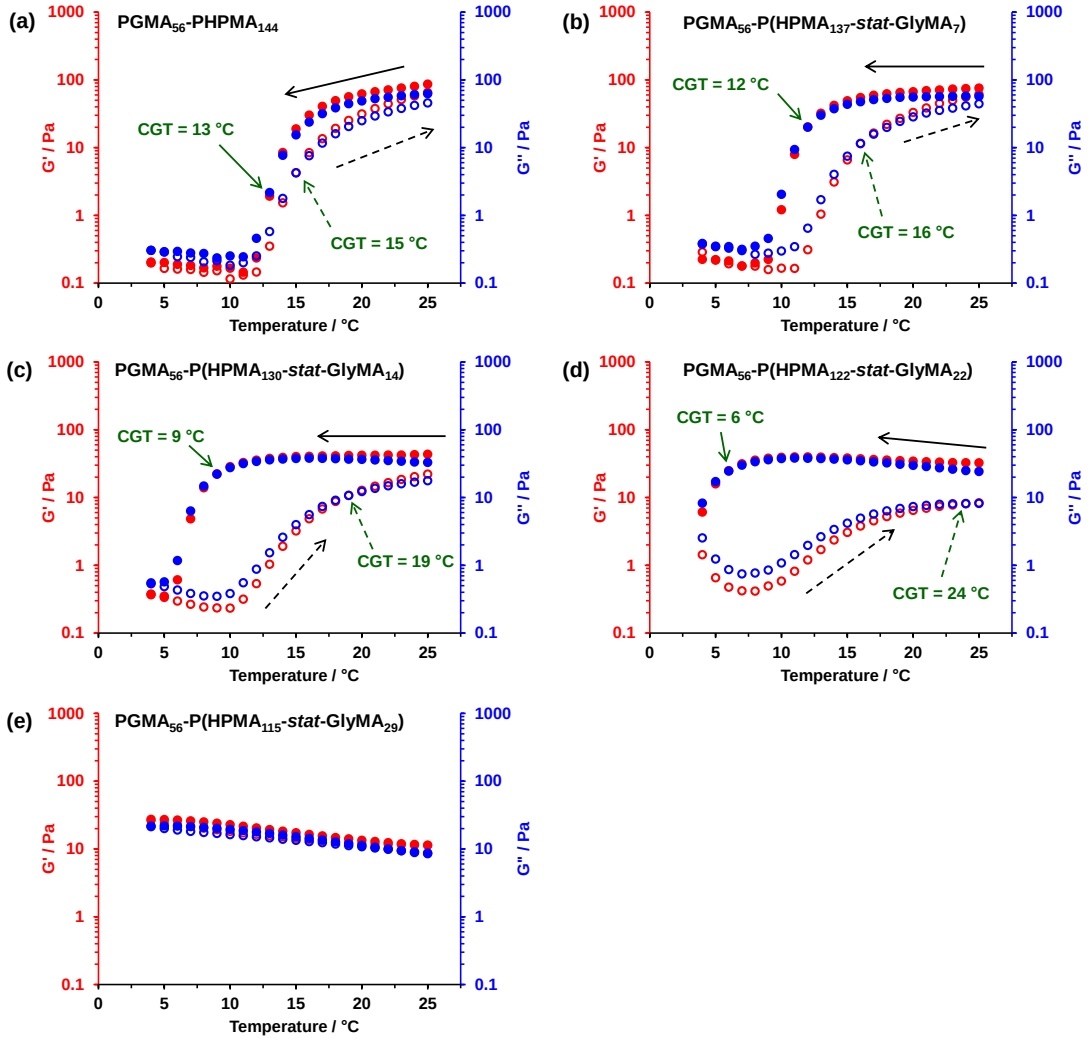

Figure 5.10 Variation of the storage modulus (G', red data set) and the loss modulus (G", blue data set) as a function of temperature. for a 7.5 % w/w aqueous dispersion of (a) $PGMA_{56}$-$PHPMA_{144}$; (b) $PGMA_{56}$-P($HPMA_{137}$-*stat*-$GlyMA_7$), (c) $PGMA_{56}$-P($HPMA_{130}$-*stat*-$GlyMA_{14}$), (d) $PGMA_{56}$-P($HPMA_{122}$-*stat*-$GlyMA_{22}$) and (e) $PGMA_{56}$-P($HPMA_{115}$-*stat*-$GlyMA_{29}$) worms before cross-linking. Closed circles denote a 25 °C to 5 °C temperature sweep and open circles denote a 5 °C to 25 °C temperature sweep. Conditions: angular frequency = 1.0 rad s^{-1}; applied strain = 1.0 %; and rate of cooling/heating = 0.5 °C min^{-1}.

	Before cross-linking				After cross-linking					
	Water		Methanol		Water		Methanol		SDS	
Copolymer composition	**Diameter / nm (PDI)**	**Derived Count Rate / Kcps**	**Diameter / nm (PDI)**	**Derived Count Rate / Kcps**	**Diameter / nm (PDI)**	**Derived Count Rate / Kcps**	**Diameter / nm (PDI)**	**Derived Count Rate / Kcps**	**Diameter / nm (PDI)**	**Derived Count Rate / Kcps**
G_{56}-H_{144}	102 (0.184)	47,000	9 (0.216)	140	n.d	n.d	n.d	n.d	n.d	n.d
G_{56}-(H_{137}-*stat*-E_7)	150 (0.210)	56,300	38 (0.252)	250	152 (0.272)	22,400	66 (0.169)	3,600	48 (0.281)	5,740
G_{56}-(H_{130}-*stat*-E_{14})	122 (0.206)	51,400	14 (0.246)	280	172 (0.345)	36,300	266 (0.411)	24,400	200 (0.255)	31,700
G_{56}-(H_{122}-*stat*-E_{22})	128 (0.238)	39,200	13 (0.354)	210	235 (0.404)	32,800	251 (0.295)	30,300	231 (0.269)	32,300
G_{56}-(H_{115}-*stat*-E_{29})	203 (0.286)	41,500	61 (0.212)	210	200 (0.412)	28,900	220 (0.242)	40,500	173 (0.238)	34,000

Table 5.1 Summary of dynamic light scattering (DLS) data obtained both before and after APTES cross-linking for $PGMA_{56}$-$P(HPMA_y$-*stat*-$GlyMA_z)$ diblock copolymers (where y + z = 144; these copolymers are denoted as G_{56}-(H_y-*stat*-E_z) for brevity) in pure water, methanol and in a 1.0 % w/w aqueous SDS solution.

5.3.2 Post-polymerisation cross-linking of PGMA-P(HPMA-*stat*-GlyMA) diblock copolymer worms

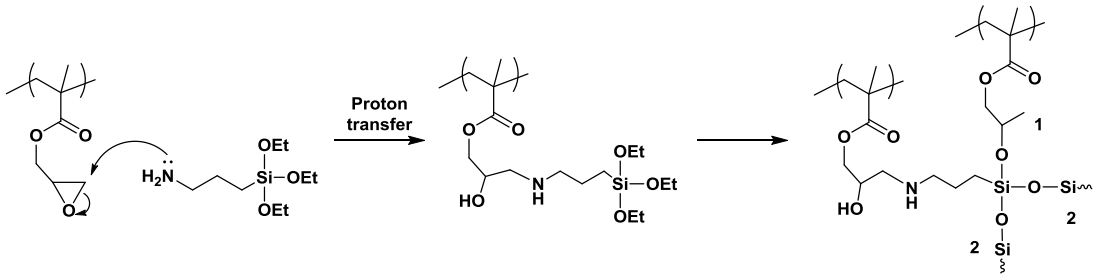

Figure 5.11 Reaction scheme illustrating worm core cross-linking chemistry by (i) epoxy ring-opening *via* nucleophilic attack with APTES and (ii) intermolecular cross-linking *via* hydrolysis-condensation. The latter step involves either reaction of the APTES with hydroxyl groups on HPMA residues on another copolymer chain (denoted as **1**) and/or condensation with other APTES groups (denoted as **2**). In reality, ^{1}H NMR studies indicate that these two steps occur more or less simultaneously, rather than consecutively as shown (see main text for details). Moreover, the chemistry is likely to be more complex than that shown as the secondary amine species may react further.

On reaching full conversion, the aqueous worm gels were immediately diluted from 15 % w/w to 7.5 % w/w to lower the gel viscosity. Once a homogeneous dispersion was achieved, APTES was added (APTES: GlyMA molar ratio = 1.0) and the shear-thinning gel was stirred overnight at 20 °C. As discussed earlier, the primary amine of the APTES reacts with the pendent epoxide groups in the GlyMA residues while the siloxane groups undergo multiple hydrolysis-condensation reactions that lead to highly cross-linked worm cores (see **Figure 5.11**). In reality, cross-linking is likely be even more complex, because the secondary amines formed *via* ring-opening of the epoxide group can in principle react with a second epoxide. One interesting question here is the following: to what extent does the time scale for the epoxy-amine reaction differ from that of the hydrolysis-condensation reactions? To address this point, the rate of reaction of APTES with the epoxide groups and the rate of hydrolysis-condensation for the $PGMA_{56}$-$P(HPMA_{115}$-*stat*-$GlyMA_{29})$ diblock copolymer worms was monitored by ^{1}H NMR using d_4-sodium trimethylsilyl propanoate (TMSP) as an internal standard (see **Figure 5.12**). Aliquots of the aqueous reaction mixture were extracted at regular

intervals and diluted using CD_3OD prior to NMR analysis. This choice of diluent enables chemical changes in the core-forming block to be monitored up to relatively high degrees of cross-linking. The rate of ring-opening by the nucleophilic APTES was determined by monitoring the disappearance of the characteristic epoxy proton signals at 3.0 ppm in the ^{1}H NMR spectra relative to the internal standard (see blue data set shown in **Figure 5.12c** and for the corresponding ^{1}H NMR spectra see **Figure 5.12a**). The integrated epoxy signal is reduced to 6 % of its original value after 8 h (and to just 3 % after 24 h). As the hydrolysis-condensation reaction proceeds, the chemical cross-links lead to worm core *swelling* in CD_3OD, rather than worm *dissolution*. At higher degrees of cross-linking, the worm cores become solid-like and hence no longer solvated by the CD_3OD, thus signals associated with the P(HPMA-*stat*-GlyMA) core-forming block gradually become undetectable by ^{1}H NMR. This can be used to infer the relative degree of cross-linking by determining either the normalised reduction in the methyl group signal assigned to the methacrylic backbone at 0.9 ppm (green data set in **Figure 5.12**), or that of the pendent methyl group assigned to the HPMA residues at 1.2 ppm (see red data set in **Figure 5.12c** and for the corresponding ^{1}H NMR traces see **Figure 5.12b**). However, the latter method is preferred, because in the former method data analysis is made more complicated by overlapping backbone methyl group signals arising from the PGMA stabiliser block, which remains soluble (and hence detectable) even after core cross-linking is complete. Perhaps surprisingly, the data shown in **Figure 5.12** indicates that the relative integral of the HPMA methyl signal is reduced *at approximately the same rate* as that of the epoxy signals. This indicates that ring-opening of the epoxide groups and the hydrolysis-condensation cross-linking reactions occur more or less simultaneously. However, the precise degree of cross-linking cannot be calculated because further cross-linking may occur that is no longer detectable by ^{1}H NMR. It is perhaps noteworthy that the reaction times shown in **Figure 5.12** correspond to the times at which each aliquot was taken from the reaction mixture – it does not include the time taken to run each ^{1}H NMR spectrum. Diluting each aliquot with an equal volume of CD_3OD may not adequately quench the reaction, so it was important to analyse each aliquot as soon as possible in order to minimise this 'dead time' (in practice, the time required for instrument set-up and

spectrum acquisition was around 15 min for each sample). Notwithstanding such minor time domain errors, this spectroscopic study confirmed that an approximate time scale of 24 h is required for extensive cross-linking of each of the four GlyMA-containing diblock copolymer worms at 20 °C under the stated conditions.

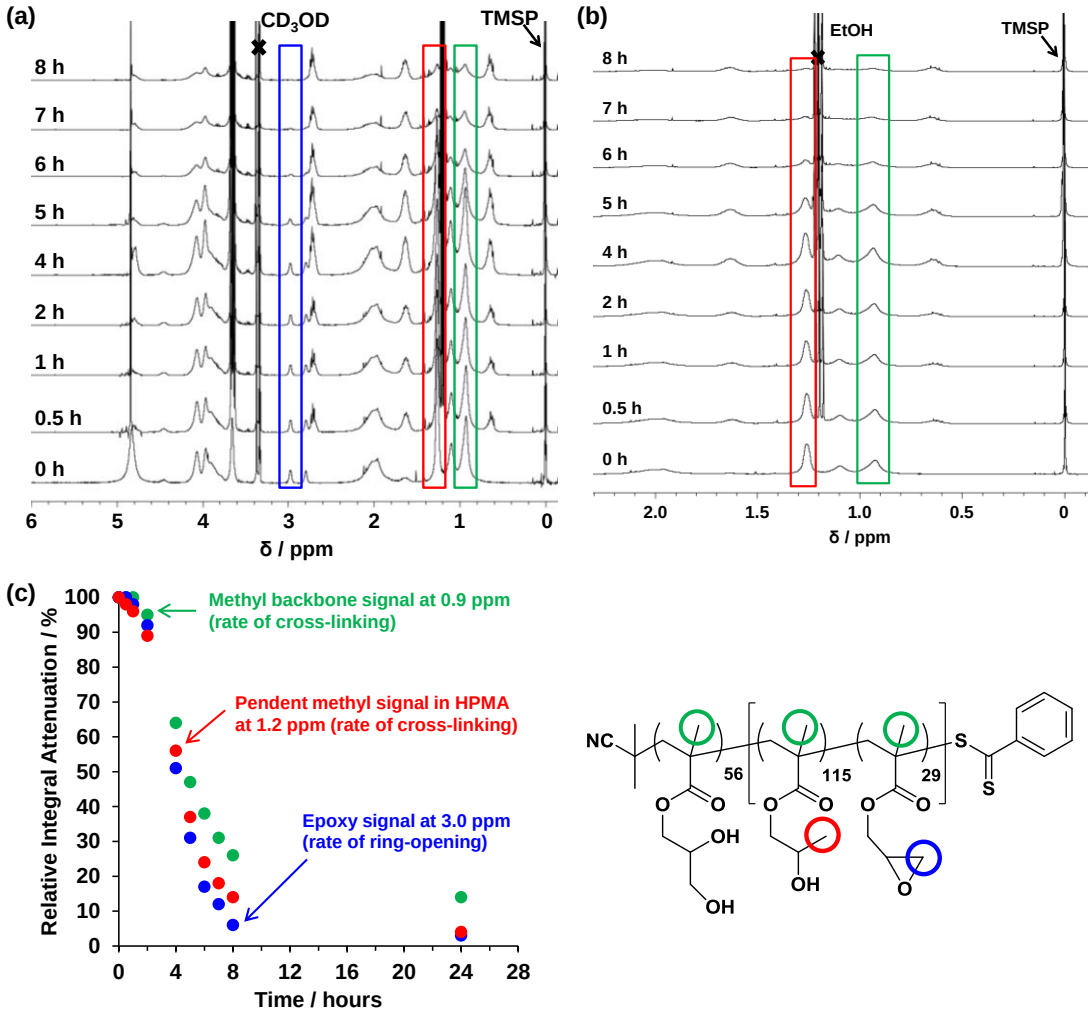

Figure 5.12 (a) and (b) ^{1}H NMR spectra obtained at various time points following the reaction of APTES with PGMA$_{56}$-P(HPMA$_{115}$-*stat*-GlyMA$_{29}$) after dilution into CD_3OD. (c) Kinetics of the ring-opening epoxy-amine reaction (blue data set) as judged by the attenuation in the relative integral of the epoxide signal at 3.0 ppm compared to an internal standard by ^{1}H NMR spectroscopy. Kinetics of worm core cross-linking as judged by the relative attenuation in the signal at 1.2 ppm assigned to the pendent methyl group in HPMA residues (red data set) and the relative attenuation in the integrated methyl signal at 0.9 ppm assigned to the methacrylate backbone (green data set) compared to the same internal standard at 0.0 ppm.

In principle, core cross-linking should prevent worm dissolution on dilution in methanol (which is a good solvent for both blocks). DLS studies conducted on 0.1 % w/w aqueous worm dispersions (see **Table 5.1**) indicates that cross-linking causes a significant increase in the apparent hydrodynamic diameters [from 122 nm to 172 nm for the $PGMA_{56}$-P($HPMA_{130}$-*stat*-$GlyMA_{14}$) worms and from 128 nm to 235 nm for $PGMA_{56}$-P($HPMA_{122}$-*stat*-$GlyMA_{22}$) worms]. However, it is emphasised that only *sphere-equivalent dimeters* are reported by DLS, so it is difficult to interpret such observations in terms of changes in either worm contour lengths or worm widths. Moreover, this apparent increase in particle dimensions could in principle simply be a result of some degree of inter-particle cross-linking. Nevertheless, TEM images obtained for the four core cross-linked diblock copolymer worms containing 5, 10, 15 or 20 mol % GlyMA (see **Figure 5.13**) after dilution to 0.1 % w/w aqueous dispersions do not indicate any discernible change in the original worm morphology. Furthermore, all four core cross-linked worm dispersions still form free-standing gels at 7.5 % w/w solids, as judged by a tube inversion test (see **Figure 5.13**).

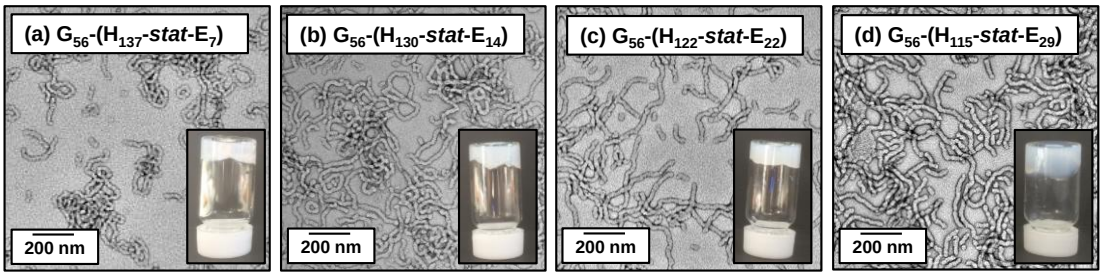

Figure 5.13 Representative TEM images obtained for dried 0.1 % w/w aqueous dispersions of $PGMA_{56}$-P($HPMA_y$-*stat*-$GlyMA_z$) diblock copolymers after APTES cross-linking of 7.5 % w/w worm dispersions at 20 °C. Inset digital photographic images recorded for the same aqueous copolymer dispersions at 7.5 % w/w solids; free-standing gels are observed in each case. These copolymers are denoted as G_{56}-(H_y-*stat*-E_z) for brevity

DLS studies conducted on the same four worm dispersions after dilution to 0.1 % w/w in methanol suggest that only worms comprising at least 10 mol % GlyMA are fully resistant to the presence of methanol (see **Table 5.1**). In contrast, the $PGMA_{56}$-P($HPMA_{137}$-*stat*-$GlyMA_7$) diblock copolymer (5 mol % GlyMA) shows a dramatic reduction in apparent hydrodynamic diameter from 152 nm in water to 66

nm in methanol, with a relatively low derived count rate (3,600 kcps) being observed in the latter solvent. This suggests that the worms undergo a morphological transition to spheres and/or short worms. However, TEM images obtained (see **Figure 5.14a**) for this latter diblock copolymer dried as a 0.1 % w/w dispersion in methanol suggest that no well-defined particles are present (i.e., worm dissolution most likely occurs under these conditions). Indeed, ^{1}H NMR studies of this copolymer in CD_3OD confirm a strong signal at around 1.25 ppm corresponding to the pendent methyl groups on the HPMA residues (see **Figure 5.15**). In contrast, DLS studies of the other three diblock copolymer worms (containing 10, 15 or 20 mol % GlyMA) in methanol indicate a much higher derived count rate of at least 22,000 kcps (see **Table 5.1**). Moreover, these diblock copolymer worms exhibit an increase in hydrodynamic diameter when dispersed in methanol as opposed to water. This is the result of *swelling* of the cross-linked worm cores because methanol is a good solvent for both blocks, but the degree of cross-linking is sufficiently high to prevent worm *dissolution*. TEM images obtained for $PGMA_{56}$-P($HPMA_{130}$-*stat*-$GlyMA_{14}$), $PGMA_{56}$-P($HPMA_{122}$-*stat*-$GlyMA_{22}$) and $PGMA_{56}$-P($HPMA_{115}$-*stat*-$GlyMA_{29}$) diblock copolymers dried from 0.1 % w/w methanolic dispersions confirmed the persistence of the pure worm morphology in each case (**Figure 5.14b-d**).

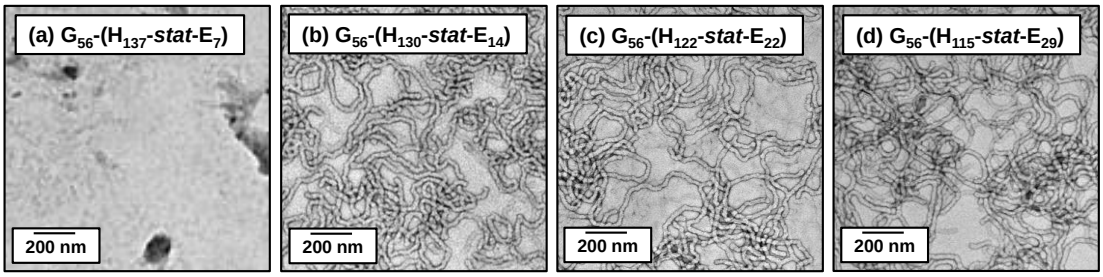

Figure 5.14 Representative TEM images obtained for core cross-linked $PGMA_{56}$-P($HPMA_y$-*stat*-$GlyMA_z$) diblock copolymers (abbreviated to G_{56}-(H_y-*stat*-E_z) for the sake of brevity) after drying 0.1 % w/w methanolic dispersions at 20 °C. (a) No well-defined nano-objects were observed at 5 mol % GlyMA, whereas the original worm morphology persists when core cross-linked worms contain higher proportions of GlyMA, see (b), (c) and (d).

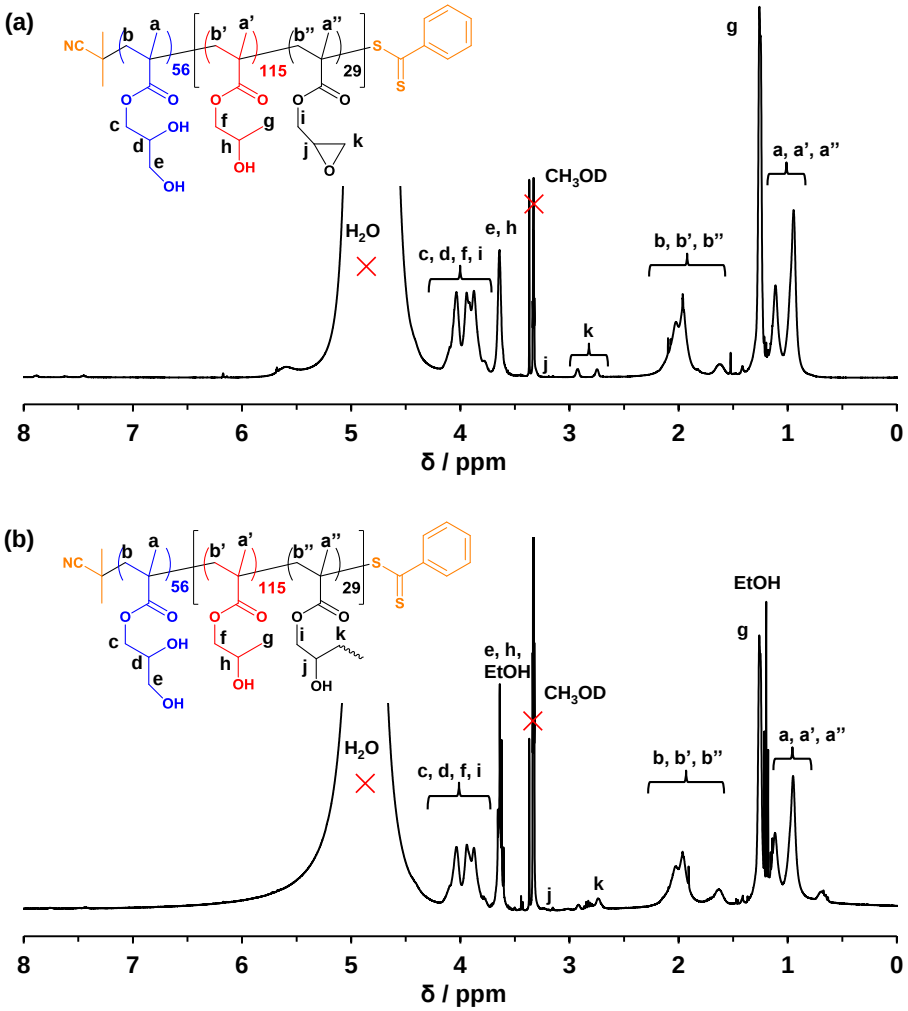

Figure 5.15 ^{1}H NMR spectra recorded in deuterated methanol for 10 % w/w $PGMA_{56}$-P($HPMA_{137}$-*stat*-$GlyMA_{7}$) diblock copolymer (a) before and (b) after APTES treatment. Note that the ethanol signals in the latter arise due its release from APTES during the hydrolysis-condensation reaction.

When APTES is reacted with the epoxy groups on the GlyMA residues, a secondary amine is generated (see **Figure 5.11**). Thus the resulting core cross-linked worms might be expected to possess weakly cationic character below neutral pH (where the secondary amine groups become protonated). In a control experiment, aqueous electrophoresis studies conducted on a 0.1 % w/w aqueous dispersion of linear $PGMA_{56}$-$PHPMA_{144}$ diblock copolymer worms indicated no cationic character from pH 10 to 3 (see **Figure 5.16**). In contrast, APTES-cross-linked $PGMA_{56}$-P($HPMA_{y}$-*stat*-$GlyMA_{z}$) diblock copolymer worms displayed cationic character below pH 7-9 (see Figure 10). However, these particles exhibit only relatively weak

cationic character (+5 to +10 mV) at pH 5. In contrast, Penfold *et al.* have recently reported that linear $PGMA_{50}$-$PHPMA_{140}$ worms prepared using a morpholine-based RAFT agent exhibit zeta potentials of around +15 mV, even though there is only one terminal morpholine group per stabiliser block in this case.[79] This discrepancy most likely arises because the cationic charge is located within the cores of the cross-linked worms in the present study, rather than in the stabiliser block.

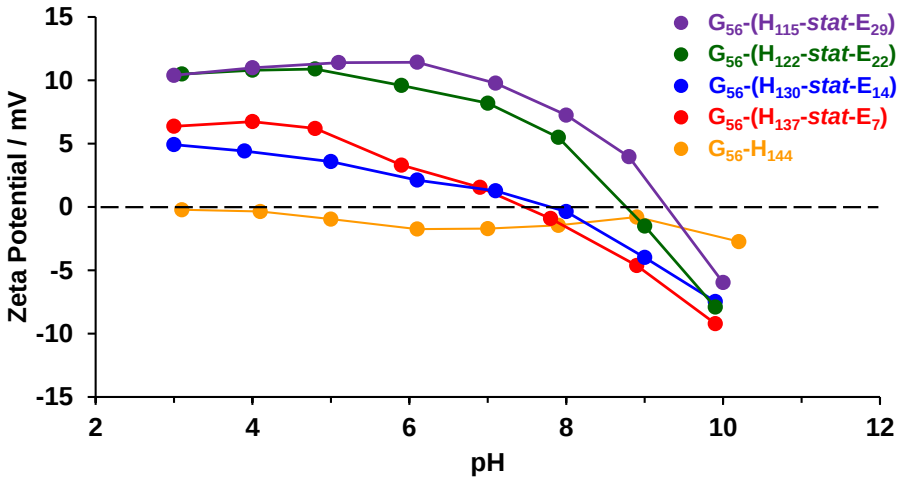

Figure 5.16 Zeta potential versus pH curves obtained at 25 °C for 0.1 % w/w aqueous dispersions of $PGMA_{56}$-$PHPMA_{144}$ diblock copolymer worms and APTES cross-linked $PGMA_{56}$-P($HPMA_y$-*stat*-$GlyMA_z$) diblock copolymer worms in the presence of 10^{-3} M KCl.

It is noteworthy that the characteristic pink colour of the worm gels that arises from the dithiobenzoate-based RAFT CTA is removed during the APTES cross-linking reaction (see **Figure 5.13**). This is the result of nucleophilic attack on the dithioester by the strongly basic primary amine groups (after APTES addition, the solution pH increases to pH 9-10).[80,81] However, as the dithioester chain-ends are located *within* the worm cores, this side reaction is unlikely to adversely affect the physical properties of these copolymer worm dispersions.

Cross-linking also causes the $PGMA_{56}$-P($HPMA_y$-*stat*-$GlyMA_z$) diblock copolymer worms to form stiffer gels, as judged by comparing the storage moduli (G') of 7.5 % w/w worm gels before and after cross-linking by oscillatory rheology (see **Table 5.2**). For example, cross-linking the $PGMA_{56}$-P($HPMA_{130}$-*stat*-$GlyMA_{14}$)

worms leads to an increase in G' from 43 Pa to 81 Pa at 25 °C (see **Figure 5.17**). Previous work by Bates and co-workers suggest that this is due to worm stiffening, which leads to a longer worm persistence length.[7] Moreover, temperature-dependent rheological studies indicate that the degelation that is observed on cooling *linear* diblock copolymer worm gels no longer occurs after worm core cross-linking (see **Figure 5.17**). Clearly, covalent stabilisation of the $PGMA_{56}$-P($HPMA_y$-*stat*-$GlyMA_z$) worms prevents their dissociation into spheres at around 5 °C. Moreover, even the relatively lightly cross-linked $PGMA_{56}$-P($HPMA_{137}$-*stat*-$GlyMA_7$) worm gel is no longer thermo-responsive (see **Figure 5.17a**), although DLS and TEM studies indicate that the same APTES-treated worms undergo dissolution when diluted in methanol (see **Table 5.1**).

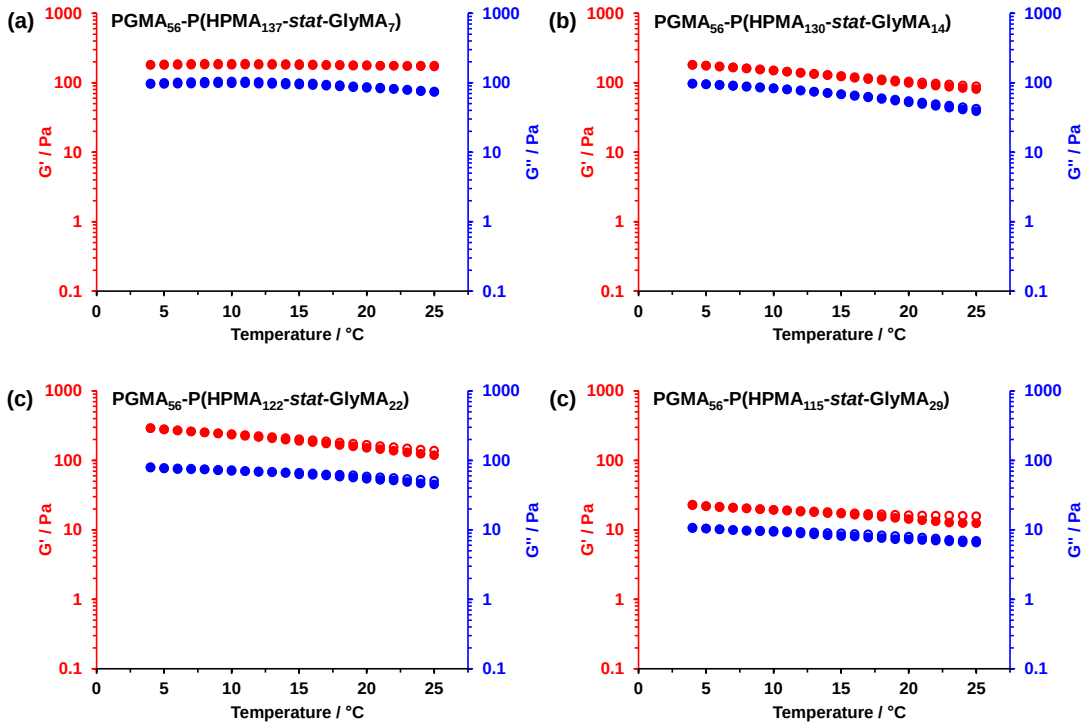

Figure 5.17 Variation in storage modulus (G'; red circles) and loss modulus (G"; blue circles) as a function of temperature for 7.5 % w/w aqueous dispersions of: (a) $PGMA_{56}$-P($HPMA_{137}$-*stat*-$GlyMA_7$), (b) $PGMA_{56}$-P($HPMA_{130}$-*stat*-$GlyMA_{14}$), (c) $PGMA_{56}$-P($HPMA_{122}$-*stat*-$GlyMA_{22}$) and (d) $PGMA_{56}$-P($HPMA_{115}$-*stat*-$GlyMA_{29}$) after worm core cross-linking using APTES (final solution pH 9-10). Closed circles denote the cooling temperature sweep and open circles denote the heating temperature sweep. Conditions: angular frequency = 1.0 rad s^{-1}; applied strain = 1.0 %; heating/cooling rate = 0.5 °C min^{-1}.

Chambon *et al*. demonstrated that $PGMA_{55}$-$PHPMA_{330}$ diblock copolymer vesicles fully dissociated to form individual copolymer chains when challenged with an anionic surfactant.[63] In contrast, $PGMA_{55}$-P($HPMA_{247}$-*stat*-$GlyMA_{82}$) diblock copolymer vesicles that had been cross-linked using a small molecule (or polymeric) diamine proved to be surfactant-resistant. In principle, similar findings might be expected for the core cross-linked diblock copolymer worms described herein. Thus core cross-linking is potentially useful because the resulting worms may be suitable as viscosity modifiers for various commercial surfactant-based home and personal care formulations. In this study, sodium dodecylsulfate (SDS) was selected to assess the surfactant resistance of the worms, as this amphiphile was previously demonstrated to be particularly disruptive towards diblock copolymer vesicles.[63] The surfactant resistance of all diblock copolymer worms was judged by TEM analysis of 0.1 % w/w copolymer dispersions conducted in the absence and presence of 1.0 % w/w SDS (i.e., a SDS: copolymer mass ratio of 10). As expected, when the linear $PGMA_{56}$-$PHPMA_{144}$ worm gels were subjected to an SDS challenge, there was an immediate reduction in turbidity and DLS studies indicated a relatively low count rate of 260 kcps (see **Table 5.1**), suggesting rapid dissociation to form dissolved copolymer chains. This was corroborated by TEM, since no nano-objects could be observed (see **Figure 5.18a**). Similarly, linear $PGMA_{56}$-P($HPMA_y$-*stat*-$GlyMA_z$) diblock copolymer worms challenged with SDS also undergo immediate dissociation. In all cases no particles could be observed by TEM (**Figure 5.18b-e**).

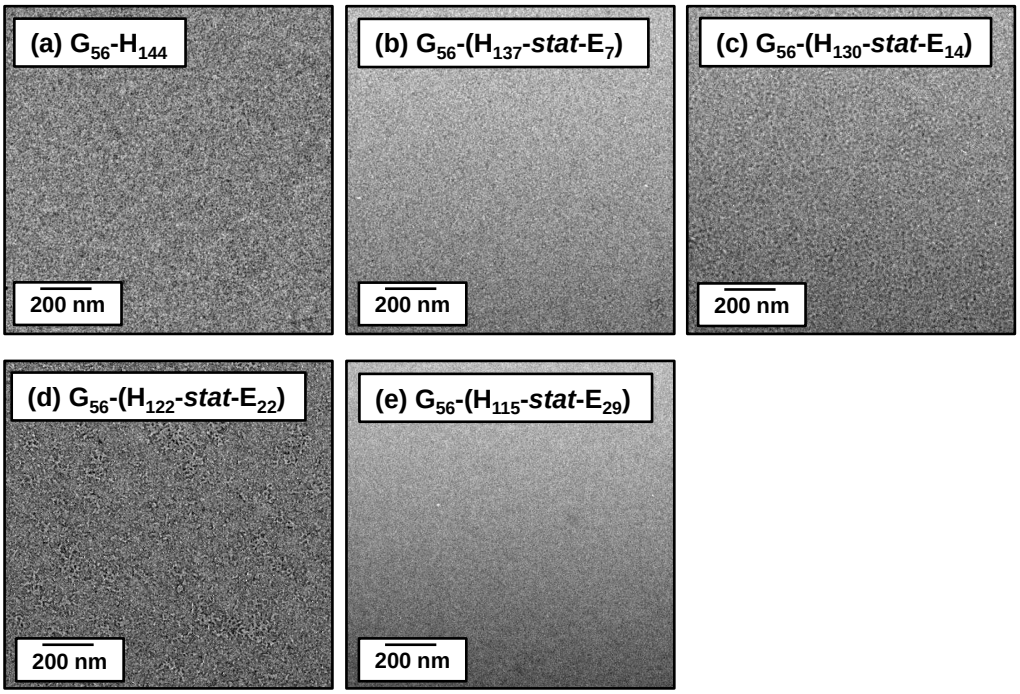

Figure 5.18 Representative TEM images obtained for $PGMA_{56}$-P($HPMA_y$-*stat*-$GlyMA_z$) diblock copolymers after dilution to 0.1 % w/w copolymer in a 1.0 % w/w aqueous SDS solution (1: 10 copolymer: SDS mass ratio) prior to cross-linking (where y + z = 144; these copolymers are denoted as G_{56}-(H_y-*stat*-E_z) for brevity). These featureless images confirm molecular dissolution of the copolymer chains under these conditions.

Interestingly, APTES cross-linked $PGMA_{56}$-P($HPMA_{137}$-*stat*-$GlyMA_7$) worms only exhibit *partial* resistance to this surfactant challenge. Rather than undergoing complete dissolution, a worm-to-sphere transition is instead observed by TEM (see **Figure 5.19a**), while DLS indicated a significant reduction in hydrodynamic diameter from 150 nm to 48 nm in the presence of SDS (see **Table 5.1**). However, on increasing the GlyMA content to 10, 15 or 20 mol % (and therefore the degree of core cross-linking) the worms became completely resistant to the presence of SDS. DLS studies of $PGMA_{56}$-P($HPMA_{130}$-*stat*-$GlyMA_{14}$), $PGMA_{56}$-P($HPMA_{122}$-*stat*-$GlyMA_{22}$) and $PGMA_{56}$-P($HPMA_{115}$-*stat*-$GlyMA_{29}$) diblock copolymer worms in the presence and absence of SDS revealed only minor changes in their apparent sphere-equivalent diameters (see **Table 5.1**). Furthermore, TEM images recorded after drying these diluted 'worm plus surfactant' dispersions

confirm that the original worm morphology is retained over time scales of months in each case (see **Figure 5.19b-d**).

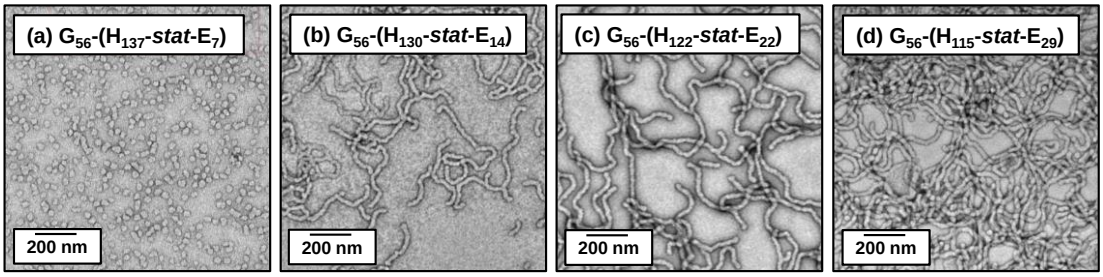

Figure 5.19 Representative TEM images obtained for APTES cross-linked $PGMA_{56}$-P($HPMA_y$-*stat*-$GlyMA_z$) diblock copolymers after dilution to 0.1 % w/w copolymer in a 1.0 % w/w aqueous SDS solution (1: 10 copolymer: SDS mass ratio). Here y + z = 144 and copolymers are denoted as G_{56}-(H_y-*stat*-E_z) for brevity.

The colloidal stability of the five $PGMA_{56}$-P($HPMA_y$-*stat*-$GlyMA_z$) diblock copolymer worms (prepared targeting the same overall mean degree of polymerisation; y + z = 144) before and after cross-linking is summarised in **Table 5.2**. Prior to cross-linking, none of the linear $PGMA_{56}$-P($HPMA_y$-*stat*-$GlyMA_z$) worms remained intact when challenged with either methanol or SDS. However, APTES treatment can significantly improve worm stability towards either reagent. In particular, for worm cores comprising at least 10 mol % GlyMA, TEM and DLS studies confirm that the worm morphology is preserved in the presence of either methanol or 1.0 % w/w aqueous SDS solution. Furthermore, temperature-dependent oscillatory rheology studies demonstrate that worm core cross-linking results in stiffer gels that no longer exhibit thermo-responsive behaviour.

Copolymer composition	Before cross-linking						After cross-linking			
	M_n / g mol^{-1} (a)	M_w/M_n (a)	G' at 25 °C / Pa (b)	Thermo-responsive degelation? (b)	Stable in the presence of methanol? (c)	Stable in the presence of SDS? (d)	G' at 25 °C / Pa (b)	Thermo-responsive degelation? (b)	Stable in the presence of methanol? (c)	Stable in the presence of SDS? (d)
G_{56}-H_{144}	37,400	1.12	86		No	No				
G_{56}-(H_{137}-*stat*-E_7)	35,400	1.13	76	Yes	No	No	170	No	No	Partial
G_{56}-(H_{130}-*stat*-E_{14})	34,300	1.14	43	Yes	No	No	81	No	Yes	Yes
G_{56}-(H_{122}-*stat*-E_{22})	35,500	1.14	32	Yes	No	No	119	No	Yes	Yes
G_{56}-(H_{115}-*stat*-E_{29})	35,000	1.15	11	No	No	No	13	No	Yes	Yes

(a) Calculated using DMF GPC against a series of near-monodisperse PMMA calibration standards.

(b) Determined for 7.5 % w/w copolymer worm gels using oscillatory rheology at an angular frequency of 1.0 rad s^{-1} and an applied strain of 1.0 %

(c) As judged by DLS and TEM studies conducted on $PGMA_{56}$-P($HPMA_y$-*stat*-$GlyMA_z$) diblock copolymer worms diluted to 0.1 % w/w in methanol

(d) As judged by DLS and TEM studies conducted on $PGMA_{56}$-P($HPMA_y$-*stat*-$GlyMA_z$) diblock copolymer worms diluted to 0.1 % w/w in the presence of 1.0 % w/w SDS aqueous solution (i.e., SDS: copolymer mass ratio = 10)

Table 5.2 Summary of data obtained for $PGMA_{56}$-P($HPMA_y$-*stat*-$GlyMA_z$) diblock copolymer worm gels in the presence and absence of methanol or 1.0 % aqueous SDS solution before and after APTES cross-linking at 20 °C.

5.4 Conclusions

In summary, a series of $PGMA_{56}$-P($HPMA_y$-*stat*-$GlyMA_z$) diblock copolymer worm gels have been prepared by PISA in concentrated aqueous solution by targeting a constant core-forming block DP (y + z = 144) in each case. Increasing the GlyMA content in such linear copolymers affords weaker gels, as judged by rheology. ^{1}H NMR studies of the kinetics of statistical copolymerisation of water-immiscible GlyMA with water-miscible HPMA indicate that the former comonomer is more reactive than the latter. Thus the comonomer composition of the core-forming statistical block becomes GlyMA-rich at its junction with the PGMA stabiliser block. This explains why temperature-dependent rheological studies indicate that worms with higher GlyMA contents gradually become less thermo-responsive, with progressively lower temperatures being required to induce surface plasticisation of the worms and hence degelation *via* a worm-to-sphere transition. Ultimately, thermally-induced degelation is no longer observed at a GlyMA content of 20 mol %. Importantly, the epoxide groups in the GlyMA residues can be reacted with APTES *via* epoxy-amine chemistry in aqueous solution, with hydrolysis of this reagent leading to condensation reactions with pendent hydroxyl groups on the HPMA residues and hence the formation of highly cross-linked worm cores. Perhaps surprisingly, ^{1}H NMR studies indicate that the ring-opening and cross-linking reactions occur more or less simultaneously. The cross-linked worms no longer undergo thermally-induced degelation on cooling. TEM studies of dried diluted aqueous worm dispersions confirmed that core cross-linking produced no discernible change in the copolymer morphology. Prior to cross-linking, the linear $PGMA_{56}$-P($HPMA_y$-*stat*-$GlyMA_z$) diblock copolymer worms are unstable with respect to the addition of either methanol (a good solvent for both blocks) or anionic surfactants such as SDS, with complete worm dissociation being observed in all cases, as judged by DLS and TEM. In contrast, the core cross-linked worms remained stable when dispersed in either methanol or in the presence of 1.0 % w/w aqueous SDS solution, provided that the worm cores comprise at least 10 mol % GlyMA. In contrast, core cross-linked worms containing 5 mol % GlyMA exhibit no resistance to methanol and undergo a worm-to-sphere transition in the presence of SDS as judged by TEM.

Finally, it is noteworthy that the cross-linking chemistry described herein (i) utilises cheap commercially available reagents, (ii) can be conveniently conducted at 20 °C in aqueous solution and (iii) produces secondary amine groups within the worm cores, which results in weakly cationic worms below pH 7, as judged by aqueous electrophoresis.

5.5 References

(1) Discher, D. E.; Eisenberg, A. *Science* **2002**, *297*, 967.

(2) Blanazs, A.; Armes, S. P.; Ryan, A. J. *Macromol. Rapid Commun.* **2009**, *30*, 267.

(3) Foerster, S.; Zisenis, M.; Wenz, E.; Antonietti, M. *J. Chem. Phys.* **1996**, *104*, 9956.

(4) Bang, J.; Jain, S.; Li, Z.; Lodge, T. P.; Pedersen, J. S.; Kesselman, E.; Talmon, Y. *Macromolecules* **2006**, *39*, 1199.

(5) Jain, S.; Bates, F. S. *Science* **2003**, *300*, 460.

(6) Wang, X.; Guerin, G.; Wang, H.; Wang, Y.; Manners, I.; Winnik, M. A. *Science* **2007**, *317*, 644.

(7) Won, Y.-Y.; Davis, H. T.; Bates, F. S. *Science* **1999**, *283*, 960.

(8) Cheng, C.; Qi, K.; Germack, D. S.; Khoshdel, E.; Wooley, K. L. *Adv. Mater.* **2007**, *19*, 2830.

(9) Geng, Y.; Dalhaimer, P.; Cai, S.; Tsai, R.; Tewari, M.; Minko, T.; Discher, D. E. *Nat. Nanotechnol.* **2007**, *2*, 249.

(10) Bhargava, P.; Zheng, J. X.; Li, P.; Quirk, R. P.; Harris, F. W.; Cheng, S. Z. D. *Macromolecules* **2006**, *39*, 4880.

(11) Petzetakis, N.; Dove, A. P.; O'Reilly, R. K. *Chem. Sci.* **2011**, *2*, 955.

(12) Dalhaimer, P.; Bates, F. S.; Discher, D. E. *Macromolecules* **2003**, *36*, 6873.

(13) Groschel, A. H.; Walther, A.; Lobling, T. I.; Schacher, F. H.; Schmalz, H.; Muller, A. H. E. *Nature* **2013**, *503*, 247.

(14) Blanazs, A.; Verber, R.; Mykhaylyk, O. O.; Ryan, A. J.; Heath, J. Z.; Douglas, C. W. I.; Armes, S. P. *J. Am. Chem. Soc.* **2012**, *134*, 9741.

(15) Sugihara, S.; Blanazs, A.; Armes, S. P.; Ryan, A. J.; Lewis, A. L. *J. Am. Chem. Soc.* **2011**, *133*, 15707.

(16) Fielding, L. A.; Derry, M. J.; Ladmiral, V.; Rosselgong, J.; Rodrigues, A. M.; Ratcliffe, L. P. D.; Sugihara, S.; Armes, S. P. *Chem. Sci.* **2013**, *4*, 2081.

(17) Jones, E. R.; Semsarilar, M.; Blanazs, A.; Armes, S. P. *Macromolecules* **2012**, *45*, 5091.

(18) Yeow, J.; Xu, J.; Boyer, C. *ACS Macro Lett.* **2015**, *4*, 984.

(19) Pei, Y.; Thurairajah, L.; Sugita, O. R.; Lowe, A. B. *Macromolecules* **2015**, *48*, 236.

(20) Pei, Y. W.; Lowe, A. B. *Polym. Chem.* **2014**, *5*, 2342.

(21) Boisse, S.; Rieger, J.; Belal, K.; Di-Cicco, A.; Beaunier, P.; Li, M.-H.; Charleux, B. *Chem. Commun.* **2010**, *46*, 1950.

(22) Zhang, X.; Boisse, S.; Bui, C.; Albouy, P.-A.; Brulet, A.; Li, M.-H.; Rieger, J.; Charleux, B. *Soft Matter* **2012**, *8*, 1130.

(23) Zhang, X.; Boissé, S.; Zhang, W.; Beaunier, P.; D'Agosto, F.; Rieger, J.; Charleux, B. *Macromolecules* **2011**, *44*, 4149.

(24) Wan, W.-M.; Hong, C.-Y.; Pan, C.-Y. *Chem. Commun.* **2009**, 5883.

(25) Wan, W.-M.; Pan, C.-Y. *Polym. Chem.* **2010**, *1*, 1475.

(26) Zhao, W.; Gody, G.; Dong, S.; Zetterlund, P. B.; Perrier, S. *Polym. Chem.* **2014**, *5*, 6990.

(27) Kang, Y.; Pitto-Barry, A.; Maitland, A.; O'Reilly, R. K. *Polym. Chem.* **2015**, *6*, 4984.

(28) Bauri, K.; Narayanan, A.; Haldar, U.; De, P. *Polym. Chem.* **2015**, *6*, 6152.

(29) Zhang, W.; D'Agosto, F.; Boyron, O.; Rieger, J.; Charleux, B. *Macromolecules* **2012**, *45*, 4075.

(30) Tan, J.; Sun, H.; Yu, M.; Sumerlin, B. S.; Zhang, L. *ACS Macro Lett.* **2015**, *4*, 1249.

(31) Warren, N. J.; Mykhaylyk, O. O.; Mahmood, D.; Ryan, A. J.; Armes, S. P. *J. Am. Chem. Soc.* **2014**, *136*, 1023.

(32) Ratcliffe, L. P. D.; McKenzie, B. E.; Le Bouëdec, G. M. D.; Williams, C. N.; Brown, S. L.; Armes, S. P. *Macromolecules* **2015**, *48*, 8594.

(33) Binks, B. P. *Curr. Opin. Colloid Interface Sci.* **2002**, *7*, 21.

(34) Thompson, K. L.; Mable, C. J.; Cockram, A.; Warren, N. J.; Cunningham, V. J.; Jones, E. R.; Verber, R.; Armes, S. P. *Soft Matter* **2014**, *10*, 8615.

(35) Thompson, K. L.; Mable, C. J.; Lane, J. A.; Derry, M. J.; Fielding, L. A.; Armes, S. P. *Langmuir* **2015**, *31*, 4137.

(36) Verber, R.; Blanazs, A.; Armes, S. P. *Soft Matter* **2012**, *8*, 9915.

(37) Won, Y.-Y.; Paso, K.; Davis, H. T.; Bates, F. S. *J. Phys. Chem. B* **2001**, *105*, 8302.

(38) Zhang, W.; Charleux, B.; Cassagnau, P. *Macromolecules* **2012**, *45*, 5273.

(39) Zhang, W.; Charleux, B.; Cassagnau, P. *Soft Matter* **2013**, *9*, 2197.

(40) Almgren, M.; Brown, W.; Hvidt, S. *Colloid Polym. Sci.* **1995**, *273*, 2.

(41) Pei, Y. W.; Dharsana, N. C.; Van Hensbergen, J. A.; Burford, R. P.; Roth, P. J.; Lowe, A. B. *Soft Matter* **2014**, *10*, 5787.

(42) Fielding, L. A.; Lane, J. A.; Derry, M. J.; Mykhaylyk, O. O.; Armes, S. P. *J. Am. Chem. Soc.* **2014**, *136*, 5790.

(43) Guo, A.; Liu, G.; Tao, J. *Macromolecules* **1996**, *29*, 2487.

(44) O'Reilly, R. K.; Hawker, C. J.; Wooley, K. L. *Chem. Soc. Rev.* **2006**, *35*, 1068.

(45) Blencowe, A.; Tan, J. F.; Goh, T. K.; Qiao, G. G. *Polymer* **2009**, *50*, 5.

(46) Kocak, G.; Bütün, V. *Colloid Polym. Sci.* **2015**, *293*, 3563.

(47) Thurmond, K. B., II; Kowalewski, T.; Wooley, K. L. *J. Am. Chem. Soc.* **1996**, *118*, 7239.

(48) Huang, H.; Kowalewski, T.; Remsen, E. E.; Gertzmann, R.; Wooley, K. L. *J. Am. Chem. Soc.* **1997**, *119*, 11653.

(49) Joralemon, M. J.; O'Reilly, R. K.; Hawker, C. J.; Wooley, K. L. *J. Am. Chem. Soc.* **2005**, *127*, 16892.

(50) Zhang, Q.; Remsen, E. E.; Wooley, K. L. *J. Am. Chem. Soc.* **2000**, *122*, 3642.

(51) Li, Y.; Du, W.; Sun, G.; Wooley, K. L. *Macromolecules* **2008**, *41*, 6605.

(52) Liu, S. Y.; Weaver, J. V. M.; Tang, Y. Q.; Billingham, N. C.; Armes, S. P.; Tribe, K. *Macromolecules* **2002**, *35*, 6121.

(53) Li, Y.; Lokitz, B. S.; Armes, S. P.; McCormick, C. L. *Macromolecules* **2006**, *39*, 2726.

(54) Butun, V.; Lowe, A. B.; Billingham, N. C.; Armes, S. P. *J. Am. Chem. Soc.* **1999**, *121*, 4288.

(55) Butun, V.; Billingham, N. C.; Armes, S. P. *J. Am. Chem. Soc.* **1998**, *120*, 12135.

(56) Hentze, H. P.; Krämer, E.; Berton, B.; Förster, S.; Antonietti, M.; Dreja, M. *Macromolecules* **1999**, *32*, 5803.

(57) Tao, J.; Stewart, S.; Liu, G.; Yang, M. *Macromolecules* **1997**, *30*, 2738.

(58) Liu, G. J.; Ding, J. F.; Qiao, L. J.; Guo, A.; Dymov, B. P.; Gleeson, J. T.; Hashimoto, T.; Saijo, K. *Chem. Eur. J.* **1999**, *5*, 2740.

(59) Li, Y.; Armes, S. P. *Angew. Chem., Int. Ed.* **2010**, *49*, 4042.

(60) Shen, W. Q.; Chang, Y. L.; Liu, G. Y.; Wang, H. F.; Cao, A. N.; An, Z. S. *Macromolecules* **2011**, *44*, 2524.

(61) Liu, G. Y.; Qiu, Q.; Shen, W. Q.; An, Z. S. *Macromolecules* **2011**, *44*, 5237.

(62) Liu, G.; Qiu, Q.; An, Z. *Polym. Chem.* **2012**, *3*, 504.

(63) Chambon, P.; Blanazs, A.; Battaglia, G.; Armes, S. P. *Langmuir* **2012**, *28*, 1196.

(64) Zhou, W.; Qu, Q.; Yu, W.; An, Z. *ACS Macro Lett.* **2014**, *3*, 1220.

(65) Wang, X.-S.; Arsenault, A.; Ozin, G. A.; Winnik, M. A.; Manners, I. *J. Am. Chem. Soc.* **2003**, *125*, 12686.

(66) Stewart, S.; Liu, G. *Angew. Chem., Int. Ed.* **2000**, *39*, 340.

(67) Figg, C. A.; Simula, A.; Gebre, K. A.; Tucker, B. S.; Haddleton, D. M.; Sumerlin, B. S. *Chem. Sci.* **2015**, *6*, 1230.

(68) Wang, X.; Liu, K.; Arsenault, A. C.; Rider, D. A.; Ozin, G. A.; Winnik, M. A.; Manners, I. *J. Am. Chem. Soc.* **2007**, *129*, 5630.

(69) Chiefari, J.; Chong, Y. K.; Ercole, F.; Krstina, J.; Jeffery, J.; Le, T. P. T.; Mayadunne, R. T. A.; Meijs, G. F.; Moad, C. L.; Moad, G.; Rizzardo, E.; Thang, S. H. *Macromolecules* **1998**, *31*, 5559.

(70) Moad, G.; Rizzardo, E.; Thang, S. H. *Aust. J. Chem.* **2005**, *58*, 379.

(71) Clayden, J.; Greeves, N.; Warren, S.; Wothers, P. *Organic Chemistry*; Oxford University Press: New York, **2001**.

(72) Save, M.; Weaver, J. V. M.; Armes, S. P.; McKenna, P. *Macromolecules* **2002**, *35*, 1152.

(73) Lovett, J. R.; Warren, N. J.; Ratcliffe, L. P.; Kocik, M. K.; Armes, S. P. *Angew. Chem., Int. Ed.* **2015**, *54*, 1279.

(74) Barner-Kowollik, C.; Buback, M.; Charleux, B.; Coote, M. L.; Drache, M.; Fukuda, T.; Goto, A.; Klumperman, B.; Lowe, A. B.; McLeary, J. B.; Moad, G.; Monteiro, M. J.; Sanderson, R. D.; Tonge, M. P.; Vana, P. *J. Polym. Sci., Part A: Polym. Chem.* **2006**, *44*, 5809.

(75) Blanazs, A.; Madsen, J.; Battaglia, G.; Ryan, A. J.; Armes, S. P. *J. Am. Chem. Soc.* **2011**, *133*, 16581.

(76) Ratcliffe, L. P. D.; Blanazs, A.; Williams, C. N.; Brown, S. L.; Armes, S. P. *Polym. Chem.* **2014**, *5*, 3643.

(77) Ratcliffe, L. P. D.; Ryan, A. J.; Armes, S. P. *Macromolecules* **2013**, *46*, 769.

(78) Zehm, D.; Ratcliffe, L. P. D.; Armes, S. P. *Macromolecules* **2013**, *46*, 128.

(79) Penfold, N. J. W.; Lovett, J. R.; Warren, N. J.; Verstraete, P.; Smets, J.; Armes, S. P. *Polym. Chem.* **2016**, *7*, 79.

(80) Willcock, H.; O'Reilly, R. K. *Polym. Chem.* **2010**, *1*, 149.

(81) Moad, G.; Rizzardo, E.; Thang, S. H. *Polym. Int.* **2011**, *60*, 9.

Chapter 6:

Conclusions and Outlook

6.1 Conclusions and Outlook

Since the invention of polymerisation-induced self-assembly (PISA) over 10 years ago, there have been significant advances in this field. Initial work was mainly based on improving understanding of the aspects of the PISA formulation. Though there are still aspects of PISA that are not fully understood (e.g., why are aqueous emulsion polymerisations so often limited to kinetically-trapped spheres?), the focus has switched to preparing diblock copolymer nano-objects by PISA that may have useful applications. Relevant to the work in this thesis is the recent use of poly(glycerol monomethacrylate)-poly(2-hydroxypropyl methacrylate) (PGMA-PHPMA) worm gels for certain biomedical applications.[1,2] For example, Gibson and co-workers reported the first solvent-free cryopreservation of red blood cells using these PGMA-PHPMA worms in combination with PVA, which constitutes the first fully synthetic formulation.[1] The worm gels act as an extracellular cryoprotectant and the PVA is a required ice-recrystallisation inhibitor. These mixtures were rapidly frozen by immersion in to liquid nitrogen and were subsequently stored at -80 °C above liquid nitrogen. After three days of storage followed by slow thawing to 4 °C, below the critical gelation temperature (CGT) of the worm gel, 68 % of red blood cells were recovered. Moreover, warming to 20 °C (i.e., above the CGT) results in regelation. Such PGMA-PHPMA worm gels also possess comparable rheological properties (10-100 Pa) to highly hydroxylated mammalian mucins (e.g., female reproductive tracts). Canton *et al.* demonstrated that a 6 % w/v worm gel can function as a suitable biocompatible 3D matrix for storage of either pluripotent human stem cells or human embryos at 37 °C.[2] Remarkably in both cases cytostasis (no cell growth) was observed, which makes them an ideal candidate the global transportation of stem cells. Moreover, the cells can be recovered by utilising the thermally-induced degelation behaviour of the PGMA-PHPMA worm gels.

In this thesis, second-generation PGMA-PHPMA worm gels are prepared with ionisable end-groups using a carboxylic acid-functionalised reversible addition-fragmentation chain transfer (RAFT) agent. Ionising the terminal carboxylic acid above pH 4.5 renders the PGMA stabiliser more hydrophilic and so induces a worm-to-sphere transition with concomitant degelation. This transition is fully reversible

and only requires minimal amounts of acid or base, thus can be cycled several times without significantly increasing the salt concentration. Similarly, pH-responsive PGMA-PHPMA vesicles can be prepared that undergo *irreversible* order-order morphological transitions provided that the PHPMA block DP is sufficiently short. It was envisaged that such pH-induced worm-to-sphere transitions may offer an alternative method for the release of cells from worm gels, rather than cooling. Similarly, it was hoped that the pH-responsive nature of the vesicles may potentially be useful for drug encapsulation and delivery when intravenously administered. However, both these examples of pH-responsive end-group-driven order-order transitions can be suppressed by the presence of added salt, i.e. 100 mM KCl. Hence, no morphology transitions are likely to be observed in physiological conditions where the salt concentration is comparable or higher than this value.[3] However, this provides a cheaper method for the preparation of PGMA-PHPMA worm gels for biomedical applications. For example, in this thesis 4-cyano-4-(2-phenyl ethanesulfanylthiocarbonyl)-sulfanylpentanoic acid (PETTC) was synthesised in-house and employed as a RAFT agent. PETTC is significantly cheaper than commercially available RAFT agents and can be isolated in high purity. Thus can be used to prepare more cost-effective PGMA-PHPMA diblock copolymer nano-objects in a phosphate-buffered saline (PBS) solution, where the pH-responsive behaviour is screened.

In related work, Penfold and co-workers have since prepared PGMA-PHPMA worms gels (and vesicles) using a morpholine-functionalised RAFT agent.[4] In this case, protonation of the morpholine end-group below pH 6.0 drives a worm-to-sphere or vesicle-to-worm morphology transition. However, these order-order transitions are also suppressed by the addition of salt. In principle, the solution pH of these nano-objects can be cycled between approximately pH 7.5 and pH 5.0 using carbon dioxide and nitrogen, which would prevent build up in salt.

Nevertheless, this research illustrates the remarkably delicate nature of these nanoparticles. Furthermore, it highlights the importance of selecting a suitable RAFT agent beyond the desired monomer class and solvent. It remains to be seen whether

similar end-group-mediated pH-responsive behaviour can be observed in other polar solvents and non-polar solvents.

In principle, chain-extending a PGMA macro-CTA *via* statistically copolymerising HPMA with 2-(diisopropylamino)ethyl methacrylate (DPA) to prepare PGMA-P(HPMA-DPA) nano-objects could enable the deleterious salt effect described above to be negated. DPA residues contain a tertiary amine ($pK_a \approx 7.2$) that can be protonated at low pH to switch these repeat units from hydrophobic to hydrophilic character. ^{1}H NMR kinetics of the copolymerisation indicated that DPA monomer is initially consumed faster than HPMA, leading to formation of a DPA-rich sequence near the block junction. This enables morphology transitions to lower order morphologies (for example vesicles to spheres or worms to spheres) when the solution pH is adjusted to below pH 7.0. Thus it is envisaged that such particles may act as drug delivery vehicles. However, the salt sensitivity of these particles still needs to be investigated. It is also perhaps worth exploring the synthesis of PGMA-P(HPMA-DPA) diblock copolymers using the morpholine-functionalised RAFT agent. This may allow for the preparation of nanoparticles with enhanced pH-responsive behaviour at high salt concentrations. Other possibilities for the preparation of pH-responsive nano-objects *via* PISA are the synthesis of PGMA-PHPMA-PDPA triblock copolymers or the incorporation of DPA units in the PGMA stabiliser block.

In Chapter 5 it was demonstrated that worms can be prepared using PISA by copolymerising a PGMA macro-CTA with HPMA and glycidyl methacrylate (GlyMA). Such worms exhibited degelation on cooling to 5 °C provided that the core-forming block contained less than 20 mol % GlyMA. This is also because the GlyMA monomer initially reacted faster than HPMA, resulting in a GlyMA-rich sequence near the block junction. Thus increasing the content of the more hydrophobic GlyMA in the core-forming block requires lower temperatures for surface plasticisation of the worms to induce a worm-to-sphere transition. These PGMA-P(HPMA-GlyMA) worms can be subsequently reacted with 3-aminopropyl triethoxysilane (APTES), which simultaneously undergo an epoxy-amine reaction and hydrolysis-condensation to produce core cross-linked worms. Oscillatory

rheology studies indicate that core cross-linked worms are stiffer and do not undergo degelation on cooling. The latter may be useful if PGMA-PHPMA worms are required at lower temperatures, since the linear worms would simply transform into spheres or dissolved copolymer chains. Furthermore, the cross-linked worms exhibit excellent resistance to anionic surfactants, whereas the analogous linear worms rapidly dissociate in the presence of surfactant. Zeta potential studies indicated that these core cross-linked worms also exhibited cationic behaviour. Thus they may potentially be capable of flocculating anionic materials such as silica. It is worth exploring the cross-linking of PGMA-P(HPMA-GlyMA) worms using cystamine (a disulfide-based diamine) instead of APTES. In principle, the resulting covalent cross-links can be cleaved by reducing the disulfide bond using a reducing agent such as tris(2-carboxyethyl)phosphine (TCEP) to give thiol groups. Moreover, these thiol groups could potentially be used to functionalise the core of such nano particles.

Utilising the same epoxide chemistry, fluorescently-labelled worms have been prepared. More specifically, PGMA-P(HPMA-GlyMA) worms containing only one GlyMA residue per copolymer chain were reacted with rhodmine B piperazine at pH 9.0. The diffusion of these 10 % w/w fluorescently-labelled worms was monitored as a function of either temperature or pH by Dr. C. Clarkson and Prof. M. Geoghegan (Department of Physics, University of Sheffield) using fluorescence correlation spectroscopy (FCS). In both cases faster diffusion was observed after inducing a worm-to-sphere transition, as expected.

Previously Cunningham and co-workers utilised poly(glycerol monomethacrylate)-poly(benzyl methacrylate) spheres as oil-in-water Pickering emulsifiers.[5] By fluorescently labelling these spheres, it was proved that they adsorbed at the interface by fluorescence microscopy. Similarly, core cross-linked PGMA-PHPMA worms can be utilised as Pickering emulsifiers. Thompson *et al.* demonstrated that such nanoparticles adsorbed significantly stronger than the corresponding spheres.[6] Therefore the fluorescently-labelled worms prepared in this thesis could be used to prove droplet adsorption. However, these particles would also require cross-linking as the high-energy homogenisation used to prepare the emulsions causes worms dissociation. The epoxide chemistry is not limited to worm-

like particles and may also enable the facile post-polymerisation modification of many other types of diblock copolymer different nano-objects with various functional groups. For example, corona-decorated particles could be prepared by incorporating a few GlyMA units into the stabiliser block.

6.2 References

(1) Mitchell, D. E.; Lovett, J. R.; Armes, S. P.; Gibson, M. I. *Angew. Chem., Int. Ed.* **2016**, *55*, 2801.

(2) Canton, I.; Warren, N. J.; Chahal, A.; Amps, K.; Wood, A.; Weightman, R.; Wang, E.; Moore, H.; Armes, S. P. *ACS Cent. Sci.* **2016**, *2*, 65.

(3) Lodish, H.; Berk, A.; Zipursky, L. S.; Matsudaria, P.; Baltimore, D.; Darnell, J. *Molecular Cell Biology*; 4th ed.; W.H.Freeman & Co Ltd: New York, USA, **2000**.

(4) Penfold, N. J. W.; Lovett, J. R.; Warren, N. J.; Verstraete, P.; Smets, J.; Armes, S. P. *Polym. Chem.* **2016**, *7*, 79.

(5) Cunningham, V. J.; Alswieleh, A. M.; Thompson, K. L.; Williams, M.; Leggett, G. J.; Armes, S. P.; Musa, O. M. *Macromolecules* **2014**, *47*, 5613.

(6) Thompson, K. L.; Mable, C. J.; Cockram, A.; Warren, N. J.; Cunningham, V. J.; Jones, E. R.; Verber, R.; Armes, S. P. *Soft Matter* **2014**, *10*, 8615.

Appendix

A.1 Rheology strain sweeps

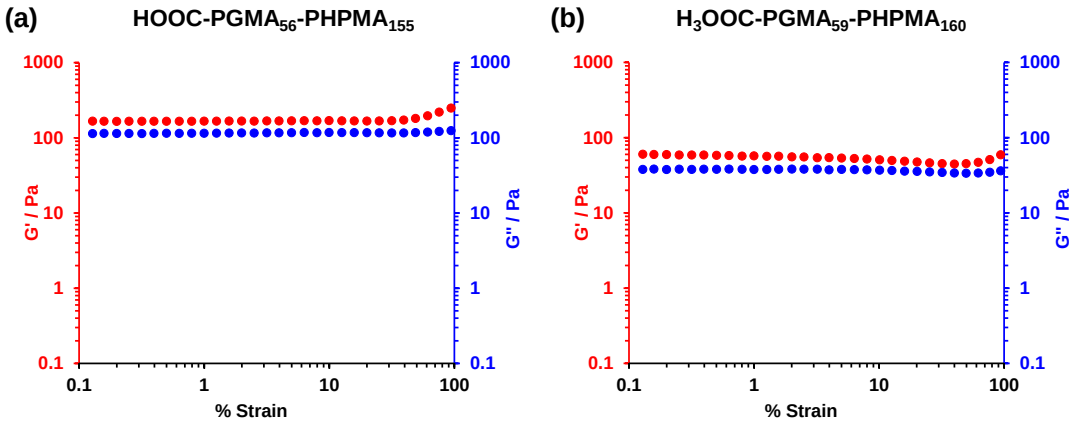

Figure A.1 Variation in storage modulus (G') and loss modulus (G") with applied strain at a fixed angular frequency of 1.0 rad s^{-1} at 25 °C for a 10 % w/w aqueous dispersion of (a) HOOC-$PGMA_{56}$-$PHPMA_{155}$ and (b) H_3COOC-$PGMA_{59}$-$PHPMA_{160}$ diblock copolymer worm gels at pH 3.5.

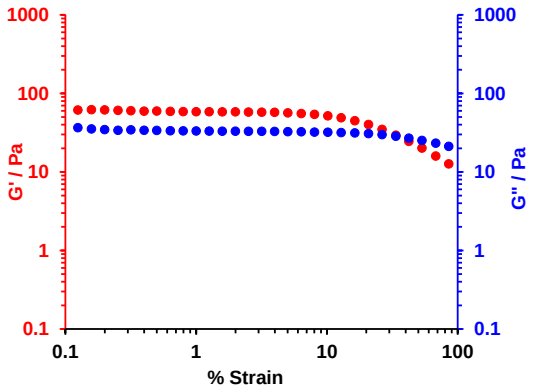

Figure A.2 Variation in storage modulus (G') and loss modulus (G") with applied strain at a fixed angular frequency of 1.0 rad s^{-1} at 25 °C for a 10 % w/w aqueous dispersion of HOOC-$PGMA_{43}$-$PHPMA_{200}$ diblock copolymer worms at pH 6.0.

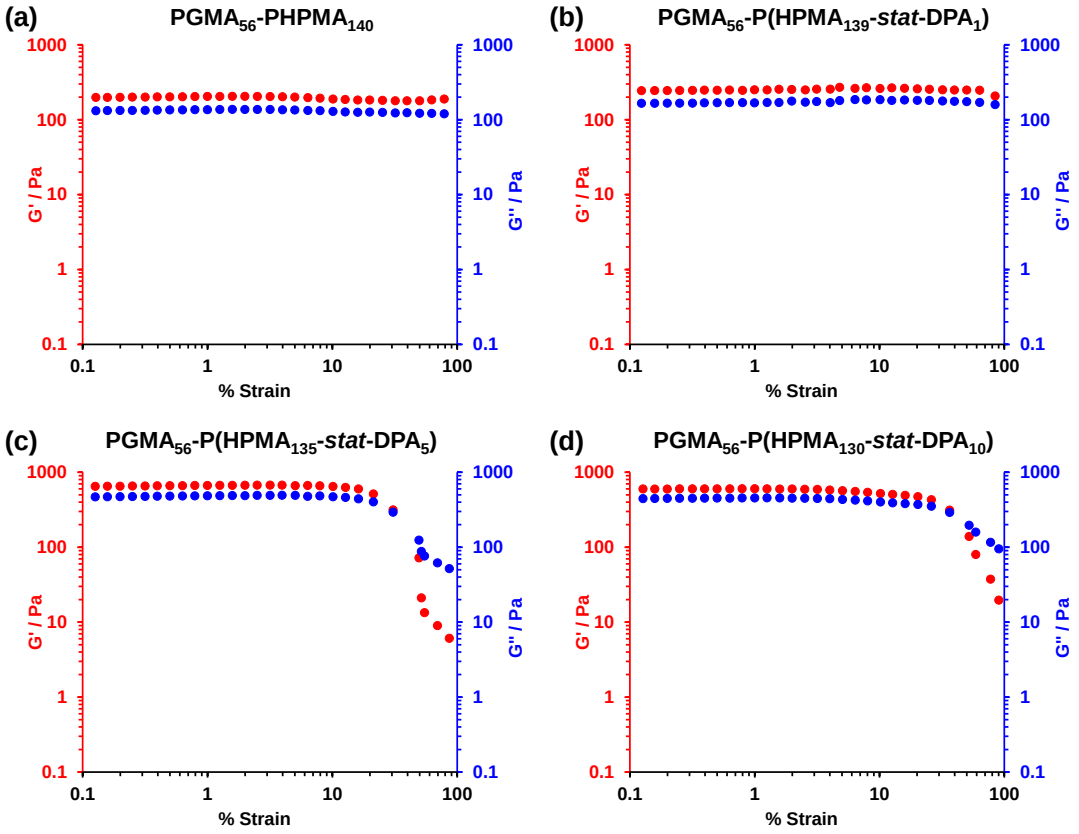

Figure A.3 Variation in storage modulus (G') and loss modulus (G") with applied strain at a fixed angular frequency of 1.0 rad s^{-1} at 25 °C for a 15 % w/w aqueous dispersion of (a) $PGMA_{56}$-$PHPMA_{140}$, (b) $PGMA_{56}$-P($HPMA_{139}$-*stat*-DPA_1), (c) $PGMA_{56}$-P($HPMA_{135}$-*stat*-DPA_5) and (d) $PGMA_{56}$-P($HPMA_{130}$-*stat*-DPA_{10}) gels at pH 8.5.

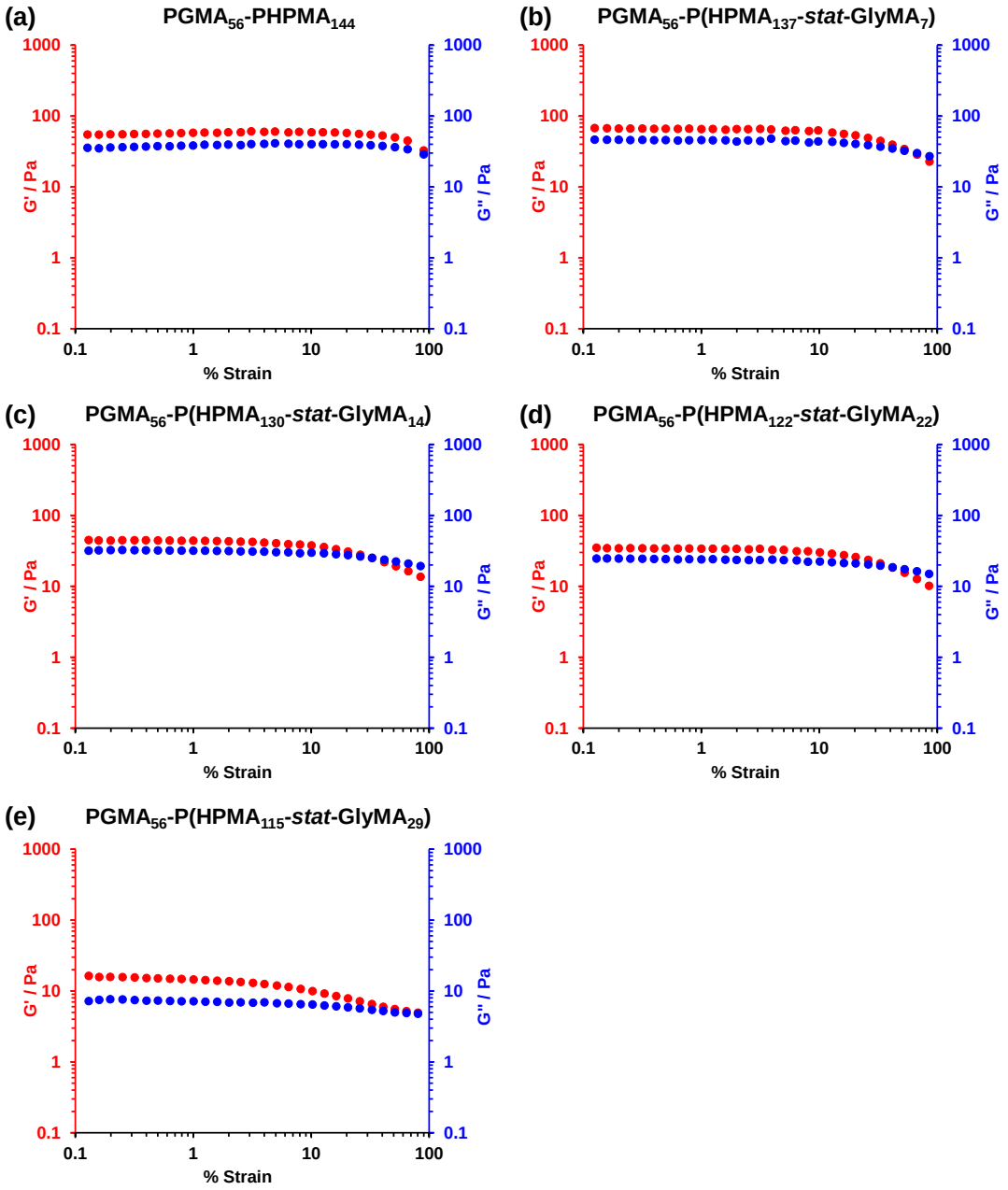

Figure A.4 Variation in storage modulus (G') and loss modulus (G") with applied strain at a fixed angular frequency of 1.0 rad s^{-1} at 25 °C for a 7.5 % w/w aqueous dispersion of (a) $PGMA_{56}$-$PHPMA_{144}$; (b) $PGMA_{56}$-P($HPMA_{137}$-*stat*-$GlyMA_{7}$), (c) $PGMA_{56}$-P($HPMA_{130}$-*stat*-$GlyMA_{14}$), (d) $PGMA_{56}$-P($HPMA_{122}$-*stat*-$GlyMA_{22}$) and (e) $PGMA_{56}$-P($HPMA_{115}$-*stat*-$GlyMA_{29}$) worms before cross-linking.